NASA Tech Briefs

National
Aeronautics and
Space
Administration

The corrosion-resistant properties of a NASA-developed inorganic zinc-dust paint are being tested on the Golden Gate Bridge.

A plasma polymerization technique may protect plastic lenses from scratching.

A commercial firm applied spacecraft fracture-toughness testing techniques, developed for checking spacecraft structure, to build stronger plows and more-powerful tractors.

Vol. 1 No. 1

SPRING 1976

Foreword

About the NASA Technology Utilization Program

The National Aeronautics and Space Act of 1958, which established NASA and the United States civilian space program, requires that "The Administration shall provide for the widest practicable and appropriate dissemination of information concerning its activities and the results thereof."

To help carry out this objective the NASA Technology Utilization (TU) Program was established in 1962. It offers a variety of valuable services to facilitate the transfer of aerospace technology to nonaerospace applications, thus assuring American taxpayers maximum return on their investment in space research; thousands of spinoffs of NASA research have already occurred in virtually every area of our economy.

The TU Program has worked for engineers, scientists, technicians, and businessmen. And it can work for you.

NASA Tech Briefs

Tech Briefs is published quarterly and is free to any U.S. citizen or organization. It is both a current-awareness medium and a problem-solving tool. Potential products ... industrial processes ... basic and applied research ... shop and lab techniques ... computer software ... new sources of technical data ... concepts ... you will find them all in NASA *Tech Briefs*. The first section highlights a few of the potential new products contained in *Tech Briefs*. The remainder of the volume is organized by technical category to help you quickly review new developments in your areas of interest. Finally, a subject index makes each issue a convenient permanent reference file.

Further Information on Innovations

Although many articles are complete in themselves, others are backed up by Technical Support Packages (TSP's). TSP's are available without charge and may be ordered by simply completing the enclosed TSP Request Card. Further information on some innovations is available for a nominal fee from other sources, as indicated at the ends of the articles. In addition, Technology Utilization Officers at NASA Field Centers will assist you directly when necessary. (See page 6.)

Patent Licenses

Many of the inventions described are under consideration for patents or have been patented by NASA. Unless NASA has decided not to apply for a patent, the patent status is described at the end of each article. For further information about the Patent Program see page 2.

Other Technology Utilization Services

To assist engineers, industrial researchers, business executives, city officials, and other potential users in applying space technology to their problems, NASA sponsors six Industrial Applications Centers. Their services are described inside the back cover. In addition, an extensive library of computer programs is available through COSMIC, the Technology Utilization Program's outlet for NASA-developed software. (See page 7.)

Applications Program

To help solve public-sector problems in such areas as safety, health, transportation, and environmental protection, NASA TU Applications Teams, staffed by professionals from a variety of disciplines, work with Federal agencies, local governments, and health organizations to identify critical problems amenable to technical solutions. Among their many significant contributions are a rechargeable heart pacemaker, a lightweight fireman's breathing apparatus, aids for the handicapped, and safer highways.

We hope you find the information in NASA Tech Briefs *useful. A reader feedback card has been included because we want your comments and suggestions on how we can further help you apply NASA innovations and technology to your needs. Please use it, or if you need more space, write us a letter.*

"The Administrator of National Aeronautics and Space Administration has determined that the publication of this periodical is necessary in the transaction of the public business required by law of this Agency. Use of funds for printing this periodical has been approved by the Director of the Office of Management and Budget through August 31, 1977."

Contents

NASA INVENTIONS AVAILABLE FOR LICENSING

Over 3,500 NASA inventions are available for licensing in the United States - both exclusive and nonexclusive.

Nonexclusive Licenses

Nonexclusive licenses for commercial use are encouraged to promote competition and to achieve the widest use of inventions. They must be used by a negotiated target date but are usually royalty free.

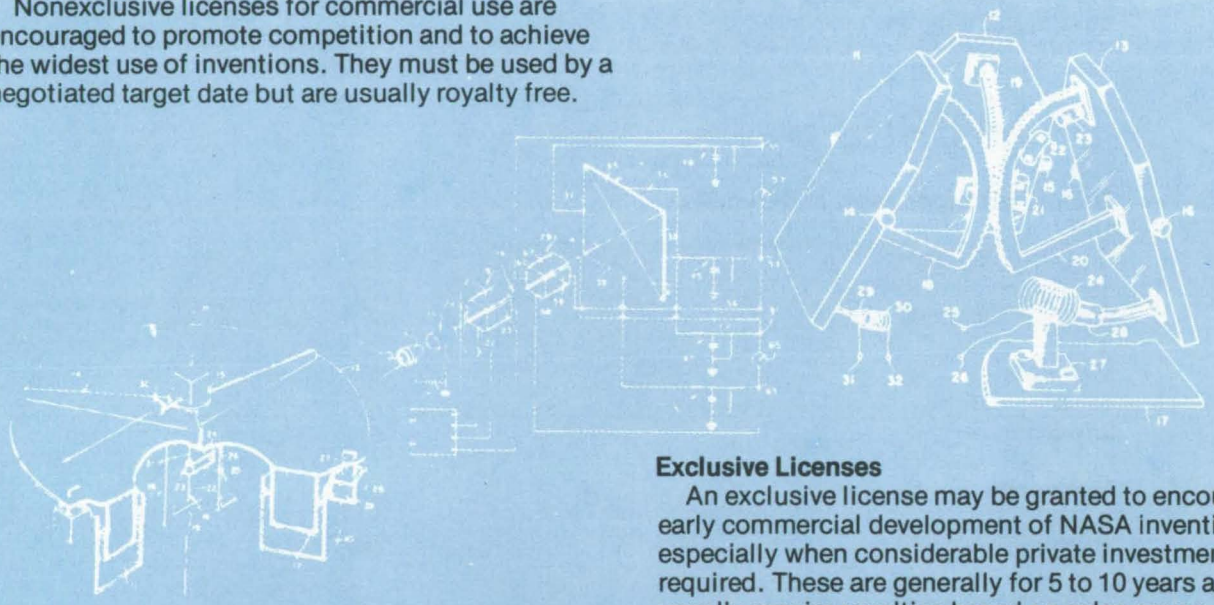

Exclusive Licenses

An exclusive license may be granted to encourage early commercial development of NASA inventions, especially when considerable private investment is required. These are generally for 5 to 10 years and usually require royalties based on sales or use.

The NASA patent licensing program also provides for licensing of NASA-owned foreign patents. In addition to inventions described in Tech Briefs, "NASA Patent Abstract Bibliography," containing abstracts of all NASA inventions, can be purchased from: National Technical Information Service, Springfield, Va., 22161. This document is updated semi-annually.

Patent Licenses and the NASA Tech Brief

Many of the inventions reported in Tech Briefs are patented or are under consideration for a patent at the time they are published. When this is the case, the current patent status is described at the end of the article; otherwise, there is no statement about patents. **If you want to know more about the patent program or are interested in license for a particular invention, write the Patent Counsel at the NASA Field Center** that sponsored the research. Be sure to refer to the NASA reference number in parenthesis at the end of the Tech Brief.

Robert F. Kempf
NASA Headquarters, Code GP
400 Maryland Ave., S.W.
Washington, D.C. 20546
(202) 755-3932

Darrell G. Brekke
Ames Research Center
Mail Code: 200-11A
Moffett Field, CA 94035
(415) 965-5104

John O. Tresansky
Goddard Space Flight Center
Mail Code: 204
Greenbelt, MD 20771
(301) 982-2351

Marvin F. Matthews
Lyndon B. Johnson Space Center
Mail Code: AM
Houston, TX 77058
(713) 483-4871

James O. Harrell
John F. Kennedy Space Center
Mail Code: SA-PAT
Kennedy Space Center, FL 32899
(305) 867-2544

Howard J. Osborn
Langley Research Center
Mail Code: 313
Hampton, VA 23665
(804) 827-3725

Norman T. Musial
Lewis Research Center
Mail Code: 500-113
21000 Brookpark Road
Cleveland, OH 44135
(216) 433-4000 Ext. 346

Leon D. Wofford, Jr.
George C. Marshall Space Flight Center
Mail Code: CC01
Huntsville, AL 35812
(205) 453-0020

Monte F. Mott
NASA Pasadena Office
Mail Code: 180-601
4800 Oak Grove Drive
Pasadena, CA 91103
(213) 354-2700

New Product Ideas

Metal Structures With Parallel Pores

Four methods of fabricating metal plates, each method yielding uniformly-dimensioned pore structures, show that the geometry of powder-metallurgy-fabricated metal parts may be readily optimized. The methods are: (1) the elongate-bundle method, (2) the wind-and-sinter method, (3) the extrude-and-sinter method, and (4) the corrugate-stack method. Plates for electrochemical cells and electrodes for certain types of fuel cells are presently made by powder metallurgy.
(See page 132.)

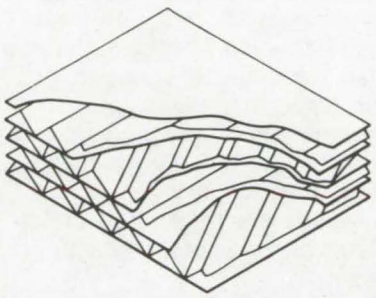

Increased Safety in Mercury-Containing Devices

A thin sheet of amalgamating metal included inside pressurized mercury-filled devices such as lamps and rectifiers reduces the amount of escaping mercury vapor if containment failure occurs. Experiments have shown that the amalgamating metals reduce the mercury pressure to approximately 6 percent of the normal value. Common heavy-duty fluorescent lamps illuminating office and factory buildings might incorporate the amalgamating metals as an extra safety factor.
(See page 20.)

Improved Wet-Slug Capacitor

An all-tantalum seal, combined with straight, ungelled, 30-percent sulphuric acid electrolyte, can reduce electrolytic capacitor leakage from the order of milliamperes to the low-microampere region. Anode damage is reduced, and the self-healing capability of the capacitor is improved. This tantalum wet-slug capacitor design offers better reliability in the severe environments encountered in military and industrial electronics systems and improved volume and weight savings resulting from the self-healing properties.
(See page 15.)

Liquid-Retention Canopy

A retention canopy prevents sloshing in fuel or liquid-gas tanks. By reducing the amount of fluid thrown against the wall, evaporation losses are reduced. This system would be particularly effective in tanks carrying cryogenic fluids such as liquid nitrogen.
(See page 101.)

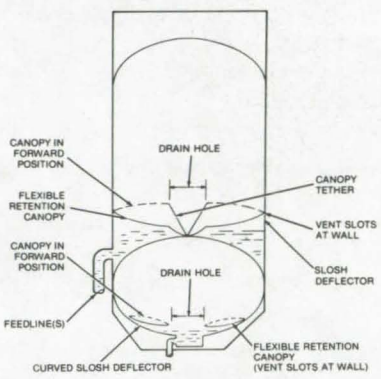

Combined Joining Process for Dissimilar Metals: A Concept

Heat dissipaters consisting of aluminum cold plates attached to stainless-steel connecting ports may be fabricated in a two-stage bonding/fluxless-brazing process that requires less than half the time and far less pressure compared to the conventional technique. Tests indicate that the resulting bond can withstand internal pressures up to 1,000 psi (6.9×10^6 N/m^2).
(See page 128.)

Graphic-to-Digital Conversion System

A computer-controlled system converts graphic data to digital data and allows the operator to record only those data points selected. It consists of a commercially-available X-Y plotter, a computer, and A/D and D/A converters. The new component is a strain-gage controller and amplifier which can be adapted to existing systems.
(See page 26.)

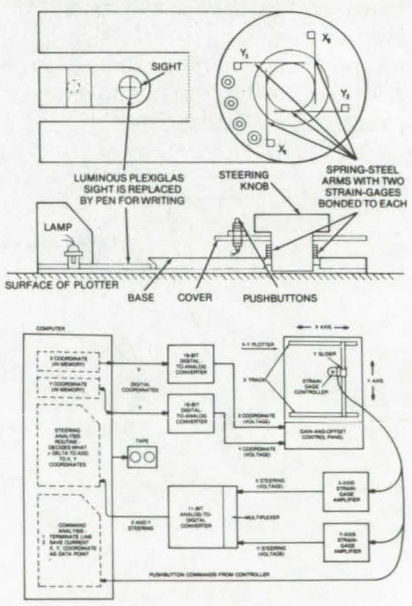

Myocardial Wall-Thickness Transducer

A new myocardium wall-thickness transducer is lightweight and small and does not interfere with normal heart functions when inserted. Heart muscle traumatization is thus avoided. The transducer, which consists of a compliant circular beam with a silicon-semiconductor strain gage attached, is connected to conventional instrumentation that is calibrated to measure the percent change in the myocardial-wall thickness from a baseline at the end of diastole to other significant events throughout the heart cycle.
(See page 83.)

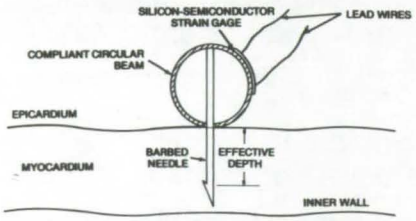

Lightweight Orthotic Appliances

Graphite-reinforced polymer materials can be used to make lightweight orthotic appliances and braces. The graphite composite material is quite stiff, even when thin. Thus orthotic supports can be made thinner as well as lighter. Furthermore, the composite supports can be made without investing in ovens, vacuum autoclaves, or other equipment required to make conventional polymer supports.
(See page 84.)

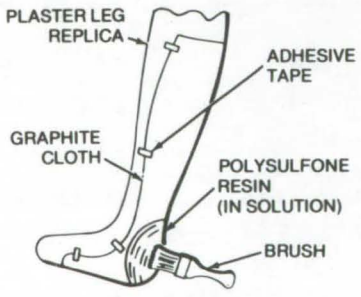

Quantitative Bioluminescent Detection of Bacteria

For infection determination, ecological measurements, and the like, the detection of bacteria by rapid, sensitive, inexpensive, and automatable methods is a necessity. Bacteria may be quantitated in such cases by measuring the phosphoflavins in the bacterial sample, using the photobacterial luciferase assay technique for flavin mononucleotide (FMN). The instrumentation used to measure the light emitted during the bioluminescent reaction offers a maximum sensitivity of 1×10^{-5} μg of FMN. Also, the costs of bacterial luciferase and the instrumentation are reasonable.
(See page 81.)

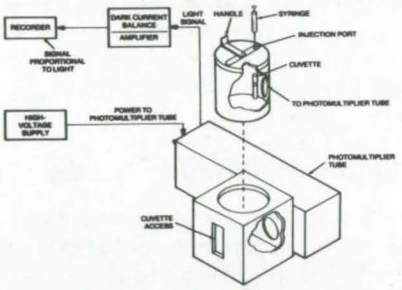

DIP Extractor Simplifies Circuit Removal

A new extractor for removing dual in-line IC's from printed-circuit boards is easy to use and inexpensive to construct. Tools of this type can be designed to extract most popular IC configurations and sizes.
(See page 10.)

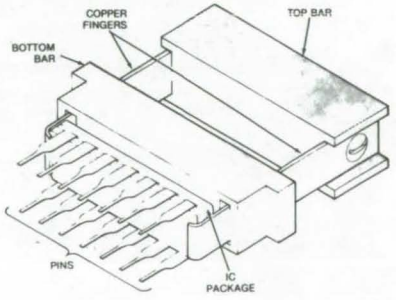

Ultraviolet Fire Detector

An ultraviolet detection system is able to detect the light emitted by a match-sized flame at a distance of 10 ft. It is not affected by high-energy or particulate radiation and is therefore particularly suited for applications around nuclear plants and X-ray equipment. The system produces a fire-warning output signal, with a low possibility of false alarms, and can be used to operate various types of alarm systems.
(See page 23.)

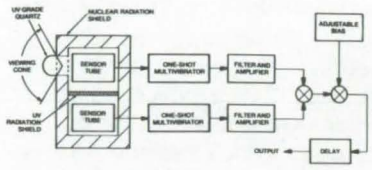

Plug-In Light Switches

A new concept in electrical hardware for buildings and similar applications is safer, less expensive to manufacture, and easier to install than conventional fixtures. A switch or outlet is integrally combined in the faceplate. This assembly is simply plugged into a recessed wall receptacle for installation. All parts are compatible with existing switch plates and socket receptacle boxes.
(See page 9.)

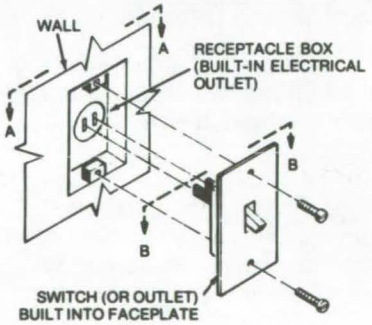

Measurement of Rapidly-Changing Heating Rates

An easily-fabricated heating-rate sensor accurately measures heating rates that are changing rapidly. The sensor consists of two metal plates, separated by a space, and a thermopile or thermocouple. The design is based on numerous heat-transfer analyses. Calibration is required, but no maintenance is needed other than for the thermocouple system.
(See page 106.)

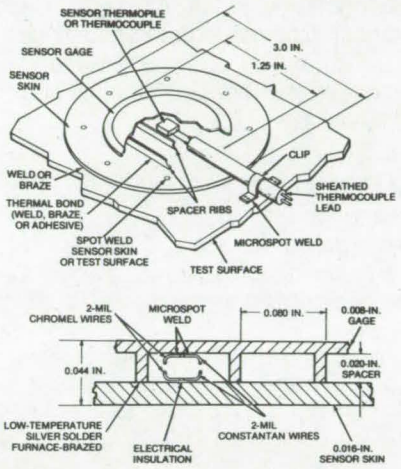

Light Pipes for LED Measurements

A high-quality light pipe directly couples LED optical output to a single detector. Essentially all of the radiated optical power is channeled to the detector. This system decreases measurement errors caused by detector instabilities and thermal effects.
(See page 43.)

Vacuum-Jacketed Line Spacer

An improved spacer for vacuum-jacketed cryogenic lines has three integral, equally-spaced leaf springs. The springs separate the outer vacuum jacket from the fluid carrying line, yet minimize conductive heat leaks and liquid boil off. The one-piece heat spring has sufficient flexibility to accommodate differential thermal expansion of the inner and outer line.
(See page 92.)

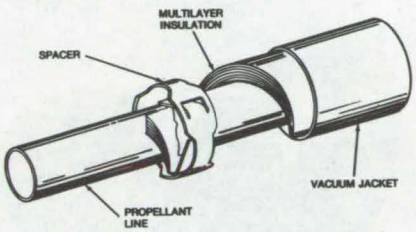

Roll-Forming Tubes to Header Plates

A technique has been developed for attaching and sealing tubes to header plates using a unique roll-forming tool. The technique is useful for attaching small tubes which are difficult to roll into conventional grooves in header plate tube holes, and for attaching when welding, brazing, or soldering are not desirable.
(See page 131.)

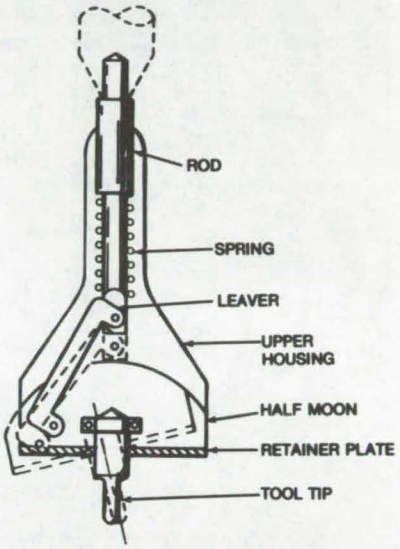

PATENT LICENSES RECENTLY GRANTED BY NASA FOR COMMERCIAL USE OF NASA-OWNED INVENTIONS

The patent licenses listed below have been recently awarded by NASA as part of its program to encourage the commercial application of its new technology. For information on how you may obtain nonexclusive or exclusive license for the commercial use of NASA inventions, see page 2 of this issue.

A nonexclusive license to Charles D. Bennett for a U.S. Patent No. 3,679,360, covering an invention entitled "Process For The Preparation of Brushite Crystals".

A nonexclusive license to Francis DeFalco for a U.S. Patent No. 3,679,360, covering an invention entitled "Process For The Preparation of Brushite Crystals."

A nonexclusive license to East-West Associates, Incorporated for a U.S. Patent No. 3,620,784, covering an invention entitled "Potassium Silicate Zinc Coatings".

A nonexclusive license to Meditron Instrument Corporation for a U.S. Patent No. 3,814,083, covering an invention entitled "Apparatus & Method for Processing Korotkov Sounds".

A nonexclusive license to PAK Manufacturing, Inc. for a U.S. Patent No. 3,197,616, covering an invention entitled "Temperature Regulation Circuit".

A nonexclusive license to PAK Manufacturing, Inc. for a U.S. pending patent application No. 545,282, covering an invention entitled "Wind Sensor".

THE NASA TECHNOLOGY UTILIZATION OFFICERS

They will help you apply the innovations described in Tech Briefs.

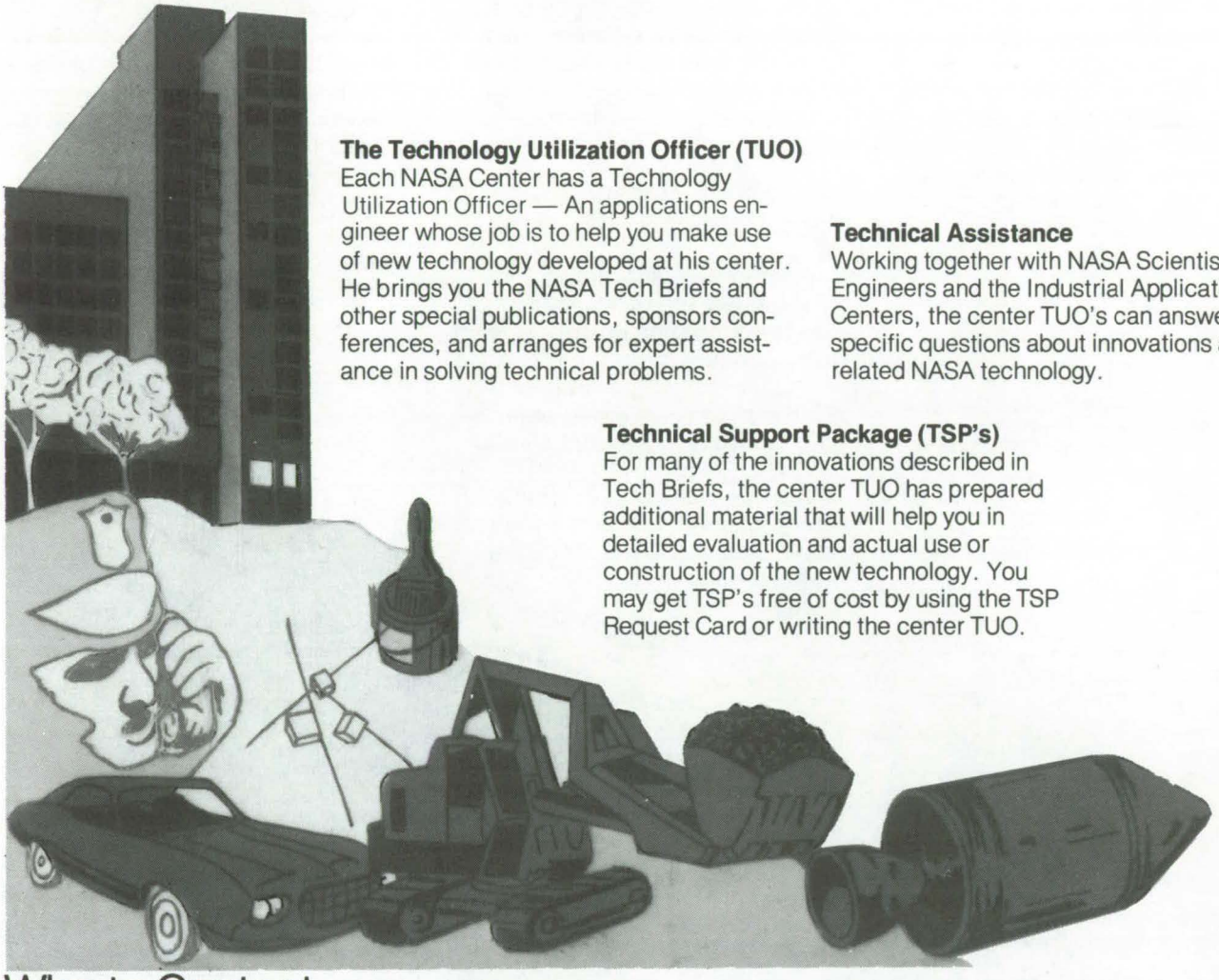

The Technology Utilization Officer (TUO)
Each NASA Center has a Technology Utilization Officer — An applications engineer whose job is to help you make use of new technology developed at his center. He brings you the NASA Tech Briefs and other special publications, sponsors conferences, and arranges for expert assistance in solving technical problems.

Technical Assistance
Working together with NASA Scientists and Engineers and the Industrial Applications Centers, the center TUO's can answer specific questions about innovations and related NASA technology.

Technical Support Package (TSP's)
For many of the innovations described in Tech Briefs, the center TUO has prepared additional material that will help you in detailed evaluation and actual use or construction of the new technology. You may get TSP's free of cost by using the TSP Request Card or writing the center TUO.

Who to Contact. Of course, many technical questions about Tech Briefs are answered in the TSP's, but when no TSP is available, or you have further questions, write the Technology Utilization Officer at the center that sponsored the research at the address listed below.

Charles K. Kubokawa
Ames Research Center
Code AU: 230-2
Moffett Field, Calif. 94035
Phone: (415) 965-5554

Clinton T. Johnson
Hugh L. Dryden Flight Research Center
P.O. Box 273
Edwards, Calif. 93523
Phone: (805) 258-3311, Ext. 568

Donald S. Friedman
Goddard Space Flight Center
Code 704.1
Greenbelt, Md. 20771
Phone: (301) 982-6242

John T. Wheeler
Johnson Space Center
Code AT3
Houston, Texas 77058
Phone: (713) 483-3809

Raymond J. Cerrato
John F. Kennedy Space Center
Code SA-RTP
Kennedy Space Center, Fla. 32899
Phone: (305) 867-2780

John Samos
Langley Research Center
Mail Stop 139A
Hampton, Va. 23665
Phone: (804) 827-3281

Paul Foster
Lewis Research Center
21000 Brookpark Rd.
Cleveland, Oh. 44135
Phone: (216) 433-4000, Ext. 6832

Aubrey D. Smith
Marshall Space Flight Center
Code AT01
Marshall Space Flight Center, Ala. 35812
Phone: (205) 453-2224

John C. Drane
NASA Pasadena Office
4800 Oak Grove Dr.
Pasadena, Calif. 91103
Phone: (213) 354-6420

Gilmore H. Trafford
Wallops Flight Center
Wallops Island, Va. 23337
Phone: (804) 824-3411, Ext. 201

Louis Mogavero
Acting Director
Technology Utilization Office
Code KT
NASA Headquarters
Washington, D.C. 20546
Phone: (202) 755-3103

COSMIC

(Computer Software Management & Information Center)

AN ECONOMICAL SOURCE OF COMPUTER PROGRAMS DEVELOPED BY THE GOVERNMENT.

COSMIC is sponsored by NASA to give you access to over 1400 computer programs developed by NASA and the Department of Defense, and selected programs from other government agencies. It is one of the Nation's largest software libraries.

COSMIC charges very reasonable fees for programs to help cover part of their expenses—and NASA pays for the remainder. Programs generally cost from $500 to $1000, but a few are more expensive and many are less. Documentation is available separately and very inexpensively.

COSMIC collects and stores software packages, insures that they are complete, prepares special announcements (such as Tech Briefs), publishes an indexed software catalog, and reproduces programs for distribution. COSMIC helps customers to identify their software needs, follows up to determine the successes and problems, and provides updates and error corrections. In some cases, NASA engineers can offer guidance to users in installing or running a program.

COSMIC programs range from management (pert scheduling) to information science (retrieval systems) and computer operations (hardware and software). Hundreds of engineering programs perform such tasks as structural analysis, electronic circuit design, chemical analysis, and design of fluid systems. Others determine building energy requirements, optimize mineral exploration, and draw maps of water-covered areas using NASA satellite data. In fact, the chances are, if you use a computer, you can use COSMIC.

COSMIC is eager to help you get the programs you need. For more information about services or software available from COSMIC, fill out and mail the COSMIC Request Card in this issue.

COSMIC: Computer Software and Management Information Center

Suite 112, Barrow Hall, Athens, Georgia 30602 Phone: (404) 542-3265

Electronic Components and Circuits

Hardware, Techniques, and Processes

Books and Reports

Plug-In Light Switches

A simplified wall receptacle saves hardware costs and installation time.

Marshall Space Flight Center, Alabama

In the conventional method of wiring electrical switches, outlets, and similar hardware in buildings, the switch or socket is hand wired in the following sequence: (1) The hardware screw terminals are connected to the wires, (2) the hardware is screwed to the flush-mounted wall receptacle, and (3) a faceplate is screwed over the hardware and is used to protect the assembly against dirt and moisture. Although this three-step procedure is time honored by its simplicity and dependability, the component costs and the labor required for installation make it more expensive than in past years; in addition, it is a potentially dangerous procedure for the inexperienced homeowner to follow.

A new concept in electrical hardware poses far less shock hazard to the homeowner when replacement is needed and is potentially less expensive to install professionally. A switch (or an outlet) assembly is integrally combined with the faceplate as shown in the illustration. A set of male lugs protrudes from the rear of the faceplate outlet assembly and is inserted into a wall-recessed outlet assembly which contains a matching female socket. The outlet, not having moving parts or other points of wear, is permanently wired to the remainder of the electrical system. The new parts are physically compatible with existing switch plates and socket receptacle boxes.

When the switch or outlet needs to be replaced, a pair of fasteners holding the plate to the wall receptacle surface is loosened, and the faulty part is removed. The repair sequence is fast and less expensive than any prior method. The integrated assemblies also would be cheaper to manufacture than those at present since fewer parts (and therefore fewer manufacturing steps) are required.

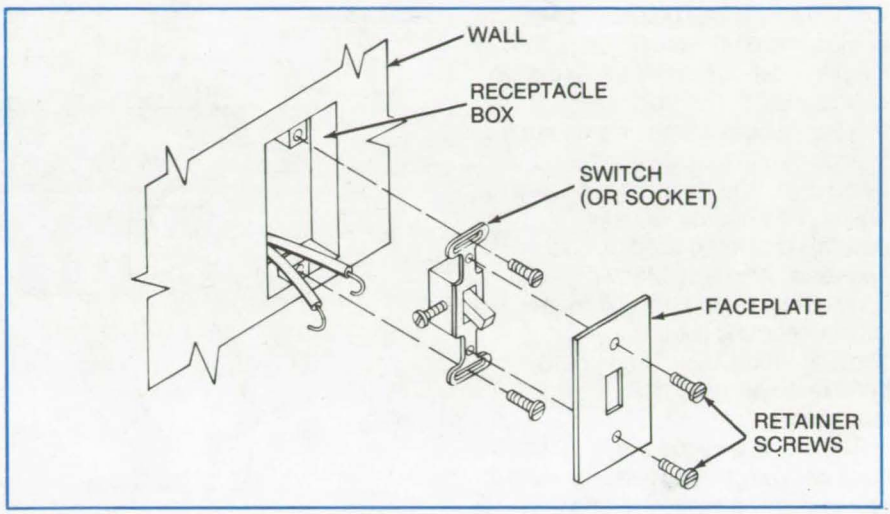

Figure 1. A **Conventional Wall Receptacle** requires several steps for initial installation. Replacement of a worn fixture also requires several steps and is hazardous for the inexperienced.

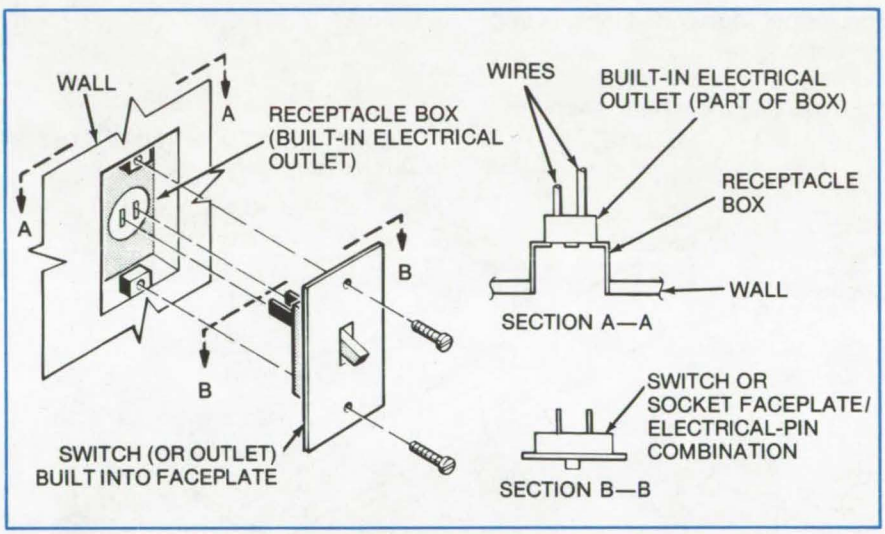

Figure 2. The **Plug-In Wall Receptacle** simplifies initial installation, and replacement of a worn fixture is considerably easier and safer than with a conventional fixture. A single switch is shown, but the method is also suitable for outlets and other fixtures.

This work was done by Eugene J. Stringer of Rockwell International Corp. for **Marshall Space Flight Center.** *For further information, Circle 1 on the TSP Request Card.*
MFS-24183

NASA

DIP Extractor Simplifies Circuit Removal

An easily constructed tool can be used to pull dual in-line packaged IC's off printed-wiring boards without damaging pins.

Lyndon B. Johnson Space Center, Houston, Texas

An integrated-circuit (IC) removal tool (Figure 1) has been made for dual in-line packages (DIP's). The simple, cost-effective tool is used to extract dual in-line packaged electronic components from circuit boards during test, prototype evaluation, and repair procedures. These components, usually consisting of integrated-circuit elements, are particularly prone to body damage, and the soft metal pins connecting the internal components to the circuit board bend or break away from the body quite easily.

The tool is designed to hold the IC body securely during removal, and it prevents pin distortion during part removal or insertion. Although the protype tool was designed to extract 14-pin IC's, a suitable tool can easily be machined to accommodate other popular package configurations and pin-out locations.

The prototype tool is machined from two aluminum bars, each 1 in. (2.5 cm) long and 0.3 in. (0.75 cm) wide. The top bar has two rectangular grooves machined into its end surfaces. These grooves hold a pair of flexible metal fingers which grip the IC along the bottom edge of the package. The fingers are held in place by machine screws. The bottom bar is longer than the top and has a pair of rectangular slits machined at either end, allowing the fingers to pass through the bar. The fingers consist of 0.03 in. (0.075 cm) beryllium copper, which is bent almost midway at an angle of 173°. A 0.07-in. (0.18-cm) flange at the bottom of the finger holds it to the integrated circuit.

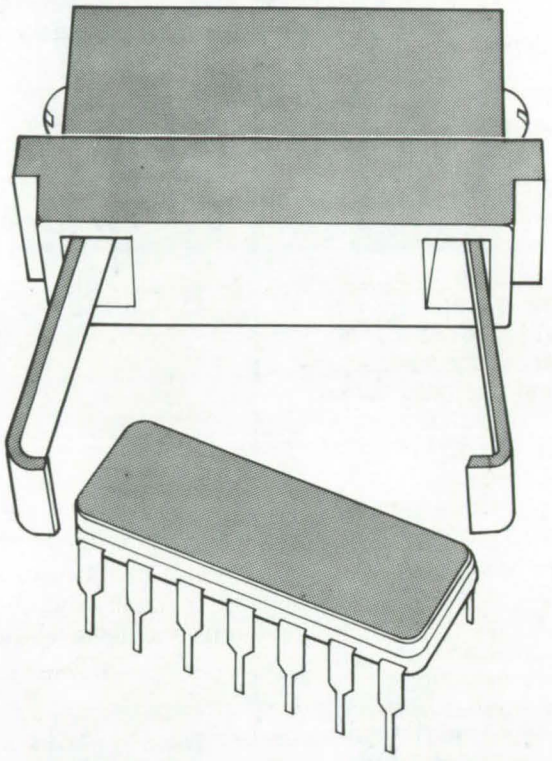

Figure 1. Pin distortion of IC package (foreground) is prevented by using DIP extractor.

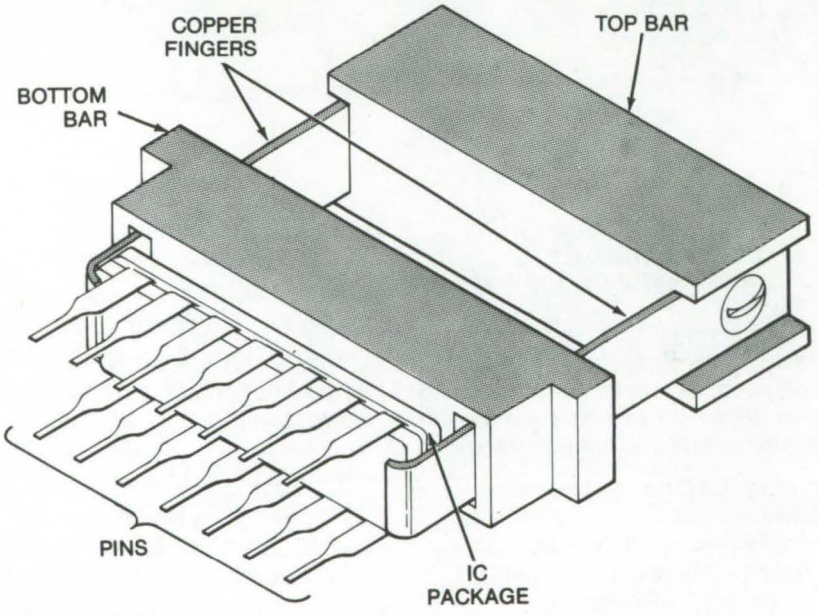

Figure 2. The shape and the exit angle of package pins are maintained by using DIP extractor.

In use, the extractor fingers are slipped over each end of the IC so that they contact the bottom edge of the package. The bottom (larger) aluminum bar is slipped downward until its bottommost edge contacts the top edge of the IC. In this position, the bar holds the fingers firmly against the IC, as seen in Figure 2, allowing it to be removed easily.

This work was done by Thomas Nies of Honeywell Inc. for **Johnson Space Center.** *For further information, including design drawings, Circle 2 on the TSP Request Card.*
MSC-12712

NASA

Superconductive Neuristor R-Junction

Formed from two superconductive neuristor lines, R-junctions propagate pulses in one direction only, with negligible attenuation.

NASA Headquarters, Washington, D.C.

Neuristors are devices that behave like nerve fibers. They have attenuationless propagation of signals. A promising feature is that these devices can be developed to simulate a nerve cell. A combination of such cells might be formed to simulate an eye or a brain and can be used in recognizing characters and other visual images.

A superconductive neuristor R-junction is formed from two neuristor lines. The lines are coupled in such a way that a pulse propagating on line 1 can induce a pulse on line 2, but a pulse on line 2 propagating in the same direction will not induce a pulse on line 1. This configuration can be constructed, using a normal metal as shown in the illustration.

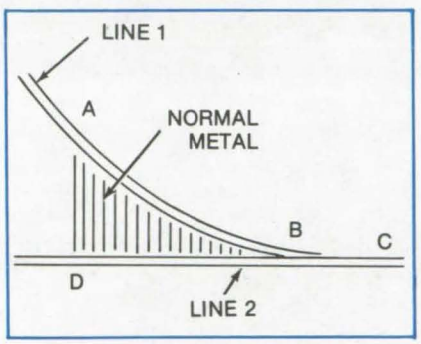

Superconductive Neuristor R-Junction incorporates a specially-configured pure metal transition region.

At points A and D the resistance of the path through the normal metal is such that lines 1 and 2 are only weakly coupled. On the other hand, the path through the normal metal at point B is short enough (or the two lines may be directly connected) so that the lines are strongly coupled. Near points A and D an active pulse on one line will only introduce a subthreshold pulse in a corresponding position on the other line. The effect of the subthreshold pulse is sufficient to introduce a refractory mode in that region of the line. Near point B the lines are so strongly coupled that an active pulse on one line in this region will always introduce an active pulse on the other line in the corresponding region.

The neuristor lines with properly-configurated normal metal patterns can be used to fabricate threshold logic devices. In this case the normal metal is used to attenuate the active pulses present on the input lines. For example, in one situation with three input lines, 1, 2, and 3, the resistivities of the normal regions may be arranged so that an active pulse on any two of the input lines is necessary to trigger a pulse on the output line. In another situation the resistivities of the normal metal regions may be arranged so that an input pulse is required on line 1 and on either line 2 or 3 to activate the output line. On the other hand, a pulse arriving simultaneously on lines 2 and 3 cannot trigger an output pulse.

The proposed methods are similar to the use of resistors to achieve threshold logic with semiconductor devices. The advantage with neuristors is that complex functions can be generated with a relatively simple setup.

This work was done by Stanley A. Reible of the Univeristy of Wisconsin for **NASA Headquarters.** *For further information, Circle 3 on the TSP Request Card.*
HQN-10871

NASA

Electrode Structure for Uniform Corona Discharge

A single corona-discharge needle is used to apply a uniform charge to a thermoplastic medium in a holograph-storage system. The needle is connected to a flat transparent electrode that is parallel to the thermoplastic.
(See page 53.)

Economical Custom LSI Arrays

Reduce custom LSI array costs using a library of standard die patterns and a computerized fabrication process.

Marshall Space Flight Center, Alabama

Custom LSI (large-scale integrated) arrays are often encountered in sophisticated electronic equipment. Until recently, high costs and long turnaround times have made these arrays impractical for low-volume applications. However, over the past 5 years computer-aided LSI array design techniques have made the custom arrays more economical. A newly-developed automatic design technique has further reduced the LSI array costs.

In the new technique standard circuit cells are used for producing the LSI arrays (see flow chart). The arrays are custom designed by using standard topological methods. After being validated each circuit cell designed is tagged with an identification or pattern number and is permanently stored in a computer memory.

Custom LSI arrays are designed by requesting the stored cells by the pattern number. The computer retrieves the requested cells from the memory. Each individual cell is represented by a collection of polygons on seven mask levels. A computer program is used to position the cells and to generate the metalization and/or tunnels to interconnect the standard cells into the required function. The program allows easy design changes and modifications of the cells. One important characteristic of this computer approach is that the program virtually guarantees successful interconnection by increasing the roadbed used for the signal interconnection.

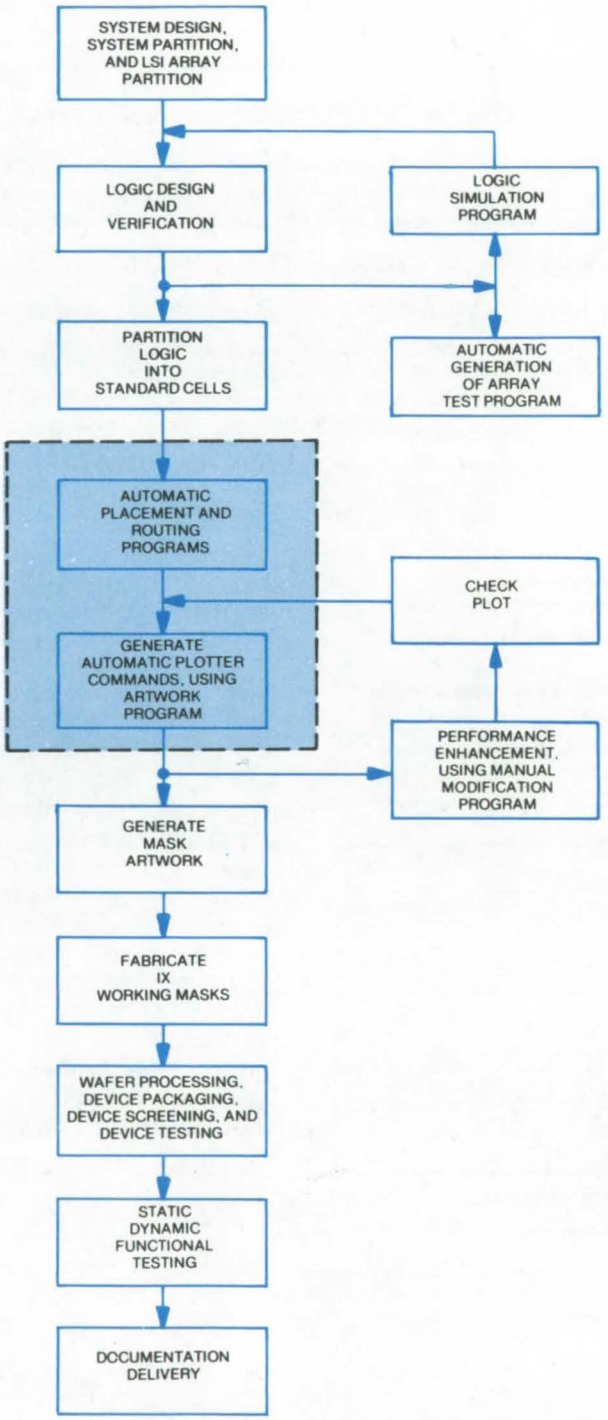

This flow chart shows the procedure for **Generating Custom LSI Arrays** using a standard cell. The cycle includes designer input, artwork generation, fabrication, testing, and packaging.

The advantages of the new technique are

- Individual cells are custom designed for high density and efficiency,
- The reliability of using tried and proved circuits,
- Computerized accuracy and reproducibility,
- Open to accommodate new cells in the same family,
- Prompt incorporation of circuit layout improvements,
- Quick turnaround time,
- The ease of corrections for changes and errors,
- Low cost,
- The utilization of semiskilled personnel,
- Circuit performance characterization, and
- Node capacity printout.

This work was done by A. Feller, A. Smith, P. Ramondetta, R. Noto, and T. Lombardi of RCA Corp. for **Marshall Space Flight Center.** *For further information, Circle 4 on the TSP Request Card.*

Inquiries concerning rights for the commercial use of this invention should be addressed to the Patent Counsel, Marshall Space Flight Center [see page 2]. Refer to MFS-23262.

NASA

Ultra-High-Vacuum Electrical Feedthrough

An electrical feedthrough utilizes the cathode dark-space region adjacent to high negative-potential surfaces.

NASA Headquarters, Washington, D.C.

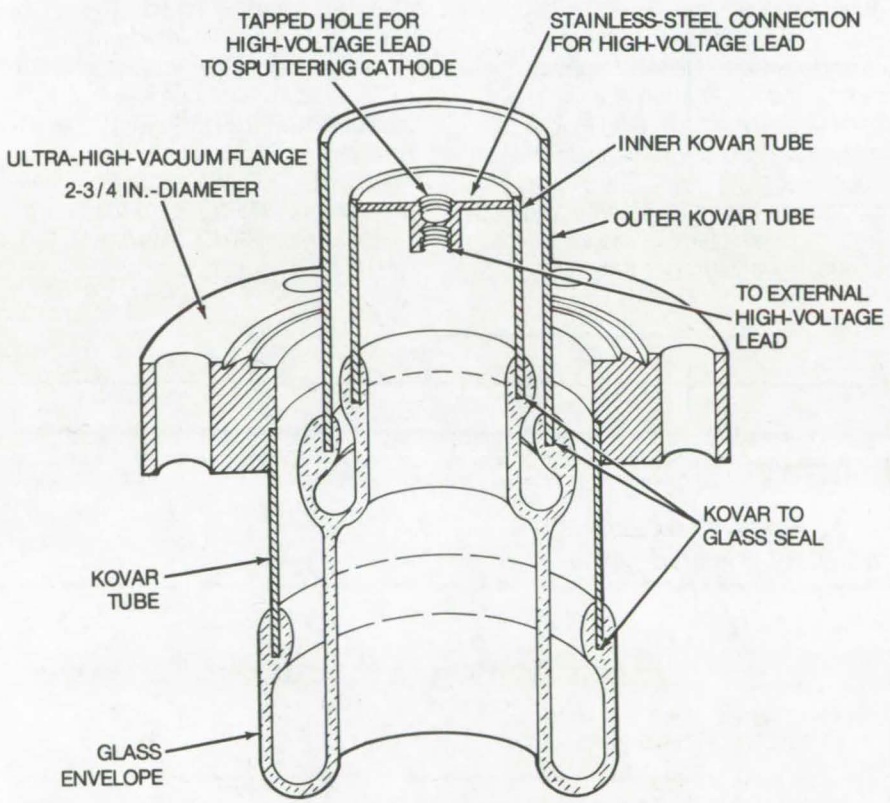

The **Vacuum Electrical Feedthrough for Cathode Sputtering** is bakeable, made of metal and glass, and is helium leaktight. It has been used in ultra-high-vacuum systems at pressures down to 2×10^{-11} torr, or less.

Techniques are known to suppress undesired cathodic sputtering, such as placing an anode within the cathode dark-space region adjacent to the high negative-potential surfaces. Although this stops the sputtering, it also stops the feedthrough. The electrical feedthrough making use of this dark-space phenomenon is the innovation described here.

The figure shows the detailed construction. The feedthrough is made exclusively of metal and glass, is helium leaktight, and is bakeable; it has been used in ultra-high-vacuum systems at pressures down to 2×10^{-11} torr, or less. This device can be incorporated easily into any vacuum apparatus, including ultra-high-vacuum systems.

This work was done by J. R. Gavaler and M. A. Janocko of Westinghouse Electric Corp. for **NASA Headquarters.** *No further documentation is available. HQN-10799*

NASA

Triple-Layer Bubble-Domain Film

Stratified bubble-domain composite improves translational velocity while providing hard-bubble suppression.

Langley Research Center, Hampton, Virginia

A triple-layer bubble-domain film is a stratified composite comprised of a layer of magnetic bubble-domain material and dual layers of magnetic material formed on either major surface of the bubble-domain layers. The dual layers have an axis of easy magnetization essentially parallel to the plane of the layers and, thus, in-plane magnetization. This stratified bubble-domain composite enhances the translational velocity and wall velocity of bubble domains while providing hard-bubble suppression and effectively eliminating coercive field inhomogeneities.

A capping layer is grown on the substrate, the bubble-domain layer is grown on this capping layer, and another capping layer is formed on the bubble-domain layer, using standard growth techniques. These techniques include liquid-phase epitaxy, chemical vapor deposition, physical vapor deposition, and, particularly in the case of amorphous materials, sputtering.

The generation of bubble domains in magnetic garnet materials requires that the bubble-domain layer must have induced magnetic anisotropy to provide a sufficient axis of easy magnetization approximately normal to the plane. Likewise, for the capping layers, an axis of easy magnetization is induced approximately parallel to the layer plane.

This composite encompasses the use of crystalline, shape, growth, and/or stress techniques to induce the required magnetic anisotropy in materials such as garnets. Assuming that the axis of easy magnetization associated with the bubble-domain layer is approximately perpendicular to those associated with the 90° capping layers, the application of a bias field generates cylindrical single-wall magnetic (bubble) domains in the bubble-domain layer. The induced anisotropy maintains the magnetization, in the plane of the capping layers, essentially parallel to the interface between the bubble-domain layer and the capping layers and essentially perpendicular to the height of the bubble domain. This perpendicular or 90° magnetization of the capping layers relative to the bubble domain forms additional domain walls at the interfaces of the capping layers with the bubble domain and provides substantially-enhanced domain wall velocities and hard-bubble suppression while precluding coercive field inhomogeneities.

This work was done by Rodney D. Henry of Rockwell International Corp. for **Langley Research Center.** *For further information, Circle 5 on the TSP Request Card.*

Title to this invention has been waived under the provisions of the National Aeronautics and Space Act [42 U.S.C. 2457(f)], to the Rockwell International Corp., 3370 Miraloma Avenue, Anaheim, California 92803. LAR-11755

NASA

Printed-Circuit Solar-Cell Array

Thinner and lighter solar-cell arrays are made with a sandwich of conductor material between two sheets of polyimide.

Marshall Space Flight Center, Alabama

A flexible solar-cell array has been made thinner and lighter than previous solar arrays. The array is placed on a substrate, which is a lamination of two sheets of plastic film with an etched electrical connector for the cells between the films. Thus, the stubstate mechanically supports the cells and interconnects them electrically.

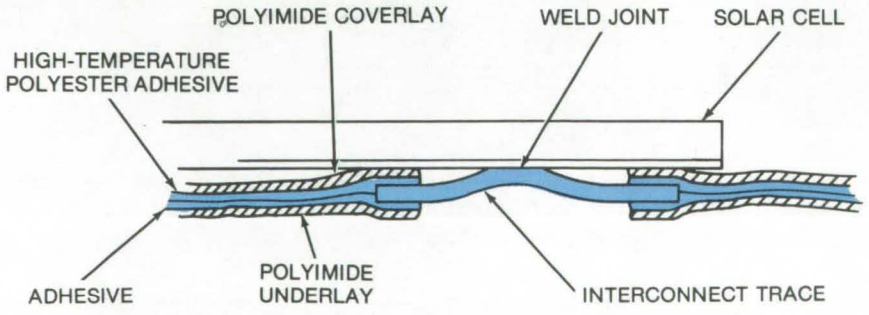

A **Typical Element** of the array is shown. The interconnect trace is part of an etched electrical solar-cell interconnect system that is held between two layers of polyimide.

The substrate configuration is shown in the illustration. The coverlay and overlay are a commercially-available polyimide film 0.5 mil (0.012 mm) thick. On one side of each layer, 0.5 mil (0.012 mm) of polyester adhesive is applied. The interconnects can be 1 mil (0.025 mm) thick copper and may constitute from 15 to 30 percent of the surface area of the substrate.

During fabrication, the polyimide sheets are prepunched so that the interconnect metal can be parallel-gap electrical-resistance welded to the solar cells. Because of the thinness of the polyimide film, its stiffness and support are reduced during fabrication, and care must be taken to control the flatness of the films and the registration of the prepunched holes in the two films.

This work was done by R. F. Currier and W. L. Palmer of Lockheed Missiles and Space Co., Inc. for **Marshall Space Flight Center.** *For further information, Circle 6 on the TSP Request Card. MFS-23138*

NASA

Improved Wet-Slug Capacitor

Tantalum capacitor leakage is reduced using all-tantalum seals and straight, ungelled, 30-percent sulphuric acid electrolyte.

Langley Research Center, Hampton, Virginia

A new capacitor design uses all-tantalum seals and straight, ungelled, 30-percent sulphuric acid electrolyte to reduce leakage from the order of milliamperes to the low-microampere region. Damage to the anode and other healable defects are also reduced.

Containment systems, such as the recently-developed Mallory TLW series, now provide a true hermetic seal with no possibility for internal electrolyte shorts. The use of ungelled electrolyte results in components which will endure two to three times more stress and with greater reliability, thus permitting applications in severe environments such as encountered in aerospace and industrial electronics. This design not only provides higher reliability due to the improved healing mode but also results in considerable weight and volume savings.

Tantalum wet-slug capacitors are used extensively in areas where, traditionally, large capacitors have been required. This is because of the large capacitance-to-volume ratio which reduces weight and volume. The electrolyte (30 percent sulphuric acid) initially had a great propensity to leak through the case seals, resulting in damage to associated components, and therefore it required a gelling agent to fix the electrolyte position.

While leakage currents of tantalum capacitors are typically below 1 μA, after stress this may rise well into the mA region and disable the circuit. This high leakage current slowly reduces back to the initial value, requiring up to 100 hours for mA-region leakers. Investigation revealed that the major cause of these long healing times was disturbance of the electrolyte in the gelled state and not the relatively minor damage inflicted on the anode surface. Prototype capacitors with a completely wet electrolyte (gelling agent eliminated) have been found to heal within minutes to μA leakage levels; even in extreme damage situations, such as a crushed anode, the maximum initial leakage is in the order of 100 μA.

Test data indicates that the elimination of the gelling agent from the electrolyte of tantalum wet-slug capacitors results in components which, even in extreme damage situations, will heal rapidly enough to permit operation of the circuit. Capacitors made under these conditions could survive 75-g rms values reliably, as compared to today's industrial standard which is a 20-g sine vibration maximum.

This work was done by Charles M. Ward of Martin Marietta Corp. for **Langley Research Center.** *Tantalum capacitors are also discussed in NASA Tech Briefs B74-10294 and B75-10274. No further documentation is available. LAR-11720*

NASA

Beam Patterns of Light-Emitting Diodes

IR-sensitive film is used to record the output beam patterns of LED's. The films are placed at varying source-to-detector distances, and the exposed beam patterns are used to determine the position of the detector surface that intercepts the maximum radiation.
(See page 49.)

Low-Cost Solar Reflectors

Foamed glass makes an inexpensive lightweight substrate for reflective elements used in solar energy converters. The glass withstands temperatures from -450° to 800° F and pressures up to 100 psi. It is shaped using an aluminum or steel master and is bonded to the reflective element with epoxy adhesive.
(See page 125.)

Uniform Solar Cells

Solar cells used in radiation sensors can be efficiently made with outputs within ±0.5 percent by individual trimming. A strip of aluminized Mylar is used to adjust the cell output to within required tolerances. This method is faster than measuring outputs of a large batch to select matched cells.
(See page 127.)

A/D Converter

Two-port dual-slope system converts both low-level (0-to-40-mV) and high-level (0-to-5-V) analog signals at 500 8-bit words/second with an accuracy of 3 percent.

Langley Research Center, Hampton, Virginia

A recently-developed analog-to-digital converter (ADC) is a two-port, dual-slope type that converts low-level analog signals (zero to 40 mV) and high-level analog signals (zero to 5 V) to 8-bit digital words. The high-level signals are referenced to a fixed single-point ground, while the low-level signals are referenced to a ground floating ±5 V with respect to the fixed ground.

The system (see Figure 1) contains a low-level amplifier, a switch buffer, an integrator, a comparator, and the necessary logic to generate the timing functions. Since the conversion technique depends on timing accuracy for overall converter accuracy, the timing functions operate at minimum-level logic to eliminate possible spurious pulse interference. All critical switches, for instance, are driven by synchronous flip-flop stages to minimize errors caused by timing.

The low-level amplifier consists of three operational amplifiers arranged to null an input common-mode voltage. They have a high common-mode range (±5 V) and high common-mode rejection. Two switches on the input of the unit (one in series with one of the operational amplifier-input terminals and the other in parallel across both of the amplifier inputs) allow the converter system to read the offset of the low-level amplifier in the presence of the common-mode voltage. This arrangement enables simultaneous nulling of amplifier-input offset voltage and recovering the low-level signal from the floating-ground source. The error contributed by the floating ground is less than ±0.01 percent.

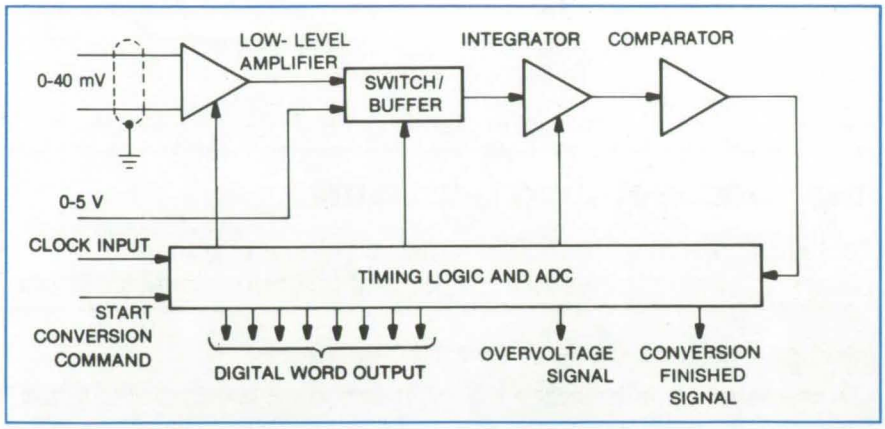

Figure 1. The A/D Converter receives 0-to-40-mV signals with respect to a single-point ground. The 0-to-5-V signals may be with respect to a floating ground within 5 V of the single-point ground.

In operation, the integrator follows the relationship

$$1/RC \int_0^T V(t)dt$$

If V(t) is a constant, the response is

$$1/RC \; V(t) \Big|_0^T = 1/RC \, VT + C$$

Time T_1 (see Figure 2) is constant and equal to 256 counts of a 288-kHz clock. During time T_1, the data voltage, V_D, is applied to the integrator. The constant of integration is equal to the comparator offsets and the time delay. At the end of T_1, the voltage on the integrator, V_i is

$$V_i = \frac{V_D T_1}{RC} + V_{CT}$$

assuming that $C = V_{CT}$.

During time T_2, which is variable, the reference voltage is applied to the integrator until the integrator output is equal to V_{CT}. The voltage change during time T_2 is $V_{Ref}T_2/RC$. At the end of T_2:

$$V_{CT} = \frac{V_D T_1}{RC} + V_{CT} + \frac{V_{Ref} T_2}{RC}$$

Solving for T_2

$$T_2 = V_D(T_1/-V_{Ref})$$

The converter has another integration period for low-level signal conditioning during which time it subtracts the static errors produced while conditioning the signal. The actual voltage, V_D, together with the low-level offset voltages, is now:

$$V_D = V_{D\,Actual} + V_z$$

and

$$T_{Ref} = -V_{D\,Actual}\,(T_D/V_{Ref})$$

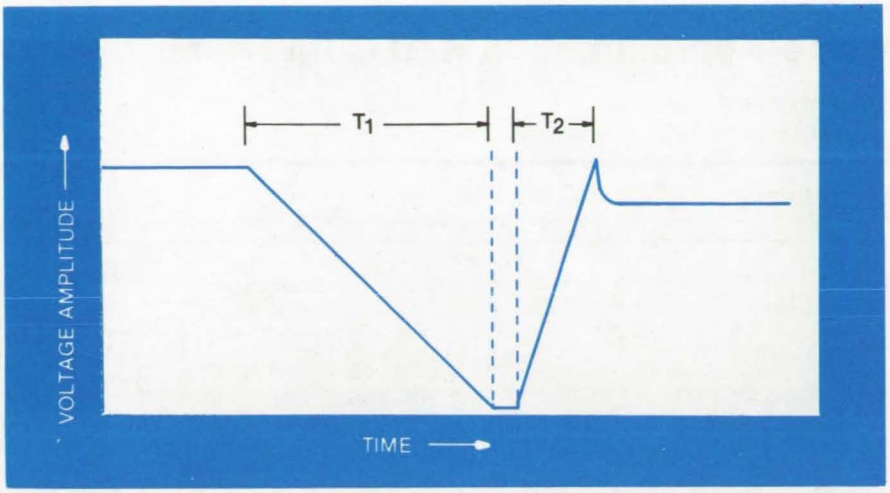

Figure 2. The **Waveform for High-Level Conversion** is shown above. Time T_1 is constant, and T_2 is variable.

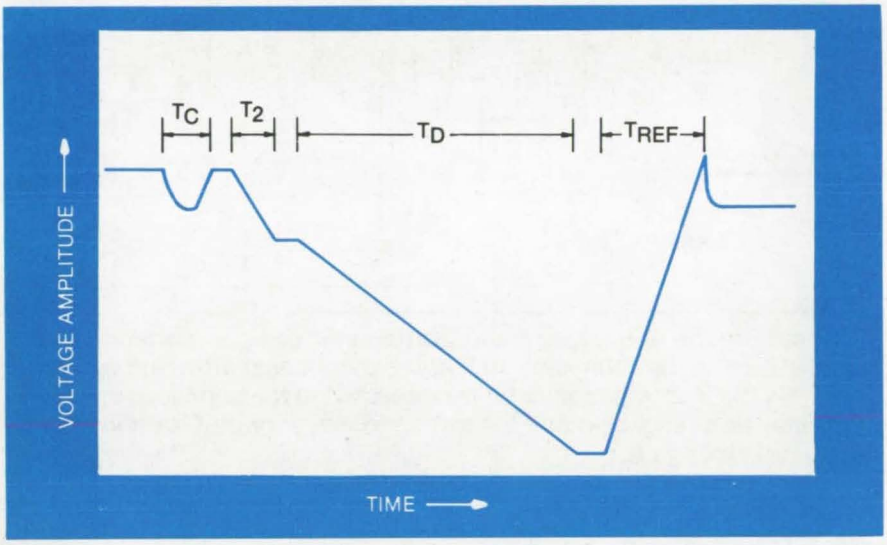

Figure 3. The **Waveform for Low-Level Conversion** includes a time T_C during which comparator errors are eliminated.

Time T_C (see Figure 3) represents the period during which the comparator errors are eliminated. This is performed by slewing the integrator to about -57 mV and then applying the reference voltage. This method initialized the converter so that overvoltage or undervoltage from the previous conversion cycle will not be passed to the next conversion. It also resets the converter when power is first applied.

This work was done by Mike D. Mason of Martin Marietta Corp. for **Langley Research Center.** *For further information, Circle 7 on the TSP Request Card.*
LAR-11319

NASA

Permanent Holographic Storage Medium

An optical information storage system with a storage unit consists of materials with specific electrical, optical, and chemical characteristics. The storage unit is an electrostatically-charged multilayered laminate. The ability of the system to store information in holographic forms is due to its material characteristics. The system is useful as a memory unit.
(See page 52.)

Battery-Cell Thermal Test Facility

A test cell is placed in a thermal vacuum chamber where heat-flow sensors monitor heat flow between the cell and a cold sink. Radiation shielding and the vacuum environment minimize radiation losses. The set-up is calibrated with a heater, and temperature is kept constant with a temperature controller. Electrical performance characteristics and sensor output are recorded.
(See page 126.)

Light Pipes for LED Measurements

A high quality light pipe couples an LED optical output to a single detector. The light pipe has a cross section area greater than the area of the light-emitting surface, and both surfaces are in contact. Physical separation is maintained between LED and detector. Capability is provided to channel the optical output of an LED from within an assembled system to a remote detector.
(See page 43.)

Control Logic for Successive-Approximation A/D Converters

A modular design which minimizes component count has the same logic structure for all bits.

NASA Pasadena Office, Pasadena, California

The design of the successive-approximation analog-to-digital converter (ADC) is sufficiently standardized so that efforts to optimize it now are based on minimizing component count. In two such updated ADC's, an iterative building-block approach is used; depending on converter resolution desired, logic architecture is expanded or diminished by simply plugging in more or fewer identical active logic stages. In one iterative design, a sequencer and a code register are used; in the other, only a single set of flip-flop (F/F) stages is connected to function both as a sequencer and a code register.

The sequencer, which can be a ring counter, shift-code counter with a simple decoder, or a binary counter with a binary-to-decimal decoder, may be implemented using available stock parts. The register requires inputs from the sequencer to set an F/F, from the control bus for reset, and one output.

In the sequencer-and-register design shown in Figure 1, each F/F in the code register is set and conditionally reset once per conversion cycle. The two-pulse outputs from the sequencer are connected to the clock terminal of the register F/F's. One of the pulses sets the register, while the other resets, as commonly controlled by the control bus. For maximum speed, the two pulses may overlap. Connecting the shift register steering gate to all but the first F/F will produce the overlapping pulse. For a nonoverlap design, the only connection necessary is to enter 2 CL as a strobe signal to the decoder.

The sequencer/register design implies that a single set of F/F's is connected to function simultaneously both as a sequencer and a code register. Fundamentally

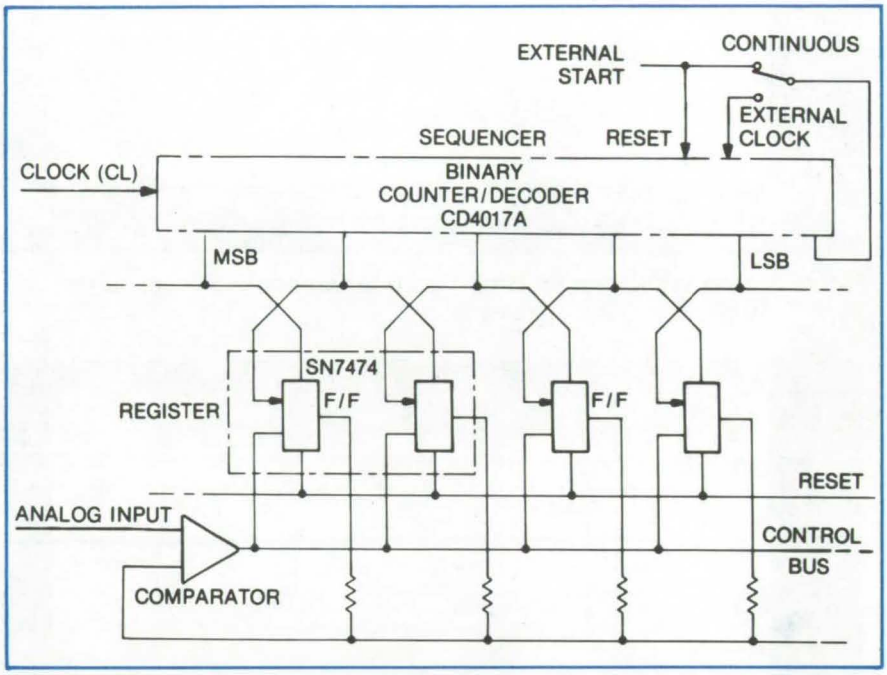

Figure 1. In the **Sequencer and Code Register** design diagramed, the sequencer may be connected so that the output next after that which controls the least significant bit is connected to the common reset line, or it may be arranged so that the same sequencer output is connected to the input clock gate.

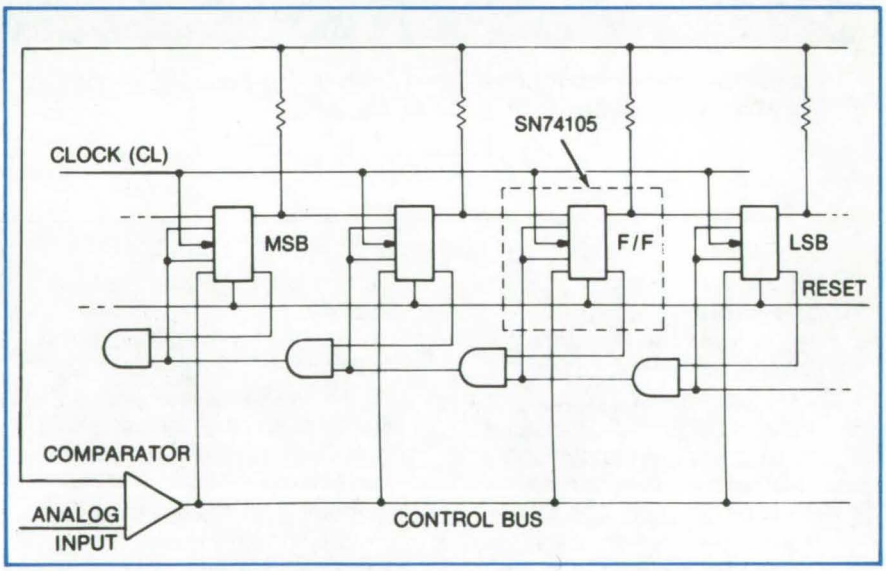

Figure 2. In the **Sequencer Register** design a single set of flip-flops functions simultaneously as both a sequencer and a code register.

higher speed of the logic is then possible; there are only minor variations. With all F/F's reset, the "0" condition of the sequencer/register is serially AND-ed via a series of AND gates from the least significant bit (LSB) to the most significant bit (MSB). A shift "1" connection from the MSB is easily identifiable. The clock is common to all F/F's. The turnoff command line is also common as is the control bus. Both turn-on and turnoff for each F/F are controlled by the AND-ed "0" condition for all bits of lesser significance.

The J/K F/F's used have two-input AND functions for both the J and K inputs. Because of pin limitations, a 16-pin package can accommodate only a single J/K F/F. Chip count for this design is high, but a slight design modification can lower it if two simple F/F's are contained per package. Two such F/F's are available in one 16-pin package.

The redesigned sequencer/register, seen in Figure 2, propagates the all-"0" condition. Only the enable terms operate on a single gate for each F/F, which then must be the clock gate. In the previous instance, J/K inputs are enabled for two clock pulses. In this case, the inputs are never disconnected; only the clock gates are automatically enabled for two clock pulses. Either sequencer/register offers higher speed architecture because transfer delay between the sequence is eliminated. Maximum control logic speed is achieved if a square-wave clock is steered to the input terminals to one-half of the F/F's used. The other F/F's are clocked from an inverted clock signal.

This work was done by Tage O. Anderson of Caltech/JPL for **NASA Pasadena Office.** *For further information, including truth tables and alternate designs, Circle 8 on the TSP Request Card.*
NPO-11937

NASA

M-ary Shift Register

Binary devices are used to construct an m-ary linear feedback shift register.

NASA Pasadena Office, Pasadena, California

A new combination of elements and mode of operation of a feedback shift register (FSR) enables an m-ary shift register with modulo m feedback to be realized with binary devices. An m-ary feedback shift register is comprised of m-state storage devices and a modulo m summing network. These shift registers can be used for scaling, counting, prescribed-sequence generation, ranging, and encoding and decoding error-correcting code. Each of the m states (i.e., 0, 1, 2, . . ., m-1) and the m-ary digit being fed back, are given binary representations, allowing the m-ary FSR to be produced using binary logic elements. Heretofore, only binary FSR's have been used, because reliable high-speed m-ary devices have not been generally available for m not equal to 2.

When m is equal to p, a prime integer, a maximal-length sequence p^r-1 (where r is the number of stages in the register) can be realized for any p. When m is not a prime, cycles of less than maximal length are realizable. The implementation involves decomposing the m-ary FSR into parallel p-ary FSR's, one for each prime factor. Each state of the p-ary register and the p-ary digit being fed back is then coded in binary. This provides a state table for designing the parallel binary shift registers that simulate the behavior of a p-ary FSR. The first register stores the most significant bit of the binary representation of each p-ary digit, the second register stores the second most significant digit, etc.

This work was done by Marvin Perlman of Caltech/JPL for **NASA Pasadena Office.** *For further information, including details of the shift register logic, Circle 9 on the TSP Request Card.*

This invention has been patented by NASA [U.S. Patent No. 3,718,863]. Inquiries concerning nonexclusive or exclusive license for its commercial development should be addressed to the Patent Counsel, NASA Pasadena Office *[see page 2]**. Refer to NPO-11868.*

NASA

Reliability of Hybrid Microcircuit Bonding

The effects of differential thermal expansion on ceramic chip capacitors are investigated for various bonding techniques. Stresses are lower in compliant bonding systems, but hard solders are less affected by thermal cycling. A strain-gage technique for measuring thermal expansion is discussed.
(See page 130.)

Transparent and Flame-Retardant Potting Compounds

A study of fire-retardant polymers has led to the development of several new potting compounds. These include a series of modified silicone RTV polymers and a series of coreacted epoxy-urethanes. Special properties can be obtained by including Br, P, and N in the polymeric structure.
(See page 76.)

Microchannel Detector Array for X-Rays and UV

One-dimensional microchannel detector array employs sensitive photoelectric electrodes and solid-state memory. It can be used at visible, UV, soft X-ray, and X-ray wavelengths. It includes nonmagnetic proximity focusing and is immune to high-energy charged-particle background.
(See page 61.)

Improved Microbridge Josephson Devices

Germanium overcoating of superconducting microbridges protects against electrical noise but does not limit sensitivity.

Marshall Space Flight Center, Alabama

Microbridge (weak-link) Josephson elements are of interest for use in superconducting quantum interference devices (SQUID's) because they can be constructed by using the techniques of integrated-circuit fabrication. However, these elements do not perform as well as expected. Microbridges are destroyed by minute noise-induced currents at room temperature. To insure survival against electrical noise these bridges are generally protected with shunts and/or current-limiting series resistors, thus limiting sensitivity.

These problems may be overcome by protecting the microbridges with a coating of a dense semiconductor material such as germanium. The semiconducting germanium will shunt the bridge electrically at room temperature, but it will behave as a dielectric at liquid helium temperatures and not affect bridge characteristics. The germanium also provides additional thermal conductivity and thermal mass at liquid helium temperatures for microbridges fabricated from niobium.

The initial niobium film is deposited via RF sputtering. To prevent the germanium from diffusing into the niobium, the substrate is allowed to cool for an hour before the germanium is deposited. To prevent the diffusion from overheating, the deposition procedure consists of alternating 2 minutes of sputtering with 3 minutes of cooling until the desired thickness is reached.

After the second germanium deposition, the microbridge is checked for continuity by using a go/no-go scheme that is particularly strenuous on the microbridge. Two multimeters set on the R×10,000-ohm resistance range are used to energize the bridge. One multimeter places 40 microamperes through the bridge; the other multimeter, 62 microamperes. The microbridge is then cooled to liquid helium temperatures, and its current and voltage (I/V) characteristics are observed.

This work was done by Palmer N. Peters of **Marshall Space Flight Center** *and Louis B. Holdeman of the National Academy of Science. For further information, Circle 10 on the TSP Request Card.*

Inquiries concerning rights for the commercial use of this invention should be addressed to the Patent Counsel, Marshall Space Flight Center [see page 2]. Refer to MFS-23274.

NASA

Increased Safety in Mercury-Containing Devices

Lamps and other mercury-containing devices are made safer by incorporating an amalgamating metal within the device.

Marshall Space Flight Center, Alabama

An amalgamating metal included inside mercury lamps reduces the amount of escaping mercury vapor when the lamps are fractured and mercury vapor escapes. The vapor is poisonous and can also contaminate equipment. A thin sheet of amalgamating metal, such as gold, tin, lead, cadmium, or indium, is placed inside the mercury lamp. Experiments have shown that amalgamating metals reduce the mercury vapor pressure to approximately 6 percent of the normal value. Should the lamp break, much of the escaping mercury will be captured by the metal sheet. This significantly reduces the possibility of mercury poisoning and contamination. A similar procedure can be used with mercury relays and mercury rectifiers.

An alternate approach can be used on some mercury fluorescent lamps that are made from strong polycarbonate tubes. For extra safety the tubes are enclosed by a shrunk-on Teflon, or equivalent, sleeve to contain glass particles, phosphor dust, and mercury vapor should the lamp break. An amalgamating metal sheet can be placed between the sleeve and the tube. Although the sleeve provides sufficient protection against the mercury vapors, still some of the vapors can diffuse through its micropores. The amalgamating metal reduces that possibility.

This work was done by George S. Evans of Westinghouse Electric Corp. for **Marshall Space Flight Center.** *For further information, Circle 11 on the TSP Request Card. MFS-23308*

NASA

Books and Reports

These reports, studies, and handbooks are available from NASA as Technical Support Packages (TSP's) when a Request Card number is cited; otherwise they are available from one of NASA's Industrial Application Centers or the National Technical Information Service.

Organic Adhesives for Hybrid Microcircuits

Extensive design guidelines for engineers

The properties of organic adhesives for use with high-reliability hybrid microcircuits are described in a report. The use of adhesives in hybrid applications is increasing because they simplify the processing procedures and eliminate the necessity for employing high temperatures during assembly and packaging. The study consists of a preliminary investigation of selected electrically insulative adhesives. The following eight criteria of adhesive selection are documented:

1. Alternate methods for determining the outgassing of cured adhesives,
2. The effects of long-term aging at 150° C on the electrical properties of conductive adhesives,
3. The effects of shelf-life age on adhesive characteristics,
4. Bond strengths of adhesives on thick-film gold metalization,
5. A copper-filled adhesive,
6. The effects of products outgassed from cured adhesives on device electrical parameters,
7. Metal migration from electrically conductive adhesives, and
8. Ionic content of electrically insulative adhesives.

The objectives of the study are to identify and investigate those adhesive properties which could cause problems and to develop an evaluation test procedure to determine the effects on the electronic die. Adhesive properties considered to be important are enumerated and briefly described, a general review of polymeric types of adhesives is given, and the major types of commercially available adhesives specifically designed for microelectronic use are identified.

The report concludes with a study of three properties of the adhesives as related to the selection process: (1) bond strength, (2) outgassing after cure, and (3) corrosivity to typical metalization systems. Specific test procedures developed to evaluate these properties are described, as are comparative results obtained for selected adhesives.

This work was done by K. L. Perkins and J. J. Licari of Rockwell International Corp. for **Marshall Space Flight Center.** *To obtain a copy of the guidelines, Circle 57 on the TSP Request Card.*
MFS-23370

NASA

Polymer Adhesives for Hybrid Circuits

Polymers found to be more durable than metal bonding

A new report compares polymer adhesives with metal bonding processes used in mounting components on hybrid-microcircuit substrates. The components are currently mounted to the substrates (e.g., ceramic) by means of soldering, eutectic bonding, and reflow brazing. These methods can cause circuit failures from component damage due to bonding heat. Also, because of the different coefficients of thermal expansion between the metals and ceramic substrates, temperature cycling may cause solder cracks which result in microcircuit failures.

Polymer adhesives are found to be more durable. Two broad categories of adhesives are used in hybrid-microcircuit fabrication: the electrically insulative and the electrically conductive. The electrically insulative adhesives are used for: (a) bonding substrates to packages, (b) lidding, (c) reinforcing edge connectors, (d) protecting fine-wire leads, (e) molding or sealing the packages, and (f) bonding the chip components (e.g., capacitors, resistors, or semiconductors) to the substrates. The electrically conductive adhesives, on the other hand, are applied in: (a) bonding the semiconductor die to substrates, (b) repairing the conductor lines, (c) attaching the capacitors to bond pads, and (d) providing the ohmic contact for connectors or lead frames.

Of these, the most important and common use for insulative adhesives is bonding of the base of metal or ceramic packages to the substrates (usually an alumina ceramic). The electrically conductive adhesives are principally used in attaching the semiconductor die and chip capacitors to the conductor pads on the substrates.

A number of tests, such as high-temperature storage, thermal shock, thermal cycling, mechanical shock, constant acceleration, and vibration, show that the polymer adhesives are more durable than the metal bonds. Results show that commercially-available nonconductive epoxies are superior in strength to the conductive epoxies and solders. These epoxies have been used to mount active and passive components to thick-film and thin-film metalized substrates. In addition, two gold-filled conductive epoxies were also tested and found to be superior to the solders.

The report discusses a number of these tests that have been used in comparing the polymer adhesives with the metal bonding processes. It includes a number of charts and photographs to illustrate the test results. The findings suggest reduced quality control costs when epoxies are used in the fabrication of the microcircuits.

This work was done by Salvadore V. Caruso and J. O. Honeycutt of **Marshall Space Flight Center.** *To obtain a copy of the report, Circle 58 on the TSP Request Card.*
MFS-23287

NASA

Electronic Systems

Hardware, Techniques, and Processes

Ultraviolet Fire Detector

A fire detector system is highly sensitive to ultraviolet radiation from a fire, but is not sensitive to background nuclear radiation.

Marshall Space Flight Center, Alabama

An ultraviolet (UV) fire-detection system is capable of detecting the ultraviolet light emitted by a small (match size) flame at a distance of 3 m (10 ft). An important advantage of this system is its ability to detect fires where there is a background of nuclear radiation. This is accomplished without reducing the sensitivity to fire when no nuclear radiation background exists.

The design (see figure) utilizes enough shielding to reduce the particulate radiation (electrons and protons) that will pass through the sensor tube to acceptable levels without restrictive weight increases. Two sensor tubes are contained within the shield, which is symmetrical to ensure that both tubes are penetrated by approximately the same amount of radiation. In addition one tube has a thick, UV grade, quartz lens. UV radiation (photons) emitted by a flame will be detected by this tube.

Each sensor tube drives a one-shot multivibrator which has an output pulse with a calibrated height and width. The pulse rate of the multivibrator driven by the fire-monitor sensor tube is equal to the number of firings caused by the radiation background plus the number caused by the ultraviolet radiation. Since the second tube cannot see the incoming UV photons, its multivibrator output pulse rate will be equal to the firings caused by the radiation background only. Each identical channel is filtered and amplified, and the resulting dc voltages are summed to eliminate the effects of the background radiation. The dc voltage output of the summer is then proportional to the ultraviolet radiation seen by the fire-monitor tube. This output is then summed with an adjustable bias level so that the intensity of the signal produced by the fire-monitor tube must overcome this threshold before a fire-warning output signal is produced. The fixed delay shown between the second summer output and the fire detector output reduces the probability of false alarms caused by statistical variations in the background radiation rates. This results in no significant reduction in sensitivity or detection time.

The design combines maximum sensitivity to ultraviolet radiation emitted by a fire with minimum probability of false alarms due to short-term variations in the nuclear radiation background environment.

This work was done by John E. Turnage, Rodney M. F. Linford, and Steve D. Cornish of McDonnell Douglas Corp. for **Marshall Space Flight Center.** *For further information, Circle 12 on the TSP Request Card.*

This invention has been patented by NASA [U.S. Patent No. 3,825,760]. Inquiries concerning nonexclusive or exclusive license for its commercial development should be addressed to the Patent Counsel, Marshall Space Flight Center [see page 2]. Refer to MFS-21577.

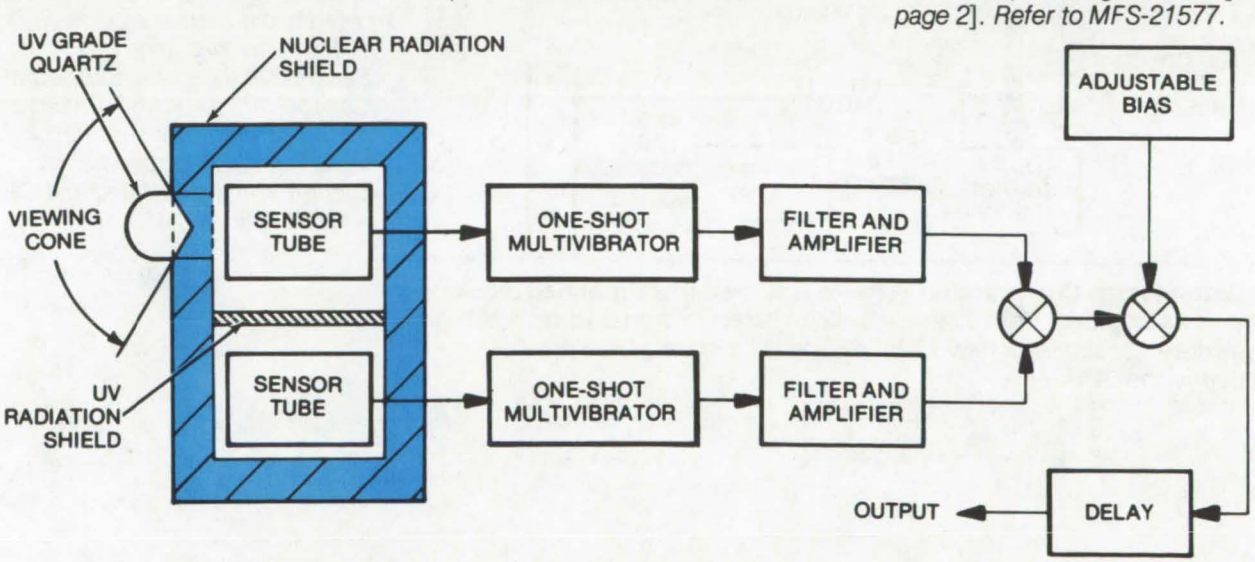

The **Ultraviolet Fire Detector** system has two sensors, one exposed to UV and the other not. Differential summing eliminates the effects of background radiation. An adjustable bias must be overcome before an alarm signal is generated, and a delay reduces the effects of statistical variations.

NASA

Data-Storage Compression Scheme

Complete binary words are transferred as data only when any bit of a previously stored word changes.

NASA Pasadena Office, Pasadena, California

One of the problems encountered in digital data measurement systems relates to the storage of redundant data samples. Conventional treatments impose requirements for large memory-storage and channel capacities.

In a new data-acquisition system (DAS), an efficient scheme of data compression is utilized which does not respond to redundant data samples. Encoded sensor output signals are transferred to the central processing unit (CPU) only when a change occurs in the encoded 12-bit word. This form of digital processing resembles delta modulation, or differential pulse-code modulation, except that the entire 12-bit word is transferred each time a change takes place. The technique is quite effective in removing redundancies and thereby provides a more efficient utilization of the CPU memory. A simplified block diagram of the DAS is shown in the figure.

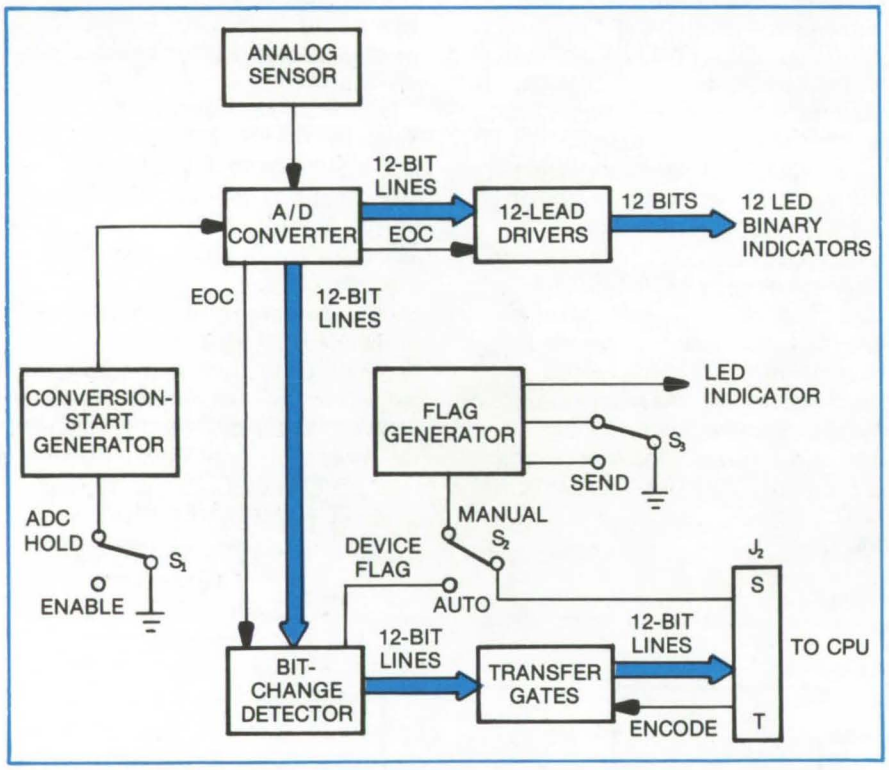

The **Data-Storage Compression Scheme** is shown in a simplified block diagram. Analog data from a sensor are converted to digital form. A bit-change detector senses a new 12-bit data word and only then provides a data flag to the CPU.

After conversion of analog sensor data to digital form, changes in the encoded 12-bit word are sensed by a group of circuits in the bit-change detector. There the current encoder word is compared with the previously stored word. A change in any bit automatically provides a data flag to the CPU, indicating that new data are ready for transfer. The new encoder word is stored for next-cycle comparison.

The bit-change detector consists of a 12-bit latch which is initially used to store the analog-to-digital converter (ADC) word. On the next conversion cycle, the ADC output is presented to a 12-bit EXCLUSIVE OR network. This network also receives inputs from the 12-bit latch which contains the previous ADC word. A difference in any of the bit values is sensed by NAND and NOR gates. A CPU flag is then generated at which time the 12-bit latch is updated to the current ADC word.

This work was done by Phil M. Salomon and Louis F. Schmidt of Caltech/JPL for **NASA Pasadena Office.** *For further information, including detailed schematics, Circle 13 on the TSP Request Card.*
NPO-13488

NASA

All-Weather Ice Information System

A system to provide near-real time information about ice location, type and thickness

Lewis Research Center, Cleveland, Ohio

A system for monitoring ice conditions on the Great Lakes and providing near-real time information about ice location, type and thickness directly to the ship's bridges for winter navigation has been developed at the NASA Lewis Research Center. At the heart of the system are two major aircraft-mounted components: a side-looking airborne radar (SLAR) system, for detecting ice cover and type, and a modified short-pulse S-band radar system for simultaneously determining ice thickness, regardless of cloud cover.

As the aircraft flies over the approximate centerline of the body of water, the ice data are taken as continuing (analog) data. The data are digitized and sent by radio transmission either directly or via a NOAA satellite to a ground receiving station. From the receiving station, the data are sent via landlines (telephone) to the U.S. Coast Guard Ice Navigation Center at Cleveland, Ohio. The data on ice cover, type, and thickness are used to produce an annotated map. The map together with the SLAR image are sent via landlines to the Marine Radio Telephone Transmitter at Lorain, Ohio. They are then transmitted via a VHF-FM radio link to facsimile recorders on board the ships and in shipping company offices (see figure). This process allows the ships and shipping companies to obtain a map of the thickness, type, location and extent of ice in the entire lake within one hour after the aircraft over-flight.

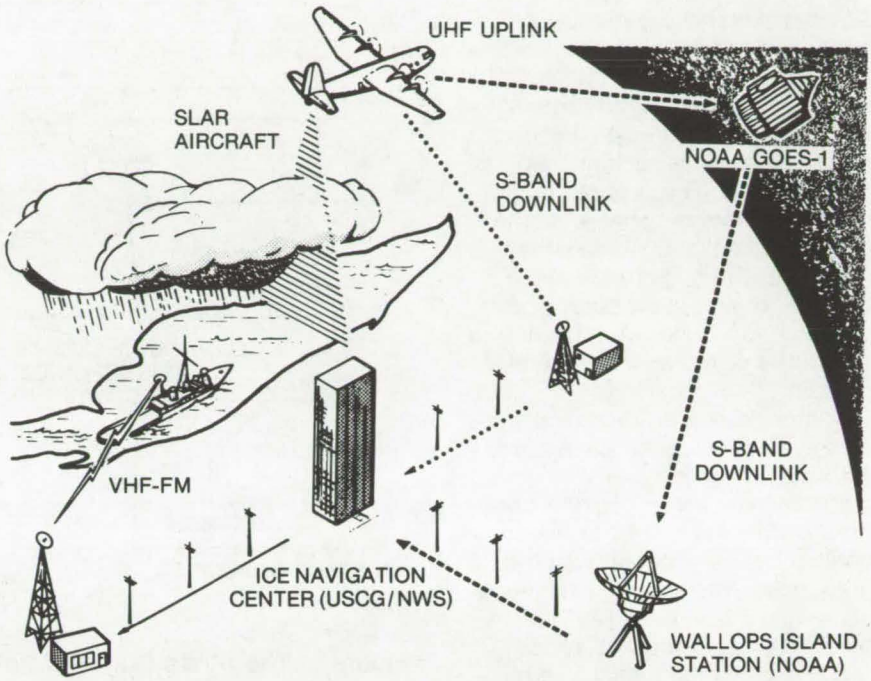

In the Great Lakes Ice Information Program, ice data are sent directly or via satellite to a ground station. The Coast Guard Center at Cleveland receives the data via telephone and then produces an annotated map. The map and radar image information are telephoned to the Marine Transmitter at Lorain, Ohio, where they are radioed to recorders on board ships and in shipping company offices.

With this map, shipping companies can dispatch ships with safe assurance and ship captains can plot safe and efficient courses.

Traditionally, the Great Lakes were closed to navigation during the winter season because of ice and particularly because of the rapidly fluctuating ice conditions often encountered. This system was made operational during the 1974-75 winter season, and enabled ships to navigate the Great Lakes without interruption through the entire winter season.

This work was done by Ronald J. Schertler, Robert A. Mueller, Russell J. Jirberg, Dale W. Cooper, John E. Heighway, A. David Holmes, Richard T. Gedney, and Herman Mark of **Lewis Research Center.** *Further information may be found in NASA TM-X-71815 [N75-33481], "Great Lakes All-Weather Ice Information System", a copy of which may be obtained at cost from the Aerospace Research Applications Center, Indiana University [see inside back cover].*
LEW-12638

NASA

Graphic-to-Digital Conversion System

A computer-controlled system to convert graphics to digital data allows the operator to record only selected data points, as well as continuous lines.

Marshall Space Flight Center, Alabama

Some graphic-to-digital conversion systems have a manually-controlled positional element which is sensed by electromechanical means. The operator positions the element and actuates a switch to record or enter its coordinates into the computer. The process is repeated, point by point, until the graphic-to-digital conversion is complete. Often, plotters have a digitizer, or an optical feedback element, which allows a drawing to be altered or redrawn by operator request.

A new graphic-to-digital conversion system has been developed with a strain gage controller. This man/machine link allows the operator to view the results of the conversion before accepting each data entry point. The system includes a converted 30-in. by 30-in. (76-cm by 76-cm) table-top X-Y plotter, and it has high accuracy and resolution over the total surface.

In this system, only the X and Y coordinate movement of the plotter is controlled by a computer, under the direction of the operator. Pushing on the strain-gage controller (SGC), seen in Figure 1, will not change the plotter position if the computer is deactivated.

The operator uses the luminous sight (position indicator) to follow a particular graphic feature. Application of a light pressure in the selected direction will bend the spring arms, changing the resistance of the 120-ohm strain gages. This causes the bridges to become unbalanced, producing small differential voltages which are amplified by the strain-gage amplifier (SGA).

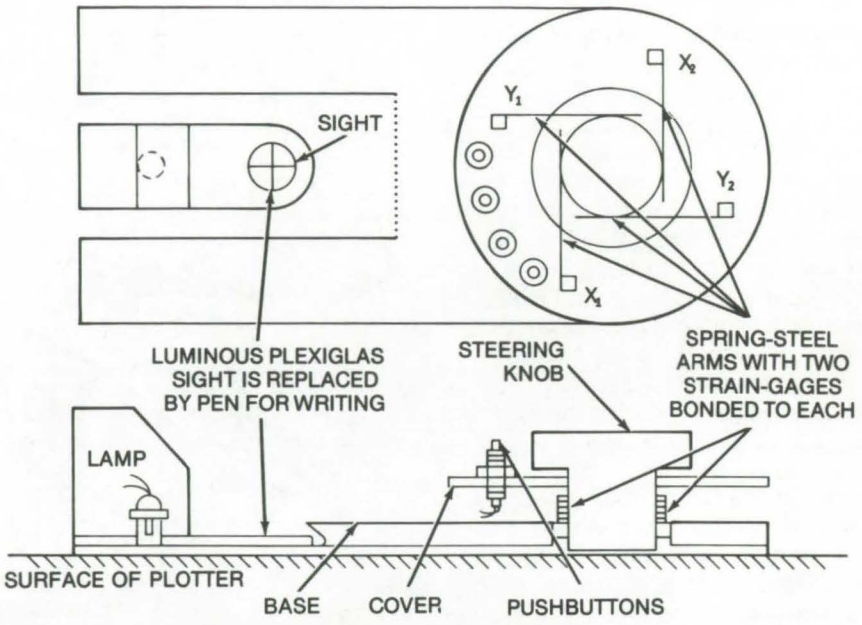

Figure 1. The Strain-Gage Controller is used by the operator to follow a graphic feature. Signals from the controller go to the computer which directs the X-Y plotter.

The two SGA analog-output steering signals are converted by an analog-to-digital converter and routed to the computer. The steering analysis routine in the computer compares the X and Y steering numbers received to the X and Y steering reference numbers. The comparison produces positive or negative difference (delta) numbers that are proportional to the direction and amount of pressure applied. These deltas are added to the X and Y coordinates in memory. The resultant coordinates are transferred to a digital-to-analog converter which produces analog coordinate voltages for the plotter. The plotter then moves in the direction of the applied pressure. The computer receives steering information and transmits updated coordinates at a rate of about 100 times per second.

Command switches are mounted on the SGC (see Figure 2). Thus, no data are recorded as the plotter X-Y position indicator is moved, unless requested by the operator. When the operator has a desired feature (data point) in his sight, he depresses a switch, and the computer picks up the current coordinate values and places them in a table. When the table is full, the computer writes a copy of it on tape and starts a new table. The

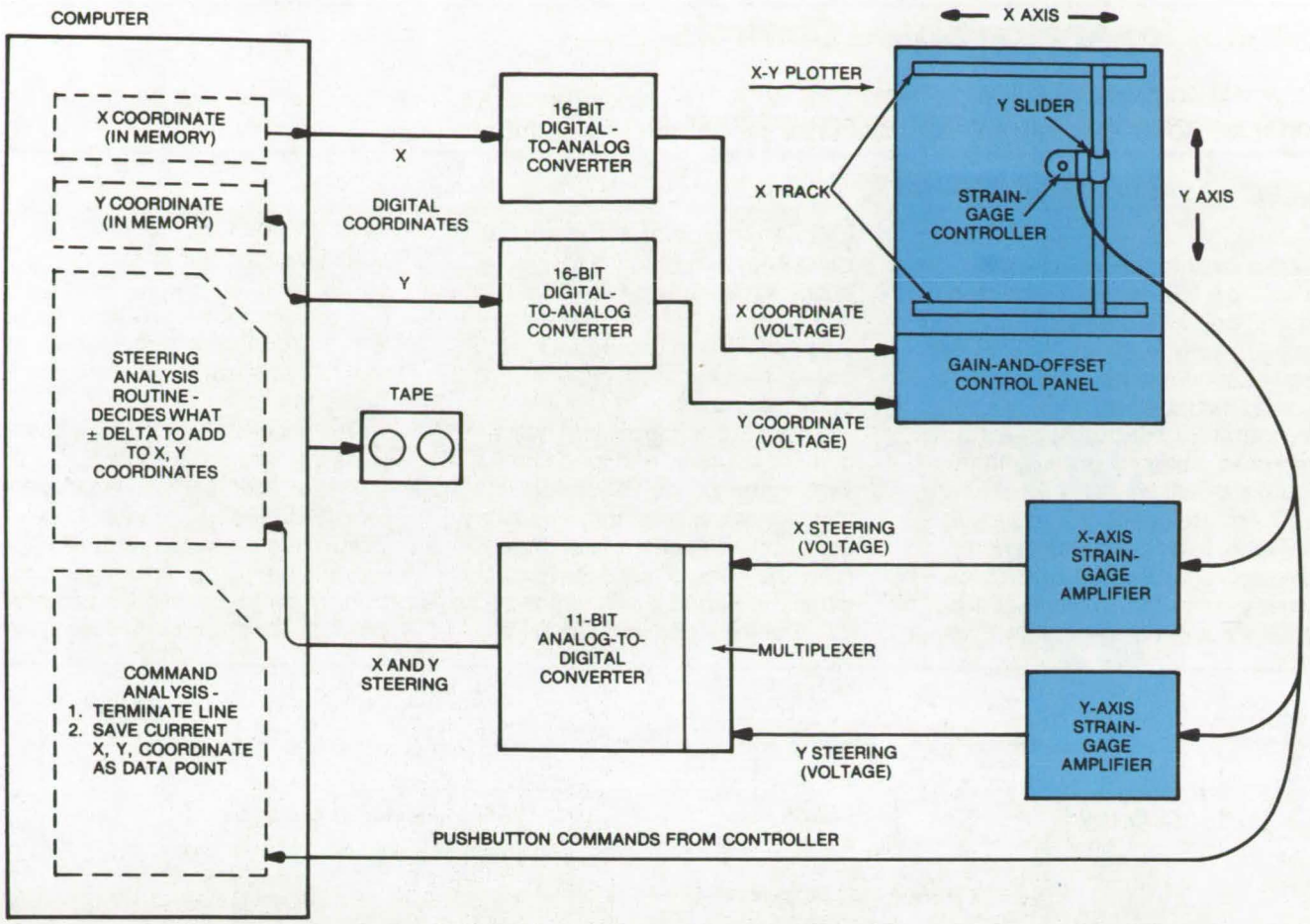

Figure 2. The **Graphic-to-Digital Conversion System** includes a specially-designed strain gage controller and amplifier and commercially available equipment, including A/D and D/A converters, a digital tape recorder, and a general-purpose digital computer.

program accepts one data point each time the (X, Y) coordinate switch is pressed.

A reset switch terminates the line by recording a raise-pen command, and also resets the steering reference. Continuous data can be recorded; however, it is more accurate to take controlled points. Data points recorded on tape are usually connected by straight lines when making any drawing.

This work was done by Frank L. Rosenthal of Rockwell International Corp. for **Marshall Space Flight Center.** *For further information, including the strain-gage circuitry, Circle 14 on the TSP Request Card.*
MFS-24410

NASA

Peak-Acceleration Limiter

A peak-acceleration statistical limiter protects test articles from damage during random vibration testing. It differentiates between normal peak-acceleration levels and damaging ones. The Gaussian distribution of peak levels is the basis of the electronic analysis of the system accelerometer outputs. The limiter aborts the test only when significant signal changes or catastrophic transients occur.
(See page 91.)

Fast Pressure-Sensor System

Miniature silicon-diaphragm pressure sensors and a signal multiplexer are mounted to ganged zero-operate-calibrate pressure selector switches. This high-speed multiport electronically-scanned pressure-sensor system was developed for wind tunnels. It allows in-situ calibration and can be computer controlled. Measurement rate is approximately 10,000 readings/second.
(See page 96.)

Stepping Optical Path Difference in an Interferometer

A stepping technique permits higher amplitude modulation of the secondary mirror of a Fourier interferometer. A closed-loop controller generates a servo error signal proportional to the offset from the previous-position servo null point. Path-length error is nulled out in the servo by counting reference laser fringes by the movement of a mirror assembly to coincide with a clock signal.
(See page 42.)

Sensor for Analog Speed Controls

A digital phase-locked-loop speed sensor improves accuracy in analog speed controls.

Lewis Research Center, Cleveland, Ohio

Analog feedback speed control systems are simple and inexpensive and allow fast, smooth, and stable operation. But for accuracies of less than one percent, highly regulated power supplies, temperature-compensated components, and temperature-controlled ovens are required. Still, drifts of less than 0.001 percent per °C or 0.1 percent per year are nearly impossible to achieve. In a crystal reference digital system, speed control accuracy better than 0.01 percent per year is easily obtained. However, expense and complexity are the most common reasons for not adopting digital systems. Also, their response tends to be slow, with step changes in the output that create transient response and stability problems.

There are primarily two types of digital frequency sensors. One senses frequency difference, typically by sensing input frequency or period and comparing it to a reference frequency or period. The sampling period is at least one-half cycle of the signal but typically several cycles. Since this is essentially a sampled data system, the output tends to change slowly and in discrete steps, causing voltage and/or frequency modulation and stability and transient response problems.

The second form of digital sensor uses a reference frequency and a phase detector. Phase-locked-loop (PLL) techniques have been used extensively in communication circuits but rarely in mechanical control systems. A PLL has a proportional control band of less than

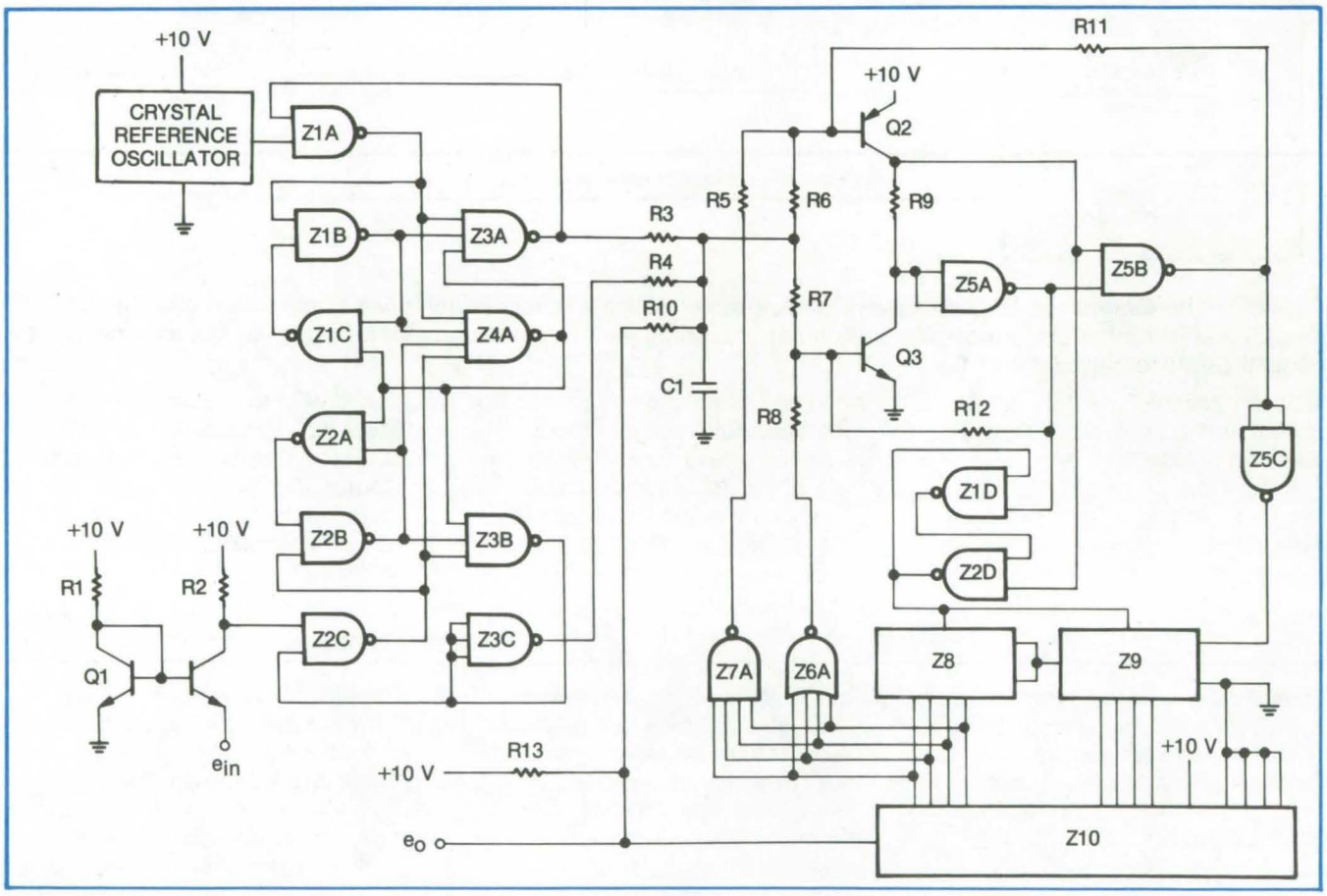

The schematic of the **Digital Speed Sensor** is shown above. The system has speed control accuracy within approximately 0.001 percent. The accuracy is limited only by the crystal reference oscillator, and there will be a negligible effect on the original system stability and transient response. The design can also be adapted to other systems and provides a compromise between either fully digital or fully analog systems.

one cycle, and mechanical systems generally respond too slowly to stay in the error band. Also, a PLL is basically an integral control with respect to frequency control. It will not result in a stable control loop on a turbine-alternator system, which is also an integrator, unless proportional control is added. However, the PLL concept has a smooth continuous real-time output and can be implemented with very little circuitry.

By combining a digital speed control with a proportional analog controller, the stability and transient response of the analog controller are retained and combined with the long-term accuracy of a crystal-controlled integral controller. A relatively simple circuit was developed for this controller by using phase-locked-loop techniques and total error storage. This overcame two problem areas, limited control range and the need for an additional proportional control loop.

The circuitry of the digital phase-locked-loop speed sensor is shown in the schematic. Complementary metal-oxide semiconductor (CMOS) logic was used throughout because of its high noise immunity and low power consumption. The components Q1, R1, and R2 convert the low-level magnetic pickup output to the CMOS logic level. The crystal reference oscillator operates at the design control frequency, 11.265 KHz for this application.

The components Z1A,B,C; Z2A,B,C; Z3A,B,C; Z4A; R3 and R4 form a phase detector. The output of this circuit is a pulse-width-modulated output whose average value varies from 0 to 10 volts, proportional to a -360° to + 360° phase error.

The components Q2, Q3, Z5A, and Z5B and the associated resistors are the pulse shaper. Separate countup and countdown pulses are formed and then combined for a single clock pulse. The separate countup and countdown pulses are detected by Z1D and Z2D to control the up or down counting of the counter.

Two four-bit counters are combined to form an eight-bit binary (256 decimal) up/down counter which extends the control range to 256 cycles of error. A R-2R DAC is driven directly from the counter and added to the phase detector output to form the output. The components Z6A and Z7A are the undercount and overcount detectors to maintain stable operation outside the normal control range.

This work was done by Arthur G. Birchenough of **Lewis Research Center.** *Further information may be found in NASA TM-X-3200 [N75-17577], "Digital Phase-Locked-Loop Speed Sensor for Accuracy Improvement in Analog Speed Controls," a copy of which may be obtained at cost from the Aerospace Research Applications Center, Indiana University [see inside back cover].*
LEW-12597

NASA

Selective Image Enhancement

A new algorithm allows selected digital enhancement of parts of an image. The same algorithm can be used with remote manipulators.

Marshall Space Flight Center, Alabama

An improved digital image-enhancement technique has been developed for TV systems. The method improves the transformation from the original image into the recorded image. It allows the observer to enhance the image areas selectively. The new transformation process is also suitable for remote manipulators. Based on the same principle, the operator can accurately transfer hand motions to the manipulator.

The transformation is accomplished using an algorithm which has four controllable parameters. An image is divided into N-by-N picture elements called pixels. Each pixel has a specific gray level X, where X varies in the interval between $0 \leqslant X \leqslant 1$. The level 0 denotes black, and 1 denotes white. Each X is then transformed into Y using the algorithm, where the Y's are corresponding gray level pixels in the displayed enhanced image. The algorithm improves the resolution of gray levels to 1 part in 2,304 rather than 1 part in 256 obtained conventionally.

Because the algorithm is based on four parameters, the operator can choose the image areas he wants to be enhanced by using a joystick having four degrees of freedom. A similar arrangement simplifies the operation of remote manipulators and can be of use for the handling of hazardous materials (e.g., radioactive isotopes).

This work was done by R. C. Gonzalez and Barry A. Fittes of the University of Tennessee for **Marshall Space Flight Center.** *For further information, including a discussion and derivation of the algorithm, Circle 59 on the TSP Request Card.*
MFS-23364

NASA

Remote Access of Modem by Digital Control

Performance of point-to-point data communications link is tested with a semiautomated data transmitter/receiver.

Goddard Space Flight Center, Greenbelt, Maryland

One means of testing the performance of a point-to-point data communications link is to equip both ends of the link with test equipment and technical personnel to operate and verify equipment condition via telephone coordination in loopback fashion. A second approach is to station a technician at the far end of the loop and perform the same task by requiring him to operate a switch at a predetermined time. The major disadvantage with this or any man/machine data set (modem) is threefold: (1) It requires a telephone call placed from point A to alert the operator at location B; (2) technical personnel are needed to identify, operate, and assist during the test; and (3) the testing of communications services is limited to the working hours of personnel at the remote location. The loopback data network is more economical to operate if both ends are automated or one operator controls the loopback function from one point.

A semiautomated system, Remote Access of Modem by Digital Control (RAMDC), enables one operator to measure the overall quality of a communications link between his console (point A) and the far-end location (point B). By transmitting a test pattern from point A, receiving it at point B, and retransmitting back to point A in loopback, the unassisted operator can evaluate overall link performance.

The RAMDC requires a parallel connection of the receive data (RD) coming from the modem, as shown in the figure. The unit constantly monitors the RD for an autocorrelation of 26 consecutive bits of a 2047 pseudorandom sequence, which is generated by a modulo-2 sum of taps 9 and 11 of an 11-bit shift register. Generators of this type of 63 and 511 bits have been standardized by the Bell Telephone Labs and CCITT, respectively, as a test pattern for data transmission systems; a more rigorous 2047 pattern has been adopted by NASCOM. The unit, having detected the presence of 26 bits by a predictor-type register, goes into a sync mode and actuates a 6144 good-bit counter. While the 6144 counter increments by virtue of the presence of the uncorrupted 2047 pattern, an 8192 counter is also incrementing toward its full count.

Three possible situations could exist: (1) the data are the customer data which look to the RAMDC to contain 50 percent errors; (2) the data from the 2047 pseudorandom generator (PRG); or (3) the data from the PRG, but 26 or more are error corrupted.

In the first case, the RAMDC ignores the data, since the 8192

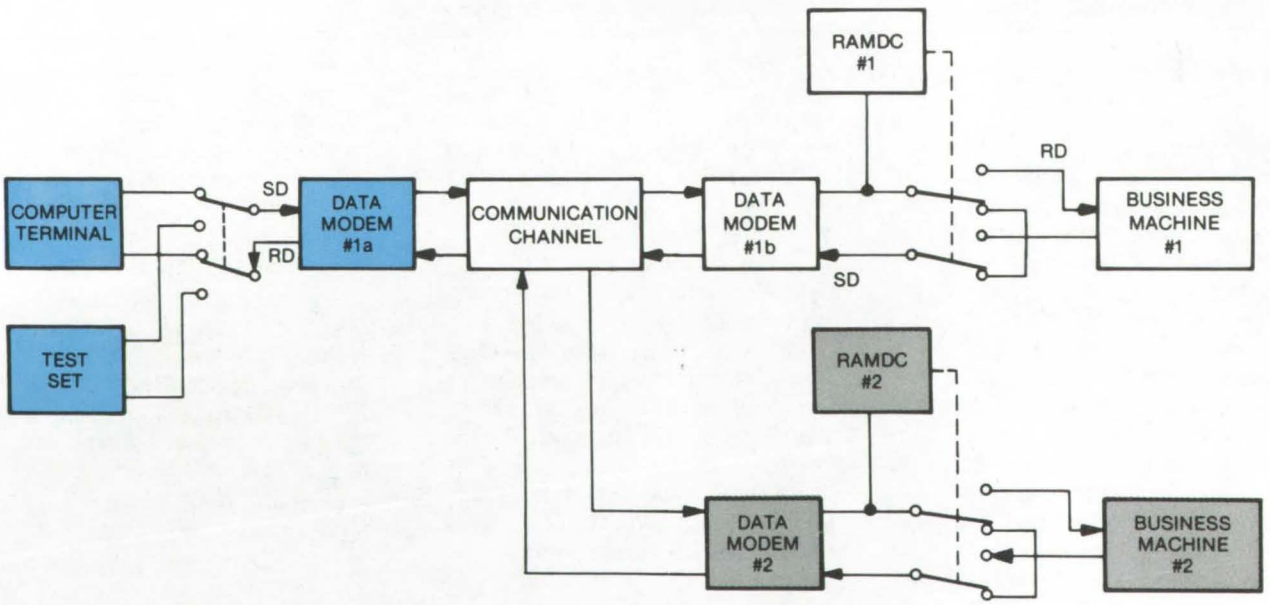

A **Data Link Employing a RAMDC** is shown. The color-tinted area represents an optional multipoint connection serving a second physically separated terminal. The gray area is a possible additional RAMDC in the send mode.

counter reached the count before the 6144 good-bit counter. In the second case, the 6144 counter reaches full count before the 8192. The RAMDC therefore detects the presence of the PRG and proceeds into a loopback. In the last case, the noisy PRG cannot increment the 6144 counter within the 8192 bit frame and resets the unit for another try.

For multipoint hook-ups of a polling network, as shown in the figure, two RAMDC's are used to isolate each segment of the system. At the main terminal location, the test set (another RAMDC) is capable of transmitting two versions of the 2047 pattern, i.e., the Q and $\overline{Q}$. At the second remote multipoint location, RAMDC (No. 2) is programed to search for the $\overline{Q}$ version of the pattern and thereby to effect the loopback without affecting the No. 1 location.

This work was done by Hiram Lopez of **Goddard Space Flight Center.** For further information, *Circle 15 on the TSP* Request Card. GSC-11943

NASA

Pulse Amplitude Discriminator Threshold Calibration

A closed-loop digital circuit, insensitive to drift with age, monitors input signals in a particle detector.

Goddard Space Flight Center, Greenbelt, Maryland

A closed-loop digital detector system has been developed for the calibration of pulse amplitude discriminator thresholds. The basic elements of the calibrator are a clock circuit, a weighting circuit, an integrator, and a chopper (see the figure). Detector systems used in instruments which measure the energy level of particles are subject to changes in sensitivity with age. The detector systems are frequently monitored to insure proper calibration by using a precision test ramp voltage. The digital detector, unlike previous systems, does not require a specific period of downtime to verify calibration.

A pulse train is used to drive a pulse height discriminator. The discriminator outputs a signal only if the input pulse amplitude exceeds the discriminator threshold. This discriminator output signal is used to control the pulse amplitude of the input signal.

The discriminator output drives the weighting circuit and the integrator. The resulting voltage is fed to the chopper, then back to the discriminator input. If the threshold is exceeded the pulse amplitude is decreased. If the threshold is not exceeded the pulse amplitude is increased. The average pulse height is therefore an exact measure of the pulse height discriminator threshold.

The clock circuit synchronizes the gate which opens and admits a discriminator pulse only when the chopper produces a pulse. The clock may also be used to inhibit inputs to the discriminator from outside sources when a threshold calibrator pulse is generated. If the calibrator pulse duty cycle is kept small the pulse height discriminator may be used for its normal function virtually without interruption.

This work was done by Daniel P. Peletier of Johns Hopkins University for **Goddard Space Flight Center.** *For further information, Circle 16 on the TSP Request Card. GSC-11912*

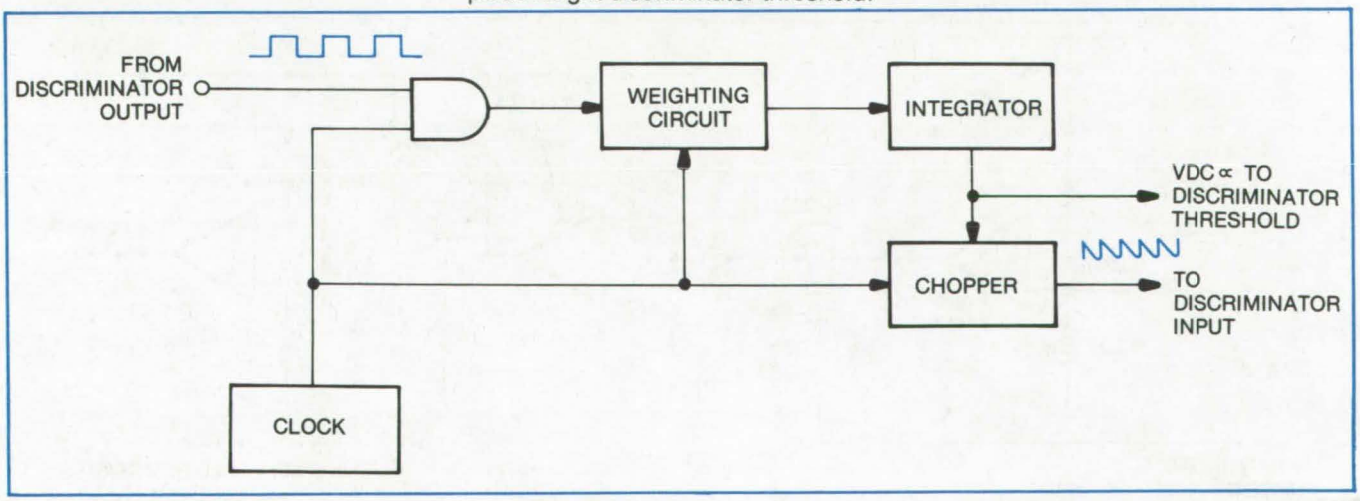

Basic elements of the **Closed-Loop System** for calibration of pulsed amplitude discriminator thresholds are shown.

NASA

Electro-Optical Liquid Depth Sensor

A compact sensor system measures the depth of a liquid flowing on a surface.

Marshall Space Flight Center, Alabama

The electro-optical liquid depth sensor (EOLDS) is a transducer in which the absorptive properties of water are utilized to determine variations in the depth of a layer of water flowing on a surface. The sensor consists of a source and a detector located on opposite sides of the liquid layer. The instrument is simple, inexpensive, small, and requires little maintenance. Thus it can easily be used instead of a direct graduated-scale readout or capacitive, ultrasonic, resistive or inductive sensors, when such instruments are impractical because of complexity, size, or cost. In addition, the sensor output is electrical so that it may be interfaced with a data system. The area required for locating both the source and the transducer is a circle approximately 1/8 in. (0.32 cm) in diameter.

The EOLDS is capable of monitoring the depth of a liquid without disturbing the liquid. The amount of light absorbed by the liquid is measured, and this depends directly on the thickness of the liquid layer. The measured liquid must, of course, be capable of absorbing light. In the present unit, an LED source emits light at 690 nm (red), and in order to make the water somewhat opaque at this frequency, it is dyed green. Absorbance can also be assured by using other LED sources, including infrared.

In order to neutralize the effect of varying ambient-light levels, the LED sources are pulsed at approximately 1 kHz (see Figure 1) and the output is sensed in a chopper-type amplifier (see Figure 2). The multivibrator, or oscillator, creates square-wave pulses in the 100-Hz range. These pulses are used to drive the LED

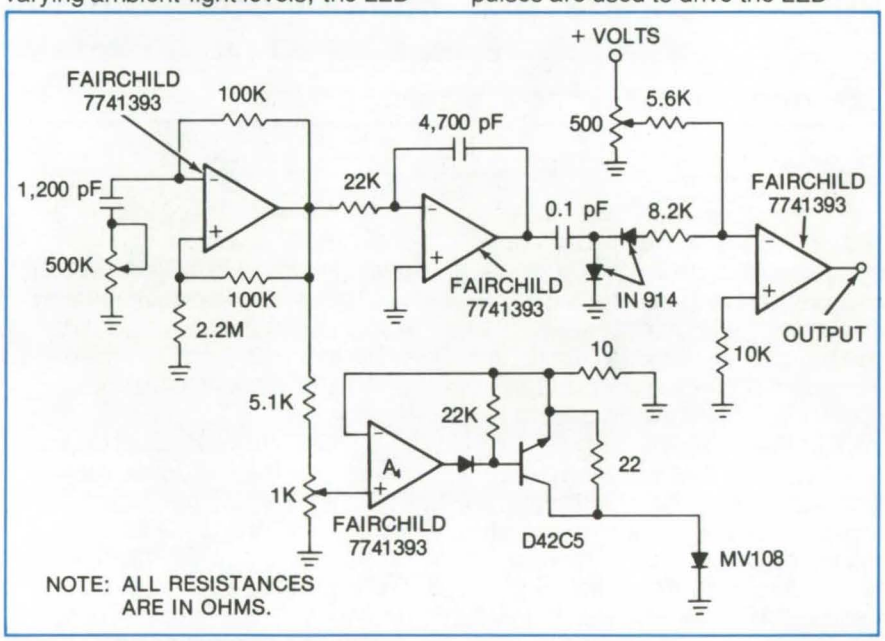

Figure 1. The **Pulsing Circuit** provides a 1-kHz pulse to the LED's. The LED's are pulsed to neutralize the effects of variations in the ambient light levels.

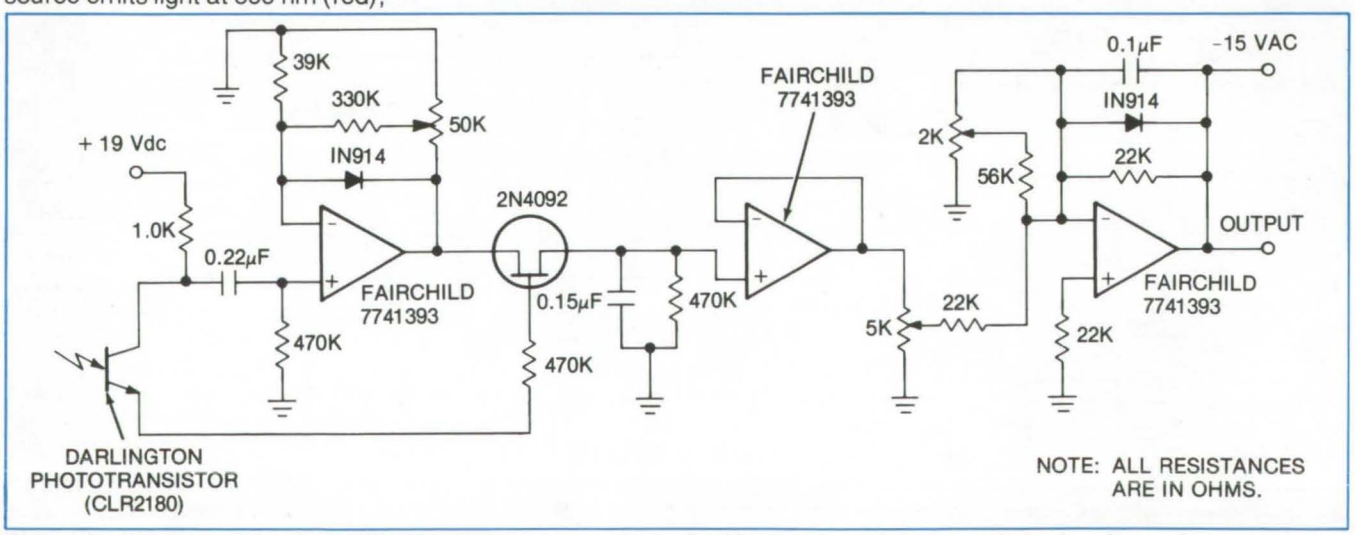

Figure 2. **Chopper-Type Amplifier Circuitry** uses a photo-Darlington transistor as a detector. It sends a square-wave output to a gated FET which is controlled by a sample-and-hold timer pulse. The sample-and-hold amplifier produces dc output which is scaled by a scaling amplifier.

sources directly. A constant-current driver delivers approximately 100 mA to the sources which are connected in series. In this fashion, several sensors can be used. The sample-and-hold timer basically takes the oscillator square wave and using an integrator creates a short-duration pulse which occurs roughly in the center of the LED driver pulse.

The detector is a photo-Darlington device. Its output is a square wave with an amplitude that is proportional to the instantaneous liquid thickness. After amplification, a short duration portion of the signal passes through a FET gate which is controlled by the sample-and-hold timer pulse. A sample-and-hold amplifier peak-detects the magnitude of each passed pulse and produces a dc output which is therefore proportional to depth. Finally, a scaling amplifier allows the output to be set at zero volts for no or minimum depth, 5 volts for maximum depth. Because of its fast response, the sensor will faithfuly reproduce signals up to the 200-Hz perturbations that are expected in dynamic flow situations.

This work was done by Dennis B. Heppner and Sedwick O. Atwood of General Dynamics Corp. for **Marshall Space Flight Center.** *For further information, Circle 17 on the TSP Request Card.*

Inquiries concerning rights for the commercial use of this invention should be addressed to the Patent Counsel, Marshall Space Flight Center [see page 2]. Refer to MFS-22921.

NASA

General-Purpose Data Link

A modem that can sample, multiplex, transmit, receive, demultiplex, and store data.

Marshall Space Flight Center, Alabama

The general-purpose data link (GPDL) is an inexpensive solution to many data communications problems. It is not just a modem but a complete communication system which is extremely versatile. It permits a wide range of input and output voltages, the number of inputs and outputs can be easily changed, it is flexible as to data rate, and provision is also made for a computer interface.

The GPDL consists of a transmitter unit and a receiver unit. It can sample, multiplex, and transmit data, as well as receive, demultiplex, and store the information. Several options are available for different interfaes. The transmission medium can be a telephone line, a video pair, or a 1,250 ohm twisted-wire pair, depending on the option selected. The GPDL output could also be used to modulate an RF carrier.

The GPDL is designed for mounting on printed-circuit boards (PCB's) which are approximately 8 in. (20 cm) square. The PCB's mount in standard enclosures. The basic blocks are: transmitter, modulator, demodulator, and receiver. The transmitter and receiver both contain a fixed amount of control logic, but the input and output matrices are expandable to handle from a minimum of 64 to a maximum of 1,536 discrete signals. Four options have been designed: (1) discrete input to remote discrete output (2) discrete input to remote computer memory (3) computer memory to remote discrete output and (4) computer memory to remote computer memory. Communication, using any of these options, is in one direction only. Two independent data links are required for two-way communications.

The data-link transmitter sequentially scans many input signals and loads them, 8 bits at a time, into a shift register. From the shift register the 8-bit characters go serially into the modulator. The modulator output is a serial phase-shift-keyed (PSK) modulated signal to a pair of wires or a transmission line. The modulator can be omitted provided that the distance between transmitter and receiver is no greater than approximately 1,000 ft (305 m), and the common mode offset can be held to ± 3 V.

Data to be transmitted is grouped in 8-bit characters (bytes). Two other bits are then added, one to distinguish sync characters from data characters and the other to provide for parity check. The first two characters in every frame are sync words, and the rest are data. The number of data characters per frame can range from 16 to 192, depending upon specific requirements.

The data-link receiver accepts serial PSK modulated input from a pair of wires, recovers the clock, demodulates the data, and provides outputs to discrete points or computer memory, depending upon the options used. The receiver, like the transmitter, has its logic partitioned for functional PCB packaging. The receiver PCB's include: a control logic board, an output matrix board, a demodulator board (when required) and a computer interface board.

This work was done by Murray J. Dinkins of General Electric Co. for **Marshall Space Flight Center.** *For further information, Circle 18 on the TSP Request Card.*
MFS-22714

NASA

Unichromatic-Carrier Color-TV System

A single-tube system produces NTSC-encoded color signals with reduced color distortion and a lower bandwidth.

Lyndon B. Johnson Space Center, Houston, Texas

In one method used to produce a color signal from a single image that is encoded according to the National Television Standards Committee (NTSC), a single image-pickup tube with a crossed, striped optical filter is used in the color-television cameras. This method, however, produces two chroma carrier frequencies and requires a large system bandwidth, making it difficult to achieve constant and accurate colorimetry characteristics. Previous attempts to use a single pickup tube to extract real-time color images from narrow bandwidth video signals have proved to be technically and economically unfeasible.

A new system produces three color signals which may be encoded according to NTSC standards. The color distortion inherent in previous single-tube systems is eliminated. Also, a single time-division-multiplexed carrier is used for red and blue color signals. This is in contrast to the separate carrier frequencies required in previous systems in addition to the luminance signal, and thus, it permits a lower system bandwidth with a higher colorimetry quality.

The optical system consists of two filter layers with each layer composed of transparent stripes alternating with dichroic color-filter stripes (see figure). The system produces a color-multiplexed light signal by vertically orienting the dichroic filter stripes perpendicular to the scan lines of the image tube. The stripes on one layer remove one primary color; the stripes on the other layer remove another color. The optical filter modulates the composite beam into a periodic light signal in the following sequence: green, green/red, green, and green/blue.

The multiplexed light, a composite of interleaved-color light signals of scene information, is projected onto a scanning-beam imaging-pickup device. As each scan line is exposed to all the multiplexed signals, the tube converts the optical signals to an equivalent video-output signal containing all of the individual colors in sequential order of scan.

The encoded video scan is therefore time-division multiplexed, and a green color signal is retrieved by a low-pass filter. Time-delay and subtractor circuits are used to obtain a single blue-and-red multiplexed-chroma carrier signal, which is demultiplexed to produce the red and the blue color signals.

This work was done by Kenneth H. Vorhaben and Phillip C. Lipoma of Lockheed Electronics Co. for **Johnson Space Center.** *For further information, including a system description at the block diagram level, Circle 19 on the TSP Request Card.*

This invention is owned by NASA, and a patent application has been filed. Inquiries concerning nonexclusive or exclusive license for its commercial development should be addressed to the Patent Counsel, Johnson Space Center [see page 2]. Refer to MSC-14683.

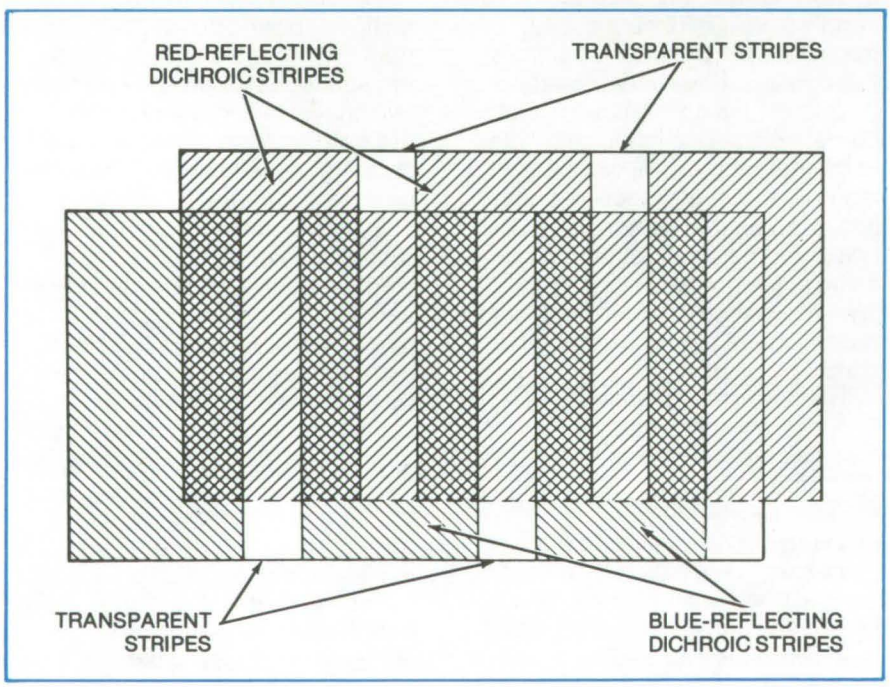

The **Filter Configuration** consists of two filter layers, each composed of alternating transparent and dichroic filter stripes. The stripes on one layer filter out red; the stripes on the other layer filter out blue.

NASA

Serial-to-Parallel Color-TV Converter

Solid-state analog-to-digital converter eliminates flicker and problems with time base stability and gain variation in sequential color-TV cameras.

Lyndon B. Johnson Space Center, Houston, Texas

Although sequential color-TV cameras are lighter and simpler than standard parallel National Television System Committee (NTSC) cameras, they have one disadvantage that restricts their application. When the image is viewed on the sequential TV monitor, there is annoying flicker, causing rapid viewer fatigue. This problem can be eliminated with sequential-to-parallel converters. However, these are conventional analog rotating-memory converters (e.g., drums or disks). They have heavy moving parts, resulting in reduced reliability, loss of resolution, and lack of field-to-field gain stability. The advantages gained with the sequential camera are lost with the converter.

An effective approach is to use a new all-solid-state sequential-to-parallel converter. An incoming serial color-video signal undergoes analog-to-digital conversion. The resultant digital data are stored in solid-state digital memories; the time-base stability and gain-variation problems of the conventional converters are eliminated.

The new converter as shown includes a 3-bit delta modulator; a two-field memory; a timing, switching, and sync network; and three 3-bit delta demodulators. The 3-bit delta modulator performs the analog-to-digital conversion. It accepts the signal from the sequential TV camera and converts each picture element of the input scan into 3 bits of digital information. The modulator is designed so that redundant information in the input scene is eliminated.

The signals are then fed to the two-field memory. NTSC compatible synchronization is provided by the timing, switching, and sync network. The signals are selectively fed from the modulator or one of the two field memories into the proper demodulator. The three demodulators do the digital-to-analog conversion. Their outputs, consisting of parallel NTSC video signals with composite sync blanking inserted, are fed to a standard color TV monitor.

The resultant 3 bits of digital data for each sample of the input video are sufficient to give the full resolution and signal-to-noise ratio performance of a conventional 6-bit PCM (pulse code modulation), which requires 6 bits of digital data for each sample of the input video signal. The resultant data compression (6 bits to 3 bits) allows a reduction of the capacity of the two-field memory by a factor of 2.

A detailed description of the converter is published in a report entitled "Sequential Color Video to Parallel Color Video Converter." This report contains a specification summary, followed by a discussion of a number of system tradeoffs that led to the selection of the delivered-system configuration.

The delta modulator/demodulator is described along with the format control and system synchronization. Also included in the report is a summary of reliability analyses and a packaging study. Finally, performance results (measured with a breadboard converter) are presented together with conclusion and recommendations for further development.

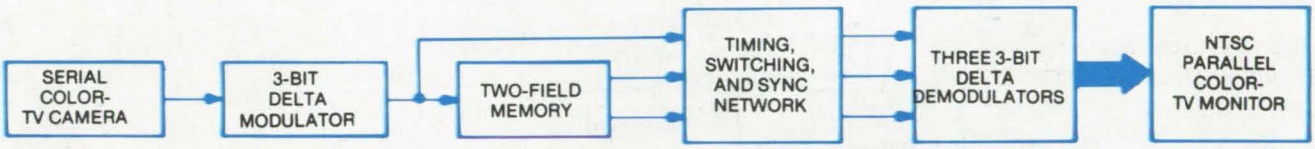

The Serial-to-Parallel Color-TV Converter transforms serial color-TV signals to NTSC-compatible parallel signals. The two-field memory is a pair of video delays implemented with PMOS shift registers.

This work was done by Thomas W. Doak, Richard B. Merwin, Samuel E. Zuckswert, and Werner Sepper of Philco-Ford Corp. for ***Johnson Space Center.*** *The report, "Sequential Color Video to Parallel Color Video Converter," NASA CR-141891 [N75-26203], may be* obtained *at cost from the National Technical Information Service, Springfield, Virginia 22151.*

Inquiries concerning rights for the commercial use of this invention should be addressed to the Patent Counsel, Johnson Space Center (see page 2). Refer to MSC-14844.

NASA

Tracking System for Moving Subjects

A camera or a spotlight can be made to focus automatically on and to follow a subject carrying a miniature transmitter.

NASA Headquarters, Washington, D.C.

A newly-proposed electronic tracking system guides cameras and spotlights that track moving objects. The system could be used in theaters to track performers with spotlights and in television and movie studios to follow actors and moving objects.

The same basic system could be used to track other subjects, such as security guards, or as part of a tracking/control system for other automatic machinery.

As shown in the illustration at least two detectors are spaced far enough apart to cover a given area. The object moving within this area is equipped with a miniature ultrasonic or radio transmitter, and the transmitted signals picked up by the detectors are phase detected and are fed to a computer. The computer determines the angular orientation of the object with respect to a camera or a spotlight and feeds command signals to a servo. A camera or a spotlight driven by the servo then tracks the object as it moves within the area.

In the system shown, the spotlight is

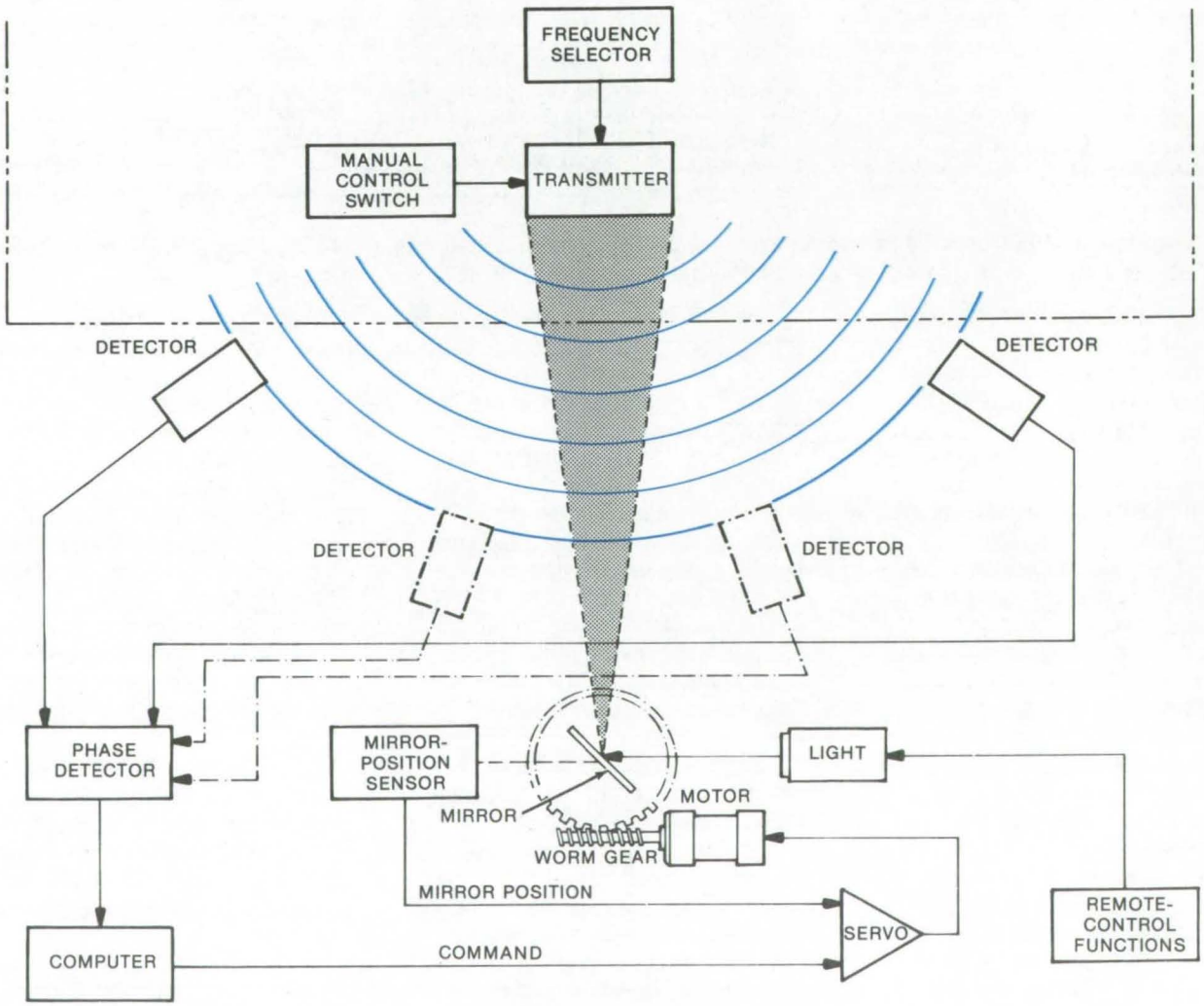

The **Spotlight Tracking System** controls a beam-directing mirror via signals received from a miniature transmitter. The detectors may be conventional radio antennas; two are required for each dimension of a subject's motion. Thus the pair shown in solid lines will track a performer moving in a straight line, and two-dimensional motion may be tracked by using the additional pair shown in dotted lines. Motion in a third dimension (up and down) requires a third pair of detectors positioned vertically.

stationary, and a mirror deflection system is used to cast the beam onto the target. This saves energy because a relatively low power servomechanism can be used to move the mirror instead of the large ones necessary to drive a spotlight directly. The mirror is driven from the servo network which develops an error signal between the mirror position and the computer command signal. The mirror position is obtained from the mirror-position sensor. Optional remote-control functions, such as spotlight size and colors, can be automatically set by an additional remote-control system.

The moving object is tracked in one-dimensional space by at least two signal detectors. Additional signal detectors are needed to track the object in two and three dimensions. The system is also capable of tracking a number of performers, using separate spotlights. Each performer may be equipped with a transmitter tuned to a different frequency. Using this setup, the performer can turn on his own spotlight when he is ready.

This work was done by Louis N. Mogavero of **NASA Headquarters** *and Edwin G. Johnsen, John M. Evans, Jr., and James S. Albus of the National Bureau of Standards. For further information, including an extended discussion of the system concept, Circle 20 on the TSP Request Card.*

This invention is owned by NASA, and a patent application has been filed. Inquiries concerning nonexclusive or exclusive license for its commercial development should be addressed to the Patent Counsel, NASA Headquarters [see page 2]. *Refer to HQN-10880.*

NASA

Readout Method for Stored Information

A technique to increase the density of stored information where the retrieval is projected onto a facsimile reproduction.

NASA Pasadena Office, Pasadena, California

Defects due to nonlinearities in scanning generators may be eliminated by a readout technique performed at an angle of 90° to the lines of recording. Storage-line structures on the order of 1 micron in width, with a similar spacing between lines, are the foreseeable requirements for future recording of video data and similar information.

Recordings are made in line sequence, with succeeding portions of the data stored in lines in descending order, similar to a printed page. Subsequent recovery of such information requires sweeping the substrate on which the recording has been made. The sweeping operation is performed in two directions, across the substrate and at a right angle to it, by ramp generators of high accuracy and linearity. Such machines, however, may develop a tendency to drift, resulting in imperfect recovery of data.

In cases in which the retrieval is projected onto a facsimile reproduction, the new technique increases the density of stored information. By scanning over an area larger than the recorded format (see figure), it ensures the recovery of all recorded information.

This work was done by George W. Lewicki of Caltech/JPL for **NASA Pasadena Office.** *For further information, Circle 21 on the TSP Request Card.*
NPO-13243

NASA

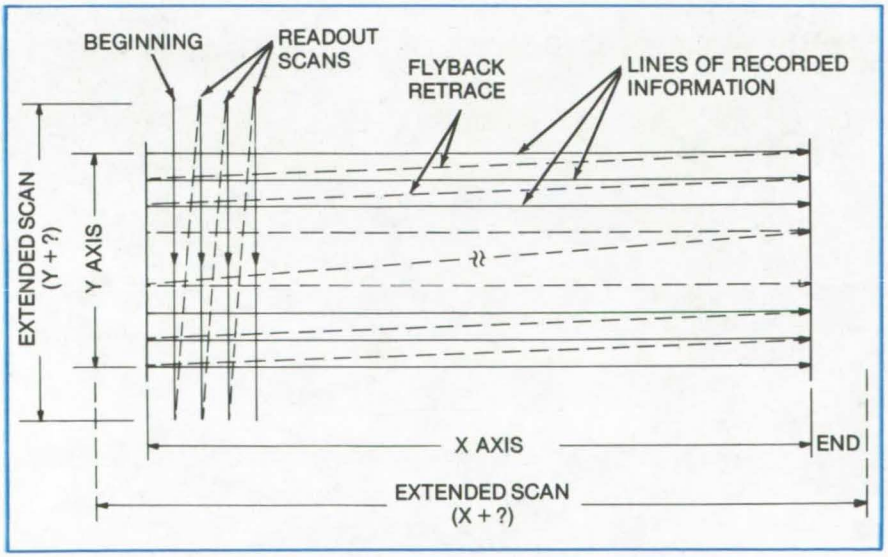

Readout Method for data stored on line structures

Physical Sciences

Hardware, Techniques, and Processes

Computer Programs

Laser Extensometer

A drift-compensated intensity-averaged laser system measures very-small thermally-induced size changes.

Marshall Space Flight Center, Alabama

In a newly-designed laser-based system, optical and photoelectric effects are used to precisely measure thermally-induced size changes. In operation, the beam of a He-Ne laser falls upon the mirror of a high-frequency galvanometer oscillating at approximately 25 kHz (see figure). An optics system then shapes the beam so that it has suitable dimensions for shadowing that part of a sample which is to be measured and has a uniform cross-sectional intensity. The beam is then allowed to fall on the sample.

After passing the sample, the beam is divided into two by a beam-splitting prism. One beam is trimmed by knife edges so that the remainder is only slightly wider than the sample shadow. This controls the sensitivity of the measurement. The second beam is also trimmed so that it no longer retains the sample shadow, thereby providing a reference which carries only information of beam intensity (lasers drift in intensity as much as 5 percent). The second beam is also trimmed to eliminate the nonuniform outer fringes.

Both beams then are chopped at a frequency of 500 Hz, pass through opal glass diffusers, and fall upon two photodiode detectors. The ac current from the detectors is rectified, thus eliminating the detector dark current, and the resulting dc signals are divided, one into the other. The final output signal is directly proportional to the size of the sample shadow and is independent of laser intensity, detector dark current, and the slight lateral motions of the sample.

This work was done by Phillip J. Stocker and Harris L. Marcus of Rockwell International Corp. for **Marshall Space Flight Center.** *For further information, Circle 22 on the TSP Request Card.*

Inquiries concerning rights for the commercial use of this invention should be addressed to the Patent Counsel, Marshall Space Flight Center [see page 2]. Refer to MFS-19259.

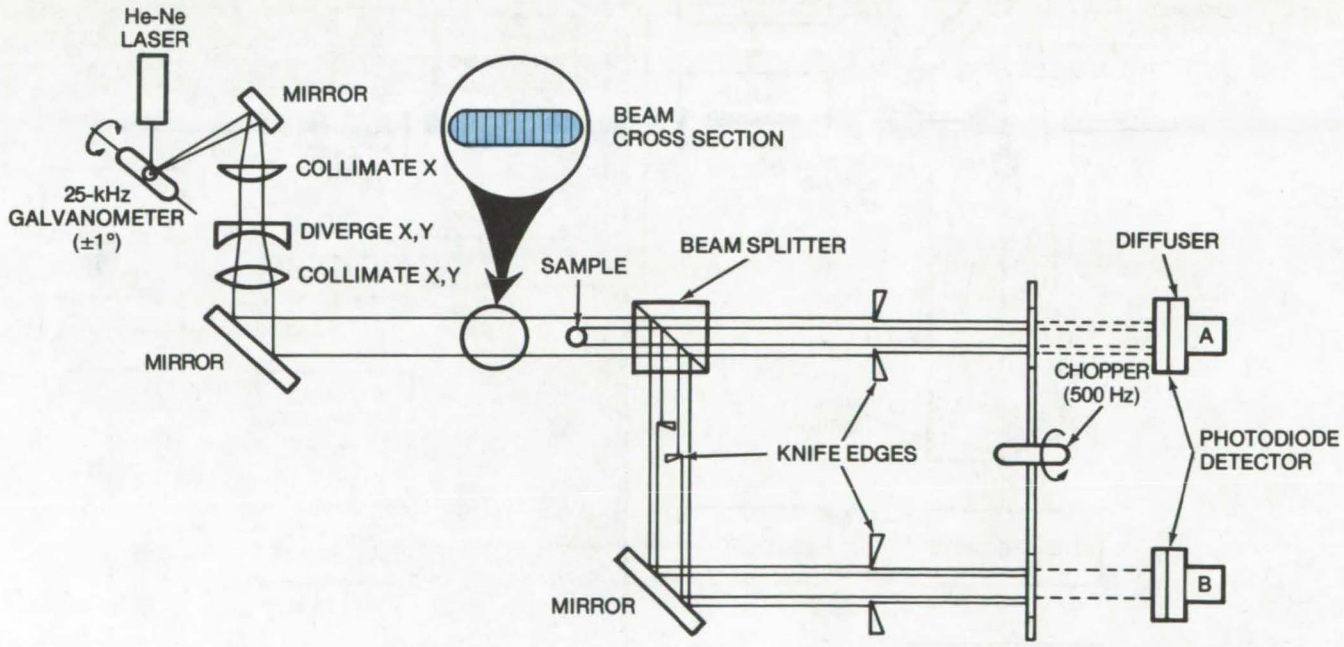

The **Laser Extensometer** has a high-frequency galvanometer and optical system that establishes a laser beam with a cross section that is uniform and larger than the sample to be measured. The sample diameter is determined by measuring the amount of light that passes by it.

NASA

Laser-Doppler Measurement of Air Turbulence

A CO_2 laser with a 10-micron wavelength tracks 1-micron dust particles to measure air turbulence.

Marshall Space Flight Center, Alabama

A laser-Doppler system has been designed to detect air turbulence and is intended for use at airports to measure and track aircraft trailing vortexes. Laser-Doppler systems function similarly to radar, but because of their much shorter wavelength, they can detect very small particles such as atmospheric dust. Since there is always dust in the atmosphere, these systems can be used to measure air movement by tracking the airborne particles.

A block diagram of the system is shown. The light from a laser passes through an interferometer and serves as a reference signal; it is then steered to the area of interest by a mirror. The reflected light is picked up by the mirror and is returned to the interferometer. The output of the detector is a herto-dyned signal which is routed to the signal-processing electronics where it is filtered and integrated.

The remainder of the electronics processes the signal for display and controls the laser scan. The scanning controller coordinates the range focus and the beam-steering mirror.

The velocity processor contains particle-velocity discrimination logic and provides velocity parameters (such as average and peak vortex velocities) as functions of position.

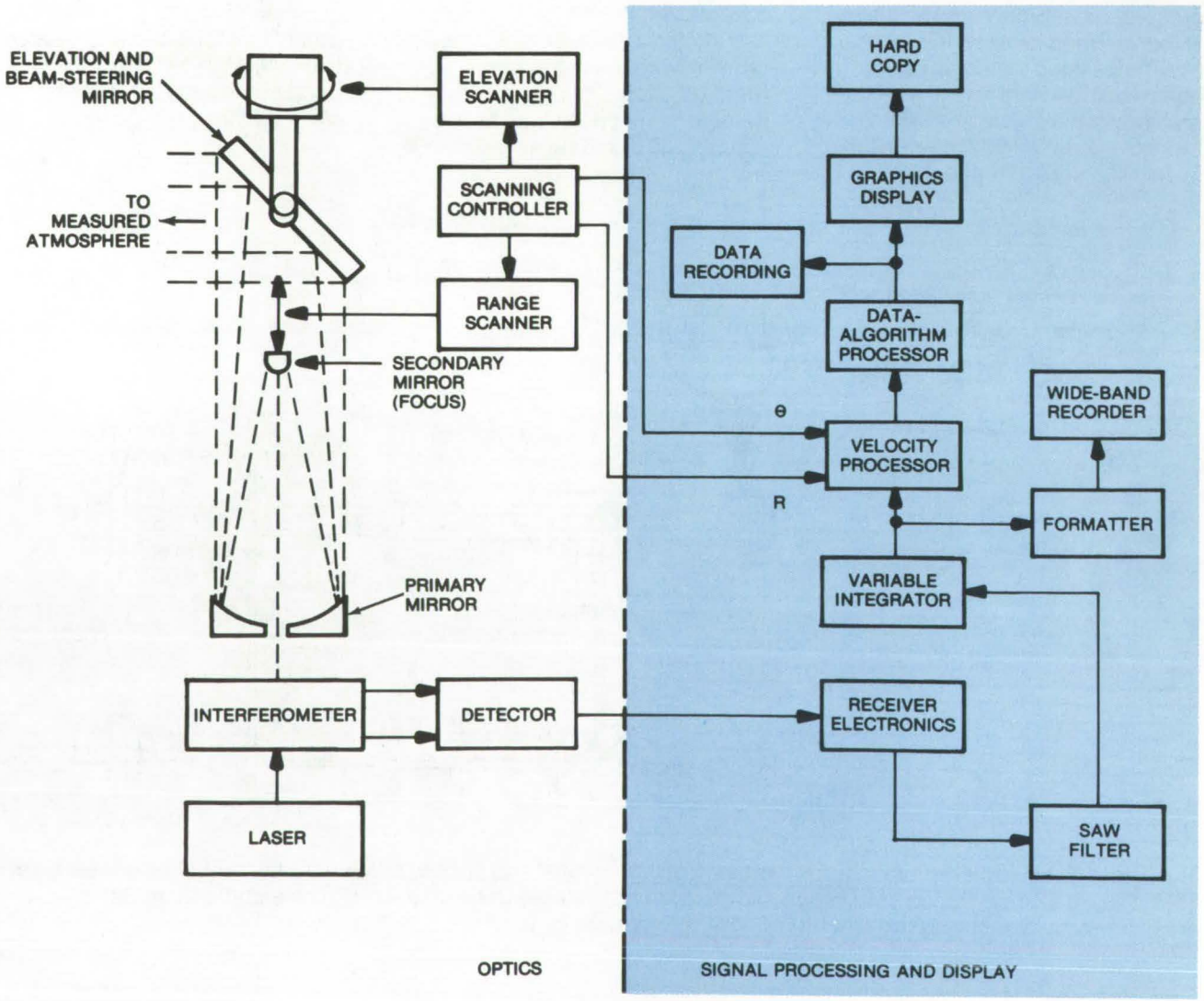

The **Laser-Doppler** system shown is a one-dimensional system with provisions for scanning for range, along a vertical line, or on a single plane.

These data are used by the data/algorithm processor to give the position of a vortex center as a function of time. The final velocity data may be displayed as functions of time, elevation, and range.

This work was done by Robert M. Huffaker of **Marshall Space Flight Center.** *For further information, including a more detailed description of the system, Circle 23 on the TSP Request Card.*

Inquiries concerning rights for the commercial use of this invention should be addressed to the Patent Counsel, Marshall Space Flight Center [see page 2]. Refer to MFS-23155.

NASA

Improved Einzel Lenses

Spherical sapphire insulators simplify fabrication and improve performance of three-electrode Einzel lenses.

Marshall Space Flight Center, Alabama

A new insulator configuration has simplified the construction of the three-electrode electrostatic electron lenses in which the center electrode has to be at a high electrical potential with respect to the two base electrodes. The lens structure is readily demountable for periodic cleaning, and it is capable of being reassembled in such a manner as to ensure concentricity of the bore holes in the three elements and parallelism between the plane faces of the elements.

In principle, the electrode assembly is similar to that of a ball race (see figure). The 20-kV center electrode is insulated from the grounded outer electrodes by three sapphire spheres, each 3/8 inch (0.97 cm) in diameter. These spheres are readily available at low cost from commercial vendors. They have tolerances in sphericity of 0.00001 inch (0.00003 cm) and in diameter of 0.00002 inch (0.00003 cm). The three spheres are located by the inner (center) electrode and outer housing grooves. The outer groove is made up of two sections: a ridge machined into the housing wall and the tapered edge of a stainless-steel ring. When the removable outer electrode is screwed down tightly onto this ring, the whole electrode system becomes self-alined. The tolerances are those imposed by the machining process.

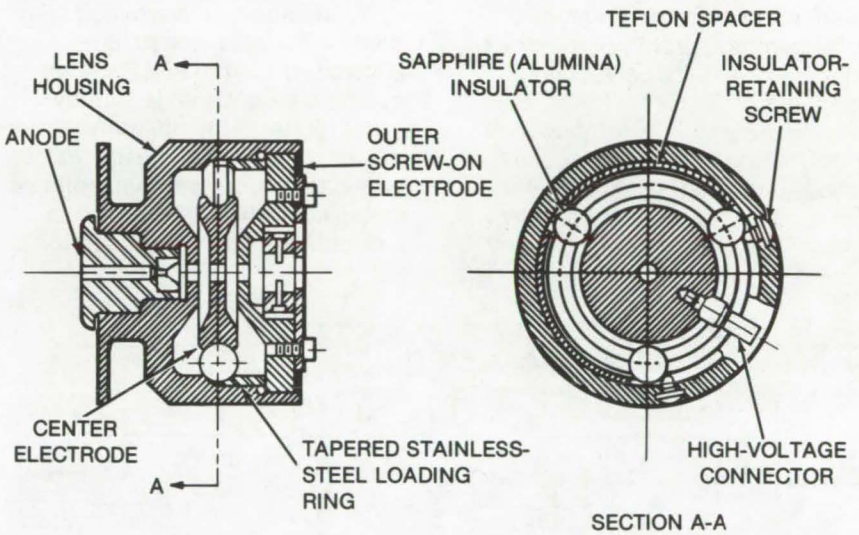

This Einzel Lens Assembly incorporates spherical sapphire insulators in lieu of the tubular ceramic or plastic insulators used conventionally.

Two Teflon strips and two retaining screws are used to keep the three sapphire spheres 120° apart. Normally the spheres are held securely enough that any movement in the cage would be impossible. However, the extra precaution of using spacers and retaining screws was taken in case the spheres should become loose as a result of differential thermal expansion during bakeout to 250° C (482° F). This bakeout is a requirement for obtaining very low residual pressures, i.e., $<10^{-8}$ torr (1.33×10^{-6} N/m^2), in the electron gun system. The insulators function satisfactorily in a 20-kV field.

This work was done by Raymond K. Hart of the Georgia Institute of Technology for **Marshall Space Flight Center.** *For further information, including detail design drawings, Circle 24 on the TSP Request Card.*
MFS-23115

NASA

Stepping Optical Path Difference in an Interferometer

A means for generating an error voltage for the interferometer servo drive, proportional to the distance offset from the proper null position

NASA Pasadena Office, Pasadena, California

A new method of stepping the optical-path difference permits a higher amplitude modulation of the secondary mirror in a Fourier interference spectrometer. In the previous version the amplitude of the mirror motion was limited to one-half the wavelength of the laser reference. With the new method the amplitude is limited only by the available voltage drive on one of the error-correcting actuators.

In the Fourier interference spectrometer, the difference in the optical-path length of two beams is adjusted by moving a secondary mirror. The mirror is controlled by a servo that uses a reference laser beam with a wavelength equal to or less than the required amplitude of the mirror modulation. The servo nulls to a 0° phase (or 2π multiple) of the sinusoidal interferogram produced by the interacting object beam and reference beam in the spectrometer.

By replacing an open-loop step controller with a closed-loop controller, a servo error voltage can be provided that is linearly proportional to the offset from the proper null position. The method for providing the error signal is shown in the illustration. In essence, a bidirectional counter is used to count the number of reference-laser fringes offset from the null position, and this is converted to a staircase or step analog voltage signal that is proportional to the offset. The laser reference signals are generated from the interferometer by a reference-signal generator (not shown). The 0°, 90°, 180°, and 270° signals are used as error null signals when the path difference is an integral number of wavelengths plus a multiple of 90°. The proper phase is selected by the quadrant selection gates controlled by quadrant logic. The switching between quadrants takes place half way between the consecutive one-quarter-wave separated null points.

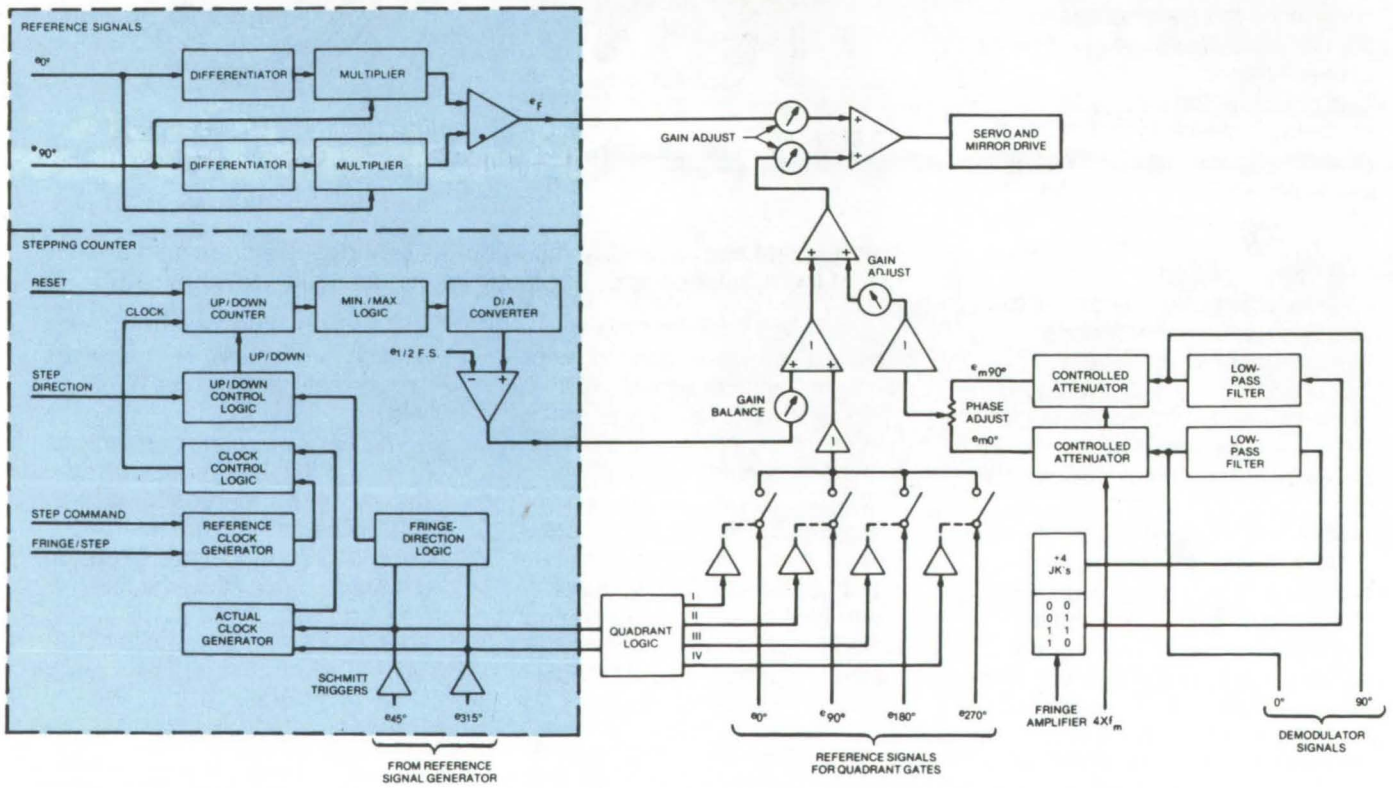

The **Error Signal System** counts the number of fringes offset from the null position with a bidirectional counter and converts this count into an analog voltage which is proportional to the offset in a staircase fashion. The analog reference voltage, in the proper phase, is then added to the analog staircase voltage.

The staircase generated by the DAC is added to the quadrant error signals. The height of each stair step is equal to the peak-to-peak value of the quadrant signal. This composite is thus the servo error signal. In order to step to the next path-difference null position (data sampling point), the count on the bidirectional counter is incremented by a series of reference clock pulses. For example, five reference clock pulses will represent five-quarters of a laser wavelength. The composite error voltage causes the actuators to drive the counter to count back down to the half-modulo count where the DAC has a zero output.

The internal modulation is applied by adding a 10,000 Hz sine-wave to the composite error signal. The peak-to-peak amplitude of the modulation can be as high as the number of DAC bits times one-quarter of a laser wavelength. Beyond this point, the modulation is no longer linear.

For amplitudes greater than the one-quarter wavelength signals, a bidirectional counter controls a digital-to-analog converter (DAC), which produces a staircase voltage proportional to the optical path difference. The counting direction is controlled by the 45° and 315° signals. For a half-modulo count, the DAC output is zero; for less than half-modulo, the output is negative; and for more than half-modulo it is positive.

In the general case, the bidirectional counter has a larger number of bits ($\cong 16$) than the DAC ($\cong 8$). The minimum/maximum logic is thus incorporated to ensure that the DAC output stays at the maximum positive or negative output instead of cycling with the least significant bits of the counter.

This work was done by Rudolf A. Schindler of Caltech/JPL for **NASA Pasadena Office.** *For further information, Circle 25 on the TSP Request Card.*
NPO-13569

NASA

Light Pipes for LED Measurements

A light pipe directly couples an LED to a single detector, overcoming problems with multidetector systems.

Goddard Space Flight Center, Greenbelt, Maryland

Light-emitting diodes radiate optical power in a diverging beam pattern, with measurable power being emitted at very large angles to the geometric axis. Because of this characteristic, it has been necessary to surround the light-emitting diode (LED) with several detector surfaces in order to measure the total radiated optical power. The use of multiple detector surfaces increases the susceptibility to measurement errors caused by detector instabilities and thermal effects. These problems could be minimized by the use of a single detector surface.

The use of a high-quality light pipe to directly couple the LED optical output to a single detector now makes it possible to use a simple, small-area detector to measure the total optical output of the diode. By using a light pipe with an end area greater than the area of the light-emitting surface, and by placing both surfaces in close contact, it is possible to channel essentially all of the radiated optical power to the detector. There will be attenuation in the optical power transmitted through the light pipe, this attenuation being a function of the quality of the light pipe and its length. The attenuation is usually small and may be easily measured and used as a correcting factor.

There are other advantages in using a light pipe to couple the optical output of a LED to a measuring detector. In addition to their optical output, light-emitting diodes generate heat. This extraneous radiation can cause measurement problems if located near thermally sensitive detectors. The light pipe eliminates this problem by physically separating the LED from the detector.

The light pipe can also channel the optical output of a LED from within an assembled system to a remote detector. This has numerous advantages in isolating failed parts prior to dismantling a system. This technique is presently being used in a parts evaluation task, as well as in screening IR light-emitting diodes.

This work was done by Samuel R. Floyd and Edward F. Thomas, Jr., of **Goddard Space Flight Center.** *No further documentation is available.*
GSC-11887

NASA

Ellipsometer for Measurement in Ultrahigh Vacuum

Combining the vacuum chamber and the optical bench allows the angle of incidence to be varied.

Marshall Space Flight Center, Alabama

An ellipsometer measures a polarized beam of light that is reflected from the surface of a sample. The instrument is widely used to study the optical constants of surfaces and thin films. When investigating an uncontaminated surface, an ultrahigh vacuum or a very well controlled atmosphere is required. Ellipsometers adapted to vacuum systems have always had fixed windows and could be used to take measurements only at a single angle of incidence. Many types of studies require measurements at several angles.

A new ellipsometer, designed for use with an ultrahigh vacuum, allows the angle of incidence to be varied. This is accomplished by incorporating the vacuum chamber directly into the optical bench system, allowing measurements at varying angles of incidence to be taken through the same region of a window. This is important, since differences in strain birefringence across a window would cause difference errors in the measurements.

The windows are mounted on the ellipsometer arms and are sealed to the vacuum chamber by flexible bellows, as shown in the illustration. The windows are optically-flat and plane-parallel glass disks, sealed to a 0.63 cm (0.25 in.) diameter glass tube with Kovar seals. After annealing, the windows are examined for strain and, if acceptable, are vacuum brazed to stainless steel bellows. The bellows are then heliarc welded to conical stainless

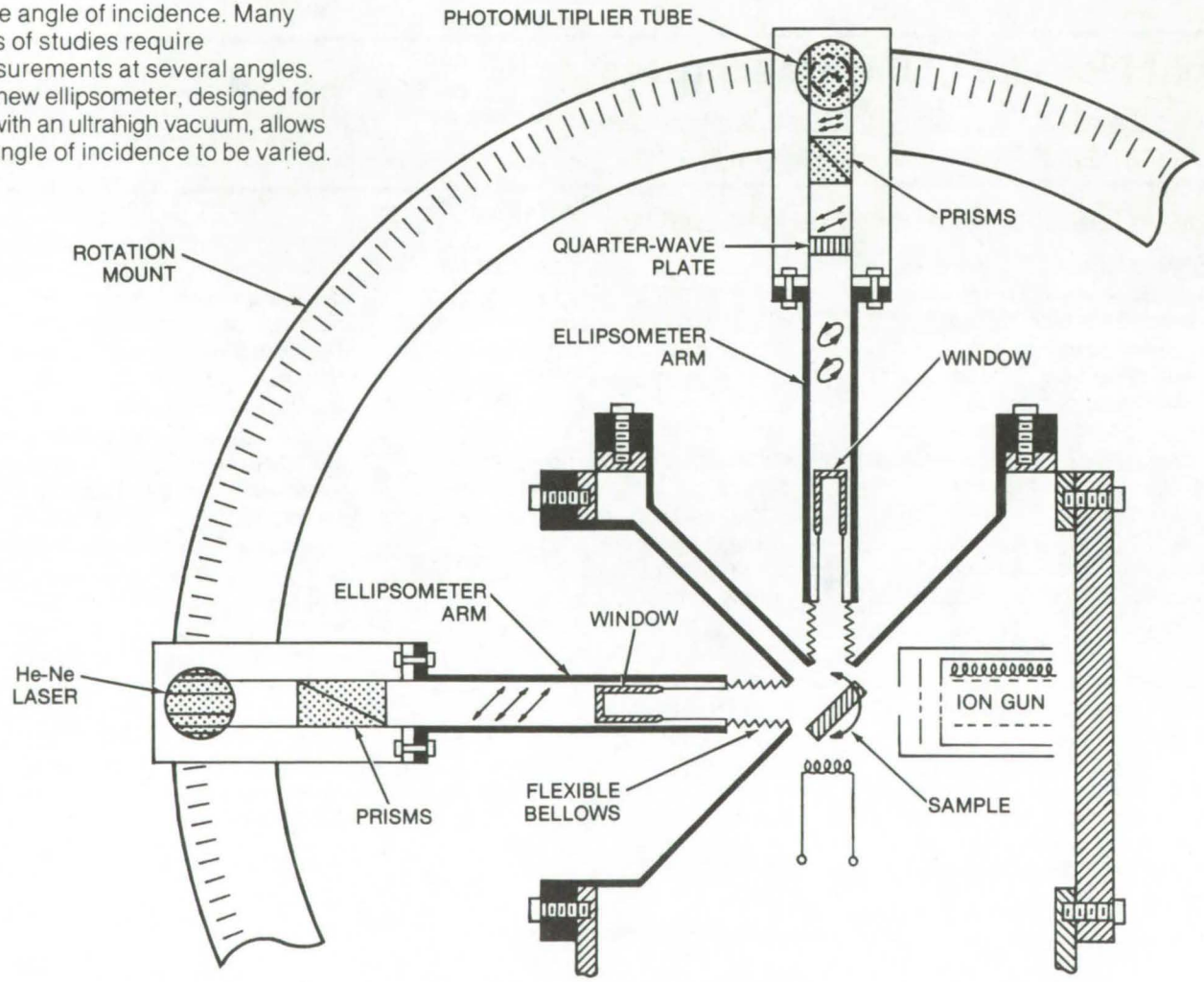

Both **Ellipsometer** arms can be rotated concentrically and independently by means of large precision ball bearings (not shown). The sample to be studied is positioned in the chamber with its surface coincident with the axis of rotation of the ellipsometer arms.

steel adapters with ultrahigh vacuum flanges.

Finally, the windows are attached rigidly to the ellipsometer frame. With a rectangular sample chamber, this system can be used at angles of incidence from 27.5° to 65° and has an accuracy of 0.0125°.

This work was done by H. U. Walter, L. A. Weitzenkamp, and P. N. Peters of **Marshall Space Flight Center.** *For further information, including details of the window assembly, Circle 26 on the TSP Request Card.*

Inquiries concerning rights for the commercial use of this invention should be addressed to the Patent Counsel, Marshall Space Flight Center [see page 2]. Refer to MFS-23130.

NASA

Calibration Source for Sensitive Optical Detectors

The spectrum of a simplified LED source for calibrating optical detectors does not change with age.

Langley Research Center, Hampton, Virginia

A light-emitting diode (LED) can be used as a constant-wavelength source to calibrate photomultipliers, photon counters, monochromators, and polychromators. Because an LED emits cold light, its luminous spectrum does not change with a decrease in intensity or age as does that of a tungsten lamp. LED composition and junction temperature determine its spectral characteristics. If the device is maintained near room temperature, the wavelength of the emitted light remains constant. It is this characteristic that makes the LED an excellent calibration source.

The source consists of an LED mounted in a housing which is physically compatible with the detector housing. Thus, when the two are mated, a lighttight enclosure is formed. All other components may be enclosed in a minibox to form a one-piece package. A typical circuit for an LED source is shown in the figure. The LED, for example an MV10B3, has a battery power source. Current flow is limited by series resistors R_1, R_2, R_3, and R_4 which are selected by range switch SW-1. This allows for the convenient selection of light levels to give calibration points in the range of the detector.

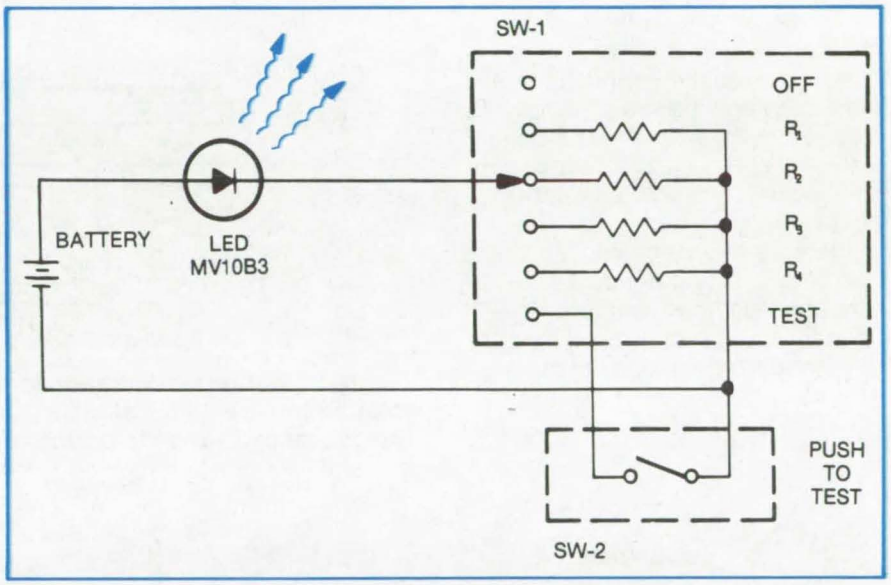

The LED Calibration Source is packaged in a housing compatible with most detector housings. Using a carbon-zinc or a mercury battery, the circuit may be left on continuously to improve stability by avoiding surface-charge accumulation during the off cycle.

The detector is protected from overexposure by range switch SW-1. The switch must turn on the smallest current flow and the lowest light level first. Additional protection for the detector is provided by the test position of the range switch. The switch must be in this position before push-to-test switch SW-2 can complete the circuit for a full intensity test of the LED. This function also provides a test of the battery.

LED's having wavelengths from infrared through the visible portion of the spectrum are commercially available and provide low-cost, stable, and convenient sources for calibrating almost any photo-optical detector. Very narrow lines are obtainable with the use of suitable filters.

This work was done by Bill T. Baugh of **Langley Research Center.** *No further documentation is available.*
LAR-11625

NASA

Measurement of Transient Reflectance

A new reflectometer can measure rapidly changing reflectances and is not susceptible to environmental contamination.

Marshall Space Flight Center, Alabama

A reflectometer is an instrument used to measure reflectance from a surface. Its uses include monitoring thin-film growth and testing the quality of mirrors. However, some applications are limited because the instrument is susceptible to environmental contamination, and it also cannot be used to measure rapidly changing reflectances. A newly-designed real-time reflectometer overcomes both these problems.

With the real-time reflectometer, measurements can be adjusted to a fraction of a second to monitor transient effects, and a sample can be exposed to its environment continuously. To minimize extraneous effects of the instrument, the reflectance and reference signals travel the same optical path. The only moving parts are the sample and one set of mirrors.

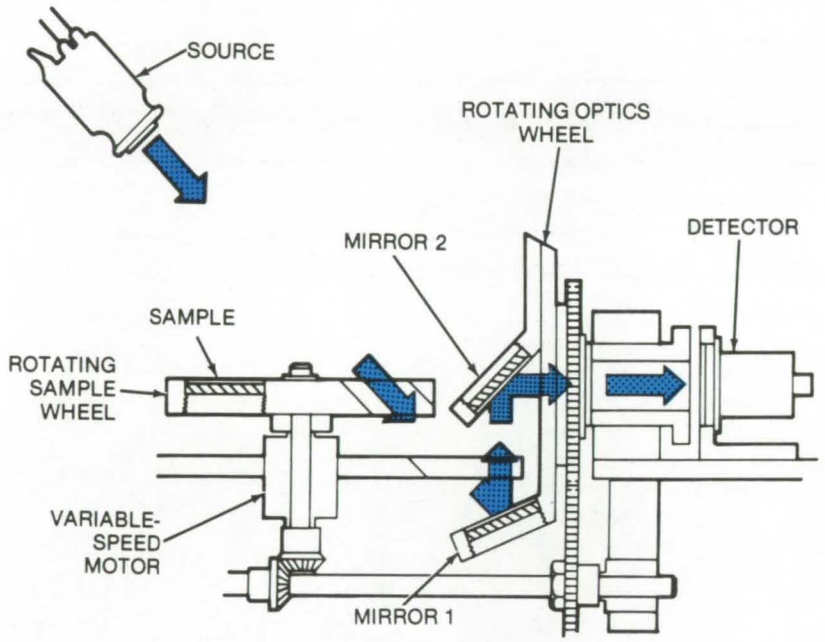

Figure 1. In the **Configuration for Reference-Signal Measurement,** the rotating wheel with the sample is positioned so that the sample is out of the optical path, and the beam is reflected to the detector by two mirrors.

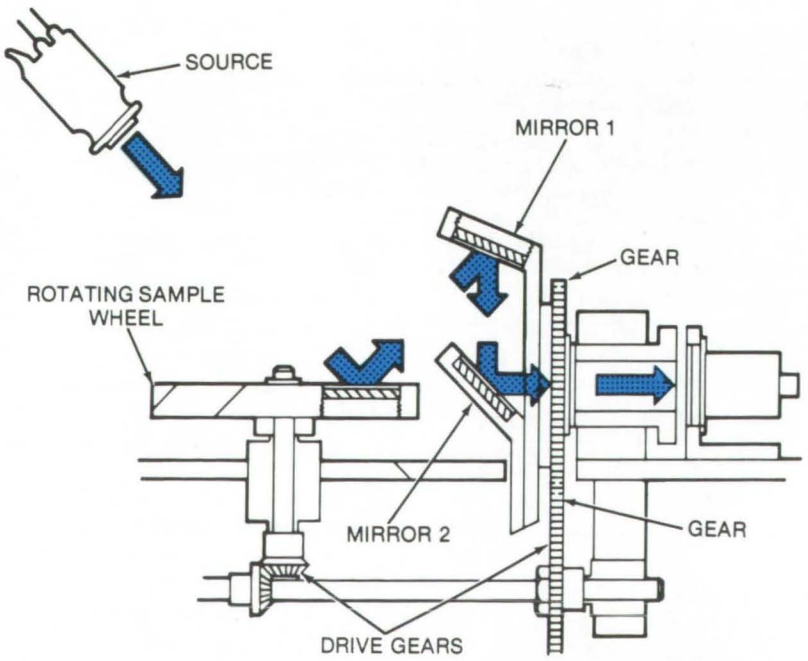

Figure 2. In the **Configuration for Reflectance Measurement,** the same mirrors are used, but the sample wheel and mirrors are rotated to place the sample in the light path.

The reflectometer is shown in Figure 1; the novel feature of this system is the optical-path configuration of the instrument. The source, the detector, and many other components are standard. It operates as a dual-beam reflectometer, but only one source is used. The two beams are created by changing the optical configuration of the instrument.

When a reference-signal measurement is to be made, the reflectometer is in the configuration shown in Figure 1. The rotating wheel containing the sample is positioned so that the sample is out of the optical path, and the beam is reflected to the detector by two mirrors. The sample and the two mirrors (also on a rotating wheel) can be moved to take a reflectance measurement as shown in Figure 2.

The rotating wheels are driven by a common drive shaft and gears that provide identical drive ratios to keep the wheels alined while rotating. The reflectance optical path has exactly the same components as the reference path with the exception of the presence of the sample. The measurement rate (sample-wheel rotation rate) is adjustable with a variable-speed motor.

This work was done by James M. Zwiener of **Marshall Space Flight Center.** *For further information, Circle 27 on the TSP Request Card. MFS-23160*

NASA

Improved Collimator for Imaging System

A high-energy-radiation imaging system has a pinhole collimator, a fiber optics scintillator, and a charge-coupled-device sensing array.

Marshall Space Flight Center, Alabama

Imaging systems for recording radiation such as gamma rays have applications ranging from the diagnoses of diseases to the inspection of welded joints. Present imaging systems, however, include coarse collimators which provide resolutions no better than 1/8 to 1/4 in. (3 to 6 mm). The collimators also have low sensitivity due partially to a 75 to 80 percent loss in the scintillation crystals.

An improved imaging system has a collimator consisting of a metal plate with many small-diameter holes and a fiber optics scintillator. It can increase system resolution to 1/23 in. (1mm) and reduce the scintillation loss to 25 percent.

The radiation is collimated by a multiplate tungsten collimator as shown in the figure. The collimator has a high coefficient of absorption and contains many small holes etched through the plates by photolithography. The collimated beams pass into a scintillator which is made of small-diameter optical fiber tubes. These tubes are of the optimal length necessary to accept the specified radiant energy range. They are partially filled with a scintillating material which converts high-energy photons to low energy ones, reducing the energy loss to approximately 25 percent.

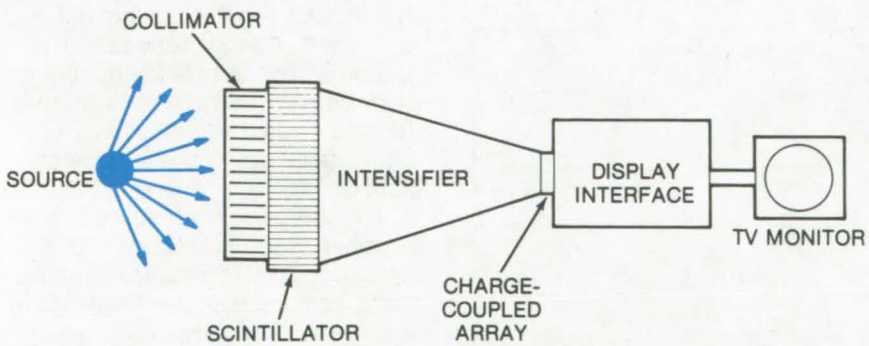

The **Improved Imaging System** has a multiplate pinhole collimator. The scintillator consists of small-diameter fiber optic tubes of a length optimal for each radiant-energy range. The fiber optics are doped with a scintillating material that converts high-energy photons to low-energy photons.

The photons then enter the intensifier tube which generates electron current in proportion to the photo input. These electrons, multiplied to some prescribed level, then impinge on a phosphor screen which emits photons. The photons are sensed by an array of charge-coupled devices, resulting in an image display on a TV monitor.

A composite scintillator constructed in this way reduces photo loss due to scattering from approximately 80 percent to about 25 percent, making it possible to reduce patient isotope dosages in medical applications. The light pipes are less than 1 mm in diameter and can thus provide excellent resolutions. Also, the charge-coupled devices are much more sensitive to photons than a standard vidicon or orthicon. They are potentially much less expensive, are less fragile, have a longer lifetime, require no warmup, and can operate on low power.

This work was done by Alvis M. Holladay and Carl T. Huggins of **Marshall Space Flight Center.** *For further information, Circle 28 on the TSP Request Card.*

Inquiries concerning rights for the commercial use of this invention should be addressed to the Patent Counsel, Marshall Space Flight Center [see page 2]. Refer to MFS-22863.

NASA

Holography With Surface Plasma Waves

Holograms are constructed using a surface plasmon resonance wave as reference beam.

Marshall Space Flight Center, Alabama

A new technique has been developed for making holograms using a surface plasma wave as the reference or object beams. Disadvantages of making holograms with surface waves have been:

a. The recording medium (a photographic emulsion) must be coated with a transparent material of a higher index of refraction than that of the medium itself, and the object light or the reference light must pass through this coating material.
b. Either the object light or the reference light must have large incidence angles in order to stimulate the surface wave.
c. Because surface plasmon resonances that are excited on blazed diffraction gratings are not used, the intensity of the surface wave cannot be controlled as effectively as with the new method.

The new technique consists of the following essential materials and steps:

a. A reflection-type diffraction grating of the type generally used in grating spectrometers is used. The grating must exhibit strong plasmon resonances (or polarization anomalies) when the incident light is p-polarized. If a grating has these resonances it can be shown experimentally. It has them if, under p-polarized light from a continuous source, narrow bright and dark bands appear in the diffraction spectra (bright for on-blaze and dark for off-blaze).
b. The grating is coated with a metal having a plasma wavelength (λp) shorter than those of the spectral region being used. For the visible region, for example, aluminum or silver is satisfactory.
c. The grating must be coated with a thin layer (on the order of 1 micron and preferably only a few hundred angstrom units) of high-resolution recording medium, having an absorption coefficient low enough so that incident light will not be appreciably absorbed before being reflected by the metal layer.

The hologram is made by first masking all but the top edge of the grating surface. The laser light is beam split so that one portion of it illuminates an object, the light from which in turn is incident on the grating. The top edge of the grating is exposed to the other portion of the laser beam (for example at 5145 Å from an argon laser), which has been spatially filtered, and is expanded about 50 cm from the grating surface. The surface wave is then stimulated. This is done by rotating the grating until one of the diffracted orders passes out of the field of view. When this critical angle is fixed, the mask can be removed (in darkness) from the rest of the grating and the hologram can be made in the usual way. The expanded light and surface wave stimulation serve as the reference beam. In Figure 1, reference beam R is incident on the grating and is diffracted into the propagating orders, 0, ± 1, and $+2$, and the surface wave -1. The hologram is formed when the surface wave interferes coherently with object light S.

To reproduce the hologram, the exposed grating is placed in the same position in the optical system. Light from the object is blocked off, and the reconstruction is made with the reference beam alone. The result is a superposition of several holographic images, real and complex conjugate.

In Figure 2, only reference beam R is used in the reconstruction. This beam again goes into the -1, 0, $+1$, and $+2$ orders. The -1 surface wave can itself be regarded as a new reference beam (R), is diffracted into its own propagating orders $(+1)$, $(+2)$, and $(+3)$. The dotted lines denote holographic

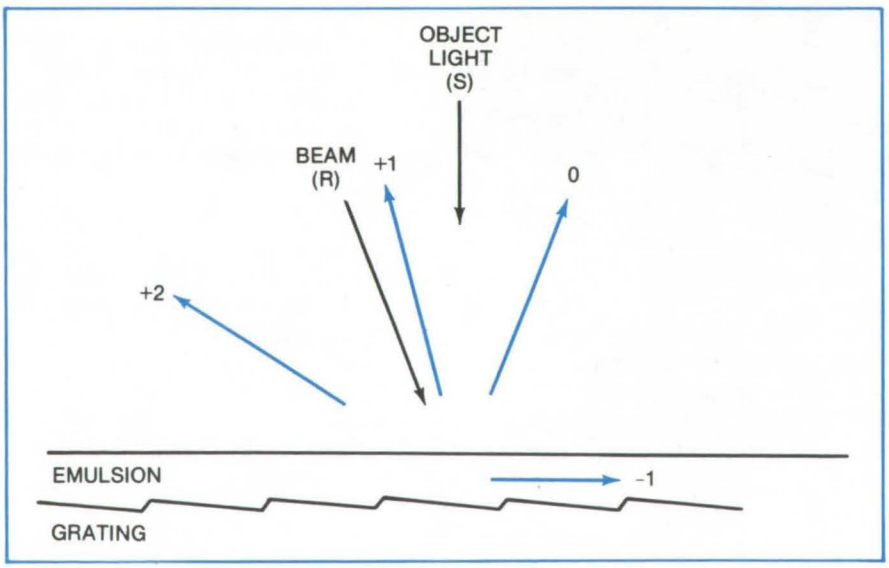

Figure 1. For **Construction of the Hologram,** reference beam R is incident on the grating and is diffracted into the propagating orders O, + 1, and + 2 and into the surface wave -1. The hologram forms when there is coherent interference with the object light S.

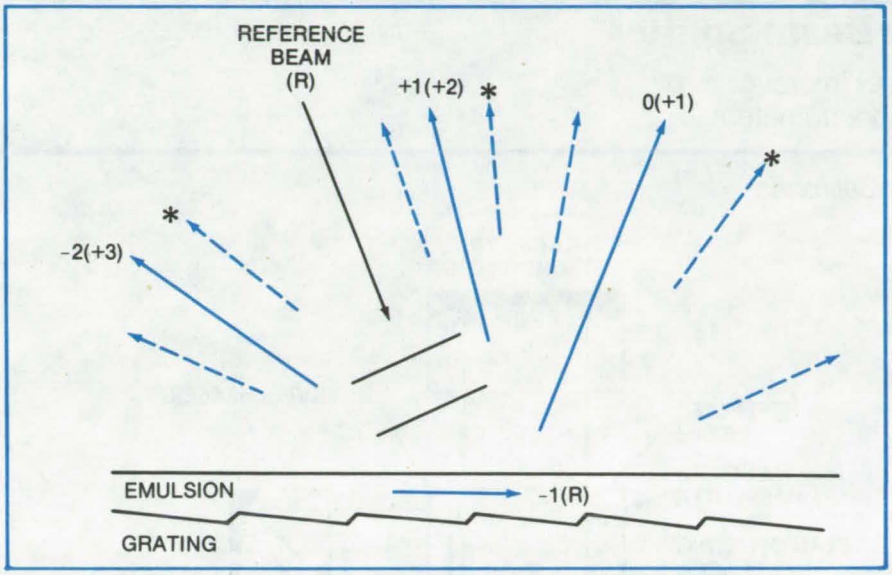

Figure 2. For **Reconstruction of the Hologram,** the reference beam R is again diffracted into the propagating -1, 0, + 1, and + 2. The -1 surface can be regarded as a new reference beam (R) which is, in turn, diffracted into propagating orders (+ 1), (+ 2), and (+ 3). The dotted lines are holographic images: the real component with no asterisk and the complex conjugate with an asterisk.

images, real (no asterisk) and complex conjugate (with asterisk). Because of the unique beam splitting properties of the diffraction grating, it should be possible to make an in-line hologram using ordinary noncoherent light of sufficient intensity.

This work was done by James J. Cowan of the National Academy of Sciences for **Marshall Space Flight Center.** *For further information, Circle 29 on the TSP Request Card.*

This invention has been patented by NASA [U.S. Patent No. 3,815,969]. Inquiries concerning nonexclusive or exclusive license for its commercial development should be addressed to the Patent Counsel, Marshall Space Flight Center [see page 2]. Refer to MFS-22040.

NASA

Beam Patterns of Light-Emitting Diodes

Infrared-sensitive film permanently records the light output of an LED. By optimizing the pattern, diode life is extended.

Goddard Space Flight Center, Greenbelt, Maryland

A new method for determining the output beam pattern of an infrared (IR) light-emitting diode permits a more efficient utilization of its power output, thus enabling it to be operated at reduced current so that longer operational life is obtained. The method is quick and easy to implement. IR-sensitive film, placed at various source-to-detector distances, records the output beam pattern of the LED. This information is then used to determine the optimum position of the detector surface so that it will intercept the maximum amount of radiated power.

Because this procedure produces a permanent record of the output beam pattern, it may be used in part inspection. Those devices having anomalous beam patterns can be identified and the appropriate action taken. Other possible applications are in failure analysis or system design parameter determinations.

This work was done by Edward F. Thomas, Jr., and Samuel R. Floyd of **Goddard Space Flight Center.** *No further documentation is available. GSC-11890*

NASA

Hydrogen Chloride Test Set

Atmospheric hydrogen chloride is selectively detected by its reaction with a tertiary amine. The reaction is monitored on a microbalance, and the reaction of approximately 10^{-8} gram of HCl has been detected.
(See page 73.)

Selective Image Enhancement

A digital image-enhancement technique for TV systems can also be used with remote manipulaors. An algorithm is used to divide an image into pixels, which may be individually enhanced. Enhancement may be controlled with a joystick. A similar arrangement simplifies remote manipulator operation.
(See page 29.)

Improved Interferometer Beam Splitter

A new drive system and beam splitter improve resolution of Fourier interference spectrometers.

NASA Pasadena Office, Pasadena, California

In a previous Fourier interferometer, a moving-coil actuator was used to change the optical path length to obtain interferograms. Weight restrictions limited the moving-coil actuator design to only 1 cm, but 2 or 3 cm are required to improve resolution significantly. Also, a moving-coil actuator designed for larger, low-frequency movements would necessarily have a poor response to higher servo-correction frequencies.

To obtain a broader range of movements, one cat's-eye retroreflector has been attached to a motor-driven lead screw. This allows relatively-large, low-frequency changes in optical path length. Smaller-amplitude, mid-frequency movements are obtained by employing a moving-coil actuator attached to the other retroreflector, and very-small-amplitude, high-frequency movements are achieved by employing a piezoelectric transducer attached to the secondary mirror of the same retroreflector. The motor-driven lead screw amplifies the displacement of the moving coil. The motor-driven lead screw could be designed to move 1 m or more in a very-high-resolution instrument.

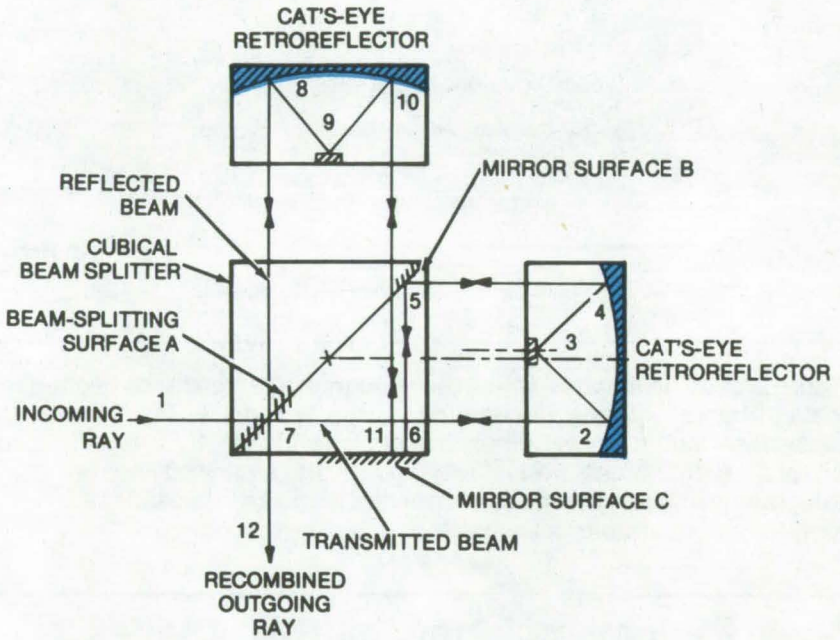

Figure 2. In the **"Single-Mirror" Beam Splitter** both rays are returned by the same mirror surface, C. The mirror at point 3 is offset to direct the transmitted ray path to mirror B to provide a different path length.

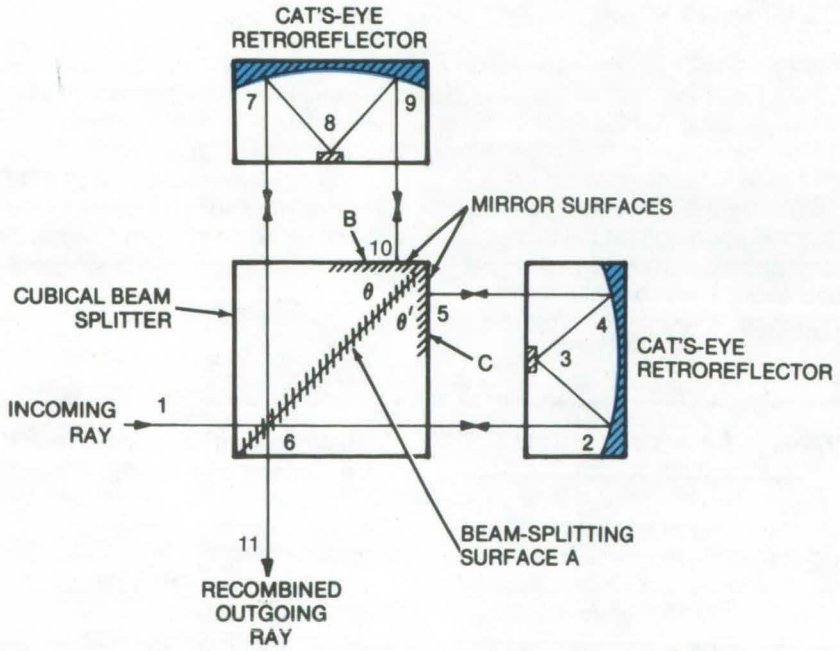

Figure 1. In a **Conventional Beam Splitter** the angles Θ and Θ′ must be made to precise tolerances or the returning rays will not be alined.

In the new scheme, the moving-coil-actuated primary mirror is linked to a potentiometer or other positional sensor. Whenever there is a positional offset of the feedback potentiometer (and of a reference potentiometer used for initial setting), a dc voltage is applied to a differential amplifier in either polarity. The lead screw will be actuated in response to signals flowing through the moving-coil actuator so as to drive to the next fringe. Since both cat's-eyes are movable, the low-frequency-response, lead-screw drive can be made to move relatively farther, allowing the mid-frequency-response, moving-coil actuator to be smaller.

A new configuration of the cubical beam splitter was also designed. Previously, two mirror surfaces adjacent to the beam-splitting surface caused beams to make two passes through the instrument. Figure 1 shows the conventional cubical beam splitter and two cat's-eye retroreflectors. The angles Θ and Θ' formed by the junction of each mirror surface with the beam-splitter surface had to differ by less than 1 second of arc, and this necessary precision made fabrication very difficult.

The newly-designed beam splitter has only one mirror surface adjacent to the beam-splitting surface. Since the transmitted and reflected beams are returned by the same mirror (see Figure 2), the positioning of the mirror is not as critical. To separate the light paths 5-6 and 10-11 (Figure 2), so that only the transmitted beam strikes mirror B, the secondary mirror at 3 has been moved off the centerline as shown.

This work was done by Rudolf A. Schindler of Caltech/JPL for **NASA Pasadena Office.** *For further information, including a description of the lead-screw drive system, Circle 30 on the TSP Request Card.*

Title to this invention, covered by U.S. Patent No. 3,809,481, has been waived under the provisions of the National Aeronautics and Space Act [42 U.S.C. 2457(f)] to: California Institute of Technology, Pasadena, California 91109.
NPO-11932

NASA

Determination of Radiative Current in LED's

The operational efficiency of an LED can be analyzed using a technique for determining the radiative and nonradiative currents.

Goddard Space Flight Center, Greenbelt, Maryland

Operational efficiency of GaAs light-emitting diodes (LED's) can be evaluated by knowing the percentage of current that contributes to the radiative output. This current, however, cannot be measured directly. Instead it is determined graphically from the LED current-voltage (I-V) plots (see figure).

In LED's a directly measurable quantity is the total forward current I_f. It is a combination of radiative and nonradiative current components. When the applied forward voltage V_f is below 1.05 V the I_f is primarily nonradiative and varies with V_f as the exp(qV/2kT), when q is the charge, V is the applied voltage, k is Boltzmann's constant, and T is the operating temperature. For any given LED the nonradiative current can be determined experimentally by using, for example, a V_f of 0.8 V and measuring the corresponding I_f. A line having a slope of q/2kT is plotted as shown on the graph (semilog) passing through the data point measured at a V_f of 0.8 V.

When the voltages exceed 1.05 V the I_f begins to deviate from the straight line (semilog) due to the radiative component entering the picture. The difference between the two curves is the radiative component, which is determined by subtracting the two curves at any given

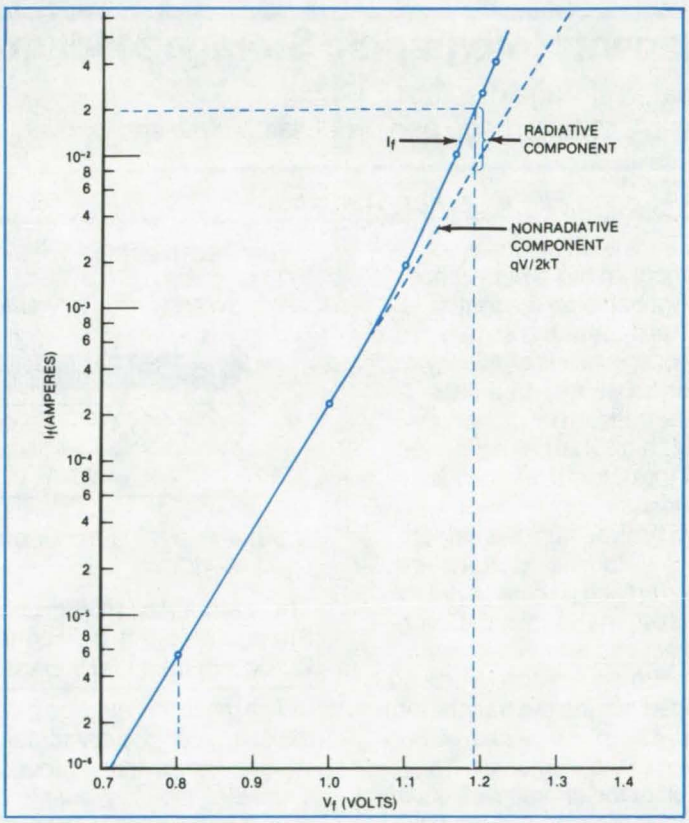

The **Current-Voltage Characteristic** for a typical GaAs light-emitting diode.

V_f. For example, at 1.19 V the I_f is 2.00×10^{-2} A while the nonradiative current is 8.2×10^{-3} A. Subtracting the nonradiative current from the total I_f yields the radiative current of 1.18×10^{-2} A, which is 59 percent of the total I_f.

This work was done by Edward F. Thomas of **Goddard Space Flight Center.** *For further information, Circle 31 on the TSP Request Card.*
GSC-12034

NASA

Voltage Control for Corona Charging Thermoplastics

An aperture is used to control the voltage of a charge deposited on a thermoplastic holographic film.

Marshall Space Flight Center, Alabama

A technique has been developed to control the voltage of a charge placed on a thermoplastic used as a holographic storage medium in an optical memory system. The charge is placed by a corona, and precise voltage control is an important consideration. Too high a voltage may cause breakdown, and too low a voltage will reduce the sensitivity of the optical memory system. Precise control is difficult to obtain because the corona charging is a function of many variables, such as the condition of the thermoplastic, air currents, and dirt.

The voltage can be controlled by placing a metal plate with a hole in it, near the surface of the thermoplastic film. Experiments have shown that the voltage on the thermoplastic will not rise above that of the metal plate. The hole on the plate is made slightly larger than the spot to be charged, and the plate is held at the voltage desired at the surface of the thermoplastic. During charging, the thermoplastic will accumulate charge only until it reaches the voltage of the plate; after that, all the charge will be deflected to the plate. A further use of this technique could be to vary the voltage on the surface of the film to control the response of the storage medium.

This work was done by R. S. Mezrich of RCA Corp. for **Marshall Space Flight Center.** *For further information, Circle 32 on the TSP Request Card.*
MFS-23102

NASA

Permanent Holographic Storage Medium

A laminated storage medium for holographic data-storage and processing systems

Marshall Space Flight Center, Alabama

A new laminated holographic-storage medium has a high write sensitivity and a high readout efficiency. The structure is shown in the illustration. It consists of five layers: (1) a glass substrate, (2) a transparent electrode, (3) a photoconductor, (4) a thin barrier layer, and (5) an RTV electric-field-polymerizable elastomer.

The storage medium is charged, and then it is illuminated by the hologram interference pattern to deform the RTV elastomer. While the interfering object and reference beams are on the storage device, a corona is developed around the transparent electrode. This places a charge on the surface of the elastomer. The distribution of the charge reflects the data (intensity patterns) in the hologram beam. This occurs because the high-intensity portions of the beam make the photoconductor more conductive at the data sites. These regions conduct more charge through to the elastomer.

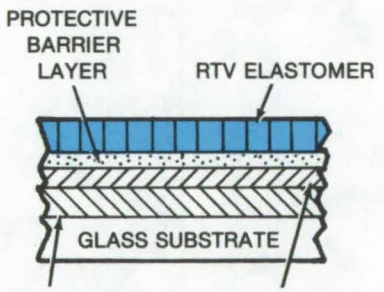

The **Laminated Holographic Storage Medium** is used to store a hologram on an RTV elastomer.

The mechanical force between the charge on the elastomer and an imaged charge in the ground plane depresses the elastomer in regions of high conductivity. These depressions become deeper and deeper until the dielectric breakdown voltage of the elastomer is reached (about 100 V). At this point the elastomer is placed in a permanent thermoset condition by electric-field-induced polymerization and crosslinking.

The photoconductor is poly-n-vinyl carbazole. The elastomer is a commercially available silicone rubber, spun on at 1,800 rpm with 3.14 g of resin, 0.31 g of hardener, and 40 cc of n-hexane solvent. Because the n-hexane can dissolve the photoconductor, a thin barrier layer of 1,200 Å of highly crosslinked and polymerized styrene is deposited before the RTV elastomer.

This work was done by Robert A. Gange of RCA Corp. for **Marshall Space Flight Center.** *For further information, Circle 33 on the TSP Request Card.*

Inquiries concerning rights for the commercial use of this invention should be addressed to the Patent Counsel, Marshall Space Flight Center [see page 2]. Refer to MFS-22588.

NASA

Electrode Structure for Uniform Corona Discharge

A corona discharge is used to uniformly charge a thermoplastic holographic-storage medium.

Marshall Space Flight Center, Alabama

One class of holographic memories consists of a thermoplastic material that is deformed by the data-carrying laser beam. The laser beam selectively activates a photoconductor which transfers charge to the thermoplastic in regions corresponding to areas of high intensity in the beam. This scheme requires that a uniform charge be placed on the surface of the thermoplastic. Grid structures were tried for deposition of the charge, but they could not provide the desired uniformity.

It was found that a uniform charge could be applied using a single corona-discharge needle. The system is shown in the illustration. The needle is symmetrically separated from the deformable surface and is connected to a flat electrostatic transparent shield (transparent electrode). The distance from the needle to the thermoplastic is about 1 in. (2.5 cm) to provide a charge shadow larger than the area over which a charge is to be deposited.

The needle is 1/2 in. (1.3 cm) long. It is held in a hole drilled ultrasonically in the transparent electrode, which is a glass substrate coated on one side with a transparent conductor. The plane of the transparent electrode is parallel to the deformable surface, and the distance between the needle and the surface is controlled by four threaded screws that connect the needle assembly and the storage device.

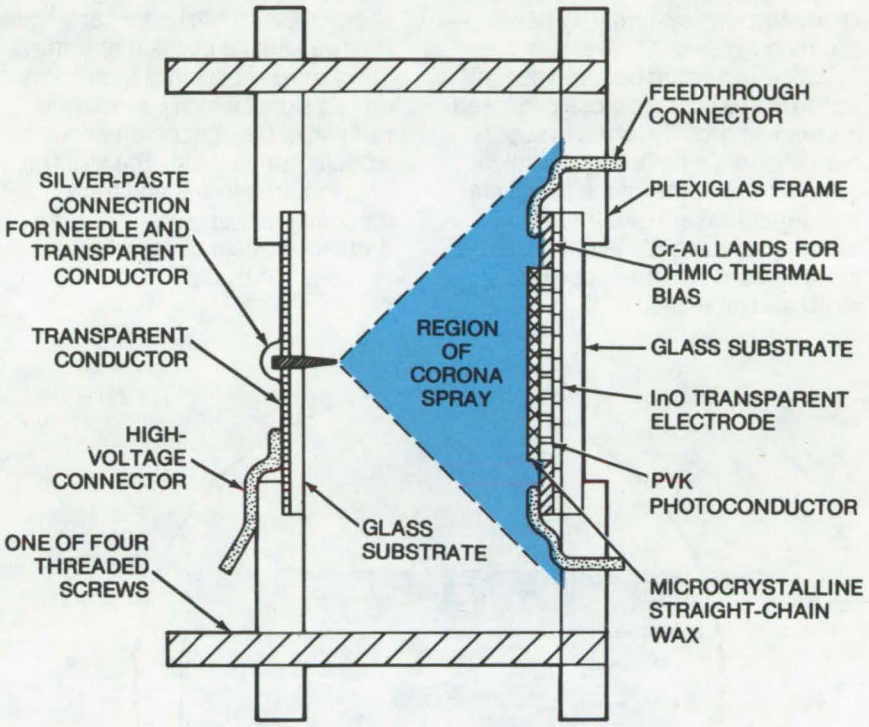

The Optical-Memory Charging Configuration was developed to generate a corona discharge that will uniformly charge a thermoplastic medium (the straight-chain wax above).

This work was done by Robert A. Gange and Carl C. Steinmetz of RCA Corp. for **Marshall Space Flight Center.** *For further information, Circle 34 on the TSP Request Card.*

Inquiries concerning rights for the commercial use of this invention should be addressed to the Patent Counsel, Marshall Space Flight Center [see page 2]. Refer to MFS-22617.

NASA

Triple-Layer Bubble-Domain Film

A stratified composite has a layer of magnetic bubble-domain material and dual layers of magnetic material on either major surface of the bubble domain. Translational velocity and wall velocity of the bubble domain are enhanced, and hard bubbles and coersive-field inhomogeneities are reduced.
(See page 14.)

Improved Microbridge Josephson Devices

Microbridge Josephson elements are protected against temperature-induced noise currents by a dense semiconductor (germanium) overcoating. Sensitivity is not limited. The germanium is deposited in layers by repeated sputtering. Test procedures are given.
(See page 20.)

Anamorphic Lens for Tracking System

A lens with a magnification on one axis twice that on the other improves the accuracy of a tracking system.

NASA Pasadena Office, Pasadena, California

An improvement made in an aerospace tracking system may have application to navigational systems and to optical-scanning pattern-recognition systems such as those proposed for reading grocery labels in supermarkets. In a modified star-tracking system the position of the target star is determined with greater accuracy using an anamorphic lens, similar to those used in CinemaScope photography and projection.

In a star tracker an image dissector tube is utilized for sensing the relative angular position of a star. The angular position is then converted to a signal which controls the rotation of the spacecraft about its roll axis during flight. The star tracker is required to see and track a particular star anywhere within a rectangular field of view that is typically 10° by 30°.

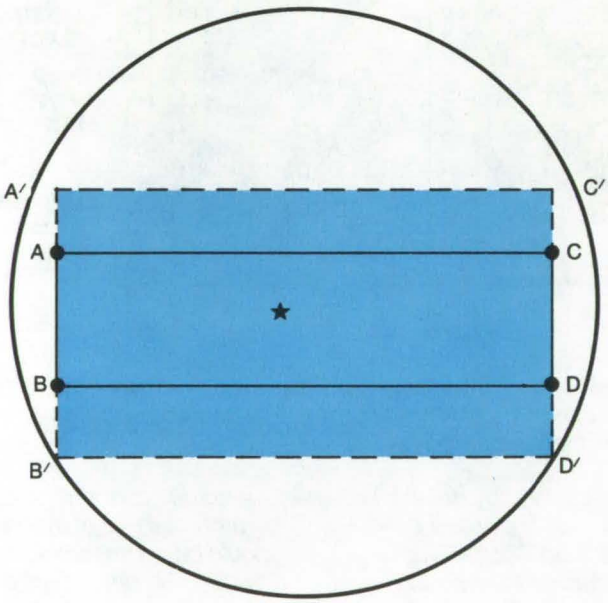

Figure 1. The **Star Tracker Field of View** projected on the image detector tube by a conventional lens system is the rectangle ABCD. The signal-to-noise ratio for up-and-down target displacement is improved by using an anamorphic lens to project an image rectangle with the increased dimension A′B′.

This field of view is imaged on the circular photocathode of the image dissector tube by a lens system which projects a rectangular image field bounded by points A, B, C, and D, as shown in Figure 1. The roll axis lies parallel to lines A-B and C-D. The aim is to maintain a star, for example Canopus, centered along the roll axis on the photocathode. The movement of the star image upward or downward produces a compensating movement of the spacecraft (by means of the roll axis attitude control system) which tends to offset the apparent star movement.

An anamorphic lens with a 2:1 focal-length ratio has been designed (see Figure 2). It consists of three spherical elements (excluding the faceplate of the tube) and two cylindrical elements. The total length of the lens from the entrance pupil to the photocathode is 7.6 cm (~3 in.). The lens was designed to minimize image spot size, with emphasis on the roll dimension, and to optimize spot location for each of four object points. These objects were located on the axis, 10° off the axis in cone, 20° off the axis in cone, and 5° off the axis in roll.

The expected root-mean-square noise equivalent angle with this lens at 1X Canopus illumination, assuming the use of the present 1.2-cm aperture, a 34-μA/lumen cathode, and a 0.1-s time constant, would be approximately 6 arc seconds. It is thought that further effort may produce a lens system having a noise level only one-third of that of previous lens systems.

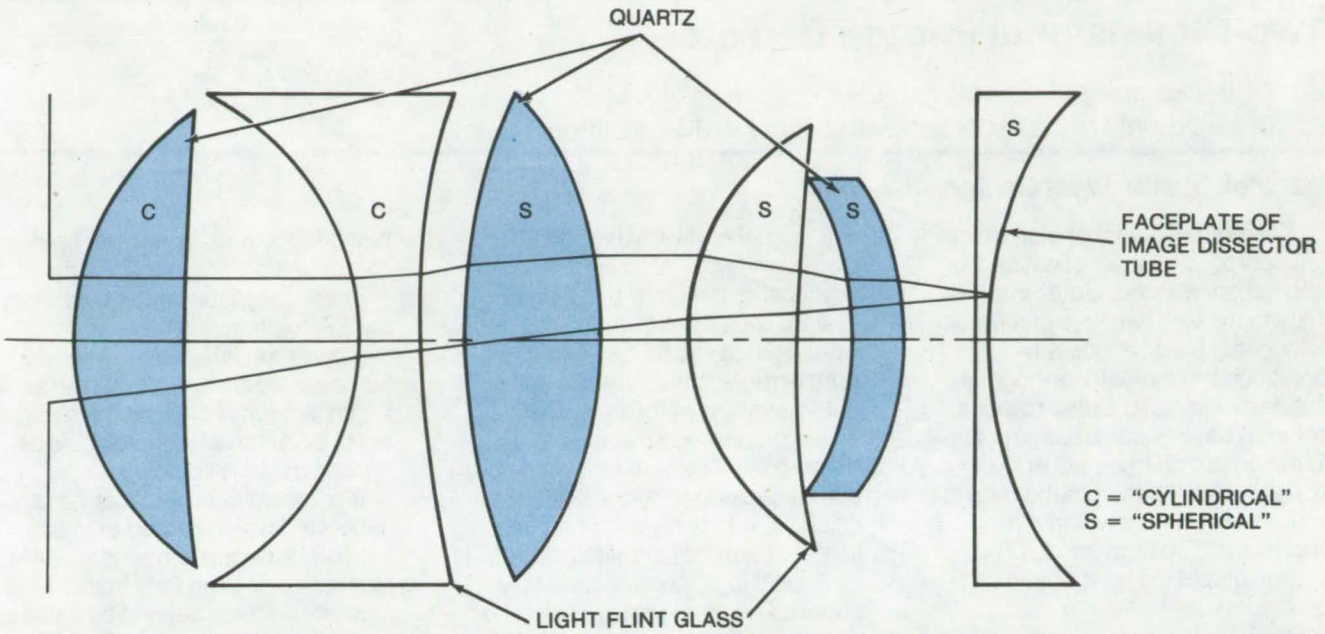

Figure 2. The **Anamorphic Lens System** is shown along with the faceplate of the image dissector tube and two ray paths. Having two cylindrical elements and three spherical elements (not including the faceplate), the lens has a focal-length ratio of 2:1 and a length of 7.6 cm.

This work was done by Richard H. Burns and Louis F. Schmidt of Caltech/JPL for **NASA Pasadena Office.** *For further information, Circle 35 on the TSP Request Card.*
NPO-13062

NASA

Solar Selective Surfaces

A simplified, low cost method of production

Lewis Research Center, Cleveland, Ohio

A new method of producing solar selective surfaces has been developed. The method consists of applying a high absorptance coating onto a thin film or foil of a low emittance material. The thin film solar selective surface is then bonded to a solar collector panel surface.

This new method has many advantages over the current coating practices of electroplating, vacuum deposition, chemical reaction, painting, etc., each full size solar collector panel. Strips or panels of film can be coated in smaller tanks than those needed for coating full size solar collector panels. In strip form, the film can be coated in a continuous operation, and handled and stored in rolls. Continuous coating also allows the quality of the finished product to be better and more easily controlled, resulting in a more uniform coating and a better quality product.

The solar selective film can be readily cut and fitted to solar collector panels of varying sizes and shapes. The flat geometry of films and foils reduces the amount of solar panel surface preparation required. The surface finish of the solar collector panel can be somewhat irregular but should be reasonably smooth, enough to allow a good bond to form between the film and the collector panel. Films can be applied to the collector panels with adhesives, solder, or any bonding agent appropriate to the type of film used.

An example of a thin film solar selective surface is black chrome electroplated onto aluminum foil. The aluminum foil is then glued or soldered to the surface of a solar collector panel.

This work was done by G. McDonald and R. W. Lauver of **Lewis Research Center,** *P. Baumeister of University of Rochester, and A. C. Benning of Harshaw Chemical Company. No further documentation is available.*

Inquiries concerning rights for the commercial use of this invention should be addressed to the Patent Counsel, Lewis Research Center *[see page 2]*. *Refer to LEW-12614.*

NASA

Two-Dimensional Photon Detector

A matrix-like array of detectors allows data from N x M picture elements to be recorded with only N + M amplifiers.

Marshall Space Flight Center, Alabama

A two-dimensional photon detector incorporates a set of cascaded microchannel-array plates in proximity focus with two sets of mutually-orthogonal linear anodes. In operation the mutually-orthogonal anode arrays (also called row and column) have equal areas exposed to the output charge packet. For correct focusing the charge packet is divided evenly between a row anode and a column anode. Thus, a charge output signal is obtained corresponding to the intersection point of the row and column anodes within the array.

Using this technique, photometric data from a total of (N × M) pixels (picture elements) can be recorded with a total of (N + M) amplifiers. Considering 512 amplifiers to be a practical upper limit, this type of system is capable of recording data from as many as 65,536 pixels. Furthermore, the array can be laid out in a variety of formats.

To demonstrate this new structure a breadboard system has been constructed, using a 32-by-32 (1,024 pixels) anode array requiring 64 amplifiers and discriminators plus additional logic control circuits, as shown. The anode array is mounted on a printed-circuit board which, in turn, is mounted on an assembly of charge amplifiers. Each anode is connected to a charge amplifier, the output of each charge amplifier being fed to a variable-threshold discriminator/one-shot circuit.

In operation the digital data from the 32-column amplifiers and the 32-row amplifiers are fed into two 32-line to 5-line binary encoders. When a column event and a row event occur simultaneously, as determined by the coincidence detection logic, an event pulse is generated which is used to initiate the random-access-memory (RAM) storage cycle. The data in the memory address defined by the two binary encoders are read into an external data register and then are incremented by one count (corresponding to the detected single photon event). The new data word is

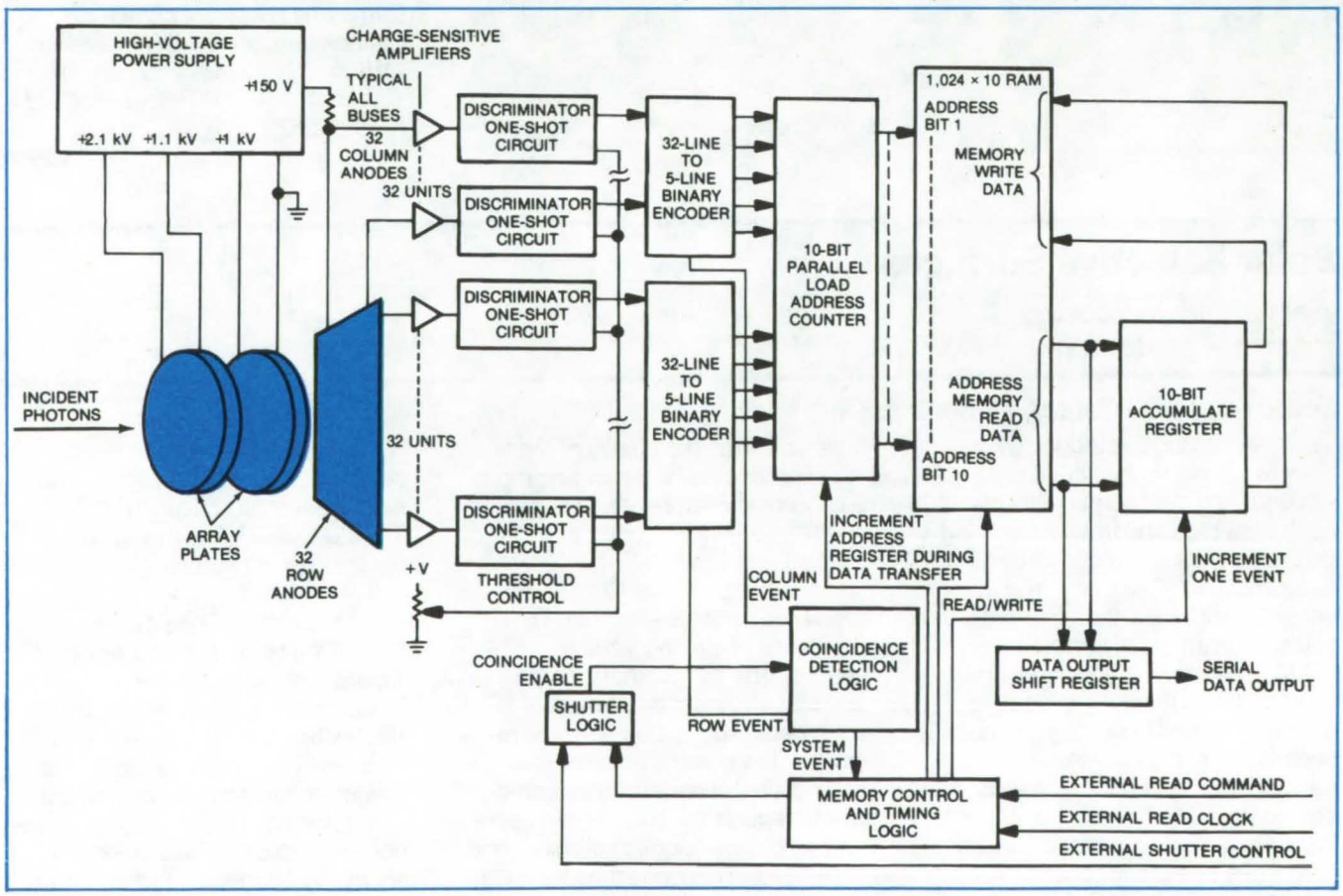

In the **Two-Dimensional Microchannel-Array Photon Detector,** bits from an anode array are processed through charge amplifiers and fed to a variable-threshold discriminator/one-shot circuit. Following encoding, simultaneous detection of array pulses activates the RAM. Logic entered into the external register is incremented by 1 count, after photon detection. Processed bits are then fed back to the original memory.

then reloaded into the original memory location. The total cycle time of this system is 1 microsecond, allowing a maximum counting rate of 10^5 counts/second (Poisson arrival) to be detected by the anode array.

At the end of the preselected integration period, the data in the system memory may be transferred to the display system memory for any subsequent data reduction or display. This permits nondestructive manipulation of the stored data in parallel with the storage of new data in the system memory.

This work was done by J. Gethyn Timothy of Harvard College Observatory and Richard L. Bybee of Ball Brothers Research Corp. for **Marshall Space Flight Center.** *For further information, including a description of the anode construction, Circle 36 on the TSP Request Card.*

Inquiries concerning rights for the commercial use of this invention should be addressed to the Patent Counsel, Marshall Space Flight Center [see page 2]. Refer to MFS-23325.

NASA

Polishing Technique for Beryllium Mirror

Repolishing a coated beryllium X-ray mirror increases efficiency and resolution.

Marshall Space Flight Center, Alabama

A polished Kanigen-coated beryllium mirror for a soft X-ray telescope has been performance tested. Polishing increases the mirror efficiency from 0.06 percent to 3.26 percent for X-rays at 8 Å (0.8 nm). The mirror resolution is increased from approximately 15 to 3.75 arc-seconds. The overall effect is to make performance comparable to previously-tested fused silica mirrors.

The tests were accomplished by inserting the entire X-ray telescope, including the polished mirror, into a vacuum line 220 ft (67 m) long and taking photographs of an X-ray resolution source. The mirror performance was then evaluated as a function of distance from the focal plane and angular distance with respect to the telescope axis. Other tests were also made in which a point source was used to study the imaging characteristics by means of a pinhole and a proportional counter placed in the telescope focal plane. X-rays were produced by an essentially monochromatic 8.34-Å (0.834-nm) aluminum source, with small contributions from 8-Å (0.8-nm) K_β and 6.94-Å (0.694-nm) tungsten radiation.

The photographs were made using a 12-wire filament configuration which produced a uniform X-ray intensity. A bar-and-dot resolution chart is used for all photographs. The bar sets and dots provide angular resolutions between 0.94 and 5.3 arc-seconds. Using the camera provided with the telescope and various types of film, both vertical and horizontal graphs ranging from 2.65 to 5.3 arc-seconds angular resolution could be resolved. This indicates that for a well polished mirror the resolutions of the telescope may be limited by the film rather than by scattering from the mirror surface.

In further tests, a 10-arc-second point source was examined by sweeping a pinhole 7.62×10^{-3} cm (0.003 in.) in diameter (9 arc-seconds) across the image in 3-arc-second steps until a 30-by-30-arc-second matrix was formed around the peak of the point source. Scan contours of the source were then made to give an indication of the scattering property of the mirror.

The efficiency is computed by measuring the flux incident on the mirror and comparing that with the intensity recorded behind the 9-arc-second pinhole. The efficiency represents the intensity from a 10-arc-second source that is focused on a spot of 9 arc-seconds diameter. The number at the peak is the efficiency of the mirror at 8 Å (0.8 nm). Both the absorption in the mirror and the scattering of intensity away from the focused beam will affect the efficiency measured.

The efficiency for this telescope using the 9-arc-second pinhole data is as follows: for 8 Å (0.8 nm), 3.26 percent; for 13.3 Å (1.33 nm), 4.1 percent; and for 44 Å (4.4 nm), 1.37 percent.

This work was done by Joseph F. Froechtenigt of Martin Marietta Corp. for **Marshall Space Flight Center.** *For further information, Circle 37 on the TSP Request Card. MFS-22923*

NASA

Standard Aerosols for Particle Velocimeters

A particle sizer velocimeter provides standard aerosols of known size-distribution and velocity for use with laser-Doppler velocimeters.

Marshall Space Flight Center, Alabama

A portable particle sizer/velocimeter has been built to provide a source of standard aerosols of known size-distribution and velocity for use with laser-Doppler velocimeters. The system consists of a laser-scattering counter and a photographic system; both can function independently or together. In addition to its design use, the instrument may be employed in determining the size-distribution and velocity of particles in fluids, in the study of vortexes, and in the study of acoustic coagulation of aerosols.

The photographic system provides an absolute method of measuring aerosol size-distributions independently of their light scattering properties. Aerosol particles are photographed while falling in a glass chamber. Their velocity is determined by comparing timed photographs. This velocity can be due to convection plus the velocity predicted by Stokes' law for falling particles. The chamber is designed to eliminate convection, thus allowing the particle size to be determined from Stokes' law.

The laser-scattering counter (LSC) comprises a 1-mW, He/Ne laser, input optics, collecting optics, a photodetector, and signal-processing electronics. It is a forward-scattering instrument in which the scattered light is collected by a camera while the direct beam is stopped. By changing the input optics and signal processing, it can act as either a particle-size counter or a velocimeter. The LSC can be used in conjunction with the photographic system by fitting the two instruments together. The particles will then pass through an overlapping portion of the sensing (focal) volumes of both instruments.

This work was done by A. Deepark, R. Ozarski, and J. A. L. Thomson of **Marshall Space Flight Center.** *For further information, Circle 38 on the TSP Request Card.*
MFS-23075

NASA

Optical Bias Assembly

An auxiliary source, or bias, is used to achieve linear response in an optical detection system.

Lyndon B. Johnson Space Center, Houston, Texas

It is often desirable to have an optical detection system which responds linearly to changing input illumination levels. Many semiconductor detectors, however, have an illumination-dependent responsivity and response time. This means that the detector signal may be a nonlinear function of both the light intensity and its duration.

The response of the detector is determined by the sum of the input flux and the quiescent background flux falling on it. If the changes in the input flux are very small compared to the background flux, the signal is a nearly linear function of the input flux. On the other hand, if the input flux is large compared to the background, then the signal is a complex nonlinear function of the input flux. The magnitude of the nonlinearity is dependent upon both the input flux intensity and the duration of the illumination. When this latter situation occurs, a newly-developed optical bias source may be used to increase background illumination until the linearity of the detector signal is acceptable for the measurement to be performed.

The optical bias assembly consists of a tungsten bulb as a source, optical filters, a fiber optics assembly, an aperture mask, a relay lens, and a folding mirror. These are illustrated schematically. The intensity for each individual detector is controlled in two independent ways. In the first place, the light is brought from the source to the aperture mask by means of five separate coherent fiber bundles in each of which a level adjustment filter is placed. The selection of filters is broad enough to allow attenuation from zero (no filters) to extinction in any one fiber bundle.

In the second place, the other end of each coherent fiber bundle is mated to an appropriately sized and spaced aperture. Each aperture sends light to either two or three detectors. If necessary, a slight adjustment of the aperture mask in three dimensions provides a fine trimming of the amount of light reaching certain detectors. The mask is imaged onto the detector array by means of a relay lens and a

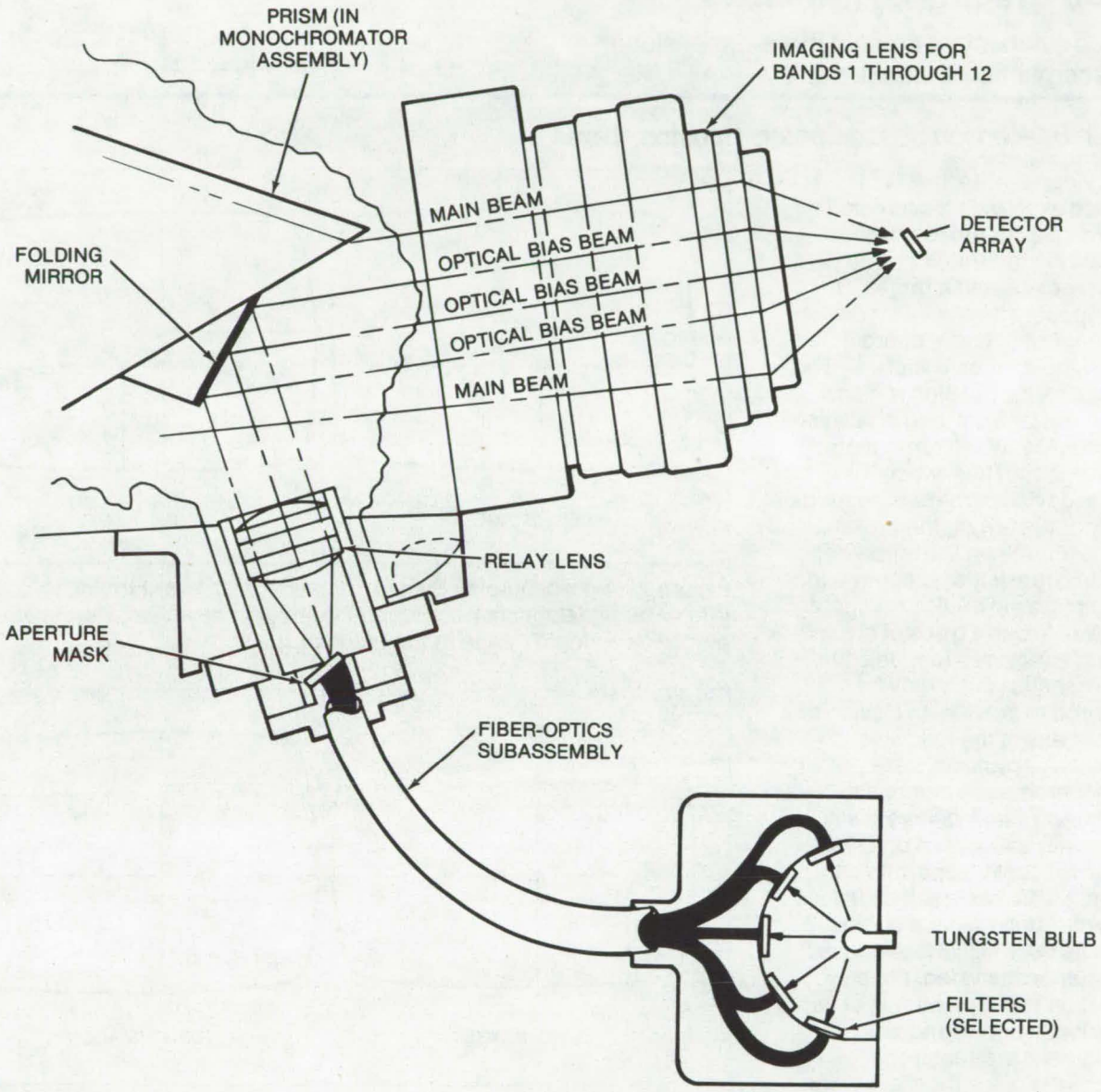

The Optical Bias System has a tungstun-bulb source that is coupled to the main assembly with fiber optics. This source provides sufficient background illumination to make the input, or main-beam, flux small compared to the background and thus makes the detector response a nearly linear function of the input flux.

folding mirror, since the optical bias assembly must not interface with the main optical path.

The light emitted by the apertures in the mask is passed through the triplet relay lens to a folding flat mirror mounted to the face of the last prism of the monochromator assembly. The folding mirror is optically located entirely within the obscuration of the main optical beam caused by the spin-mirror assembly. The optical bias assembly therefore does not interface with the main optical path. After reflection from the folding mirror, the optical bias reduction passes through the imaging lens and is focused upon the detector array.

The lens holder assembly holds the triplet relay lens; it also provides two-axis gimbal adjustment and two-axis lateral translation adjustment for optical alinement. Focus is adjusted during assembly by means of shims between the lens holder assembly and the light-and-filter assembly.

This work was done by Robert Weagant and Nancy Aldrich of Honeywell, Inc., for **Johnson Space Center.** *No further documentation is available.*
MSC-14412

NASA

Video Display Synthesizer

A video synthesizer depicts three-dimensional displacement on a planar display.

Lyndon B. Johnson Space Center, Houston, Texas

The video synthesizer (VS) is designed to provide a simulated stereo display of the relative positions and orientations of a terminal device and a target. The target appears as a dot with displacements in X and Y coordinates on a monitor screen (Figure 1). The terminal device position is also represented by a dot, and in addition its pitch and yaw are represented by a crosshair. Thus, when the terminal device camera is pointed directly at the target, the crosshair will be centered on the target dot.

The VS translates dc command voltages from an analog computer into any of several types of display. The output includes four dots and two crosshairs which may be configured to provide an illusion of depth via any of the following presentations: planar or stereo either in monochrome or color and if stereo, using dual monitors, a single monitor with split screen or a single monitor with color separation. In addition, the VS has a self-contained sync generator so that a complete composite video signal is developed. Using composite video, the only connection to the monitor is at its normal input, and no monitor modifications are required.

The center of the monitor screen represents the (0, 0, 0) coordinate position. The X and Y coordinate axes are in the plane of the screen, with the Z axis projecting outward toward the viewer. Using dual monitors or a single monitor with a split screen, displacements in the Z direction are simulated by superimposing suitably coordinated changes, ΔX in the X coordinate (Figure 2). This technique, however, has proved to be unsatisfactory from a human factors standpoint, as it was found to be difficult to converge the eyes on spots of light in different planes.

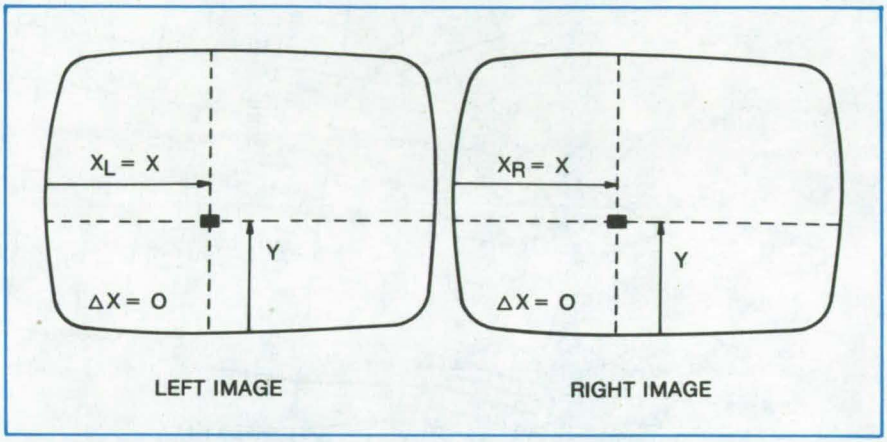

Figure 1. A Two-Display System presents a different image to each eye. When the two dots are positioned identically, as above, the viewer perceives a single image in the plane of the screen.

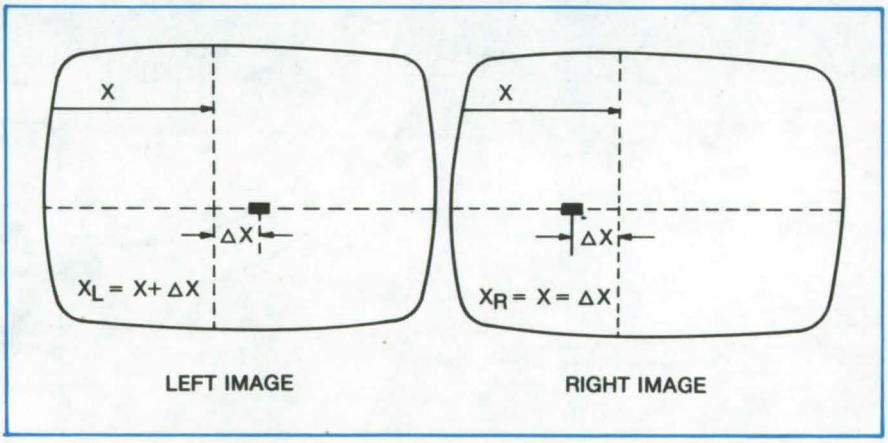

Figure 2. Motion in the Two-Display System appears to be in plane if the dots move identically. If the changes in their X coordinates are different, they appear to move perpendicular to the screen.

An alternative method based upon a color depth indicator was also devised. The target in this configuration is represented by a single blue dot on a color monitor. The end effector position is represented by a white cross. The end effector translation is represented by two dots — one red and one green, the horizontal separation represents the distance from the depth plane of the target.

When the manipulator end effector is closer to the camera than the target, the green dot is to the left of the red dot as in Figure 3a. As the end effector moves outward, the green and red dots move closer together until, as in Figure 3b, the dots merge into a single yellow dot when the end effector and the target are in the same depth plane. If the end effector moves farther out, the two dots

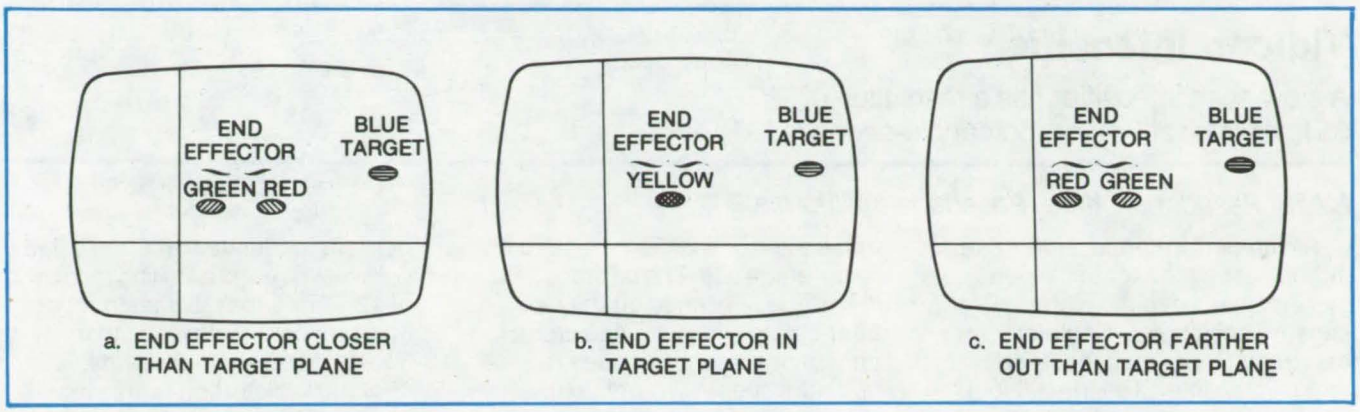

Figure 3. In the **Color Display System,** depth is indicated by the relative positions of a red and a green dot.

reappear, this time the red dot to the left of the green as in Figure 3c. Thus, the necessary depth information is displayed without the convergence difficulties encountered using stereo.

The video synthesizer can be applied in any situation where a three-dimensional displacement is desirable in a display. These displacements can be in response to computer or manual commands. Typical applications might be in rangefinders, object position indicators (three-dimensional), video games, target tracking, navigation system evaluation, manipulator control law evaluation, and stereo acuity measurements.

This work was done by Christopher Grant of Martin Marietta Corp. for **Johnson Space Center.** *For further information, Circle 39 on the TSP Request Card.*
MSC-14620

NASA

Microchannel Detector Array for X-Rays and UV

One-dimensional charged-particle detector combines photoelectric array with solid-state memory.

Marshall Space Flight Center, Alabama

Conventional X-ray and ultraviolet radiation detectors utilize either photographic equipment for image storage or photoelectric devices for improved sensitivity. A new detector array combines the advantages of both methods by employing sensitive photoelectric electrodes with solid-state memory.

The detector incorporates an anode array consisting of 64 linear electrodes, each of which is 1.3 mm long and 25 μm wide, set on 50-μm centers. Each anode is connected to a charge-sensitive amplifier. The amplifier output is connected to a variable threshold discriminator/one-shot circuit. This circuit generates a 300-ns 10-V logic pulse that exceeds a preset threshold level (between 5×10^6 and 7×10^7 electrons). The output pulses derived from each of the 64 electrodes are accumulated in 12-bit counters, and the contents of each of the 64 counters are periodically transferred in parallel to shift registers and are serially shifted to the display circuits.

The detector array can be operated in a windowless configuration at extreme ultraviolet and soft X-ray wavelengths, or it can be integrated with a semitransparent or opaque photocathode for use at ultraviolet and visible wavelengths. It is designed to be rugged and compact and is immune to high-energy charged-particle background. The device incorporates nonmagnetic proximity focusing which eliminates bulky magnetic components, making it also immune to external magnetic fields.

This work was done by J. Gethyn Timothy of Harvard College Observatory and Richard L. Bybee of Ball Brothers Research Corp. for **Marshall Space Flight Center.** *For further information, Circle 40 on the TSP Request Card.*

Inquiries concerning rights for the commercial use of this invention should be addressed to the Patent Counsel, Marshall Space Flight Center [see page 2]. Refer to MFS-23324.

NASA

Vidicon Intensifier

A slow-scan intensifier has a resolution of 35 lines/mm at 3×10^{-3} footcandle-seconds.

NASA Pasadena Office, Pasadena, California

A high-performance, slow-scan intensifier vidicon for television systems has been developed. The sensor consists of a single-stage, electrostatically-focused, triode image intensifier. The intensifier is fiber-optically coupled to a 1.5 in. (38 cm), all-magnetic, direct beam vidicon (see figure).

The computer-designed image intensifier provides high quality imaging characterized by exceptionally-low geometric distortion, low shading, and a high center-and-corner modulation transfer function. The intensifier may be electrically gated by the application of a 2000-V pulse to the focus electrode. The photocathode is surface deposited on the input fiber-optics window. The output phosphor screen is chosen for optimum spectral match to the vidicon photoconductor.

The vidicon electron optics are designed to provide high center-and-corner aperture response and low shading. The slow-scan photoconductor exhibits high sensitivity, good image storage-and-erase characteristics, very low dark current and good stability. When coupled, the image intensifier and the vidicon provide as much as 50 percent modulation at 600 TV lines (17 lines/mm) and a limiting resolution of 1250 TV lines (35 lines/mm) at an exposure level of less than 3×10^{-3} footcandle-seconds. The geometric distortion is less than 1 percent. The gate cutoff transmission ratio is greater than 10^5.

This work was done by Robert P. Carpentier, Johannes P. Pietrzyk, Rolf R. Beyer, and Jerome S. Kalafut of Westinghouse Electric Corp. for **NASA Pasadena Office.** *No further documentation is available.*
NPO-11912

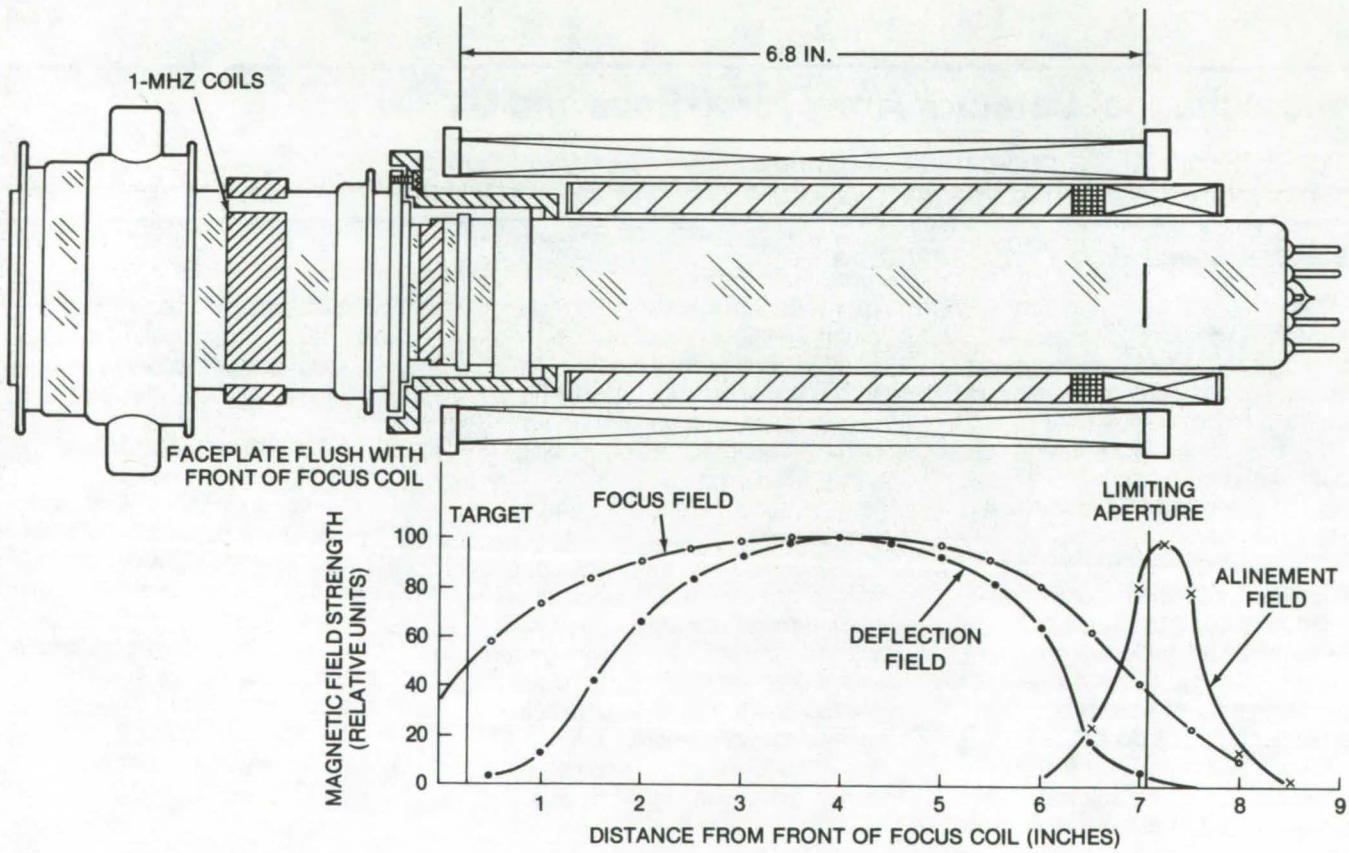

The **Vidicon Intensifier** consists of a single-stage electrostatically-focused triode image intensifier. It is coupled to a 1.5-in. all-magnetic direct-beam vidicon with fiber optics.

NASA

Calibration of Image Dissector Tubes

A computer-controlled LED beam sweeps across the detector to provide an intensity pattern.

Marshall Space Flight Center, Alabama

An image dissector tube measures the intensity of incident light as a function of position by selectively monitoring portions of the photoelectron beam emitted from the illuminated photosensitive surface of the tube. The position of the selected portion of the screen is determined indirectly and is a function of aperture size, tube geometry, deflection current, and stray electromagnetic fields in the tube. For this reason a calibration device is very desirable.

Prior methods of calibrating image dissector tubes depended upon focusing a known light pattern on the photo surface and using this pattern to measure the beam deflection rate. The method is relative rather than absolute. It is also time consuming, and it interferes with the ordinary operation of the instrument during the calibration period.

A new calibration device is shown in Figure 1. The computer turns on the light-emitting diode (LED) and floods the masked face of the image dissector. By sweeping the monitored portion of the beam across the face of the image dissector, an intensity pattern is obtained, as is shown in Figure 2. The binary position of the beam at x_1 and x_2 is provided to the computer by the dissector or tube via an analog-to-digital converter (ADC). This binary information allows exact calibration of position and internal scaling or compensation for stray fields (which are assumed to be constant over the dimensions of the viewed field).

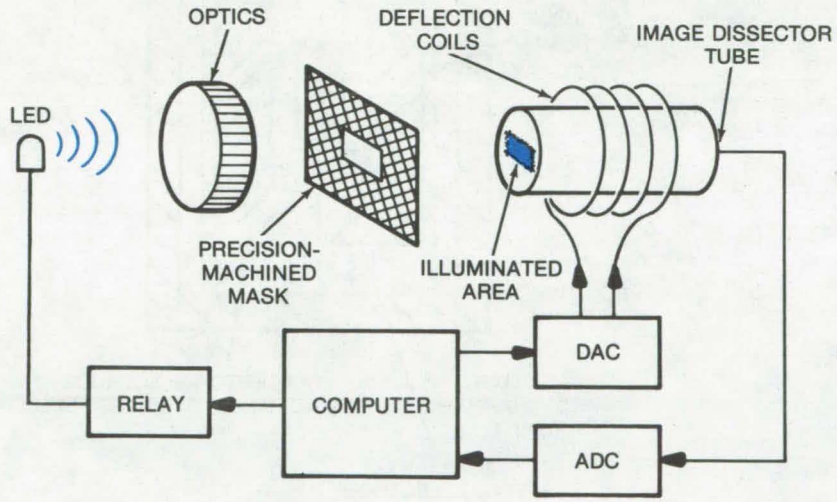

Figure 1. **Calibration Device** for the computer-controlled image intensifier is illustrated. (Note: The mask is shown away from the tube for clarity.)

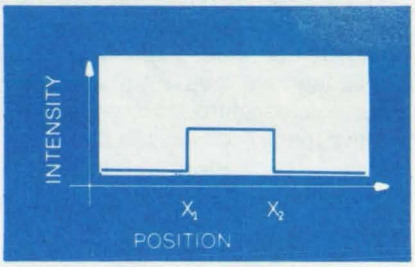

Figure 2. An **Intensity Pattern** as shown above is obtained as a function of beam position.

Computer control of the beam deflection coils is implemented by the digital-to-analog converter (DAC). The speed with which the calibration may be performed (milliseconds) makes it possible to calibrate the tube every few seconds or minutes without unduly interfering with the operation of the instrument. The LED can be out of the functioning field of view and therefore need not interfere.

This work was done by Edwin E. Klingman III of **Marshall Space Flight Center.** *For further information, Circle 41 on the TSP Request Card.*

Inquiries concerning rights for the commercial use of this invention should be addressed to the Patent Counsel, Marshall Space Flight Center [see page 2]. Refer to MFS-22208.

NASA

Hybrid-Mode Thermionic Converter

An efficient thermoelectric-energy transducer

NASA Headquarters, Washington, D.C.

A typical cesium thermionic converter has two electrodes. When the converter operates, a spontaneous low-voltage arc is established between these electrodes to generate positive ions which sustain the plasma. The disadvantage in this arrangement is that a voltage across the electrodes is taken directly from the converter output voltage. This reduces the converter efficiency. Auxiliary ion sources are no improvement because additional power supplies are necessary to operate these devices. A new hybrid-mode thermionic converter has a built-in auxiliary region which improves efficiency.

The new converter also has two electrodes. The collector electrode has a uniform low-work-function surface. It is operated at a sufficiently low temperature to produce negligible electron emission. The emitter electrode, on the other hand, is divided into main and auxiliary regions. The main region has an intermediate work function and is capable of emitting a large electron current at the operating temperature. The auxiliary region of the emitter electrode has a relatively-high work-function surface. This region is in good electrical and thermal contact with, and is at the same potential (Fermi level) and temperature as the main region of the emitter electrode. The work function of the auxiliary emitter region is high enough that the contact potential difference between it and the main region is sufficient to maintain an ignited discharge (i.e., is greater than the arc drop) but is low enough to emit the electron current required by the auxiliary discharge.

The main and auxiliary regions of the emitter are made of platinum and niobium, respectively. The collector is made of stainless steel. Different electrode surfaces and gases other than cesium can be used to obtain the same performance, provided similar work functions and discharge characteristics are used.

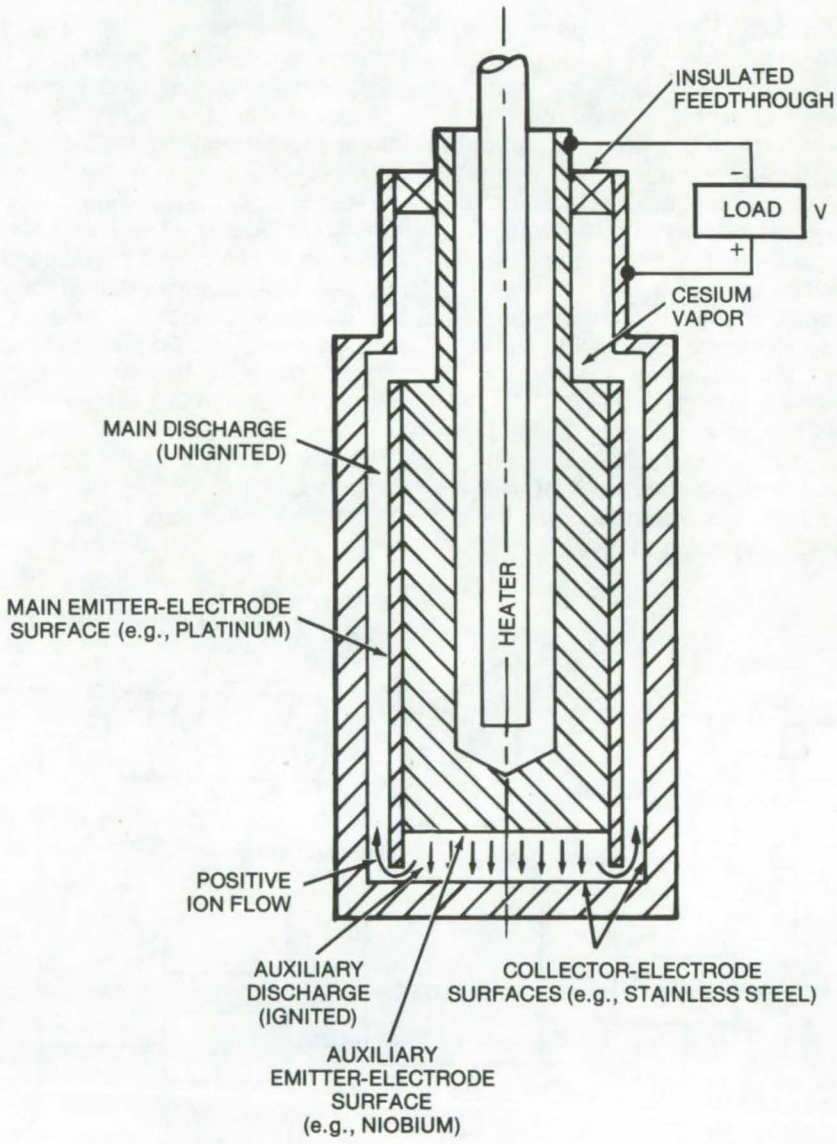

The Thermionic Converter has two emitter-electrode surfaces. The main and auxiliary emitters are made of different materials so that there is a work-function-produced, contact-potential difference that produces a sustainer discharge in the auxiliary region.

In operation, the output voltage of the converter is adjusted to produce no voltage drop across the main discharge region. Under this condition an ignited discharge occurs in the auxiliary region and is maintained by a potential difference across that region. This potential difference is equal to the contact potential difference between the two emitter regions. The auxiliary discharge is partially isolated from the main dis-

charge by an extension of the main emitter cladding. This provides sufficient coupling between the two regions to allow enough ions to flow from the high-potential plasma of the auxiliary discharge to sustain a neutral plasma in the main discharge.

Efficient ion distribution is obtained by using ion-retaining (electron-rich) sheaths at both electrode surfaces in the main discharge region. This means that both the emitter and collector surfaces are operated under conditions that they can emit slightly more electron current than the plasma is able to accept with the local ion supply. A slightly-modified emitter configuration has to be used in cases where the size of the electrode is so great as to preclude efficient ion distribution from a single auxiliary region.

This work was done by Ned S. Rasor and Edward J. Britt of the Atomic Energy Commission for **NASA Headquarters.** *For further information, Circle 42 on the TSP Request Card.*

Inquiries concerning rights for the commercial use of this invention should be addressed to the Patent Counsel, NASA Headquarters [see page 2]. Refer to HQN-10878.

NASA

Computer Programs

These programs may be obtained at very reasonable cost from COSMIC, a facility sponsored by NASA to make new programs available to the public. For information on program price, size, and availability, circle the reference letter on the COSMIC Request Card in this issue.

CONVERT

Technique and computer program for calculating photographic film-density variations

A computer program has been developed to convert binary-coded-decimal (BCD) microdensitometer output into film densities that have been corrected for atmospheric backscattering and lens vignetting. The densitometer output is converted into a number representing the film-density difference between the unexposed film border and any data point on the photograph, while also correcting for atmospheric backscattering and lens vignetting.

The microdensitometer uses a double-beam system in which two light beams from a single source are alternately impinged on a photomultiplier tube. The photomultiplier is exposed to one beam going through the specimen and then to the other beam which goes through a reference linear-density wedge, thus providing an electrical signal which controls a servomotor that brings the linear wedge into optical balance with the specimen beam. A pen attached to the linear-wedge carriage plots the position of the wedge, resulting in a plot representative of the density.

The vertical distance that the tracing pen moves equals the distance that the linear wedge is shifted to optically balance the refererice and specimen beams. The multiplication of this vertical pen distance by the slope (density/mm) of the linear-density wedge would give the film-density difference value. A magnetic-tape encoder system is mounted on the rear of the microdensitometer and is attached to one of the pulleys driving the linear-density wedge. The encoder provides a binary-coded-decimal (BCD) output corresponding to 1 of 175 positions evenly spread out along the length of the linear wedge. Thus, there is a direct proportionality between the magnitude of the difference in BCD numbers between any two points and the vertical pen distance between those points.

The program CONVERT calculates the vertical pen distance of each data point by taking the difference between AVERAGE (the BCD film density of the unexposed border) and the BCD number of a specific data point. Multiplication by a proportionality constant (mm/BCD) will put the distance in units of length. The angle off the principal axis of the lens is computed for each data point, and from that a correction factor is calculated which is used to determine the corrected vertical pen distance. The multiplication of this vertical pen distance by the slope of the linear-density wedge used will give the desired film-density difference value.

FORTRAN IV
CDC 6000, Calcomp plotter
SCOPE 3.0

This program was written by Craig W. Ohlhorst of **Langley Research Center.** *For further information, Circle A on the COSMIC Request Card.*
LAR-11873

Materials

Hardware, Techniques, and Processes

Books and Reports

Novel Aminobenzyl and Imidobenzyl Benzenes

A new class of aromatic polyamines is derived from nitrobenzyl alcohols or halides and alkylated benzenes.

Langley Research Center, Hampton, Virginia

Aromatic amines are extremely useful chemicals in the polymer industry. They are employed as cross-linking agents for polyepoxides and polyurethanes, as intermediates for thermally-stable addition-type polyimides, and, in the case of the diamines, for the synthesis of polyamides and condensation-type polyimides. The imide derivatives of the amines are also useful as intermediates for the preparation of the addition-type polyimides.

Several examples of a new class of aromatic amines, polyamines derived from nitrobenzyl alcohols or halides and alkylated benzene compounds, have been synthesized. These compounds have the following formula:

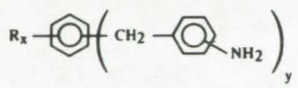

Note: The positions of the substituted amine groups have not been determined.

where R = alkyl, x = 2, 3, or 4, and y = 6 minus x.

These compounds are useful as intermediates for several classes of polymers. The amines can function as cross-linking agents for epoxide and urethane polymers, as well as intermediates for the synthesis of thermally-stable addition-type polyimides. Where R is 4, the compounds are diamines which are useful for the synthesis of polyamides and condensation-type polyimides.

These amines can be further reacted with certain monoanhydrides containing olefinic unsaturation, thus giving imide derivatives with the following general formula:

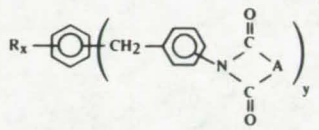

Note: The positions of the substituted imide groups have not been determined.

where R = alkyl, x = 2, 3, or 4, and y = 6 minus x and A = one of the groups:

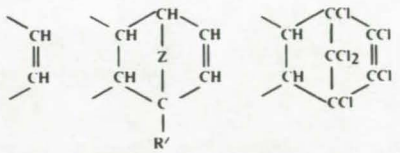

where Z = $-CH_2-$ or $-O-$ and R′ = CH_3 or H.

There are several features which make these amines uniquely suitable for use in polymer preparation. The alkyl groups substituted upon the central benzene ring can serve to increase the solubilities of polymer intermediates, such as the imide-terminated derivatives of the amines, as well as to decrease the melting points of the same polymer intermediates and the softening points of the resulting polymers.

These changes in physical properties make the polymers markedly easier to process. The fact that the alkyl groups can be located at various isomeric positions on the central benzene ring can also alter the solubilities of the intermediates and the softening points of the resulting polymers. The fact that the amine groups are separated by three benzene rings leads to easier processing of the polymer intermediates and the resulting polymers. Countless variations of isomers based upon the positions of attachment of the amine groups on the benzyl moieties, as well as the positions of the alkyl groups on the central benzene ring, can be used to alter the properties of the amines, imide derivatives, and polymers as desired.

The first step in preparing the new compounds involves reacting two, three, or four molar equivalents of ortho-, meta-, or para-nitrobenzyl alcohols or halides with one molar quantity of a benzene substituted with four, three, or two alkyl groups, respectively. The resulting bis-, tris-, or tetrakis-nitrobenzyl benzene intermediates can then be reduced by any of a number of methods, both catalytic and chemical, to yield the corresponding bis-, tris-, or tetrakis-aminobenzyl benzene compounds.

When a nitrobenzyl alcohol is used as the starting material for the initial reaction, the reaction with the alkyl-substituted benzene receptor is best conducted in concentrated sulfuric acid as the solvent catalyst and at temperatures of -25° to +75° C for periods of time ranging from 1 hour to 10 days. The optimum times and temperatures of reaction vary with the choice of nitrobenzyl alcohol and substituted benzene substrate.

The use of a nitrobenzyl halide as a reactant with a substituted benzene reactant requires the use of an acidic catalyst, such as anhydrous aluminum chloride, although many of the Lewis acid type catalysts normally used for Friedel-Crafts condensations can be successfully employed.

This work was done by Vernon L. Bell of **Langley Research Center,** *J. Richard Pratt of the University of Southern Mississippi, and Billy L. Stump of Virginia Commonwealth University. No further documentation is available.*

Inquiries concerning rights for the commercial use of this invention should be addressed to the Patent Counsel, Langley Research Center [see page 2]. Refer to LAR-11843.

NASA

Atmospheric Particle Sampler

Positive and/or negative gas pressure drives particulate matter against a filter element for capture.

NASA Pasadena Office, Pasadena, California

An atmospheric sampler has been designed to collect particles from rocket exhausts and could be used to monitor industrial emissions as well. The sampler is more efficient and collects smaller particles than comparable systems. A known volume of atmosphere is captured, and particles in the sample are forced against and trapped by a filter element. The particles are forced by positive or negative pressure, or both.

The sample chamber is shown in Figure 1. It consists of a 90° ball-cock valve with a uniformly machined passageway alined with the atmosphere inlet and outlet tubes when the valve is open. By rotating the hand lever, a sample is trapped within the cylindrical passageway. Figure 2 shows the sampler and pressure system at a right angle to the view of Figure 1 and after the sample chamber has been sealed off.

The ball-cock valve has a small threaded inlet on one side and a large recessed opening on the other. When the pressure-release and vacuum-operating valves are opened, pressurized helium is forced into the cylindrical passage. Helium is used rather than air because it imparts a higher velocity to the particles. The pressure and vacuum drive the sample against the filter where it is trapped. The gases may be retained in the gas cylinder for later analysis, or they may be evacuated; the filter is removed for analysis (e.g., under an electron microscope).

The filter element is a thin sheet of plastic with perforations on the order of 1 micron (10^{-6} m) or less. It is made by exposing plastic sheet to bombardment by radioactive fission fragments; this produces minute straight-line weaknesses in the plastic. The sheet is subsequently etched to form pores at the weaknesses.

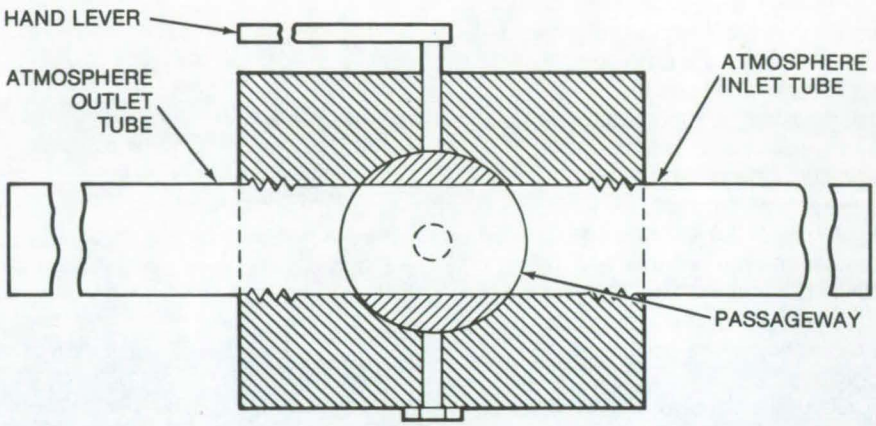

Figure 1. When the **Sample Chamber** valve is open as shown, the uniformly-machined cylindrical passageway is alined with both the inlet and outlet tubes. The atmosphere passes through the tubes and valves until the hand lever is turned 90 degrees to capture a sample within the passageway.

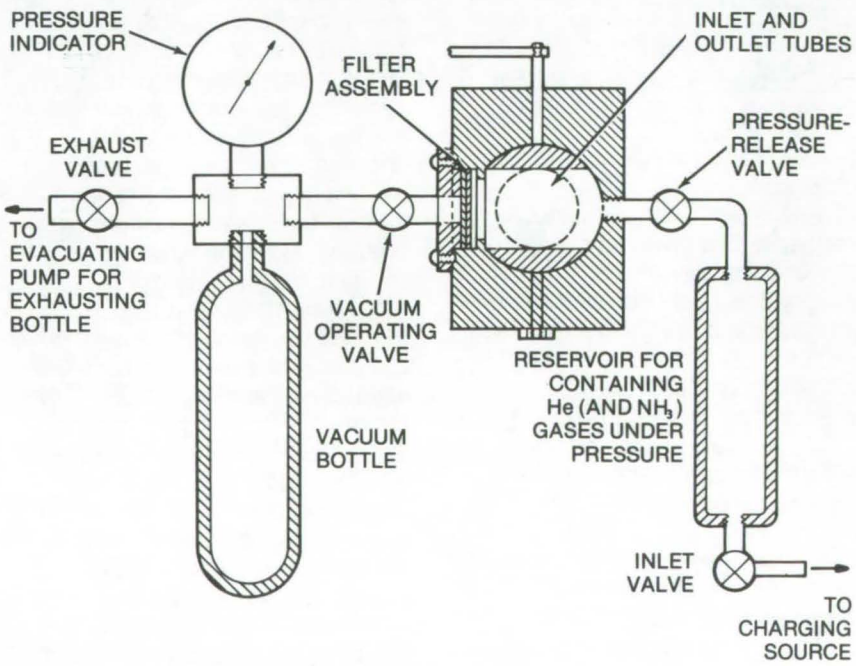

Figure 2. The **Sampler and Pressure System** are shown at a right angle to the view in Figure 1, and the lever has been turned to seal off the passageway. In this position the release and operating valves are opened and the trapped sample is driven against the filter.

The amount of HCl vapor in the sample can also be determined by including NH_3 in the pressurized gas. This will react with any HCl in the sample to produce a white solid (NH_4Cl) that will be trapped by the filter.

This work was done by Charles G. Miller and James B. Stephens of Caltech/JPL for **NASA Pasadena Office.** *For further information, including a discussion of the filter elements, Circle 43 on the TSP Request Card.*

This invention is owned by NASA, and a patent application has been filed. Inquiries concerning nonexclusive or exclusive license for its commercial development should be addressed to the Patent Counsel, NASA Pasadena Office [see page 2]. Refer to NPO-13396.

NASA

Continuous HCl in Air Indicator

Atmospheric HCl is converted to an ammonium chloride cloud which is scanned photometrically.

NASA Pasadena Office, Pasadena, California

A new monitoring system can be used to detect continuously or intermittently the presence of hydrochloric acid (HCl) in air. A steady stream of air is drawn into the system and passes between a light source and a photocell. There the incoming gases are sprayed with ammonia (NH_3) forming a white cloud of NH_4Cl if any HCl is present. This cloud passes between a second light source and photocell, and the difference between the transmitted light before and after the NH_3 is added is proportional to the HCl content in the intake sample.

The indicator system is outlined in the figure. A horn-shaped conversion chamber is connected to an air intake. The measurement taken between the first light source and cell includes the effects of all particulate matter in the air. The light-transmission decrement measured at the second photovoltaic pair is due only to the difference caused by the NH_4Cl vapor. Thus this indicator could be used near smokestacks or other particle emitters without complex and expensive filtering.

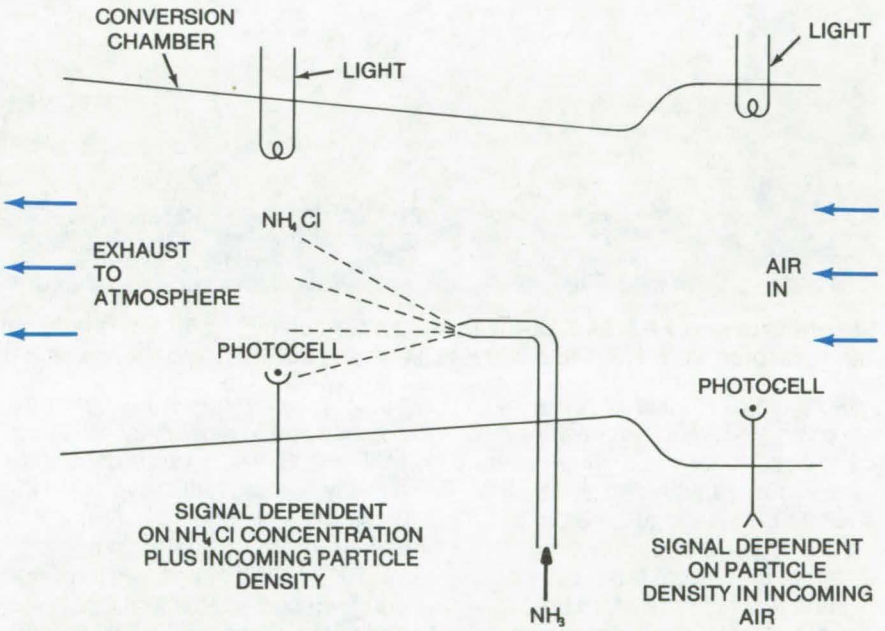

The HCl Indicator is essentially a conversion chamber through which the sampled air is drawn. Inside the chamber the intake sample is mixed with NH_3, and any HCl present forms a cloudy suspension of ammonium chloride.

This work was done by Ralph E. Bartera and Charles G. Miller of Caltech/JPL for **NASA Pasadena Office.** *For further information, Circle 44 on the TSP Request Card.*

This invention is owned by NASA, and a patent application has been filed. Inquiries concerning nonexclusive or exclusive license for its commercial development should be addressed to the Patent Counsel, NASA Pasadena Office [see page 2]. Refer to NPO-13474.

NASA

Thermal Fatigue-and-Oxidation-Resistant Alloy

NASA Alloy TAZ-8A has superior thermal-fatigue and oxidation resistance.

Lewis Research Center, Cleveland, Ohio

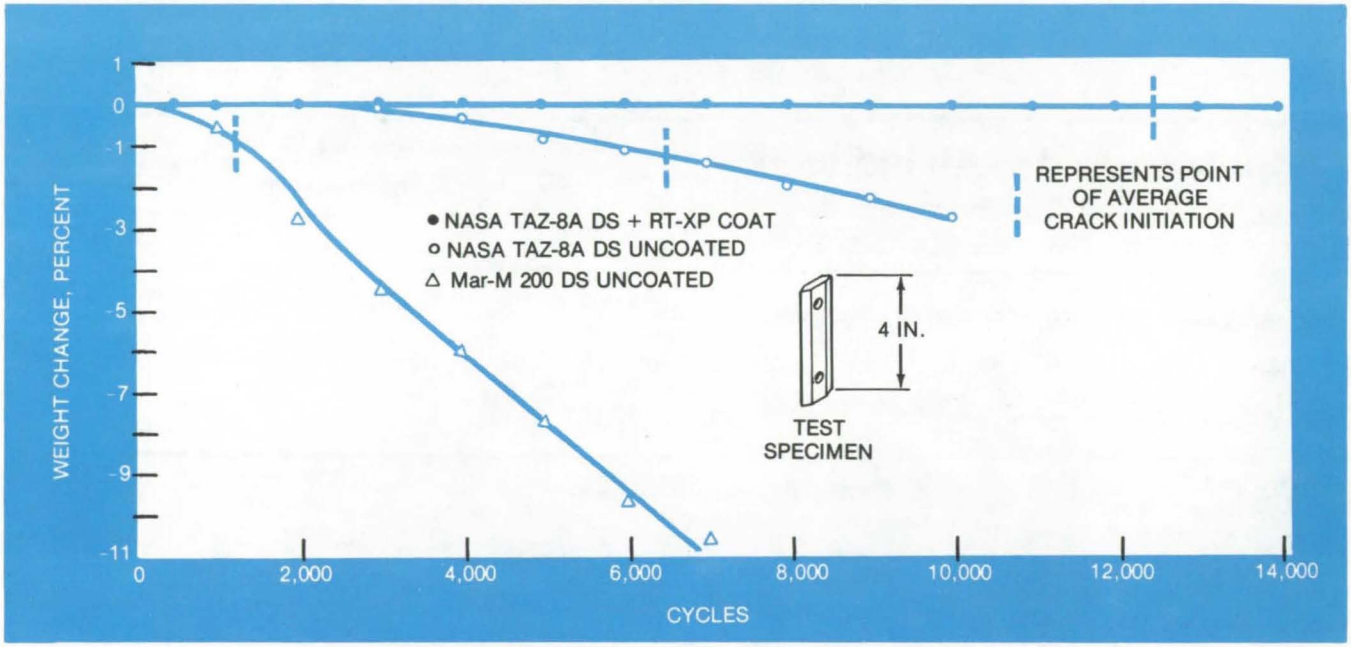

Weight Change of NASA TAZ-8A ia shown for two alloys, directionally solidified from fluidized bed tests. Bed temperatures were 1,361 and 589 K (1,990° and 600° F), and there was 3-minute immersion in each bed.

A cast nickel-base alloy designated as NASA TAZ-8A has been developed for use in high-temperature aircraft engine components such as first-stage turbine blades. This alloy exhibits superior resistance to thermal fatigue and oxidation, which are often the life-limiting modes of failure for engine components. In addition, its high-temperature strength, both short- and long-time, compares favorably with that of current nickel-base alloys.

When cast by the directional solidification process and coated with RT-XP*, the thermal fatigue resistance of NASA TAZ-8A (tested by temperature cycling in fluidized beds) is superior to that of 34 other combinations of alloys and coatings, both current and advanced (see the Tech Brief article following: "Comparative Thermal Fatigue Resistance"). Its thermal fatigue life (12,500 cycles) was almost double that of the next best alloy-coating combination, directionally solidified MAR-M200 with a vapor-deposited overlay coating (6500 cycles). In these tests, wedge specimens were alternately heated to about 1347 K (1965°F) for three minutes and then cooled to about 622 K (660°F) for three minutes by immersion in fluidized beds.

The cyclic oxidation resistance of coated and uncoated directionally-solidified TAZ-8A determined from these tests is compared with that for directionally-solidified MAR-M200 in the figure. Note first the much smaller weight loss of TAZ-8A. Tests with RT-XP coating on directionally-solidified TAZ-8A showed almost no weight loss throughout the duration of testing (14,000 cycles), signifying excellent oxidation resistance.

The NASA TAZ-8A composition is 8Ta, 6Cr, 6Al, 4Mo, 4W, 2Cb, 0.5Zr, 0.125C, 0.004B, and balance Ni (weight percent). Its specific gravity at room temperature is 8.65. Some other nominal properties of the directionally-solidified form of this alloy are shown in the table.

At 1033 K (1400°F)	
Proportional Limit	96,300 N/cm² (140,000 psi)
Ultimate Tensile Strength	107,000 N/cm² (155,000 psi)
Reduction of Area	5%
At 1255 K (1800°F)	
100 Hour Rupture Stress	17,200 N/cm² (25,000 psi)
Reduction of Area	30%

Properties of NASA TAZ-8A

*The RT-XP coating is a proprietary process of the Chromalloy American Corporation Research and Technology Division. It is a coating containing an aluminide with a case depth of about 70 μm (2.7 mil). This coating process was selected because of its ability to coat the interior of the small holes found in film-cooled turbine blades.

This work was done by Peter T. Bizon, William J. Waters, and David A. Spera of **Lewis Research Center.** *Further information may be found in:*

NASA TN-D-8071 [N75-33429] "Comparative Thermal Fatigue Resistances of 26 Nickel- and Cobalt-Base Alloys" and NASA TN-D-3597 [N66-34938] "Investigation of Columbium-Modified NASA TAZ-8 Superalloy."

Copies of these reports may be obtained at cost from the Aerospace Research Applications Center, Indiana University [see inside back cover].

LEW-12564

NASA

Printed-Circuit Solar-Cell Array

This is a technique for interconnecting solar cells to form multiunit arrays. It consists of sandwiching a network of electrically conductive material between two sheets of thin plastic, and adhesively bonding the resulting structure to the solar cell assembly. This is a substantial advance in the weight reduction of flexible printed circuit solar array substrates.

(See page 14.)

Metalworking Methods for Composites

Drawing, rolling, extrusion, and swaging were studied as fabrication methods for Al/C and Al/B composites. Experimental equipment was designed. Hot/cold drawing produced satisfactory Al/B tubes with excellent filament distribution. Metalworking processes were not successful with Al/C, but resistance and ion-beam heating may be useful.

(See page 133.)

Comparative Thermal Fatigue Resistance

Comparative data on 26 nickel- and cobalt-base alloys

Lewis Research Center, Cleveland, Ohio

To aid in the selection of alloys for fluctuating high-temperature service, a comparative study was made of the resistance to thermal fatigue and cyclic oxidation of a wide variety of alloys and coatings. Nineteen cast nickel-base alloys, five cast cobalt-base alloys, and two wrought nickel-base alloys were included in this study. Five of the nickel-base alloys had a directionally-solidified polycrystalline grain structure. Three diffusion coatings (Jocoat[1], RT-1A[2] and RT-XP[2]) and one vapor-deposited overlay coating (NiCrAlY[1]) were also included in this investigation.

The number of thermal cycles required to initiate cracks in the 35 combinations of alloys and coatings are shown in the figure. This chart shows that the thermal fatigue lives under identical test conditions ranged from less than 15 to 12,500 cycles. The class of materials having the longest thermal fatigue lives was found to be cast alloys with directionally-solidified polycrystalline grain structures. This is attributed to two factors: (1) their lower modulus of elasticity in the longitudinal direction (varying from about 2/3 at room temperature to about ½ at 1366 K (2000 °F) that of the same alloy in the random polycrystalline form) resulting in lower thermal stresses, and (2) the absence of transverse grain boundaries which might serve as crack nuclei.

The alloy-coating combination with the highest thermal fatigue resistance (12,500 cycles) was directionally-solidified NASA TAZ-8A with an RT-XP coating. Its thermal fatigue life was almost double that of the next best alloy-coating combination, directionally-solidified MAR-M200 with the vapor-deposited overlay coating, NiCrAlY, (6500 cycles). In all cases, the application of a coating improved the thermal fatigue resistance of the substrate alloy.

Of all the random polycrystalline alloys tested, hafnium modified B 1900 with Jocoat had the highest thermal fatigue resistance (1480 cycles). However, of the nineteen uncoated random polycrystalline alloys tested, NASA TAZ-8A again had the highest thermal fatigue resistance (700 cycles).

The comparative thermal fatigue resistance was determined experimentally by simultaneously testing specimens of the different materials with the same geometry in fluidized beds and comparing the number of cycles required to initiate the first crack. The number of cycles to crack initiation was taken as the average of the number of cycles at the last inspection without cracks and the number of cycles at the first inspection with a crack.

Groups of up to 18 prismatic bars 10 cm (4 in) long with double-wedge cross sections (see insert on bar chart) were alternately heated for three minutes and cooled for three minutes. Materials were tested with the heating bed temperature held at 1361 K (1990 °F) and the cooling bed temperature held at 589 K (600 °F). Maximum metal temperatures were about 1347 K (1965 °F) and minimum metal temperatures were about 622 K

[1]Pratt and Whitney Aircraft proprietary process
[2]Chromalloy American Corporation Research and Technology Division proprietary process

(continued next page)

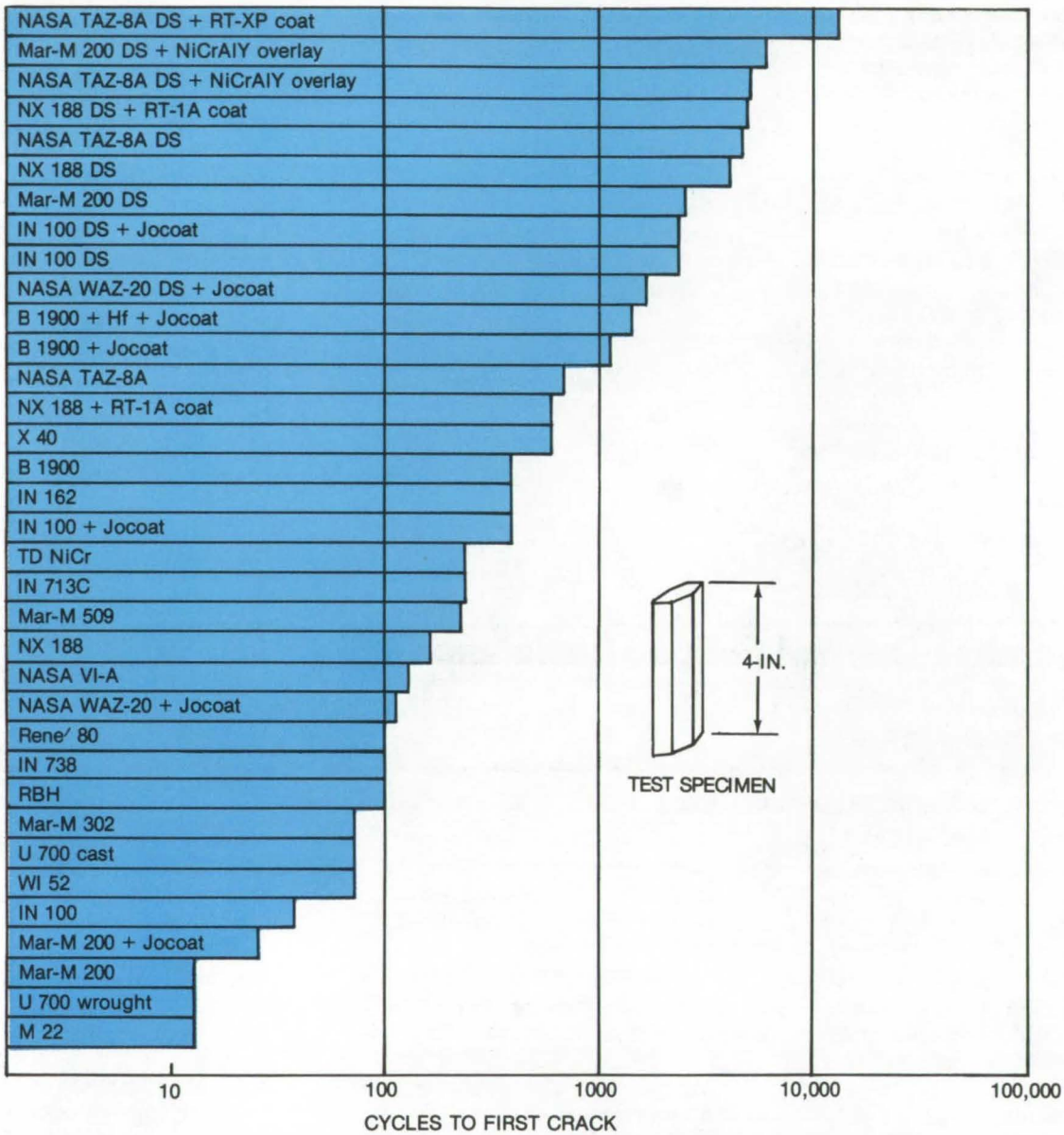

Cast alloys with directionally-solidified polycrystalline grain structures are shown to have the longest fatigue lives. Comparative Thermal Fatigue Resistances are shown for nickel- and cobalt-base alloys. Bed temperatures were 1,361 and 589 K (1,990° and 600° F), and there was 3-minute immersion in each bed.

(660°F). Since the test conditions were selected to represent those expected in advanced aircraft gas turbines, the metal temperatures in this study may have exceeded the recommended maximum use temperatures for many of the alloys tested. However, to obtain comparative thermal fatigue resistance for all materials, a uniform thermal cycle was necessary.

A more detailed study of the results including oxidation resistance of directionally-solidified NASA TAZ-8A with RT-XP coat is presented in the preceding Tech Brief article "Thermal-Fatigue-and-Oxidation-Resistant Alloy."

This work was done by Peter T. Bizon and David A. Spera of **Lewis Research Center.** *Further information may be found in NASA TN-D-8071 [N75-33429], "Comparative Thermal Fatigue Resistances of 26 Nickel- and Cobalt-Base Alloys", a copy of which may be obtained at cost from the Aerospace Research Applications Center, Indiana University [see inside back cover].*

LEW-12563

NASA

Hydrogen Chloride Test Set

Atmospheric hydrogen chloride can be detected selectively and at low concentrations using tertiary amines.

Marshall Space Flight Center, Alabama

Hydrogen chloride gas is a noxious byproduct of many industrial chloride processes. In order to monitor gas content in the atmosphere, a portable and sensitive hydrogen chloride monitor is needed. Monitoring techniques relying on acid-base reactions or chemiluminescence have limited specificity, since most acid and some redox reactions are similar to the HCl reactions used. Mass spectrometry, which has also been used, is sensitive and selective, but is too expensive for many applications.

A new hydrogen chloride detector has been developed, using the chemical reaction

$$R_3N + HCl \rightarrow R_3NH^+Cl^-$$

where R_3 represents an organic radical attached to the amine nitrogen. The use of a tertiary amine (R_3N) makes the reaction fairly specific for the relatively-small highly polarized HCl molecule.

The reaction is monitored by any microbalance capable of measuring extremely-small mass differences in real time. The sensitivity of the detector is determined by the sensitivity of the microbalance. The ultimate range of detectability is determined by the characteristics of the microbalance, the total number of amine molecules which can be deposited on the microbalance, and the total number of nitrogen atoms per molecule.

Excellent results may be obtained by using a quartz crystal microbalance (QCM) as the mass indicator and triphenylamine as the tertiary amine. The QCM is coated with a film of the amine which will change in weight as it reacts with the HCl. Since the detector operates as an accumulative collector, very low concentrations of HCl can be detected. Tests on a prototype device have indicated a sensitivity of 10^{-9} grams/frequency, enabling the detector to respond to $\cong 10^{-8}$ grams of hydrogen chloride, or 2.5×10^{14} molecules.

This work was done by Gary L. Workman of Athens College for **Marshall Space Flight Center.** *For further information, including test data, Circle 45 on the TSP Request Card.*

MFS-23357

NASA

Combined Joining Process for Dissimilar Metals: A Concept

Combined brazing and diffusion bonding of aluminum and stainless steel is investigated. The metals are brazed and diffusion bonded in the same retort with less than conventional pressure and time. The bond will withstand internal pressures up to 1,000 psi.

(See page 128.)

Metal Structures With Parallel Pores

Four methods are used to make metal plates with parallel pores: elongate bundle, wind and sinter, extrude and sinter, and corrugate stack. Such plates are particularly suitable for electrodes for electrochemical and fuel cells.

(See page 132.)

Field Sampling Fine-Vacuum Systems

A portable pumping station consisting of a roughing pump, an air-cooled diffusion pump, and a liquid nitrogen cold trap can be used for onsite sampling of vacuum systems. Subsequent chemical analysis of sampled gases shows good agreement with laboratory results.

(See page 119.)

Increased Safety in Mercury-Containing Devices

An amalgamating metal included inside mercury lamps reduces the amount of escaping mercury vapor when the lamps are fractured. The amalgamating metal, gold, tin, cadmium, or indium, reduces the mercury vapor pressure to approximately 6 percent of the normal value.

(See page 20.)

Thermal Insulation for High-Temperature Systems

Laminated platinum-foil insulation can be used at 1,700° F.

Goddard Space Flight Center, Greenbelt, Maryland

A novel thermal-insulation concept can be used under an air atmosphere and/or in a vacuum with temperatures up to 1200 K (1700°F). Forty layers of 0.00064-cm (0.00025-in.) platinum foil, sprayed with zirconia during assembly, comprise the laminated insulation with microquartz felt set into the corners. The foil layers are grouped and/or proportioned as shown in the figure. The foil separation distances vary so as to produce a linear temperature gradient from the inside to the outside surfaces.

A key feature is the utilization of a noble metal, platinum, as an insulation material at high temperatures in either vacuum or air. Platinum was chosen because its emissivity is stable at temperatures up to 1200 K (1700 °F), in either air or vacuum and it resists oxidation when used in air, even at high temperatures. However, the cost of this insulation material must be kept in mind for any specific industrial applications.

This work was done by Andrew J. Parker of Hittman Associates Inc. for **Goddard Space Flight Center.** *For further information, Circle 46 on the TSP Request Card.*
GSC-10954

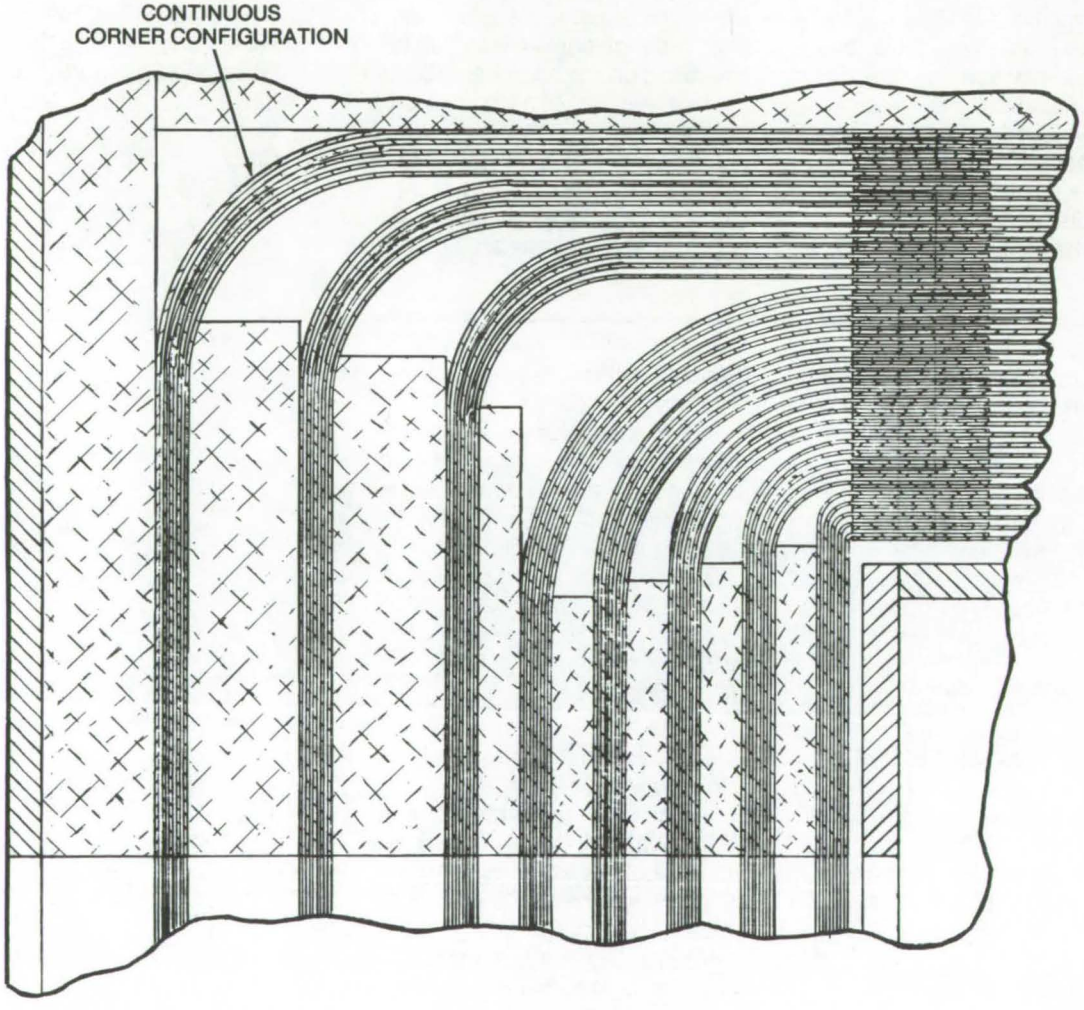

Forty layers of platinum foil, sprayed with zirconia, are used for a laminated insulation system.

NASA

Polymeric Foams Stable at High Temperatures

Crosslinked poly(N-arylenebenzimidazoles) are stable up to 370° C.

Ames Research Center, Moffett Field, California

Crosslinked polymeric foams made from poly(N-arylenebenzimidazoles) are stable at temperatures up to 370° C (700° F) and are also self extinguishing. The polymers are made by mixing the appropriate stoichiometric amounts of a tetramine such as N,N′-bis(2-aminophenyl)benzidine and an aromatic dicarboxylic acid anhydride with phenol or an alkyl-substituted phenol. The phenol, which may be varied from 5 to about 50% of the total weight, serves as a flux and a blowing agent. The mixture is heated to complete dissolution and to advance the condensation of the monomeric composition to a prepolymer state. A dianhydride is incorporated to provide crosslinking, and it is desirable to provide about 5% of a crosslinking agent in order to limit shrinkage and deformation in later stages of cure.

The optimum time and temperature required to bring the monomeric mixture to the prepolymer state will vary with concentration and the nature of the tetramine and monoanhydride as well as the amount of tetrafunctional dianhydride added as a crosslinking agent. Naturally, polymer-forming mixtures with greater amounts of crosslinking agent are more sensitive to premature gellation owing to the insolubility induced by the crosslinking action.

After the prepolymer has been formed, the resulting mixture is allowed to cool and solidify. The resin is ground to a uniform particle size and placed in an enclosed foaming fixture. The overall density of the final foam is determined by the charge mass-to-volume ratio in the fixture (allowing for loss of volatiles). The loaded fixture is placed in an oven preheated to 150° C (300° F) and allowed to come to equilibrium; to form the foamed part, the temperature is raised at a programed rate from 35° to 150° C (100°-300° F) per hour to about 260° C (500° F). Finally, the temperature is raised to 340° C (650° F) and held for about 30 minutes.

When cold, the finished part is removed from the mold and postcured for 2 hours at 400° C (750° F) in an inert atmosphere. Densities as low as 0.032 g/cm^3 (2 lb/ft^3) have been obtained.

This work was done by Salvatore R. Riccitiello of **Ames Research Center** *and Edward S. Harrison and Chadwick B. Delano of Whittaker Corp. For further information, Circle 47 on the TSP Request Card.*

This invention is owned by NASA, and a patent application has been filed. Inquiries concerning nonexclusive or exclusive license for its commercial development should be addressed to the Patent Counsel, Ames Research Center [see page 2]. *Refer to ARC-11008.*

NASA

Quantitative Bioluminescent Detection of Bacteria

The flavin content of bacteria is determined rapidly using bioluminescence. Boiling perchloric acid is used to rupture cells to free bound flavin, and to hydrolyze FAD to FMN. A base-stabilized water solution of sodium borohydride is used as a reductant.
(See page 81.)

Reducing Cold Flow in Elastomeric O-Rings

Cold flow in elastomeric O-rings is reduced by special pretreatment. The seal is pressure loaded and heated. A load is then applied to the heated seal to cause material flow. Finally the parts are cooled to room temperature, and the load is removed.
(See page 94.)

Nondestructive Inspection of Multilayered Insulation

Radio-frequency techniques are used to evaluate multilayered cryogenic insulation. The insulation is probed with an electromagnetic field generated by an induction coil. The coil impedance is a function of metal loss and layer density.
(See page 129.)

Transparent and Flame-Retardant Potting Compounds

Several new flame-retardant and transparent polymers make excellent potting, encapsulating, and conformal coating materials.

Lyndon B. Johnson Space Center, Houston, Texas

As part of an exhaustive study of the development of and the properties of fire-retardant polymers, several new potting and encapsulating compounds have been produced. These compounds could also be useful as adhesives for other polymeric structural materials, such as those used in prefabricated housing, furnishings, and marine construction.

Among the compounds developed and tested are a series of modified silicone RTV polymers which have excellent flame-retardant properties and are easily molded and cured. Also, another interesting group of flame-retardant polymers has been formulated: coreacted epoxy-urethanes. These are self-extinguishing, transparent, do not melt when exposed to high temperatures, and exhibit less than 0.5 percent outgassing when exposed to 4×10^{-6} torr.

The coreacted epoxy-urethanes have a high tear strength and good elongation. The reaction incorporates a mixture of diepoxide, dihydroxide polyol, and diisocyanate in the ratio of 1:1:2. With this composition, it is possible to include bromine, phosphorus, and nitrogen in the polymeric structure. In this way properties can be developed which, in the past, required the addition of diluents, nonreactive additives, or plasticizers. Such additions cause shrinkage, outgassing, and migration. These problems are eliminated with the coreacted formulation.

This work was done by Sheldon L. Lieberman of Furane Plastics, Inc., for **Johnson Space Center.** *Further information may be found in "Final Report: Production Development of Organic Non-Flammable Spacecraft Potting, Encapsulating and Conformal Coating Compounds":*

NASA CR-134234 [N74-21159] Vol. I Discussion, Figures, and References
NASA CR-134235 [N74-21160] Vol. II Tables
NASA CR-134236 [N74-21161] Vol. III Appendices
NASA CR-134237 [N74-21162] Vol. IV Executive Summary

Copies of these reports may be obtained at cost from the National Technical Information Service, Springfield, Virginia 22151.
MSC-14669

NASA

Coatings for Mullite Insulation

A family of ceramic coatings waterproofs mullite insulation and protects it from physical damage.

Langley Research Center, Hampton, Virginia

Panels of fibrous mullite insulation are porous and friable. These properties make the mullite insulation vulnerable to moisture absorption, dust penetration, and damage from careless handling; anyone of which could seriously impair its thermal efficiency. A series of coatings has been developed which provides the fibrous mullite panels with a hard, impermeable, waterproof layer. In addition, the inclusion of selected color oxides in the coating composition imparts high emittance to the surface.

The coating is water repellent and thermally compatible with the mullite. In selecting the coating, various kinds of glass frit, refractory fillers, and colorants were screened. Refractory fillers investigated included TiO_2, $BaO\cdot ZrO_2$, $SrO\cdot TiO_2$, zircon, spodumene, petalite, and kryptonite. Colorants included Cr_2O_3, NiO, and CoO.

This preliminary screening produced combinations of kyanite, petalite, NiO, Cr_2O_3, and various kinds of glass frit. Selected dry mixtures of these constitutents were ball milled. A small amount of each mixture was then slurried with a 3-percent aqueous solution of polyvinyl alcohol and applied to mullite panels for evaluation. The coated mullite was dried at 230° F (110° C) then fired at 2,500° F (1,370° C) for at least ten minutes. Several very good coatings resulted from this work. Fibrous mullite panels, ranging in size from one-inch cubes to panels 13 × 11 × 2 in. (33 × 28 × 5 cm) have been coated with these mixtures and have then been tested for thermal endurance and thermal shock resistance. The mixtures were found to be waterproof and thermally compatible with mullite even after extended exposure to at least 2,100° F (1,150° C).

This work was done by Phillip N. Bolinger and Harry W. Rauch, Sr., of General Electric Co. for **Langley Research Center.** *For further information, Circle 48 on the TSP Request Card.*
LAR-11150

NASA

Specific-Ion Electrodes for Measuring Ag^+

Silver-conductive epoxy prevents rapid electrode failure caused by corrosion.

Lyndon B. Johnson Space Center, Houston, Texas

Specific-ion electrodes used for measuring the quantity of silver ions in aqueous solutions often fail due to the electrode structure. A typical electrode is made by compressing silver sulfide powder around a silver wire to form a pellet. The wire is subsequently soldered to an external cable, and the pellet is cemented into a plastic housing. During the measurements the pellet comes into direct contact with the aqueous solutions. Since the pellet is porous the liquids migrating through it cause rapid corrosion of the soldered connection. The result is failure after a short period of time.

The migration of fluid through the pellet, and thus the corrosion of the soldered connection, is prevented by modifying the structure as follows: The same silver sulfide membrane is used. However, the silver wire, rather than being embedded in place, is attached with silver-conductive epoxy. In addition, the epoxy is thinned with toluene, and two coats are applied to a pressed pellet. Each coat is allowed to cure at 100° C for one-half hour. Unthinned epoxy is then used to attach the silver wire to the pellet. The epoxy coats prevent fluid from entering the pellet.

This work was done by J. L. Day of **Johnson Space Center** *and J. M. Walsh of Beckman Instruments, Inc. For further information, including detailed fabrication procedures, Circle 49 on the TSP Request Card.*
MSC-14906

NASA

Reduction of Acoustic Losses by Outgassing

Heat treatment at low pressures reduces acoustic losses in porous materials.

Lyndon B. Johnson Space Center, Houston, Texas

A method of removing volatiles from porous materials (outgassing) has been found to increase the internal-friction quality factor (Q factor) of treated samples. The procedure is heat treatment at very low pressures. This thorough outgassing can reduce the propagation losses in porous ferroelectric ceramics by as much as a factor of 100.

The process was developed as part of a study of the Q factors of lunar basalt; measurements made on the Moon showed Q factors of from 3,000 to 5,000. Similar lunar specimens examined in Earth laboratories had Q factors of less than 100. The difference has been shown to be due to absorbed atmospheric volatiles.

In a typical outgassing procedure, the sample is cleaned by boiling in trichlorethylene for an hour, boiling in ethanol, and boiling in water. Also very effective is boiling in a 30-percent H_2O_2 solution for several hours. The cleaning increases Q factors from around 20 to nearly 100.

One drying procedure is to heat the sample at 150° C for about a day. This can further increase the Q factor to about 400. Further processing by several hours' exposure to a vacuum of 1×10^{-7} torr (1.33×10^{-5} N/m^2) can result in an increase in Q of up to 700. Finally, a series of heating and cooling cycles under vacuum (at peak temperatures of 100°, 140°, and 170° C successively) has been shown to raise the factor to 1,700.

If the sample is exposed to the atmosphere after outgassing, the Q factor will drop back to around 100, indicating the reabsorption of atmospheric volatiles. Some reabsorption will take place even upon cooling in a vacuum.

Tests on the relative effectiveness of various volatiles in reducing Q factors are summarized in the table. All vapors tested have similar effects, and the gases are at least an order of magnitude less effective.

This work was done by E. H. Cirlin, R. M. Housley, and B. R. Tittmann of Rockwell International Corp. for **Johnson Space Center.** *For further information, including laboratory procedures for outgassing, Circle 50 on the TSP Request Card.*
MSC-15985

Vapors With a Large Effect on Q Factors	Gases With Some Effect on Q Factors	Gases With Little or No Effect on Q Factors
water	carbon monoxide	nitrogen
methanol	carbon dioxide	helium
ethanol	oxygen	
acetone	hydrogen	
trichloroethane	ammonia	
carbon tetrachloride	hydrochloric acid	

Effect of Some Vapors and Gases on the Q Factors of Porous Materials

NASA

REDOX - Electrochemical Energy Storage

A promising new electrochemical bulk energy storage concept

Lewis Research Center, Cleveland, Ohio

The storage of electrical energy to match efficient generation with fluctuating demand is a growing concern.

A preliminary study has been made of the practicality of a REDOX (reduction-oxidation) electrochemical bulk energy storage concept. On the basis of capital cost estimates, size estimates, and other necessary considerations, the REDOX system has considerable promise as a bulk energy storage system. The estimated capital cost of a 10-megawatt, 85-megawatt-hour, REDOX system ranges from $325 (70 percent efficiency) to $200 (85 percent efficiency) per kilowatt. For this power and energy, the estimated volume of the tanks and power cells is approximately one-fiftieth the value required of pumped hydroelectric storage with a 250-meter (825-foot) operating head. Siting, environmental, and hazard concerns are modest for the REDOX system.

The REDOX energy storage system consists of two electrolyte storage tanks connected to a flow cell (see figure). One tank contains an analyte, an aqueous titanium trichloride/titanium tetrachloride ($TiCl_3/TiCl_4$) solution; the other tank contains a catholyte, an aqueous ferric chloride/ferrous chloride ($FeCl_3/FeCl_2$) solution. The flow cell consists of two compartments connected to the separate electrolytes and containing inert carbon electrodes separated by an anion-permeable, selective-ion-exchange membrane. In operation, the two electrolytes are circulated through their respective flow cell compartments. On discharge, with an electrical load applied to the cell, the $FeCl_3$ is reduced to $FeCl_2$ giving up electrons and chloride ions while the $TiCl_3$ is oxidized to $TiCl_4$. The ion exchange membrane allows passage of the chloride ions from one compartment to the other to maintain electro-neutrality. The system is recharged simply by reversing the direction of the current flow. The system operates at relatively low temperatures from room temperature to about 353 K (176 °F).

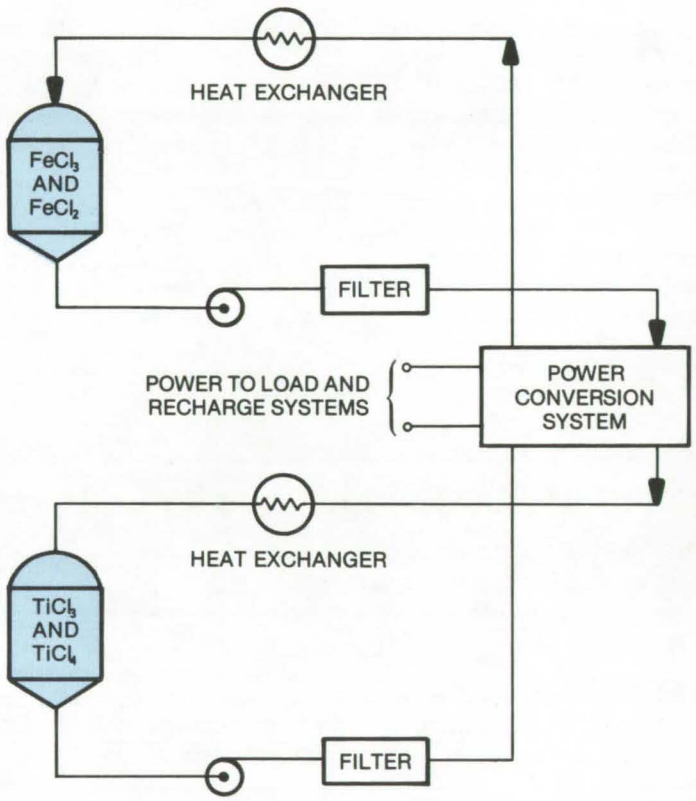

The Power Generation System shown is an electrically rechargeable redox-flow-cell power generator. This bulk energy storage concept appears particularly attractive where space and/or siting concerns limit the use of conventional storage systems.

This work was done by Marvin Warshay, Lyle O. Wright, and Lawrence A. Thaller of **Lewis Research Center.** *Further information may be found in:*

NASA TM-X-71805 [N75-32593] "Cost and Size Estimates for an Electrochemical Bulk Energy Storage Concept," and NASA TM-X-71540 [N74-21688] "Electrically Rechargeable REDOX Flow Cells."

Copies of these reports may be obtained at cost from the Aerospace Research Applications Center, Indiana University [see inside back cover].

Inquiries concerning rights for the commercial use of this invention should be addressed to the Patent Counsel, Lewis Research Center [see page 2]. Refer to LEW-12220.

NASA

Books and Reports

These reports, studies, and handbooks are available from NASA as Technical Support Packages (TSP's) when a Request Card number is cited; otherwise they are available from one of NASA's Industrial Application Centers or the National Technical Information Service.

Passive Thermal-Control Coatings

A handbook of data on coating techniques, surface selection, and damage mechanisms

A design engineer's handbook on passive thermal-control coating contains a large collection of data and a discussion of coating techniques. This information has been collected from many reports, journal articles, and proceedings. Now available in a single reference, it is a valuable tool for comparison and selection of thermal-control coatings.

Part I of the handbook discusses passive temperature-control techniques, the selection of control surfaces, and some environmental damage mechanisms in passive thermal-control surfaces. Part II presents data on the coatings, including a tabular summary.

Emphasis is placed on those references relating to extreme environments such as the vacuum of space. In selecting the data to be included in the Handbook, many data sources were evaluated, and the results of the more experienced researchers were given preference.

This work was done by T. K. Mookherji and J. D. Hayes of Teledyne Brown Engineering for **Marshall Space Flight Center.** *To obtain a copy of the handbook, Circle 51 on the TSP Request Card. MFS-22794*

NASA

Handbook of Liquid Metals

Physical properties of 20 different liquid metals

A new handbook describes physical properties of liquid metals. It is divided into three sections. The first section presents data on 20 liquid metals from aluminum through zinc. Each metal is described by physical appearance followed by atomic weight, atomic number, and valence. Other important parameters are listed as follows: (a) latent heat of fusion, (b) latent heat vaporization, (c) thermal conductivity, (d) surface tension, (e) viscosity, and (f) volume change.

Laboratory handling and safety procedures are also outlined, for each metal. An additional paragraph describes corrosion characteristics for some metals. This section is concluded with a number of graphs showing density as a function of temperature.

The second section discusses heat-transfer correlations in liquid metals. Heat-transmission mechanics are analyzed between liquid metals and the solid surfaces with which they are in contact.

The third section examines diffusion coefficients in liquid gallium/indium solution. A number of equations are used to describe the diffusion mechanism. Based on experiments conducted using gallium/indium solution and gallium liquid solvent, diffusion coefficients for liquid gallium/indium have been obtained. The section includes a diagram of the test apparatus and graphs to display test results.

An appendix section includes an expanded table for 40 metals, showing their melting-points and boiling-points. Additional tables for selected metals show thermal conductivity, density, heat capacity, and electrical resistivity at various temperatures.

This work was done by Anthony O. Ukanwa of Howard University for **Marshall Space Flight Center.** *To obtain a copy of the handbook, Circle 52 on the TSP Request Card. MFS-23355*

NASA

Life Sciences

Hardware, Techniques, and Processes

Computer Programs

Quantitative Bioluminescent Detection of Bacteria

Photobacterial bioluminescent assay of flavins are used to measure the presence of bacteria.

Goddard Space Flight Center, Greenbelt, Maryland

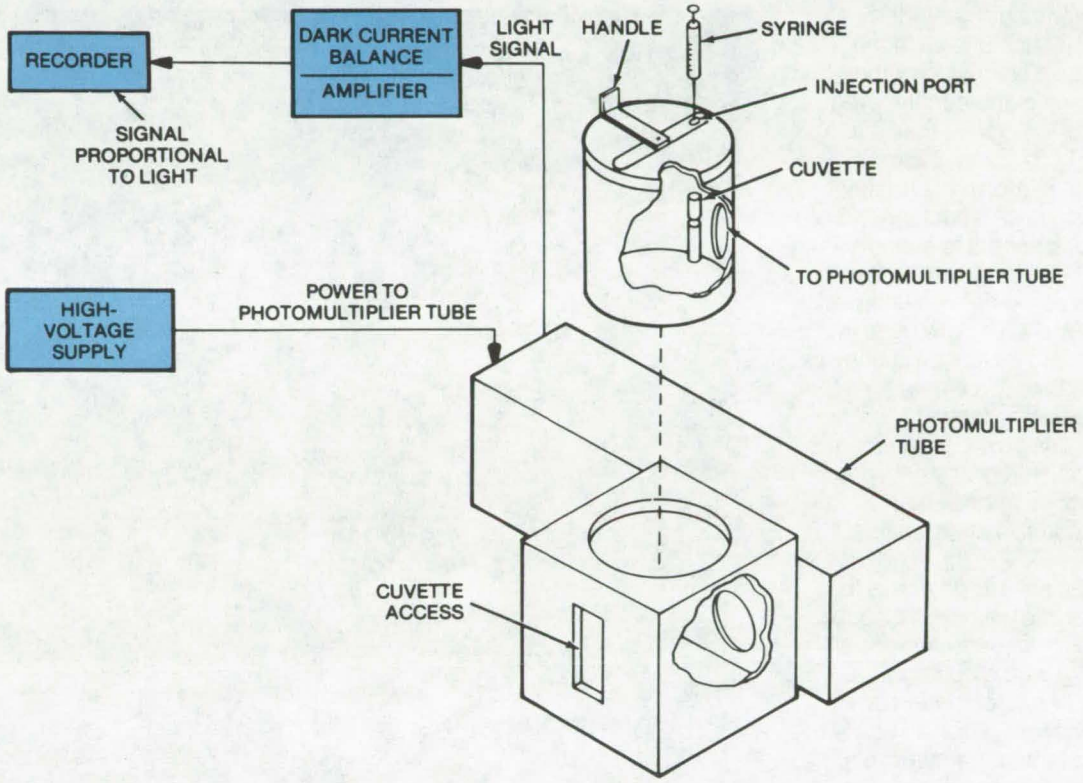

The **Instrumentation for Light Measurement** consists of a reaction chamber, a photomultiplier tube, and an amplifier/recorder.

For infection determination, ecological measurements, and the like, the detection of bacteria by rapid, sensitive, inexpensive, and automatable methods is a necessity.

In such cases, bacteria may be quantitated by measuring the phosphoflavins in a bacterial sample, using the photobacterial luciferase assay for flavin mononucleotide (FMN). The basic reaction in photobacteria is as follows:

$FMNH_2$ + long-chain aldehyde + bacterial luciferase $\xrightarrow{O^2}$ FMN + products + light

The material is boiled in perchloric acid to rupture the cells under assay. This frees bound flavin and hydrolyzes the flavin adenine dinucleotide (FAD) to FMN. Sodium borohydride with $PdCl_2$ as a catalyst is used to reduce the FMN.

The assay is performed by injecting 0.1 ml of the reduced FMN solution into 0.3 ml of the enzyme solution. The conditions of the reaction are such that the initial peak intensity is proportional to the injected FMN. The maximum sensitivity is 1×10^{-5} μg of FMN.

The instrumentation used to measure the light emitted during the bioluminescent reaction is illustrated. The reaction chamber, which is attached to the photomultiplier tube housing, is a rotary cylinder mounted in an aluminum block and cut out to accommodate a 6-mm by 50-mm glass cuvette. Immediately above the cuvette holder is a small injection port through which FMN is injected by needle and syringe into the enzyme solution. The signal from the photomultiplier tube is amplified, and the dc signal from the amplifier is read out on a chart recorder. Commercial instrumentation is also suitable. The costs of bacterial luciferase and the instrumentation are reasonable.

This work was done by Emmett W. Chappelle and Grace Lee Picciolo of **Goddard Space Flight Center.** *For further information, see "Assay of Flavin Mononucleotide [FMN] and Flavin Adenine Dinucleotide [FAD] Using the Bacterial Luciferase Reaction," in Methods in Enzymology, vol. XVIII, part B, ed. D. B. McCormick and L. D. Wright [1971], by Chappelle, E. W., and Picciolo, G. L.*

GSC-12003

NASA

Exercise Support for Therapy

Constant-value weight-relieving device is cantilevered to exert a constant support force during walking, stooping, and climbing.

Langley Research Center, Hampton, Virginia

The constant-value weight-relieving apparatus shown in the illustration is an extension of the principles used in the cantilevered constant-tension device that is a part of the Flying Lunar-Excursion Experimental Platform at Langley Research Center. A constant part of the weight of a patient is supported during rehabilitation exercise by a combination of multiple pulleys and spring clusters, which are used in conjunction with a cammed pulley to create a constant force over a specified operating range. The support harness provides the means for the user to shift pressure from hands to armpits to crotch as dictated by comfort and personal preference.

The purpose of this device is to assist individuals who are incapable of supporting their entire weight with their legs. It exerts a constant weight-relieving force during any vertical movement, such as walking, stooping, squatting, going from a sitting to a standing position, or climbing stairs during a walking exercise. The supporting force is preselected for the particular patient but can be easily changed from one value to another as the patient improves or when the device is used by a different person.

The illustration shows the evaluation prototype in use. The supporting mechanism moves on rollers engaged in an overhead track. The harness is supported by a strap attached to a cammed pulley which in turn is attached to the central shaft. Other pulleys with spring clusters attached are also mounted on this shaft, and each pulley contributes to the constant tension an amount depending on the spring force of its cluster. The desired constant tension is imposed at the supporting strap by selecting the proper combination of spring clusters and engaging the keys of those pulleys to the shaft.

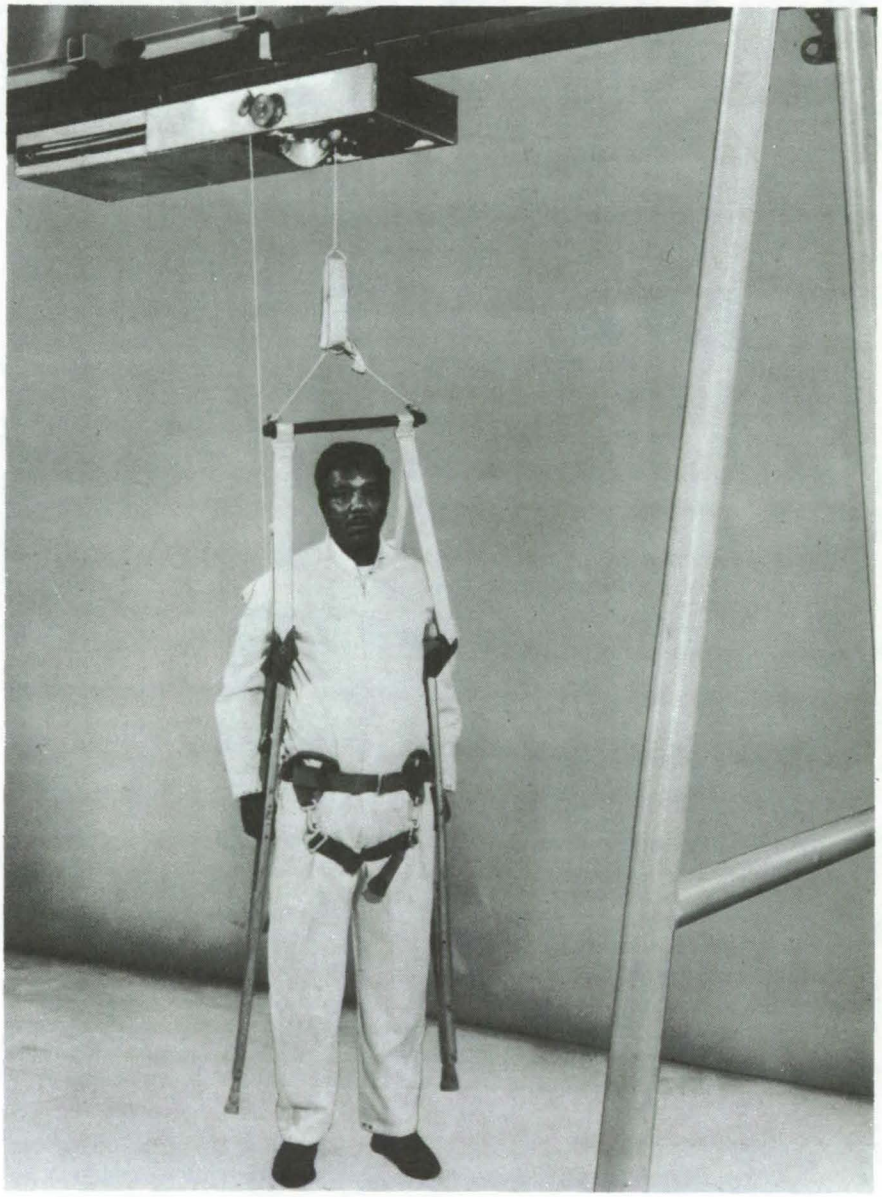

The **Constant-Value Weight-Relieving Device** moves on rollers in an overhead track. A constant percentage of the patient's weight is supported during all movements. The shortened crutches are not for assisting in walking but let the patient feel he can support himself during a fall. However, should he fall, pulleys will bring him to a smooth stop and prevent him from striking the floor.

The harness supports the patient under the arms, at the hands, under the seat, and around the upper legs. The multiple contact points permit the patient to relieve pressure at any one point by shifting it to another. The crutches do not rest on the floor, so the patient's weight, other than the constant force, is supported by his legs. If the patient should begin to fall, the cammed pulley is contoured to bring him to a smooth stop before striking the floor. It is thought that the shortened crutches may also add confidence that he will not be hurt by falling.

The patient exercises by walking back and forth under the framework. The overhead supporting mechanism is either towed along by the supporting strap or moves at a speed selected by the therapist to lag behind, to match the movement of, or to lead the patient slightly. The use of a selected speed motor and a gear box relieves the requirement for the patient to overcome the initial inertia and weight drag of the apparatus.

A spring-loaded pawl and a rachet are used to lock the mechanism in place for donning and removing the harness. An inertial locking reel is attached to a pulley on the main shaft and prevents rapid inadvertent retraction. In a modification of the supporting harness, flexible straps are used in place of the crutches to enable the patient to don the harness while in a sitting position. Industrial applications of this device have also been suggested for locations such as warehouses and equipment storage facilities where heavy equipment is handled, particularly shock-sensitive equipment and instrumentation.

This work was done by Moses J. Long and Stephen C. Irick of **Langley Research Center.** *For further information, Circle 53 on the TSP Request Card.*

Inquiries concerning rights for the commercial use of this invention should be addressed to the Patent Counsel, Langley Research Center [see page 2]. Refer to LAR-11975.

NASA

Myocardial Wall-Thickness Transducer

A lightweight, small transducer allows measurement of the heart wall without significantly disturbing normal heart functions.

NASA Pasadena Office, Pasadena, California

A new transducer has been developed for measuring the wall thickness of myocardium, the middle and thickest layer of the heart wall. Conventional myocardium transducers have been bulky, difficult to install, and tended to traumatize the muscle, thereby interfering with the measurement in progress. Through the use of mechanical and electronic miniaturization techniques, the new transducer, shown in the figure, is lightweight and small. When it is inserted into the myocardium the disturbance of normal functions is minimal.

The wall-thickness transducer consists of a highly-compliant circular beam to which are attached a silicon-semiconductor piezoresistive strain gage and a barbed needle. To measure radial deflection of the myocardium, the needle is pushed into the tissue until the circular beam rests firmly on the epicardium. A change in the thickness of the myocardium will deform the beam and cause the resistance of the piezoresistive strain gage to change. The gage is connected to conventional instrumentation that is calibrated to measure the percent change in the myocardial-wall thickness from a baseline at the end of diastole to other significant events throughout the heart cycle.

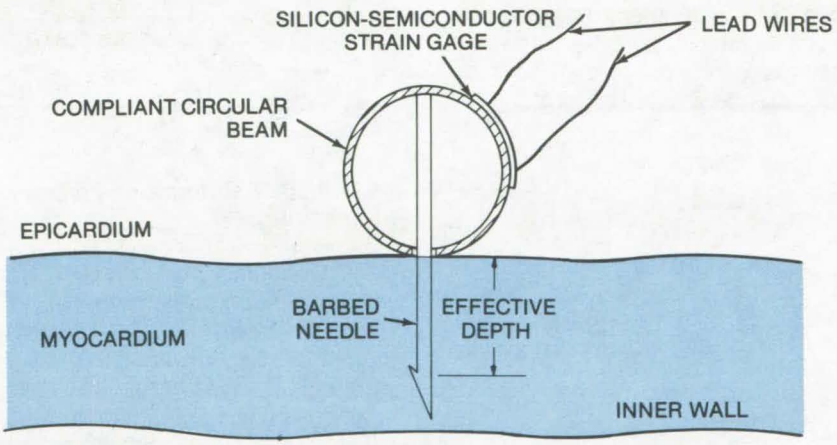

The **Biotransducer** with piezoresistive strain gage and a highly-compliant circular beam is shown embedded in the myocardium. The lead wires are connected to conventional instrumentation. Note that the needle does not penetrate the inner wall of the myocardium.

This work was done by Cyril Feldstein, Gilbert W. Lewis, Robert H. Silver, and Virgil H. Culler of Caltech/JPL for **NASA Pasadena Office.** *For further information, Circle 54 on the TSP Request Card.*

This invention is owned by NASA, and a patent application has been filed. Inquiries concerning nonexclusive or exclusive license for its commercial development should be addressed to the Patent Counsel, NASA Pasadena Office [see page 2]. Refer to NPO-13644.

NASA

Lightweight Orthotic Appliances

Graphite-filament-reinforced polymer materials used to fabricate body braces are stronger, yet thinner than components made from polypropylene.

Langley Research Center, Hampton, Virginia

A new technique has been devised for the fabrication of complex, high-strength, and lightweight articles and structures such as orthotic appliances and braces. It provides an alternative to the plastic materials and attendant processes currently utilized in a variety of orthotic brace components. To sustain the loads and subsequent deflections applied to orthotic appliances and braces made of materials such as unfilled polypropylene (one of the most widely used plastic materials) it is commonly necessary to use very thick material. The required thicknesses can result in skin chafing, excessive weight, and an undesirable appearance. Furthermore, the use of a polypropylene ankle support, as shown in Figure 1, frequently requires orthopedic shoes of different sizes for each foot to compensate for the increased interior volume necessary for the shoe with the support.

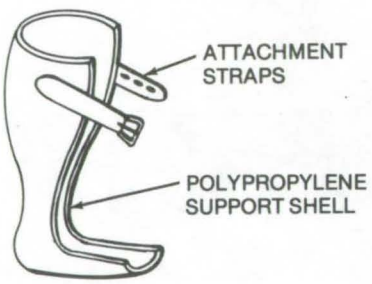

Figure 1. **A Polypropylene Ankle Support**

Graphite-filament-reinforced polymer materials, such as woven graphite-cloth-reinforced polysulfone, are used in a wide variety of applications requiring high tensile strength and modulus. This material is on the order of 20 times stronger and about 50 times stiffer than the unfilled polypropylene. These superior properties permit the fabrication of orthotic devices which are considerably lighter, thinner, and stiffer than conventional components.

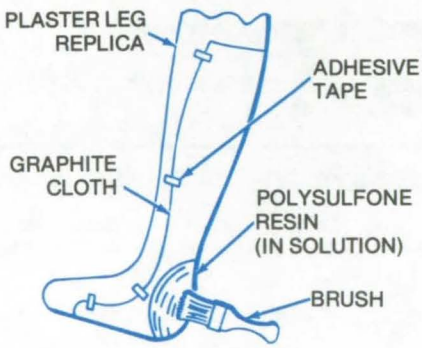

Figure 2. **Fabrication of a Drop Foot Support**

To manufacture a complex curved support, such as the drop foot support shown in Figure 2, woven graphite cloth is draped to the contour of a plaster replica of the patient's leg. Polysulfone, in solution with a low-boiling-point solvent such as chloroform, is then applied to the cloth with an applicator such as a brush or by spraying or dipping. The solvent readily evaporates to leave a solid polysulfone matrix around the graphite cloth. These steps are repeated as many times as necessary to build up the required thickness. A support produced by this technique eliminates the problems encountered with the thick-section polypropylene.

These composite materials and this process can be applied to a variety of orthotic appliances and braces with a capital outlay generally much less than that required for polypropylene devices. Since the reinforcement (graphite cloth) and the matrix (polysulfone in chloroform solution) are combined on the desired contour form with no subsequent processing required, many pieces of auxiliary equipment such as heated ovens, vacuum forming equipment, and autoclaves are not required as in the case of polypropylene, heat-curing polymers, and post-curable reinforced thermoformable systems.

This work was done by Robert M. Baucom and Terry L. St. Clair of **Langley Research Center.** *For further information, Circle 55 on the TSP Request Card.*
LAR-11918.

NASA

Remote, Unattended, Forest Fire Detector

Two concepts for scanning large land tracts: an ultrasensitive temperature transducer and a slow-scan TV.

Marshall Space Flight Center, Alabama

Many forest fires start in remote areas too distant to be detected from fire lookout towers. Only on rare occasions are these fires spotted by anyone (e.g., pilots) and reported before huge tracts of land are destroyed. In view of this, current NASA technology has been surveyed to see if it can be applied for early fire detection.

Various monitoring instruments developed for the Ranger, Surveyor, Mariner, and Lunar Orbiter programs have been examined. One of the applicable instruments is a temperature-sensing system developed for the lunar soft lander. The system is capable of detecting a match flame many miles away. Conceivably it can be mounted on a pedestal above a forest and can scan the surrounding area (e.g., every 5 minutes). The system output would be amplified and converted to a tone with frequency in proportion to the temperature of the scanned area. This signal can be readily transmitted to a central station through a conventional telephone line.

The central station will include a strip-chart recorder with a ramp or a triangular wave generator. The incoming intensity signal frequency would then be converted to an ac signal with an rms or a peak-to-peak voltage directly proportional to the temperature of the scanned sector. This ac signal then is added as a dither signal to the dc ramp-generating signal, indicating azimuth and slant position of a fire.

An alternate approach is to use a television camera. This involves two possibilities. In the first, a standard industrial television camera is installed on a tower overlooking a forest. The camera would be provided with automatic light balance and remote control of position, filter, and focus. This system would convert a single full-field image into a series of tone-modulated signals transmitting over a telephone line. The signals generated by the camera are slowed electronically by using a television disk for conversion and transmission on a line-by-line basis. The process is reversed at the central station to reconstruct the scene viewed by the camera.

The second possibility is to use a flying-spot scanner similar to that in the Surveyor soft lander. In this case a photocell would see only the intensity of the flying spot brought to it by the mechanical sweep-and-scan mechanism. This single bit of information is easily encoded for transmission over a telephone line. Again, a regeneration technique is used to reconstruct the image at the central station.

To date the telephone lines seem to be the most economical means of communication with the fire-monitoring equipment. Microwave and laser communication systems have also been considered; however, they are restricted to line of sight. Lasers in addition are easily obscured by smoke, haze, and fog. Coaxial cables used in television transmission are more costly.

Another possible method of fire detection is to use weather satellites. At this stage, however, they do not have sufficient resolution to pinpoint fires from space. With further development these satellites may become very effective fire monitors.

This work was done by David J. Winslow of **Marshall Space Flight Center.** *For further information, Circle 56 on the TSP Request Card.*

Inquiries concerning rights for the commercial use of this invention should be addressed to the Patent Counsel, Marshall Space Flight Center [see page 2]. Refer to MFS-21221.

NASA

Computer Programs

These programs may be obtained at very reasonable cost from COSMIC, a facility sponsored by NASA to make new programs available to the public. For information on program price, size, and availability, circle the reference letter on the COSMIC Request Card in this issue.

Proton Tissue Dose

Exposure to isotropic radiation

Design of radiation shields and dosimeters requires calculation of the anticipated dose distribution in the human body for the pertinent radiation environment. A new program calculates the proton dose averaged over five major segments (upper limbs, lower limbs, upper trunk, lower trunk, and skull) of the blood-forming organ (BFO), treating the human body geometry in detail but assuming isotropicity of the incident primary particles.

An approximate form of transport theory is used, incorporating nuclear star effects. The three basic functions generated are the areal density distribution function, the fluence-to-dose conversion factors for normal incidence on a slab, and the incident fluence spectrum. Two numerical integrations are used to evaluate an intermediate equation and then the dosage equation. Integrations over areal density and energy use the Gauss-Legendre quadrature formula.

FORTRAN IV
CDC 6000, Run compiler

This program was written by John W. Wilson of **Langley Research Center** *and Govind S. Khandelwal of Old Dominion University. For further information, Circle B on the COSMIC Request Card.*
LAR-11802

NASA

Mechanics

Hardware, Techniques, and Processes

Books and Reports

Computer Programs

Hydrostatic Lift-Off Seal

A high-pressure seal for a rapidly rotating shaft restricts leakage when the shaft is stationary and allows a small controlled leak when it is rotating.

Marshall Space Flight Center, Alabama

A seal on a dynamic interpropellant turbopump serves as a static seal at rest and as a dynamic seal with shaft rotation. The dynamic pressure differential, sealed, is up to 7,000 psi (48×10^6 N/m^2) with surface velocities on the order of 500 ft/s. The seal operates in an oxidizer propellant, with the seal diameter established by rotor axial thrust.

The interpropellant turbopump oxidizer seal consists of four basic parts: (1) the smooth flat surface on the back of the second-stage oxidizer impeller, (2) the floating seal ring, (3) the semistatic piston-ring secondary seal, and (4) the low-pressure flexible-bellows static secondary seal. The seal performs the two discrete functions of static sealing at rest and controlled-leakage sealing in operation.

The single inner land serves as the static seal and the control clearance to the overboard vent. A low-pressure intermediate cavity is vented to pump suction, thus resulting in minimum leakage to the overboard vent. Upon shaft rotation, high pressure from the impeller discharge enters the hydrostatic seal face, through the outer land and the compensating orifice to separate recesses; it exits across the adjacent land to the intermediate cavity.

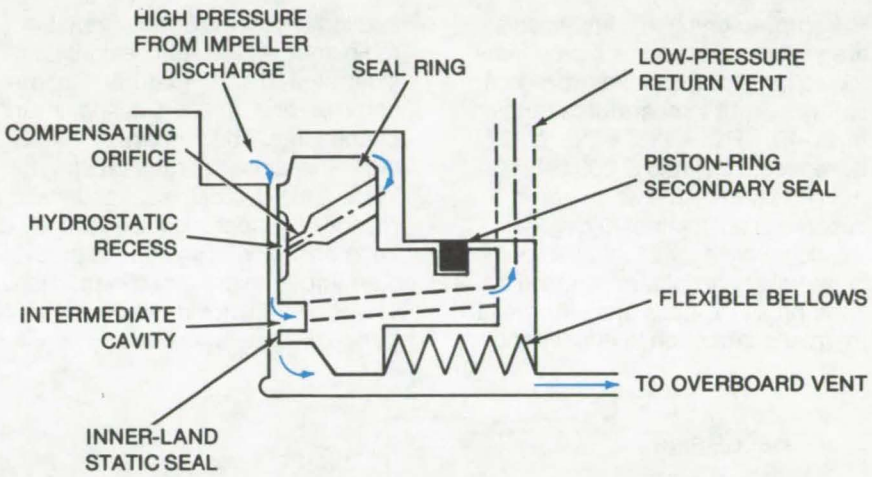

The **Interpropellant Turbopump Seal** is shown with arrows indicating the hydrostatic pressure flow that occurs upon shaft rotation.

The hydrostatic action causes the seal ring to lift off and track the running ring on a thin fluid film with extremely high restoring forces, due to the high-pressure drop across the seal. To allow the seal ring to track the running ring while minimizing leakage to the low-pressure return vent, a piston ring is used as a high-pressure semistatic secondary seal. Since the low-pressure secondary seal must be a positive seal in parallel with the static-sealing land, a flexible welded metal bellows is used. Pressure balancing assures minimum relative deflection between the running ring and the seal ring. The diameter of the flexible bellows is selected to provide a positive sealing force under any tank pressure.

Due to the high pressure supply and the heat generated, the sealed fluid (LOX) will change phase, somewhere between the low-pressure intermediate cavity and the atmospheric overboard vent. This phase change is designed to occur at the exit of the inner land.

This work was done by Paul S. Buckmann of Aerojet Liquid Rocket Co. for **Marshall Space Flight Center.** *No further documentation is available.*
MFS-21496

NASA

Atmospheric Particle Sampler

Positive and/or negative pressure is used to trap airborne particles against a filter. Positive pressure is provided by a low-molecular-weight gas (He or H) to achieve a high particle velocity and a high capture percentage. Trapped particles are examined under an electron microscope.
(See page 68.)

Myocardial Wall-Thickness Transducer

A small, lightweight transducer consists of a highly-compliant circular beam attached to a piezoresistive strain gage and a barbed needle. It measures radial deflection of the myocardium with minimal disturbance of normal heart functions.
(See page 83.)

Nondestructive Inspection of Multilayered Insulation

Radio-frequency techniques are used to evaluate multilayered cryogenic insulation. The insulation is probed with an electromagnetic field generated by an induction coil. The coil impedance is a function of metal loss and layer density.
(See page 129.)

Improved Cryogenic Shaft Seals

High-pressure shaft seals accommodate radial and axial play including tilting motion

Marshall Space Flight Center, Alabama

Improved cryogenic shaft seals are designed for use with propellant (liquid oxygen and liquid hydrogen) ball valves, at temperatures ranging from -400° F to +130° F (33 to 327 K, respectively) and 8,000 psig (55×10^6 N/m^2). The seals are capable of sustaining 90-degree rotation, with a substantial amount of lateral and axial play, caused by large pressure loads and differential thermal contraction in their intended application on the Space Shuttle main engine. The seal designs, as illustrated, display features that are common and, in some cases, interchangeable. The primary differences are the method of loading the dynamic seal and the means of supporting the seal body or cage on the housing against pressure thrust, to prevent dynamic seal extrusion and provide low-friction torque.

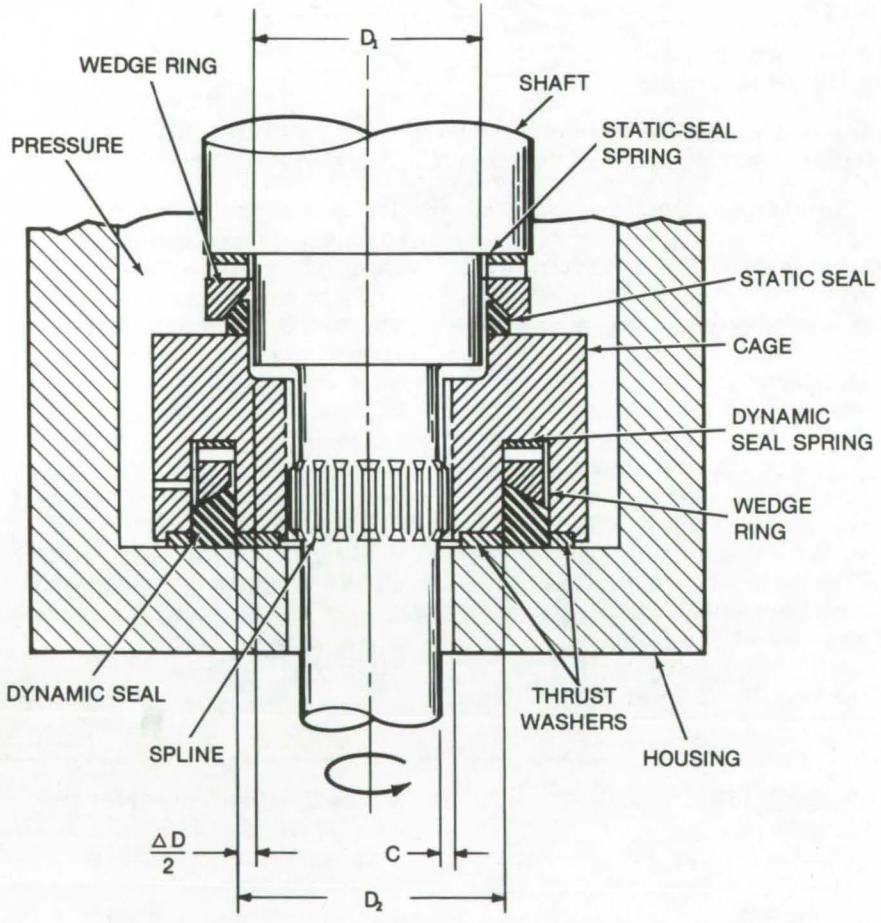

Figure 1. The **Journal-Bearing Shaft Seal** has a cage that is spline keyed to the shaft and provides a strong metal body for the two polymer seals.

The journal-bearing seal is comprised of a cage which is spline keyed to the shaft and which provides a strong metal body for two polymer seals, one dynamic and one static. Diametral clearance for the static seal is small [less than 0.002 in. (0.05 mm)] to preclude high-pressure extrusion. The static seal is spring loaded through a metal wedge ring to provide a low-pressure seal, and also to load the cage against the housing and provide an intimate low-pressure contact between the housing and the thrust washers. The dynamic seal is keyed to the cage and loaded by a metal wedge ring and a spring. Seal sliding is thus confined to the interface between thrust washers, dynamic seal, and housing. Dynamic-seal extrusion is prevented by the intimate contact between thrust washers and housing.

Dynamic seal wear is accommodated by the seal loading spring and the axial feed of the seal into the housing seal face. Minimum shaft torque is obtained by partially balancing the pressure thrust force with a stepped shaft. Only sufficient annular pressure area is exposed (i.e., ΔD) to ensure intimate contact between thrust washers and housing.

The roller-bearing seal cage is loaded onto the housing by the static polymer seal spring. The dynamic polymer seal is spring loaded independently by approximately eight pins through a metal wedge ring. This technique provides for a substantial amount of dynamic seal wear. The seal cage is keyed to the shaft through a single tang, although the spline approach could be used also.

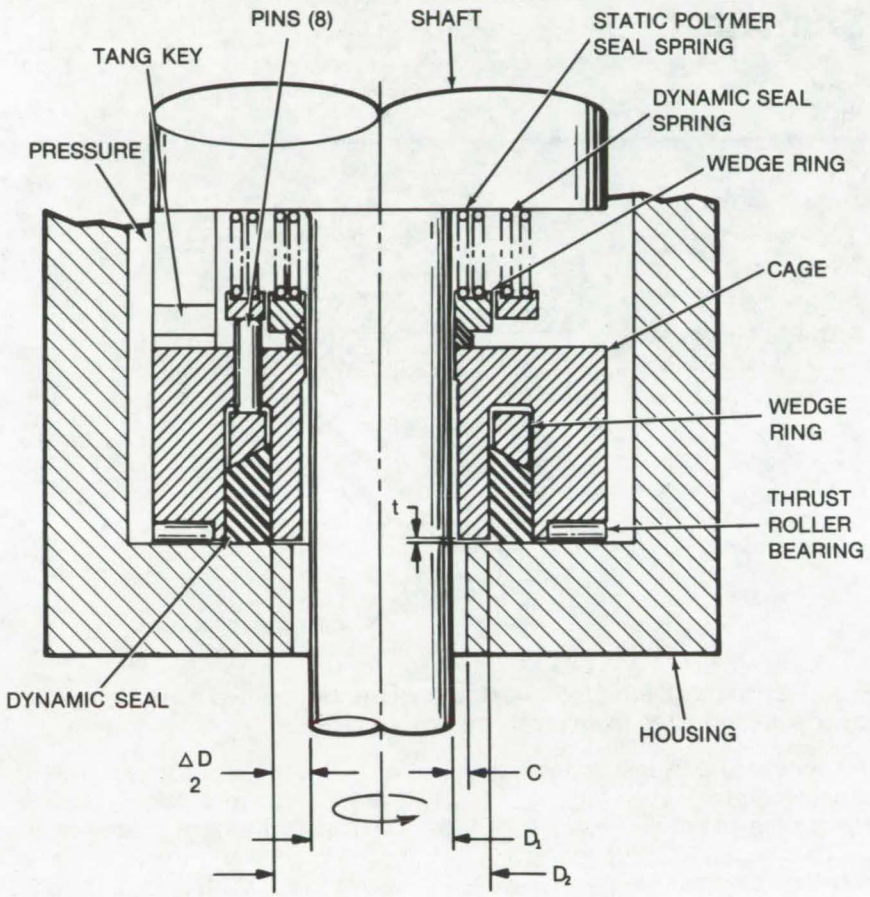

Figure 2. The **Roller-Bearing Shaft Seal** has a cage that is loaded into the housing by a static polymer seal ring.

Thrust loads are considerably larger with the straight shaft as compared with the stepped shaft seal, because of much larger exposed unbalanced annulus. With journal thrust washers, torque would be excessive; therefore, the thrust roller bearing is used. Dynamic seal extrusion and wear is minimized by providing a small clearance (t) between the seal cage and the housing face.

This work was done by Willard A. Gillon, Jr., and Gilbert F. Tellier of Rockwell International Corp. for **Marshall Space Flight Center.** *For further information, Circle 60 on the TSP Request Card.*
MFS-19153

NASA

Calibration of Image Dissector Tubes

An image dissector tube calibration technique consists of a computer-controlled light-emitting diode (LED), a precision machined mask, and analog-to-digital converter (ADC). The computer turns on the LED which floods the masked face of the tube. An intensity pattern, generated as the tube is electromagnetically swept, is fed to the ADC which controls tube calibration.
(See page 63.)

Measurement of Transient Reflectance

A real-time reflectometer which is not susceptible to environmental contamination can be adjusted to a fraction of a second to measure transient effects. To minimize extraneous effects of the instrument, the reflectance and reference signals travel the same optical path. The only moving parts are the sample and one set of mirrors.
(See page 46.)

Anamorphic Lens for Tracking System

An anamorphic lens with a 2:1 focal-length ratio consists of three spherical elements and two cylindrical elements. The total length of the lens is 7.6 cm, and is designed to minimize image spot size. When used in conjunction with an image dissector tube, the expected root-mean-square noise equivalent angle is approximately 8 arc seconds.
(See page 54.)

Cost-Saving Synergistic Shaft Seal

An elastomeric seal lip may be replaced with a pair of segmented carbon rings.

Lewis Research Center, Cleveland, Ohio

Elastomeric lip seals as used on some aircraft and accessory transmissions tend to leak excessively at the higher sliding speeds. Elastomeric lip seals are usually satisfactory at sliding speeds below 1219 m/min (4000 ft/min); however, at higher speeds, the temperature of the lubricating film (under-lip temperature) exceeds the useful temperature limit of the elastomer causing elastomer degradation and leakage of the lubricant out of the transmission. Also, as rotative speed increases, the elastomeric lip ceases to follow the runout motions of the shaft.

Conventional carbon ring seals (circumferential and face types) can run successfully at high sliding speeds, but the cost is ten times (or greater) that of a lip seal.

This problem may be overcome by replacing the lip of the elastomeric seal with a pair of segmented carbon rings (see Figure 1). If wear occurs in the carbon ring bore, then the elastomeric flex section and garter springs act to maintain contact between the carbon rings and the shaft. The two rings are segmented with the gap between the rings indexed so that leakage paths are blocked. The carbon rings can withstand the high temperature developed in the lubricant film and can even run dry against the shaft.

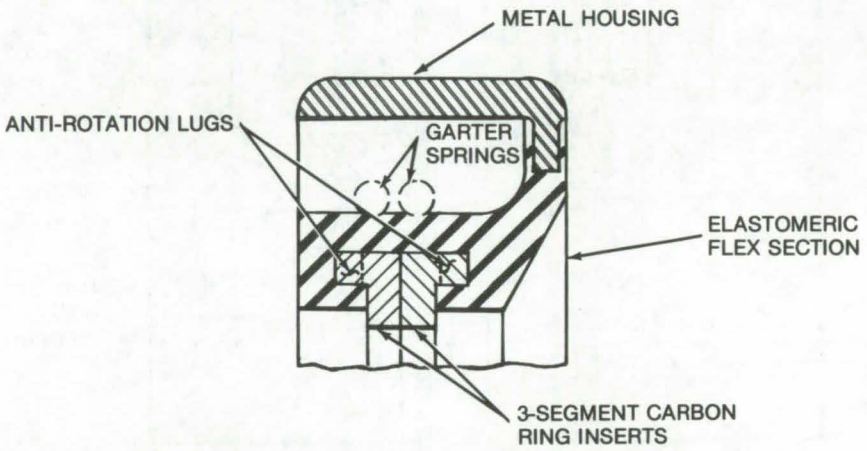

Figure 2. In the Synergistic Seal shown the segmented carbon ring inserts are mounted in an elastomeric ring section.

The synergistic shaft seal is a marriage between the lip seal and the conventional segmented carbon ring seal. The segmented rings provide the resistance to the high temperature generated in the lubricating film, but the machining and close manufacturing tolerances of the conventional segmented seal are avoided by mounting the segmented rings in an elastomeric flex section (see Figure 2). The elastomeric band contains suitable lugs for anti-rotation purposes. The elastomeric flex section has an additional advantage of allowing the segmented rings to align themselves to the shaft O.D. (In a conventional segmented seal, simultaneous alignment of the rings to the shaft and seal housing is difficult to achieve and is one of the principal causes of leakage.)

Bench tests were run on a synergistic seal having an 11.258 cm (5.481 in) bore. The seal was operated to sliding speeds of 20,000 ft/min with a radial runout of 0.010 cm (0.004 in). The sealed pressure was 2.07 N/cm^2(3 psi). These tests revealed that the synergistic seal has at least three times the speed capability of elastomeric lip seals, and a speed capability comparable to that of conventional carbon ring seals with an anticipated cost of less than one-half that of conventional carbon ring seals.

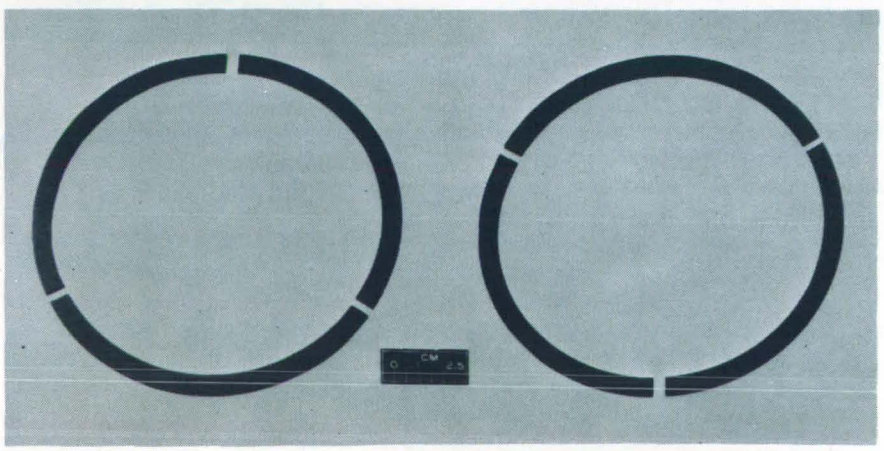

Figure 1. Segmented Carbon Rings are used to replace the elastomeric seal lip.

This work was done by Lawrence P. Ludwig and Thomas N. Strom of **Lewis Research Center.** *No further documentation is available.*

Inquiries concerning rights for the commercial use of this invention should be addressed to the Patent Counsel, Lewis Research Center [see page 2]. Refer to LEW-12119.

NASA

Peak-Acceleration Limiter

A statistical limiter protects test specimens during random vibration testing.

NASA Pasadena Office, Pasadena, California

A peak-acceleration statistical limiter has been designed to protect test articles from damage during random vibration testing. The limiter differentiates between peak acceleration levels that are normal components of the vibration signal and those that exhibit damaging characteristics. Unlike conventional peak-acceleration limiters, which abort the vibration test whenever a peak signal exceeds a given level, the statistical limiter aborts the test only when the statistical properties of the vibration signal change significantly or when a catastrophic transient occurs.

The output signal of an accelerometer monitoring a random vibration test exhibits instantaneous peak levels with amplitudes ranging from a fraction to four times the rms signal level. The amplitude distribution with respect to time is random. Thus the distribution of peak levels can only be described in statistical terms. If the rate of occurrence of peak levels is measured at some given level, such as three times the rms value, it will be found that for wideband random noise the rate will be about 20 peaks per second on the average. At four times the rms level, the rate will average about 4 peaks per 10-second time interval.

The Gaussian distribution of the peak levels provides the basis for the statistical peak limiter. Two comparators form a voltage amplitude window of variable width. The rms value of the acceleration signal is taken as the reference voltage. The variable voltage is then the absolute value of the peak signal. When the variable voltage is within the amplitude window, an EXCLUSIVE OR gate generates an output that is registered by a decade counter. This process continues for 1 second until the counter is reset. Thus the counter indicates events per second which occur within the amplitude window.

Since the probability distribution of the events versus time is known, the output of the decade counters can be used to initiate the shutdown of the vibration system. For example, if the expected number of peak signals at 3 sigma is known not to exceed 26 peaks per second 99.97 times out of 100, then the counter can be set to indicate when a count of 27 is reached. Therefore a count of 27 indicates that a statistically significant change has occurred, and the vibration test is automatically aborted.

A second counter system detects transients exceeding four times the rms level. It determines the time interval during which the transient exceeds the 4-sigma reference level. This is useful because the width of the transient determines its damage potential. The greater the pulse width, the greater the damage potential.

A relatively narrow pulse (0.5 ms) has a broad frequency distribution, and each spectral component has low-energy content. A relatively wide pulse (6 ms) has a narrow frequency spectrum concentrated in a lower frequency range than the more narrow pulse. This type of pulse may be very damaging and must be suppressed. The transient detector circuit measures the pulse width and can be set to shut down the vibration system quickly if the pulse exceeds safety criteria. Pulse width is measured by gating a periodic wavetrain into the counter during the transient.

This work was done by Raymond C. Woodbury of Caltech/JPL for **NASA Pasadena Office.** *For further information, including schematics and a more detailed description, Circle 61 on the TSP Request Card.*
NPO-11940

NASA

Selective Image Enhancement

A digital image-enhancement technique for TV systems can also be used with *remote manipulators.* An algorithm is used to divide an image into pixels, which may be individually enhanced. Enhancement may be controlled with a joystick. A similar arrangement simplifies remote manipulator operation.
(See page 29.)

General-Purpose Data Link

A communications modem comprising a transmitter, a demodulator, a modulator, and a receiver is compatible with a telephone line, a video pair, or a 1,250-ohm twisted-wire pair. It permits a wide range of input and output voltages and flexible data rates, and it has provision for a computer interface.
(See page 33.)

Vacuum-Jacketed Line Spacer

Direct radiative heat paths between inner and outer spacer are eliminated.

Lyndon B. Johnson Space Center, Houston, Texas

Cyrogenic lines must be well insulated in order to prevent the cryogenic fluid from heating up. At the same time, the lines must have enough flexibility to thermally contract when first filled with cold fluid. Vacuum jacketing is a well-known technique that could provide good insulation, except that the required spacers constitute a heat-conduction path that can cause excessive boil off in the line.

An improved spacer for vacuum jacketed lines is shown in Figure 1. It has three integral, equally-spaced, leaf springs, shown in detail in Figure 2. Conductive heat leaks into the cryogenic line are minimized through material selection and leaf length. Additionally, the spacer configuration minimizes radiation by eliminating direct radiative paths between the inner and outer lines.

There are four novel features in this concept: (1) the use of a leaf spring to provide interline structural support, (2) the use of a leaf spring to lengthen the thermal conduction path and reduce heat transfer, (3) the use of a leaf-spring spacer fabricated from a single piece, and (4) the use of a leaf spring to accommodate differential thermal expansion of the inner and outer line.

This work was done by Fred A. Houte, Harris B. McKee, and Thomas C. Patten of McDonnell Douglas Corp. for **Johnson Space Center.** *No further documentation is available.*
MSC-14365

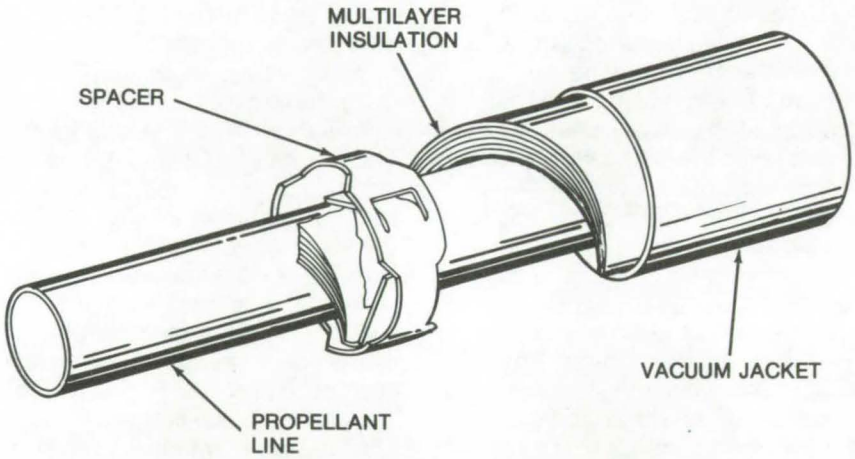

Figure 1. The **Vacuum Jacketed Line Assembly** employs a spacer consisting of a circumferentially-supported three-leaf spring.

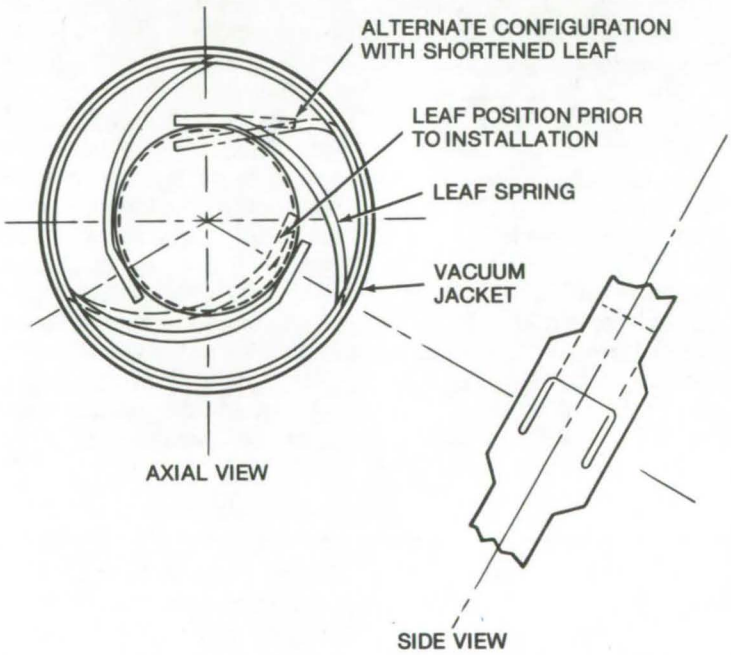

Figure 2. Detail of **Leaf Springs** for vacuum-jacketed spacer

NASA

Inexpensive Leak-Detector Envelope

An easily-constructed vacuum envelope is used with a mass spectrometer to locate leaks in large systems.

Lewis Research Center, Cleveland, Ohio

An inexpensive vacuum envelope for locating leaks in large systems can be constructed from readily available and inexpensive components. The figure shows the parts of such a small vacuum envelope, constructed to leak-check a helical coil of tubing in a large system.

The chamber is basically a stainless-steel 3.5-in. (8.9-cm) pipe elbow [4.0-in. (10.1-cm) O.D. by 0.083-in. (0.211-cm) wall] which is split lengthwise. A 1.0-in. (2.5-cm) hole is drilled in one-half of the elbow, into which is welded a 1.0-in. (2.5-cm) tube for the leak-detector connection. The end seals are rubber stoppers, each with an axial hole in the center to fit tightly around the tube of the helical coil. Each stopper is split along a radius with a sharp blade so that the stopper can be slipped over the tube. Sections of a 3.5-in. (8.9-cm) tube are welded into each end of the elbow so that the stoppers seal against a cylindrical surface. In assembling the chamber around the tube, the two halves of the pipe are sealed with silicon rubber sealant and clamped together with large hose clamps. The rubber stoppers are then slipped over the tube and forced into the ends of the pipe.

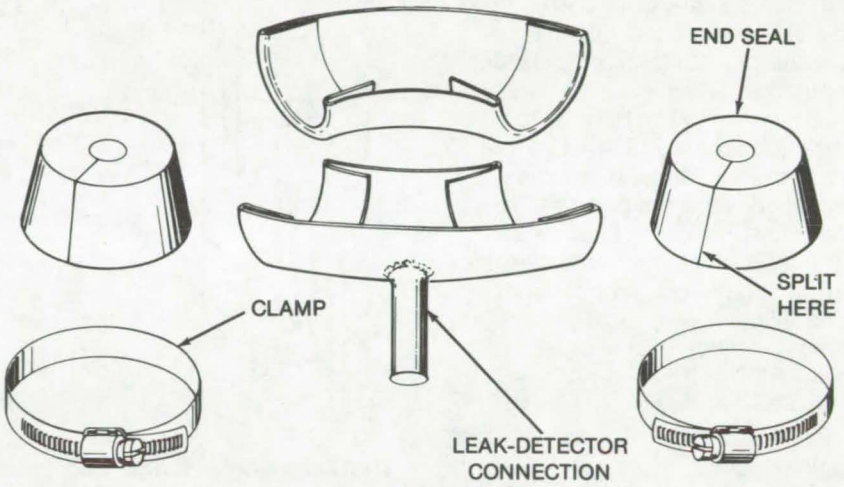

The **Leak-Detector Envelope** components shown above form a small vacuum chamber designed to fit around a helical coil.

A helium mass-spectrometer leak detector is attached to the envelope, and the section of the system enclosed in the envelope is filled with helium. If no leakage is indicated in the section which is enveloped, the envelope is moved to the adjacent section and the process is repeated. This procedure is continued until a leak is located, or the system is determined to be free of leakage.

The vacuum-envelope method is a much more sensitive technique when high helium pressure can be employed, which may decrease the response time by several orders of magnitude.

This work was done by T. F. Lyon of General Electric Co. for **Lewis Research Center.** *No further documentation is available.*
LEW-11305

NASA

Exercise Support for Therapy

A constant-value weight-relieving apparatus supports the weight of a walking, stooping, squatting, or standing patient with a combination of multiple pulleys and spring clusters. The individually preselected support force is constant for all movements. The supporting mechanism moves on rollers on an overhead track.
(See page 82.)

Ultra-High-Vacuum Electrical Feedthrough

An ultra-high-vacuum electrical feedthrough for cathodic sputtering makes use of the cathode dark-space region adjacent to negative-potential surfaces. Made of metal and glass, it is helium leak-tight, and bakeable, and has been used in vacuum systems at pressures down to 2×10^{-11} torr.
(See page 13.)

Zero-Angle Helical Coil

A specialized helical coil has no linear axial motion from thermal expansion or coil-winding movements.

Goddard Space Flight Center, Greenbelt, Maryland

A specialized type of helical coil has been developed which could be useful in various types of actuators, such as temperature controls.

When using wide bimetallic coil stock, a necessity to meet torque requirements, small-diameter helical coils are not practical. Winding such a coil requires a large helix angle, and considerable torque capability is lost because bimetallic action causes motion along the winding axis instead of around it.

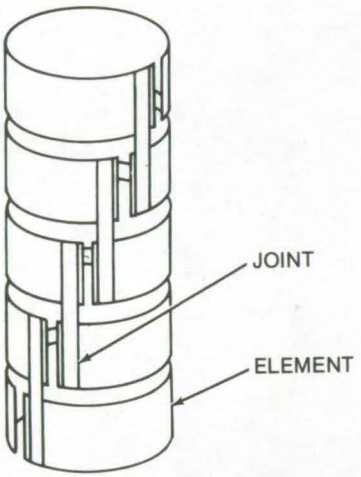

The **Zero-Angle Helical Coil** is constructed of bimetallic stock material. It was originally developed for a Sun-tracking device, but could be used where minimal axial spring force is needed.

To avoid this problem, a zero-angle helical coil may be constructed as shown in the figure. Bimetallic stock of any width may be formed into segments of small diameters and fastened together by metal strips as shown. In this way it is possible to wind small-diameter coils of relatively-wide bimetallic stock which exhibit no linear axial motion due to thermal expansion.

This work was done by J. A. Troendle of Lockheed Missiles & Space Co. for **Goddard Space Flight Center.** *No further documentation is available.*
GSC-10969

NASA

Reducing Cold Flow in Elastomeric O-Rings

A mechanical and thermal treatment markedly reduces cold flow in O-ring seals.

Marshall Space Flight Center, Alabama

A new technique accelerates the compression set of elastomeric O-rings. These and other seals incorporating this procedure do not require an auxiliary load or torque to compensate for cold flow.

Elastomers have higher compressive strengths as the temperature lowers. However, many applications require that an elastomeric seal be exposed to cryogenic temperatures during only a portion of its use. Thus, the vacuum held by the seal can change as the cold flow occurs, causing the shape and compressive strength of the elastomer to change.

It has been found that seals made by other hot-forming techniques maintain a constant vacuum under temperature changes. The built-in

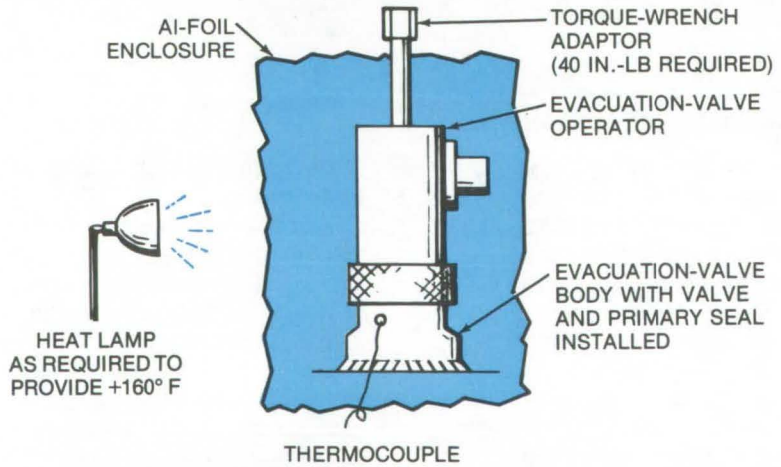

Figure 1. **Hot-Formed O-Rings** can be made with the apparatus shown. A thermocouple is used to control a lamp which, together with an aluminum-foil reflector, provides the heat. Mechanical force is applied with a torque wrench.

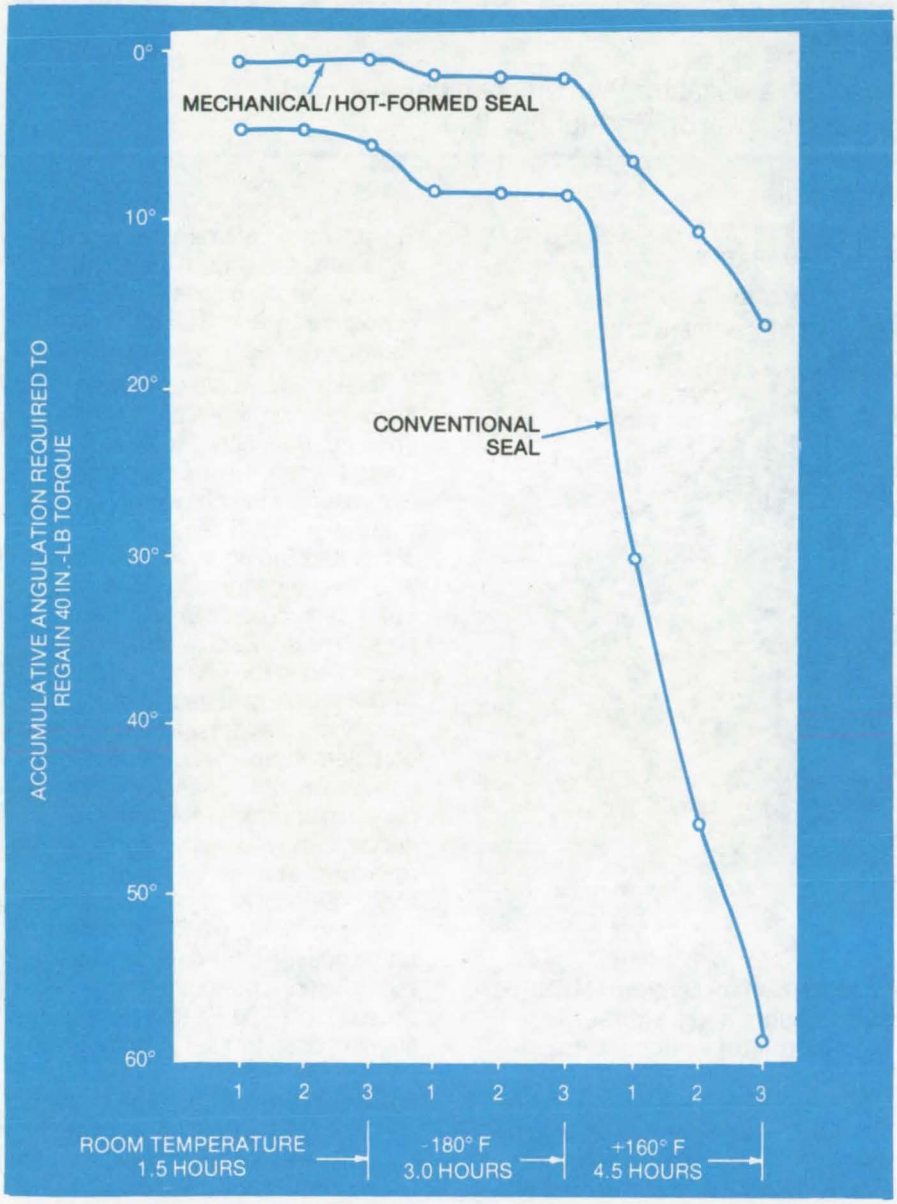

Figure 2. **Vibration Tests** were made on conventional and hot-formed O-ring seals on the same evacuation valve. Three different frequencies (designated as 1, 2, and 3 on the abscissa) and three different temperatures were used. Cold flow was measured as the angulation needed to regain the required sealing torque. The performance of the hot-formed seal can be seen to be definitely superior.

cold flow is accelerated, by quickly molding the seals into the shapes they will tend to assume over extended periods of time.

Figure 1 shows the setup used to form a seal. The operation is as follows:

1. The seal is pressure loaded.
2. The seal and loading mechanisms are heated to 160°F (345K).
3. A load is applied to the heated seal, causing the material to flow.
4. The parts are cooled to room temperature.
5. The load is removed.

Figure 2 shows a test on an evacuation valve using an elastomeric O-ring seal. Two runs were performed: the first with a conventional seal; the second with the hot-formed seal. It can be seen that greater angulation was required to maintain the vacuum with the conventional seal.

This work was done by Robert H. Henry and Owen K. Olsen of Rockwell International Corp. for **Marshall Space Flight Center.** *For further information, Circle 62 on the TSP Request Card.*
MFS-24336

NASA

Fast Pressure-Sensor System

Electronically-switched pressure-sensor array is faster than mechanical systems and allows real-time analysis and display of wind-tunnel data.

Langley Research Center, Hampton, Virginia

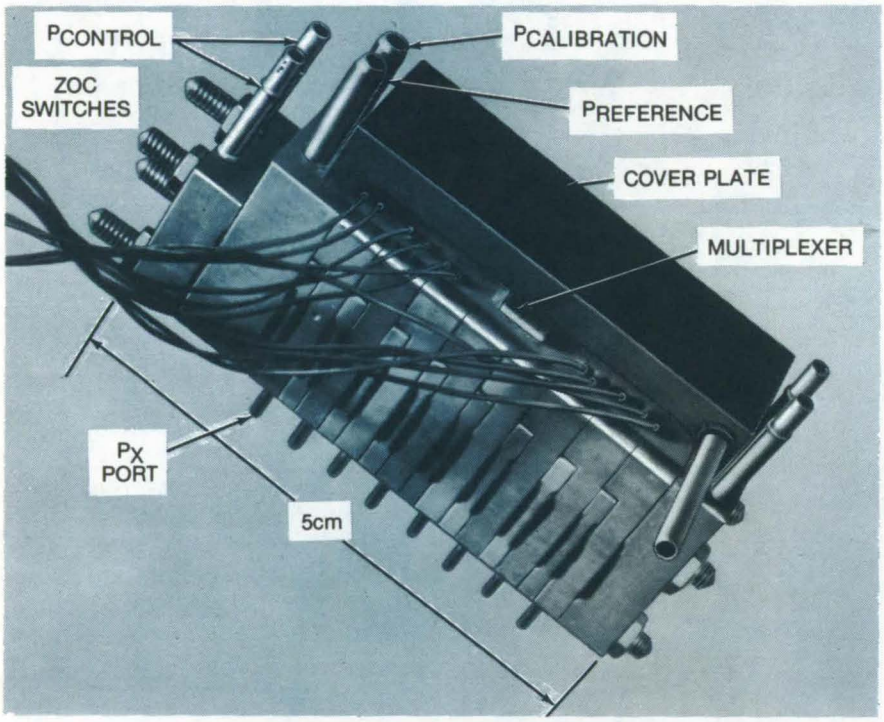

The **Multiport Electronically-Scanned Pressure-Sensor System [MESPS]** uses miniature silicon-diaphragm pressure sensors and a signal multiplexer, mounted to ZOC (zero-operate-calibrate) switches. An 8-channel system is shown.

For a number of years there has existed a need for higher data rates for wind-tunnel pressure measurements. This need arises from requirements for: (a) short run times such as in blowdown tunnels, (b) the reduction of wind-tunnel operation costs, (c) the minimization of errors resulting from temporal variations in tunnel flow conditions, and (d) real-time data display and analysis. Presently, mechanically-scanned pressure measurement systems that have sufficient accuracy for wind-tunnel measurements are limited to data rates of generally less than 10 readings/second.

Faster data rates may be obtained with miniature pressure sensors that are electronically switched and are used in conjunction with pressure selector switches that permit in-situ calibration. Miniature silicon-diaphragm pressure sensors, along with a signal multiplexer, are mounted to ganged zero-operate-calibrate (ZOC) pressure selector switches as shown in the figure. The ZOC switches, which are pneumatically controlled, permit the pressure sensor to be calibrated in situ by sequentially applying a zero differential pressure and known pressures to each pressure sensor.

The ability to calibrate in situ largely eliminates the usual problem of thermal zero and sensitivity shifts encountered when using silicon-diaphragm pressure sensors.

The system would usually be used in conjunction with a computer-oriented, data acquisition-and-control system. The ZOC switch is controlled by the computer, and the calibration coefficients are computed and updated in memory whenever a calibration is required. For measurements of unknown pressures the ZOC switch is positioned to the operate (P_X) ports.

The pressure sensor outputs can be randomly addressed through the complementary metal-oxide semiconductor (CMOS) analog multiplexer in approximately 1 microsecond, and the output signal can be measured at a rate of 10,000 readings/second, using standard analog-to-digital (A/D) conversion techniques. At this data rate faithful reproductions of fluctuating pressures of 100 Hz (the frequency limit imposed by inlet ports and the internal volume of the ZOC switch) can be obtained. Prototype systems of 8 and 48 channels have allowed pressure measurements to be made to an accuracy of about 0.25 percent of a full-scale pressure of 15 psid (1.04×10^5 N/m^2).

This work was done by Chris Gross of **Langley Research Center.** *No further documentation is available.*
LAR-12003.

NASA

Noncontaminating Method for Visualizing Gas Flow

A noncontaminating fog is formed from dry ice and warm water.

Lewis Research Center, Cleveland, Ohio

To visualize the flow of a gas used as a film coolant, the coolant was ejected from holes in the parts to form a protective film. The interaction between the gas and the hot air flowing over it had to be understood in order to determine the most efficient means of ejection. Conventional means of visualization, such as smoke in the coolant gas, were unsatisfactory because the smoke contaminated the apparatus and the instrumentation.

A noncontaminating fog, formed from dry ice and warm water, was used to simulate the coolant; and its interaction with the mainstream flow was observed visually and photographed.

A metal basket filled with dry ice is submerged in warm water at about 325 K (125° F), inside a pressure-tight tank, to produce a carbon dioxide-water fog. As the dry ice vaporizes, pressure builds up inside the tank; the fog flows to a plenum chamber, where large waterdrops are removed, and then to the coolant ejection holes.

Photographs were taken of the coolant flow using a high-intensity strobe light and a light source positioned on the opposite side of the jet from the camera.

This work was done by F. S. Stepka and D. Poferl of **Lewis Research Center** *and R. J. Goldstein of University of Minnesota. Further information may be found in NASA CR-72991 [N72-14945] "Film Cooling Effectiveness and Heat Transfer With Injection Through Holes." A copy may be obtained at cost from the Aerospace Research Applications Center, Indiana University [see inside back cover].*
LEW-12076

NASA

Fluid Classifier and Disseminator

A modified air-jet mill for separation of submicron particles

NASA Headquarters, Washington, D.C.

A commercially-available air-jet mill that pulverizes and disseminates solid particles may be modified to remove, classify, and disseminate submicron particles.

The figure illustrates the two modifications: a particle channel (M_1) and a large-particle exhaust port (M_2). The channel directs the material around the periphery of the classification chamber. In the area labeled S, the submicron particles are separated from larger ones. The larger particles are then ejected through the second modification, the large-particle exhaust at the end of the channel. The small particles are exhausted through the port in the center of the mill.

This work was done by Warren C. Kocmond and Vito A. DePalma of Cornell Aeronautical Lab. Inc., for **NASA Headquarters.** *No further documentation is available.*
HQN-10748.

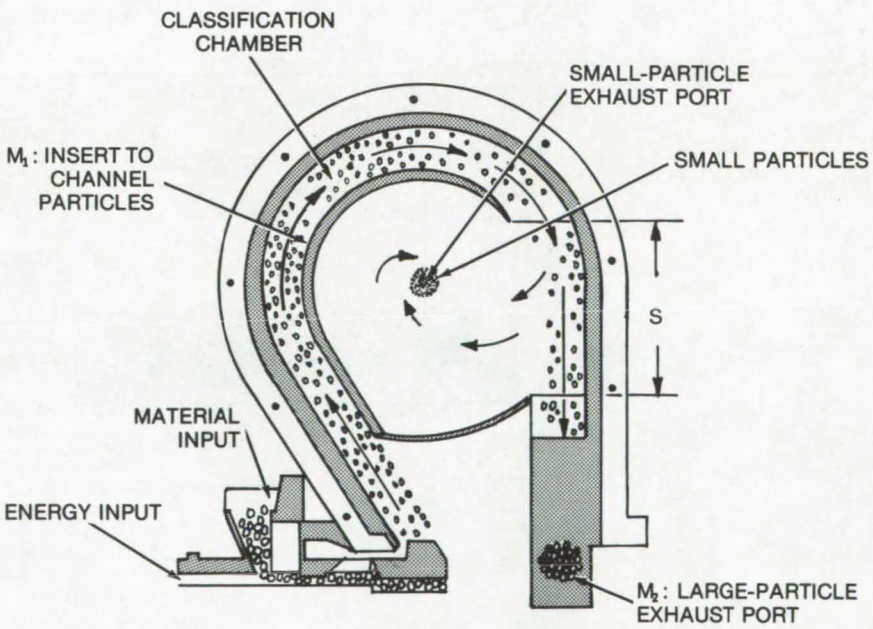

A **Modified Air-Jet Mill** has an insert (M_1) that channels material around the classification chamber. Large particles are disseminated at M_2, and submicron particles are separated in area S.

NASA

Shock-Tube Driver

An improvement in triggering a shock tube provides higher shock velocities and reduces contamination.

NASA Pasadena Office, Pasadena, California

A new type of shock-tube driver, the annular-arc accelerator (ANAA), has been developed in order to obtain the data needed to design lightweight dependable heat shields. The development of entry probes to explore the atmospheres of the outer planets, such as Jupiter and Saturn, requires the construction of heat shields to withstand the severe heating experienced during atmospheric entry at speeds of 30 to 60 km/s. The simulation of the fluid flow and intense radiation that such a probe would encounter has required a significant advance from the shock velocities of 15 to 34 km/s attainable in other facilities.

The ANAA shock tube consists of a cold-gas driver, an expansion section, the electrode sections, and the shock-tube test section (see Figure 1). A stream of helium driver gas is produced by bursting a diaphragm disk in the cold-gas driver. The expanding driver gas pushes a weak shock wave through the electrode sections. As the gas passes through the anode section, the energy of a high-voltage capacitor bank is discharged into the gas. The arc-heated plasma immediately expands and cools, driving a shock wave down the tube. This immediate expansion greatly reduces the opportunity for the gas to lose energy by radiative cooling.

The ANAA driver has two key advantages over other types of electric discharge shock tubes. The use of external capacitor-bank switches eliminates the need for exploding metal trigger wires which introduce large amounts of contaminants into the flow. Since there is no diaphragm present within the electrode sections, the energy loss and radiative cooling associated with diaphragm opening are avoided. Thus, higher shock velocities are possible, using the same input energy. Also, contamination from the vaporization of the diaphragm is eliminated.

The high-voltage discharge is triggered by a glow-discharge gage

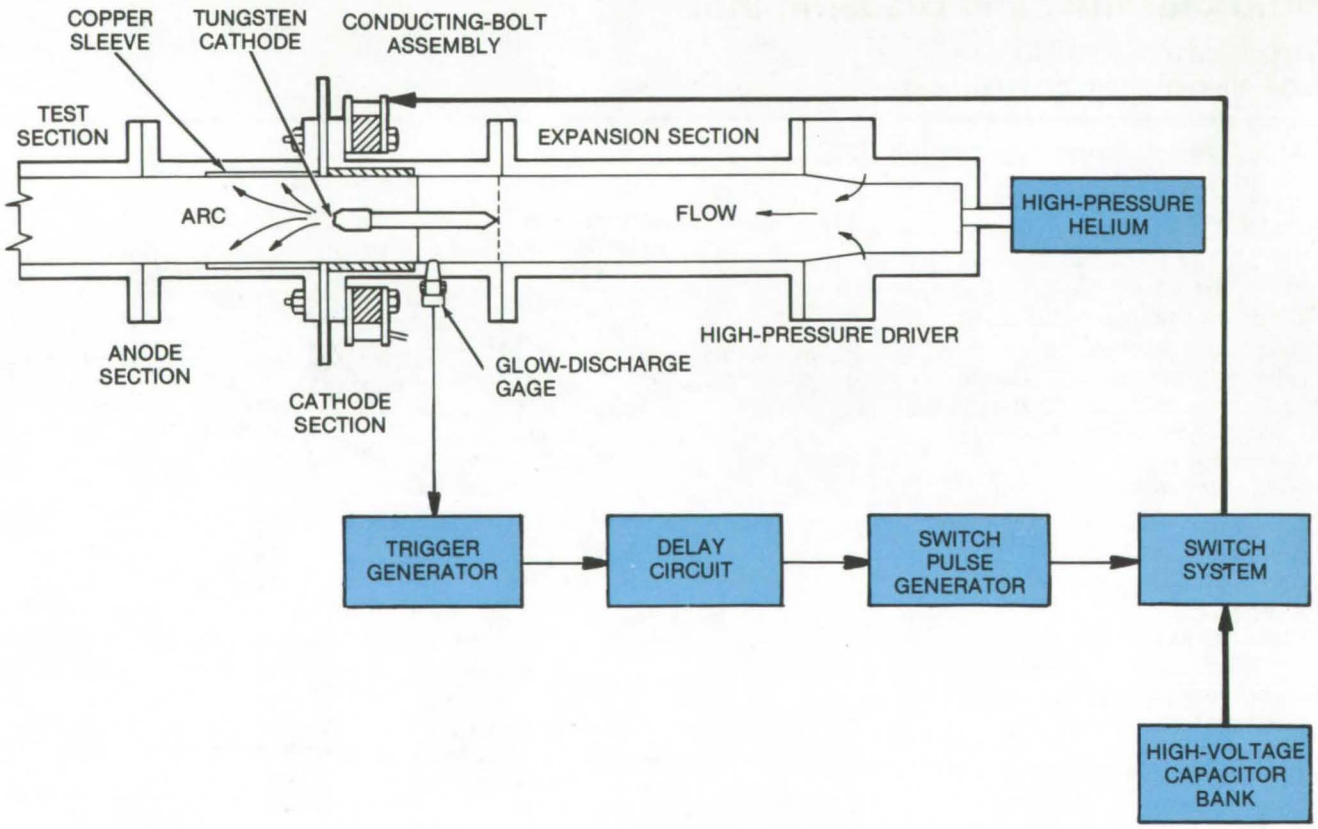

Figure 1. The **ANAA Shock Tube** consists of a cold-gas driver, an expansion section, the electrode sections, and the shock-tube section.

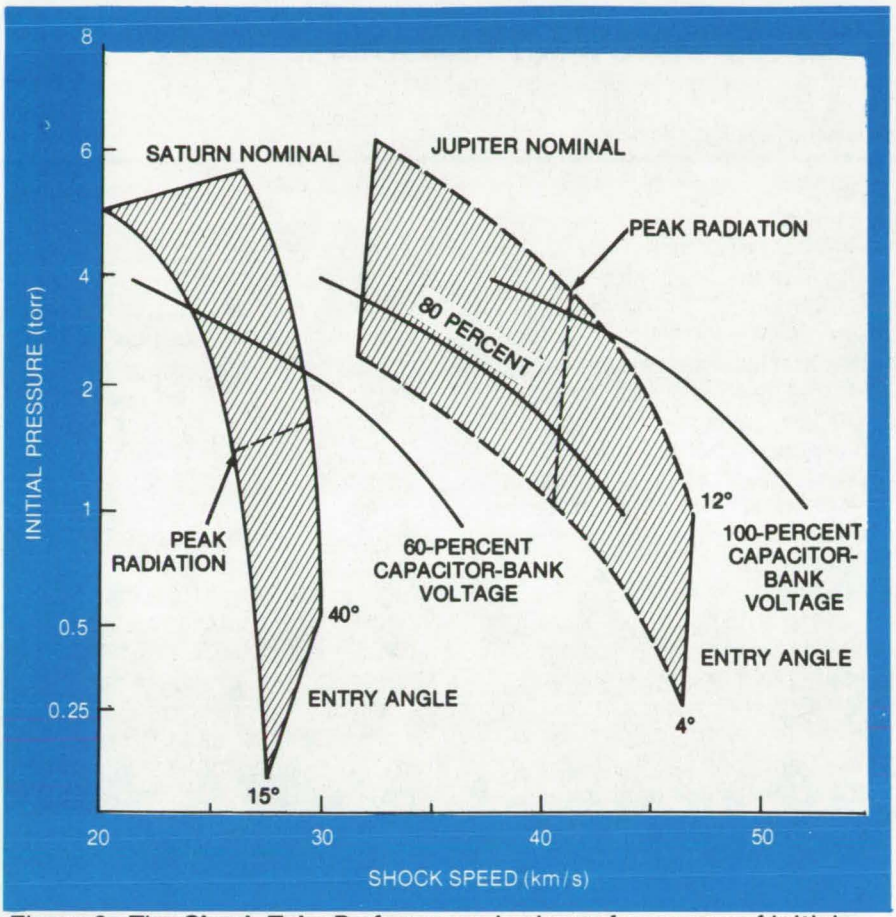

Figure 2. The **Shock-Tube Performance** is shown for a range of initial pressures and capacitor-bank voltages. The shaded areas are the ranges of Jupiter and Saturn entry conditions which the system was designed to simulate.

mounted on the cathode section. This device is sensitive to the small density change produced by the initial shock wave and can withstand the discharge-produced environment. The signal from the glow-discharge gage passes through a high-voltage isolator, a delay circuit which allows time for the driver gas to reach the anode section, and then triggers the capacitor bank switches. The ANAA driver has been used successfully with both a 290-kJ, 20-kV, spark-gap-switched capacitor bank and a 1-MJ, 20-kV, ignitron-switched bank. Peak currents of up to 1.5×10^6 A are produced with discharge times less than 50 μs.

With the ANAA shock tube the full range of outer planet entry conditions of current interest can be simulated. In Figure 2 the actual performance of the ANAA shock tube is shown in relation to Jupiter and Saturn entry conditions. Shock velocities up to 55 km/s into 1.0-torr outer planet mixtures have been obtained. Test times and attenuation rates have been tested and shown to be adequate for use in experimental investigations. Thus, this facility provides a tool for developing the confidence in entry technology that is needed for outer planet probe missions.

This work was done by Lewis P. Leibowitz of Caltech/JPL for **NASA Pasadena Office.** *For further information, Circle 63 on the TSP Request Card.*

This invention is owned by NASA, and a patent application has been filed. Inquiries concerning nonexclusive or exclusive license for its commercial development should be addressed to the Patent Counsel, NASA Pasadena Office [see page 2]. *Refer to NPO-13528.*

NASA

Self-Contained Constant-Temperature Heat Absorber

A reliable lightweight system for precise control of a heat-producing component is unaffected by pressure, heat, or rotation.

Marshall Space Flight Center, Alabama

A reliable lightweight system that can maintain precise thermal control of a heat-producing component has been developed. It is not affected by changes in external pressure, ambient thermal environment, or gravity, and can be operated in both static and spinning attitudes.

Other methods for the thermal control of components include active cooling loops and cold plates, space radiators, thermal coatings, and insulation schemes. Each of these methods has disadvantages. Active cooling loops and cold plates are normally heavy, expensive, and require moving parts, such as valves, pumps, or fans, which do not enhance reliability. This type of system is not compatible with lightweight, restricted-area design requirements. The space radiator requires an unobstructed surface area, and it cannot compensate for external thermal environment variations unless it is attached to an active cooling loop. Other passive systems, such as thermal coatings and insulation, are also sensitive to variations in the ambient thermal environment.

The self-contained heat absorber (see figure) is lightweight, compact, and reliable. It does not require mechanical components, such as pumps or fans. It is a simple, easily adaptable system that affords positive thermal control for components operated in conditions ranging from room environments to hypersonic flight conditions with spin.

The size chosen for the liquid container depends on how often it must be filled. In one version, the liquid container is divided into 16 compartments by bulkheads. The compartments keep the liquid from migrating to the outer periphery of the container, as would occur in a nonsegmented container subjected to a centrifugal force. They also add to the rigidity of the container and enhance the thermal flux from the heat transfer surfaces to the liquid. The bulkhead openings allow the working fluid to reach all the compartments during filling but do not allow liquid interchange during spin.

The vent connection is located below the orifice outlet to prevent the working fluid from collecting in the orifice during filling when the container is oriented in the fill attitude as shown in the figure. The container

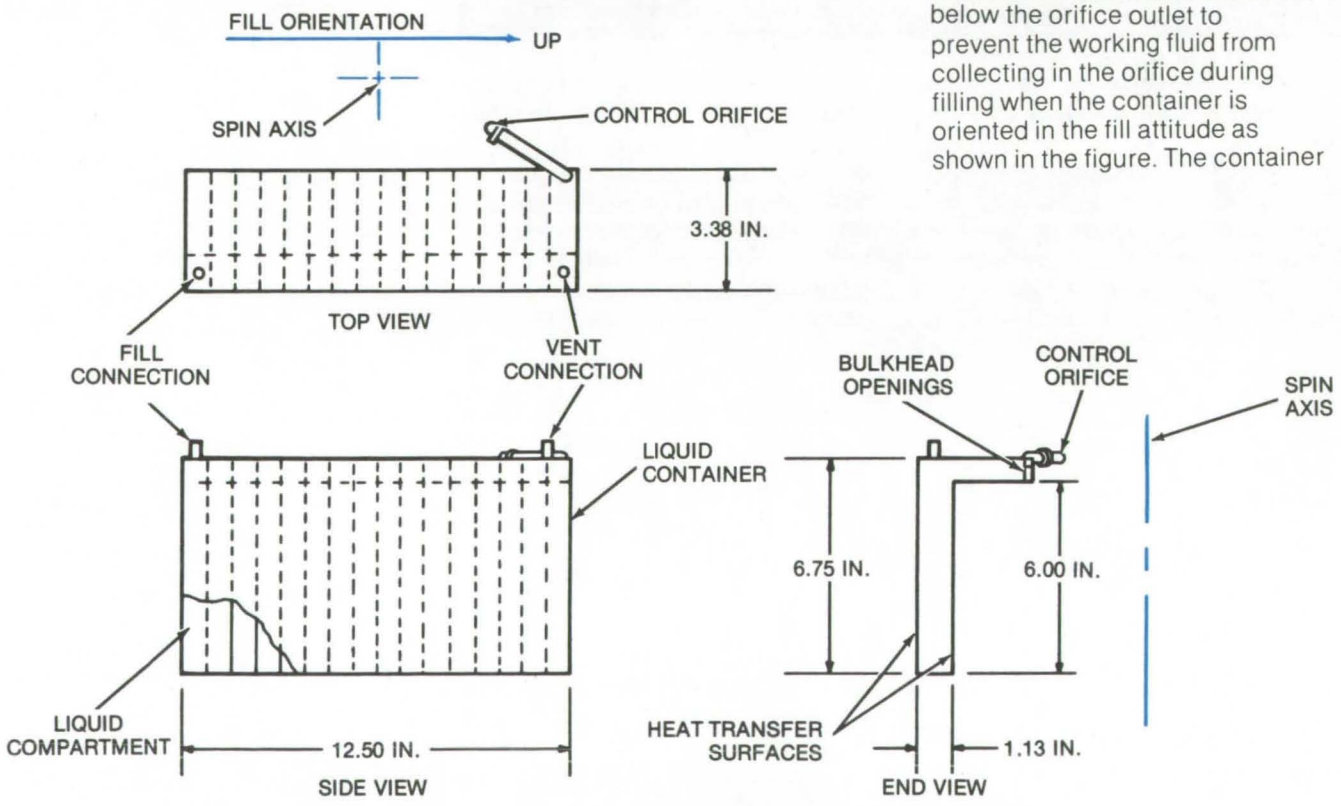

The **Constant-Temperature Heat Absorber** has an orifice oriented toward its spin axis. The orifice size determines the container pressure which establishes the boiling temperature of the heat-absorption medium.

is simple to fill, even when utilizing liquids with low boiling points. The first step is to connect the source to the fill connector (the liquid source pressure must be greater than the operating pressure of the container). With the orifice closed, the container is filled until the liquid escapes through the vent. Then the liquid fill bottle is disconnected, the control orifice is opened, and the vent is closed.

The absorber will provide thermal control in any attitude that does not allow the flow of liquid into the control orifice. This orifice is the key to the thermal control capability. It is oriented toward the center of the spin axis to force any liquid that may have collected in the orifice tube, prior to spinning, back into the container. The orifice size selected determines the container pressure, which in turn establishes the boiling temperature of the liquid utilized for heat absorption. Thermal input to the heat transfer surfaces is removed from the system by the liquid phase change. Three parameters determine the orifice size: (1) the amount of heat generated, (2) the required operating temperatures, and (3) the existence of choked flow conditions at the highest expected ambient pressure.

The size and shape of the container and the heat absorption media used can be custom fitted to particular thermal requirements. The relative position of the fill and vent connections and the control orifice can be varied to enable the absorber to operate in different attitudes. If the absorber is to be used in a constant ambient-pressure environment, a relief valve can be substituted for the control orifice.

This work was done by Raoul W. Lopez, Jerold L. Vaniman, and Robert R. Fisher of **Marshall Space Flight Center.** *For further information, Circle 64 on the TSP Request Card.*
MFS-22989

NASA

Liquid-Retention Canopy

An antislosh canopy might be used in tanks of volatile fuel or liquid nitrogen to reduce vaporization losses.

Marshall Space Flight Center, Alabama

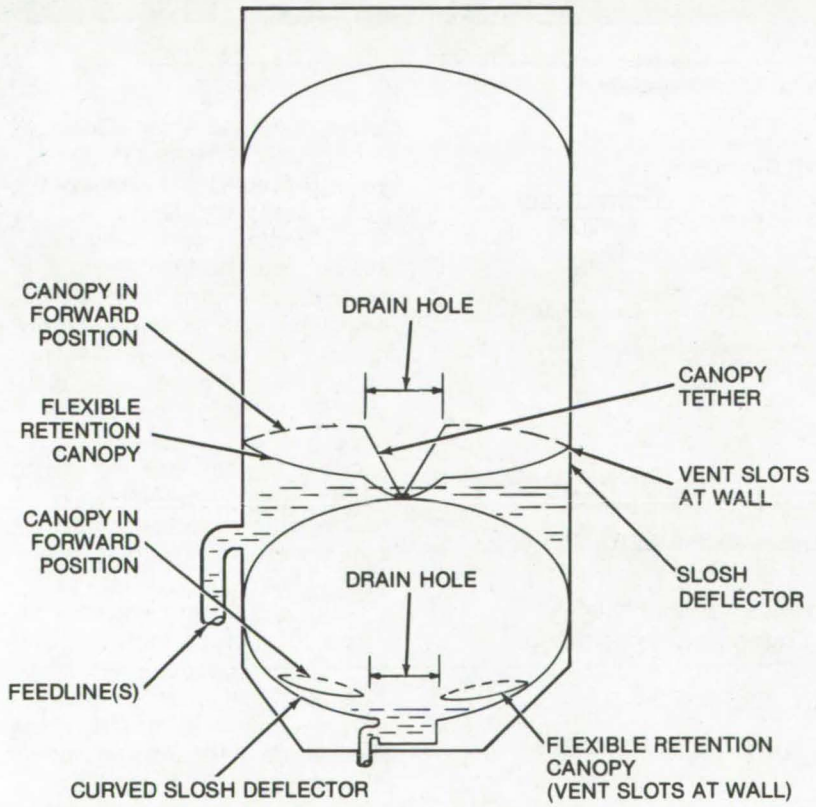

The **Retention Canopy** shown here was designed for a cryogenic tank. A similar arrangement could be used for other applications.

A retention canopy (see figure) serves as a fuel tank antislosh baffle and divides the tank into upper and lower sections. The lower section contains liquid and the upper section contains gas. The flexible canopy is fastened to the tank wall above the expected liquid level and has a drain hole in the center and vent slots at the tank wall. The canopy prevents severe sloshing and bubbling and redirects the fluid motion toward the tank bottom. This reduces cryogenic boiloff, wetted-wall area, and pressure collapse. In addition there will be fewer structural problems from differential thermal expansion. The position of the canopy can be varied up and down within the tank as the liquid volume varies. This device may be of interest to tank car designers.

This work was done by John H. Dawson and Adolph F. Brux of Rockwell International Corp. for **Marshall Space Flight Center.** *For further information, including design drawings, Circle 65 on the TSP Request Card.*
MFS-24133

NASA

Introducing Controlled Matter Into a Fluid System

A premeasured quantity of particles can be injected into a closed fluid system without unwanted contamination.

Marshall Space Flight Center, Alabama

When a fluid system is required to be free of contaminants, the extent of its cleanliness is measurable by instruments such as a nephelometer. For this purpose, a device has been developed to handle controlled particulate-contamination samples.

The device consists of a two-piece capsule holder and a one-piece glass inner tube, defined as the contamination capsule. The capsule holder is fabricated from several modified standard MS-type reducer unions, a vacuum fitting, a piece of 5/8-in. (1.5 cm) outside-diameter tubing, and a "B" nut fitting (see Figure 1). The two end fittings (reducer fittings) are machined to accept the glass tube [3/8 in. (0.9 cm) in diameter]; they support the tube and restrict its axial movement. The contamination capsule is fabricated from 3/8-in. outside-diameter glass (Pyrex) tubing. One end of the glass tube is vee-notched, to assure that equal pressures are maintained on both sides of the tube.

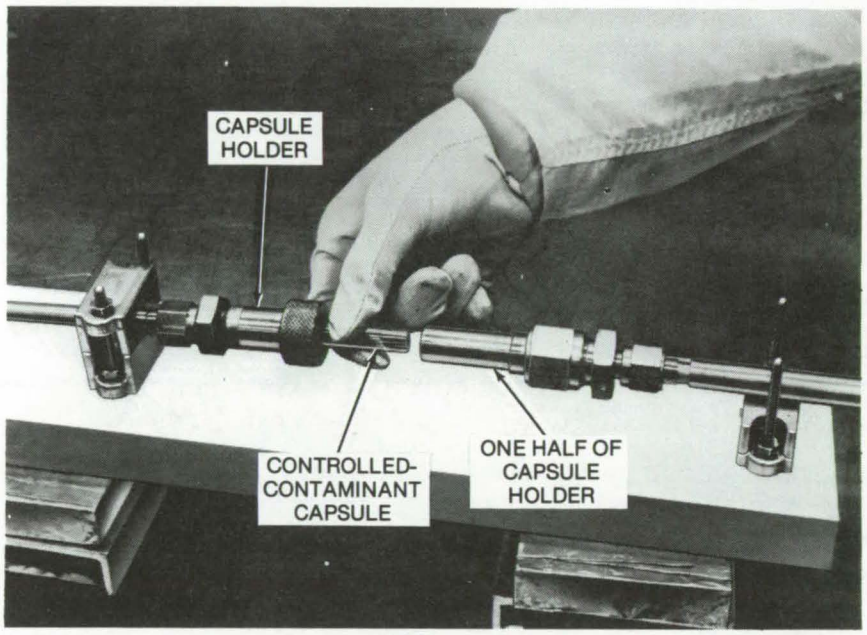

Figure 2. A **Controlled Contaminant** is shown being loaded into a simulated test system.

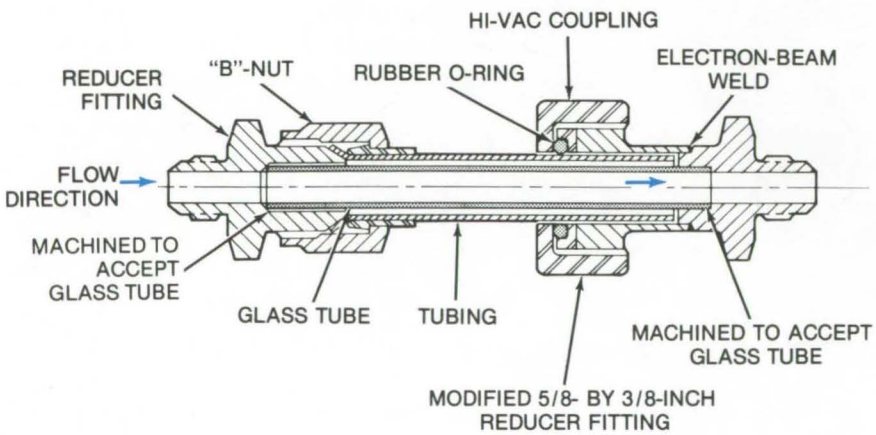

Figure 1. The **Contamination Capsule and Holder** assembly is constructed with stainless-steel fittings and tubing except as noted.

The contamination capsule is inserted into the holder with the vee-groove end of the glass tube coinciding with the inlet-end of the holder. The opposite end of the glass tube is ground perpendicularly to the axis of the tube. This is done to obtain a butt joint, between the tube and the mating holder surface, that will not allow the entrapment of contaminates as they are blown from the contaminant holder.

The capsules are loaded with a preselected cross section of particulate, using a stereomicroscope. This operation is performed in a controlled environment to ensure against the introduction of foreign contamination. The capsule is installed in the capsule holder at the time of the test (see Figure 2).

After the capsule, loaded with the predetermined amount of particulate, is loaded into the holder, the particulate is blown from the holder by a gas stream through the precleaned test system. Monitoring of the particulate travel through the test system and collection at the distal end yield the necessary test data for evaluation.

This device could be adapted to similar applications where particulate contamination must be handled, measured, and introduced into fluid test systems.

This work was done by Charles E. Hoffman of Rockwell International Corp. for **Marshall Space Flight Center.** *For further information, Circle 66 on the TSP Request Card.*

Inquiries concerning rights for the commercial use of this invention should be addressed to the Patent Counsel, Marshall Space Flight Center [see page 2]. Refer to MFS-24309.

NASA

Propellant Side Feed

The thrust-to-power ratio of a solid-propellant pulsed-plasma microthruster is increased.

Langley Research Center, Hampton, Virginia

Two new solid-propellant configurations increase the thrust-to-power ratio of a pulsed plasma microthruster and provide the possibility of varying the thrust. The techniques are adaptable to other uses, such as the sputter coating of polymeric material (more mass sputtered per discharge energy) or pulsed ablating light sources.

A conventional thruster (Figure 1) is used. Additional solid propellant is fed downstream from the discharge by using a Vee-shaped propellant or by side feeding (see Figures 2 and 3). An electric arc between two electrodes is surrounded by the propellant on the downstream side. By using a Vee-shaped propellant with the arc initiated at the apex of the Vee, it is possible to feed the propellant continuously as it is being consumed. The included angle of the Vee affects the thrust/power ratio by determining the amount of propellant fed through the breach and from the sides. Similar results may be obtained by feeding conventional rectangular propellant from the side, as well as through the breach.

This work was done by William J. Guman of Fairchild Hiller Corp. for **Langley Research Center.** *No further documentation is available. LAR-11082*

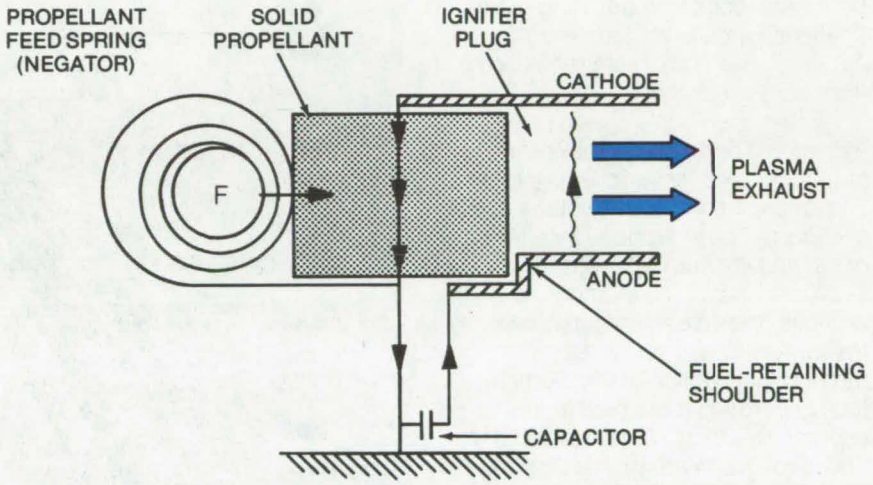

Figure 1. **Standard Thruster** with simple negator spring that is used to feed the propellant.

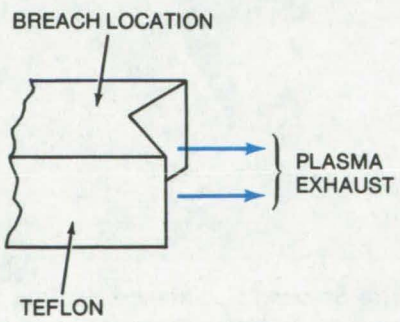

Figure 2. With a **V-Shaped Propellant Rod** the angle of the V determines the amount of propellant fed from the breach and the side.

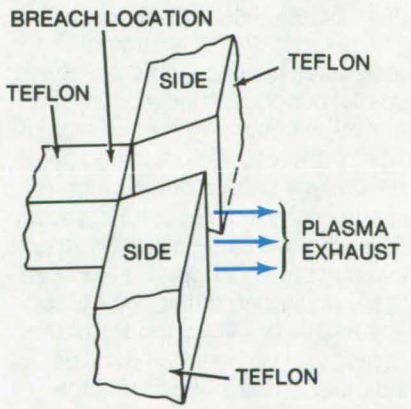

Figure 3. Independent **Breach and Side Feed,** like the V-shaped feed, increases the thrust-to-power ratio.

NASA

Resistance Heating Elements With Specific Heating Profiles

Bundled, interrupted, resistance heating elements provide specific heating profiles.

Lewis Research Center, Cleveland, Ohio

Several applications require an electrical resistance heating element having a specific or tailored heating profile. It is desired that certain sections of the element (located at specific longitudinal positions) should possess a greater heat intensity than other sections. Prior heating elements utilized a uniform cross section or machined exterior variations in the cross-sectional area, resulting in additional fabrication costs (such as machining modifications for different temperature patterns) and in short life resulting from easy breakage.

An improved heating element is assembled by stacking or bundling a number of resistance rods together. The location and intensity of the "hot section(s)" is determined by altering or varying the internal cross-sectional area of the element. By reducing the cross-sectional area, the current density is increased through that section of the element, thus generating more heat in the section, resulting in the creation of a "hot section." With this design only straight resistance rods of several diameters need to be stocked for ready construction of a wide variety of "tailored" heating elements.

The cross-sectional area of the resistance heating element is made up of a bundle of smaller elements or rods in contact with each other. The "hot section" is obtained by removing a section of the inner rod(s). For example, stacking seven rods all of the same diameter results in a compact configuration as seen in the upper part of the photograph. The middle one-inch section of the center rod has been removed as indicated in the lower part of the photograph, thereby producing a "hot section."

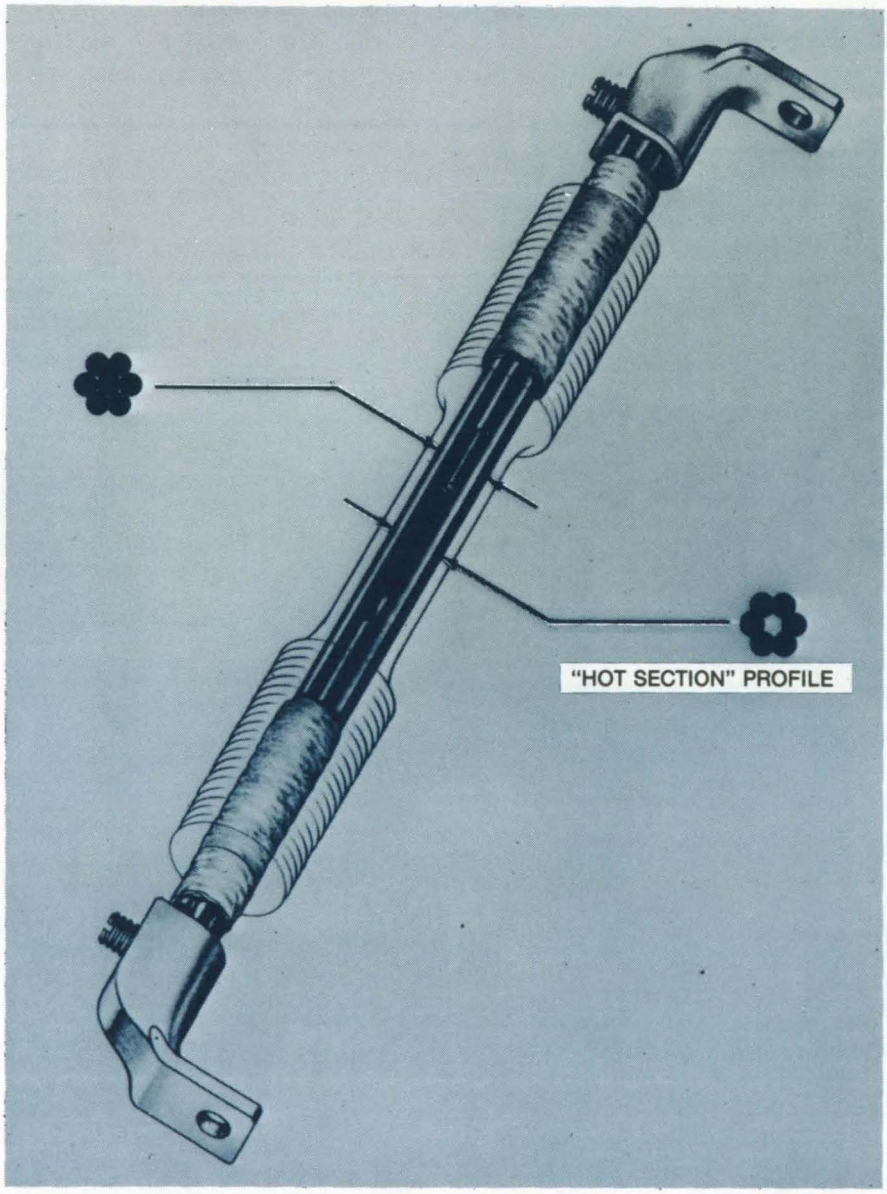

The **Stacked Resistance Heating Element** is shown with a "hot section" created by removing a one-inch section of the center rod.

Variation in the diameter of the center rod (D) and the outer rods (d) as a function of the number of outer rods (N), i.e., $D/d = (1-\text{Sin } 180/N)/(\text{Sin } 180/N)$, results in different area ratios and therefore different degrees of heat in the "hot section(s)." Other geometries can be used, e.g., square bars, hexagonal bars, etc., and stacked so that any number of sections may be removed to form the "hot section." Multiple "hot sections" can also be produced.

In effect, while internally varying or changing the cross-sectional area of the heating element assembly in order to get the desired heat intensity at the "hot section," the exterior radiating surface is unaffected and thus the distance between heating element surface and the surface of the article being heated remains constant.

This new flexible heating element design offers the following advantages: (1) larger surface areas for heat radiation, and (2) easily "tailored" lengths and locations of "hot sections," as well as degrees of heat intensification, by controlling the cross-sectional areas of the sections removed.

This work was done by Marvin H. Hirschberg of **Lewis Research Center.** *No further documentation is available.*
LEW-10719

NASA

Analytic Numerical Solutions for Shock Waves

Accurate prediction of shock waves occurring in inviscid supersonic flows

Ames Research Center, Moffett Field, California

A study has been made of the weak solutions of the simple wave equation, the inviscid Burgers equation, and the Euler equations in order to develop a technique for accurately predicting the shock waves that occur in inviscid supersonic flows. A numerical method of second-order accuracy in two forms, differential and integral, was used to calculate the weak solutions of the equations for several initial value problems, including supersonic flow past a wedge, a double symmetrical wedge, and a sphere. Additionally, there was examined the effect of computational mesh on the accuracy of computed weak solutions, including shock waves and expansion phenomena.

As a result of the study, modifications to the finite-difference method are suggested that aid in obtaining desired solutions for initial value problems in which the solutions are nonunique. In the study of flow past a sphere, comparison was made between the use of a fixed computational mesh and an adjusting mesh. In the first instance, the mesh was determined initially by a best quadratic fit to the theoretical shock wave and thereafter held fixed; in the second instance, the mesh was allowed to adjust with time according to the Rankine-Hugoniot relations. Although the difference in the final or converged position of the adjusting mesh differed only slightly (a few percent of the standoff distance) from that of the fixed mesh, the accuracy of the computed solutions differed significantly; the solution computed with the adjusting mesh compares well with theory.

This work was done by Robert W. MacCormack of **Ames Research Center** *and Alvin J. Paullay of Bronx Community College/CUNY. Further information may be found in: "The Influence of the Computational Mesh on Accuracy for Initial Value Problems with Discontinuous or Nonunique Solutions," R. W. MacCormack and A. J. Paullay, Computers & Fluids, vol. 2, p. 339, 1974. No further documentation is available.*
ARC-10959

NASA

Measurement of Rapidly-Changing Heating Rates

An easily-fabricated heating-rate sensor accurately measures rapidly-changing heat-flux levels.

Langley Research Center, Hampton, Virginia

Rapidly-changing heating rates are not sensed accurately as a function of time when a heating rate sensor with a slow response is employed. Heretofore such changes were detected with a thin, thermally isolated sensor. Changes in sensor temperature were detected by changes in its electrical resistance, by a thin thermocouple or by thermal-radiation measuring devices. The utility of the sensor was limited by its slow cooling at low temperatures, its poor cooling by thermal radiation, and by its delicate nature. As an example, no currently practical device could be found that would accurately sense heating rate changes over a range of 0.05 to 35.00 Btu/ft^2-s when the rate of change was about 100 $Btu/ft^2/s^2$ for both heating and cooling.

A new heating rate sensor (see figure) consists of two metal plates separated by a spacer. Modifications to the configuration shown are possible as long as the outer and inner elements are connected by a suitable resistive heat path. When subjected to a heat flux, the temperature of the exposed outer plate rises at a rate determined by the heat flux, the plate heat capacity, the thermal resistance between the outer and inner plates, and the inner plate heat capacity. The differential temperature between outer and inner plates is directly proportional to the applied heat flux. A small phase lag, which is readily determined by calibration or by analysis, exists between changes in the heat flux and the differential plate-temperature response.

The spacer serves as a conductive-heat resistance path having a value required by the particular design. Thermal conductivity may also be controlled through variations in the material used and its thickness and in the physical arrangements of the resistive elements (e.g., parallel ribs or truss arrangements).

Thin thermocouple wire is attached to the outer and inner plates to sense plate temperatures and/or differential temperatures between plates. The unit is fastened at its periphery to the side of the surface that will be subjected to a varying heating rate input. The thermocouple leads are connected to a suitable recording device. Calibration with a known method of heating is required to assure high accuracy, but no maintenance is necessary beyond that required for thermocouple systems.

Numerous transient heat transfer analyses, employing a model that simulates the heating rate sensor, have been conducted using a large digital computer. The time lag in response to heating rate

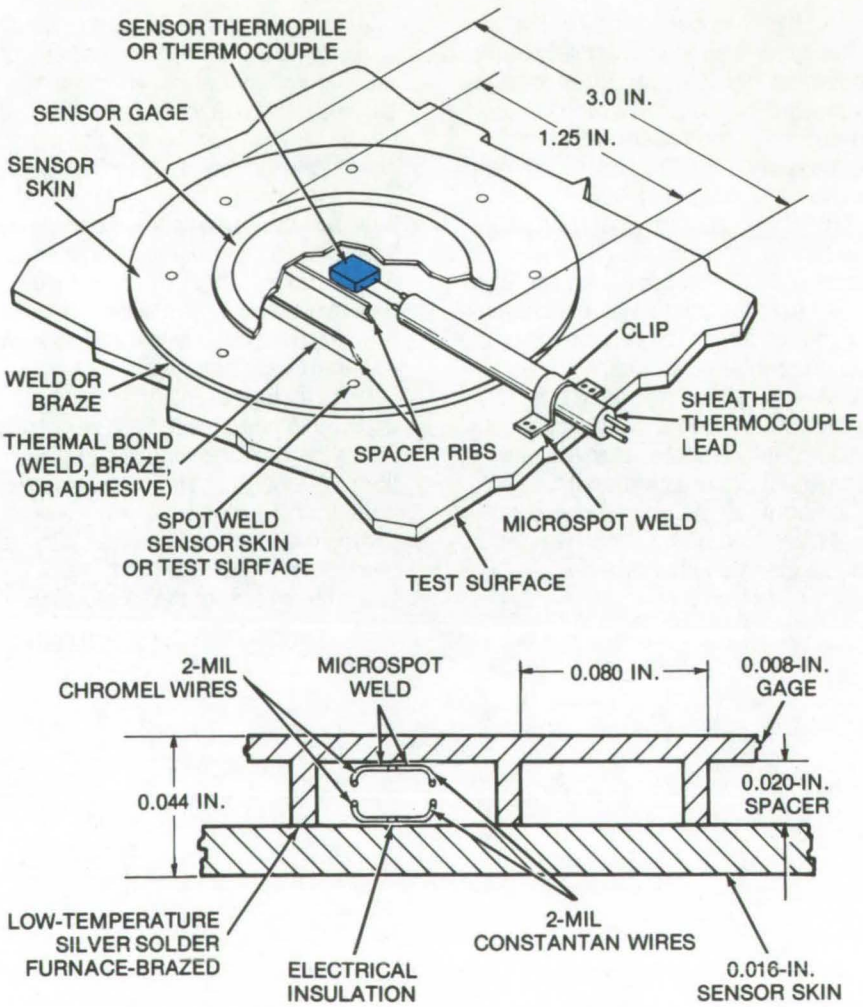

The **Heating-Rate Sensor** is shown in cross section and as installed for measurements on the Atlas tank skin.

changes and the changes in the thermal characteristics of materials with temperature, or time, or both, are possible sources of error. The sensor requires an essentially-uniform heating rate over the entire outer surface for accurate measurement. When this condition is not present, errors may occur in the output.

To minimize the errors introduced by conduction from the peripheral fasteners to the centrally-located temperature sensors, the radial dimensions involved must be adequate for the intended application. Thus, there is an advantage in using a plate material with relatively-poor thermal conductivity.

This work was done by Edward W. Schwartz of General Dynamics Corp. for **Langley Research Center.** *For further information Circle 67 on the TSP Request Card.*

Inquiries concerning rights for the commercial use of this invention should be addressed to the Patent Counsel, Langley Research Center [see page 2]. Refer to LAR-11380.

NASA

Books and Reports

These reports, studies, and handbooks are available from NASA as Technical Support Packages (TSP's) when a Request Card number is cited; otherwise they are available from one of NASA's Industrial Application Centers or the National Technical Information Service.

JPL Solar Power Experiments

Solar power systems for terrestrial applications

A report has been prepared describing the evolution of photovoltaic power systems designed and built for terrestrial use. The problem areas discussed are those currently impeding the further development of such systems. The focus is technological rather than economic; seven different types of solar panels and six different types of material test specimens are considered. A detailed description of these experiments together with accumulated test data and its interpretation are presented.

Solar photovoltaic power systems may someday see large-scale application for terrestrial use. However, to date, terrestrial use has been limited to systems with low power requirements. Typical applications include radio repeater stations, lighthouses, lightbuoys, wireless telephones, beacons, highway call systems, and field transmitters and receivers. Although such systems are currently in use, the development of photovoltaics for terrestrial use has been impeded by a number of fundamental problems, not all of which are related to cost.

This report is a followup to a 1968 study investigating the use of surplus spacecraft hardware and aerospace technology to identify some of the problems in designing solar arrays for terrestrial environments. Early experiments, including the design, fabrication, and testing of several seismic observatories, a portable radio transmitter, and a rooftop power supply, provided the basis for compiling a rather extensive list of design considerations for terrestrial photovoltaic-powered systems. Applicable considerations then were factored into some recently designed and fabricated systems. These include an onshore beacon located at Point Vincente, California and two buoys located in the San Diego Harbor. These recent experiments have identified system, environmental, and material considerations which will be applicable in future experimental solar-powered systems.

This work was done by Robert K. Yasui of Caltech/JPL for **NASA Pasadena Office.** *To obtain a copy of the report, Circle 68 on the TSP Request Card.*
NPO-13461

NASA

Gust Alleviation for STOL Aircraft

An analytical study suggests a method of improving flight performance.

New ride improvements for airplanes are always in demand, particularly for those having relatively-low wind loading and those flying at low altitudes where air turbulence may be expected.

A gust-alleviation system, for a STOL airplane in cruise condition, could reduce the root mean square of the normal acceleration in random turbulence by as much as 50 percent. It operates by driving the flaps in response to normal acceleration, and by moving the elevator in proportion to the command flap-deflection angle and to a pitch-rate signal.

These findings were arrived at by analytical studies. The calculations were based on airplane dimensions, mass, flight conditions, and aerodynamics.

This work was done by Waldo I. Oehman of **Langley Research Center.** *A copy of this report, NASA TND-7201 [N73-20013], "Analytical Study of the Performance of a Gust-Alleviation System for a STOL Airplane," may be obtained at cost from National Technical Information Service, Springfield, Virginia 22151.*
LAR-11413

NASA

Outer Flow and Turbulence in Boundary Layers

Turbulence propagates from the outer to the inner region.

In fluid dynamics the processes involved in the initiation and proliferation of turbulence in a flat-plate boundary layer are not well understood. Earlier experiments support the hypothesis that turbulence generated near the wall migrates outward and is ultimately associated with the convoluting outer edge of the boundary layer.

The following experiment was conceived and performed in an attempt to determine if any correlation exists between the convoluting outer edge and the production region near the wall; that is, to see if there is some correlation which would support the hypothesis of an inward flow of information from the outer edge that may be responsible for the initiation of turbulence near the wall. The results are published in a report.

The experiment was performed in a small open-return-type wind tunnel. A honeycomb, which was located in a large circular inlet, was used to straighten the inlet flow and to break up any large-scale disturbances. From the inlet the flow passed through a settling chamber and then accelerated into a test section, where the cross section narrowed to 45.7 by 45.7 cm. The tunnel ceiling was adjusted so as to develop a near-zero pressure gradient, flat-plate boundary layer.

The correlation measurements were performed at 1.22 m from the start of the test section. Two standard constant-temperature hot-wire anemometers were used with 0.01-mm-diameter platinum/iridium wire. Normal annealing and calibration of the hot wires were performed previously. One hot wire was placed in the undulating outer edge of the boundary layer, and the other one was placed very near the wall. The boundary layer was approximately 7 cm high. Signals from the hot wires were fed directly into a commercial time-delay correlator, an rms meter, and a tape transport.

Measurements have been obtained of the correlation between the two hot-wire anemometer signals, one from the intermittent outer region and the other from the turbulence production region of a turbulent boundary layer. Space/time correlation curves for the two signals indicate that a measurable correlation exists only for the case where the hot wire in the outer flow is slightly upstream of the probe near the viscous sublayer. No correlation could be measured when the other wire was slightly downstream of the sublayer wire.

The correlations indicate that information is propagated from the outer region to the inner region. The migration of turbulence away from the wall has been previously discussed in the literature. The results presented in this report along with the migration results lend support to the "limit-cycle" model for turbulence production. That is to say that the perturbations travel through the boundary layer and give rise to the turbulence production process which occurs near the viscous sublayer. A part of the turbulence produced near the wall, in turn, moves outward and eventually produces the convoluting outer edge of the boundary layer to reproduce and sustain itself.

This work was done by William C. Cliff and Virgil A. Sandborn of **Marshall Space Flight Center.** *To obtain a copy of the report, Circle 86 on the TSP Request Card.*
MFS-23286

NASA

Pressure Tube Instrumentation

Standards for design, fabrication, and installation.

A set of standards in the form of a set of drawings has been prepared that provides detailed information on the design, fabrication, installation and quality control for a large variety of static and total pressure tube instrumentation. These standards document many of the types of pressure tube instrumentation that have been tried and proven at the NASA Lewis Research Center in its aerospace programs. The methods and techniques have resulted from the great variety of requirements that have been encountered in aeronautics and space research. The purpose of these standards is to outline certain basic practices that are necessary with pressure tube installation and to standardize these practices.

Details such as materials, fastening techniques, surface finishes, critical dimensions and quality control specifications are included. Methods of installation are shown for solderable and non-solderable materials, and for removable and non-removable total pressure probes. Instrumentation shown is of the steady-state type but includes one design of a dynamic total pressure probe because of increased interest in this unit. Also included are compact and unique pressure tube surface attachment methods.

Currently used information and documentation covering the design, fabrication, and installation of pressure tube instrumentation is often incomplete, and in many cases varies widely. These variations in existing information, together with incomplete data in many areas, indicated the need for reliable and realistic criteria for the installation of pressure tube instrumentation.

Besides assuring accuracy of measurement, these standards can improve the understanding of quality levels, increase the engineer's ability to distinguish special requirements and reduce costs by eliminating the specification of unnecessary rigid limits where they are not required.

This work was done by George Foerster, Oral Mehmed, and Richard Mueller of **Lewis Research Center.** *To obtain a copy of the standards, Circle 69 on the TSP Request Card.*
LEW-12539

NASA

Joule-Thomson Data Curves

Temperature-pressure curves over a wide range of both parameters

A series of graphs shows the temperature-pressure relationship for the gases air, nitrogen, helium, oxygen, and hydrogen when flowing across a line restriction (the Joule-Thomson effect) over a wide range of temperatures and pressures. Also, an error in predicted temperature has been plotted as a function of the downstream Mach number to provide an understanding of the limitations of the Joule-Thomson assumption. The graphs can be applied as an engineering design guide for the prediction of the temperature change across a line restriction as a result of flowing air, nitrogen, helium, oxygen, or hydrogen at temperatures ranging from -400° to 300° F, for pressures up to 6,000 psia.

These graphs would be useful to component manufacturers in selecting materials. Designers of piping systems would benefit by the ease with which the temperature change could be predicted and then applied, to provide allowances for insulation, expansion joints, and the like.

The data curves are the first known compilation on the above-named gases showing the Joule-Thomson effect in standard engineering units of temperature (°F) and pressure (psia). They are also the first known demonstration of the relative error of the Joule-Thomson assumption.

This work was done by H. W. Beimgraben of The Boeing Co. for **Kennedy Space Center.** *To obtain a copy of the report, Circle 70 on the TSP Request Card.*
KSC-10538

NASA

Optimal Insensitive-Controller Synthesis

A theoretical examination of the effects of parameter variation

A report describes an investigation of the methods used in the design of optimal controllers. This report is of interest in that it treats, in a rigorously sound mathematical manner, a problem that perplexes designers in virtually all engineering disciplines: How to account for and minimize the degrading effects of parameter variations.

The report includes the proof of two important theorems. The first theorem provides a local sufficiency condition for the existence of optimal insensitive controllers, that is, in the case of sufficiently-small parameter variations. This theorem also implies that such controllers are optimal controllers corresponding to boundary points of admissible parameter variation sets. The second theorem states a necessary condition for an optimal controller corresponding to a point in the boundary of the domain of admissible parameter variations to be an optimal insensitive controller. Here, the expression "optimal insensitive controller" refers to a controller which is optimal for some admissible value of the parameters which minimizes the maximum of the performance over the range of admissible values.

The goal of explicitly including parameter variation constraints within the quadratic optimization formulations motivated study in two directions. One phase of the study was aimed at discovering properties of the optimal performance over a segment of parameter space, and utilizing such properties to find optimal insensitive controllers. The other phase of the study was aimed at reducing the sensitivity to parameter variations by introducing proper compensators into the controller. Promising results of both theoretical and practical value were obtained.

The technical development is predicated on the so-called normal-form representation of system performance, $\dot{x} = fx+gu+n$. While this form always exists for linear systems and most nonlinear systems, it generally happens that f and g for a given practical system are difficult to find. Further, the research assesses the effects only on small changes in the nominal parameter values. Consequently, further work to relax the normal-form characterization and to extend the results to large changes in parameters is needed for a more practical application of this research.

This work was done by C. A. Harvey and Y. S. Lee of Honeywell, Inc., for **Marshall Space Flight Center.** *To obtain a copy of the report, Circle 71 on the TSP Request Card.*
MFS-21666

NASA

Computer Programs

These programs may be obtained at very reasonable cost from COSMIC, a facility sponsored by NASA to make new programs available to the public. For information on program price, size, and availability, circle the reference letter on the COSMIC Request Card in this issue.

NASTRAN Component-Mode Synthesis

Efficient Determination of vibration characteristics of large structures

Using the DMAP feature of the NASTRAN computer program, a vibrational analysis capability for large structures, which is known as component mode synthesis, has been developed. This is a dynamic substructuring analysis technique known as component modes, using NASTRAN via alterations to rigid format number 3. The method generally follows the outline in the NASTRAN User's Manual. The steps are as follows:

a. The calculation of component modes;
b. The selection of component normal modes, the calculation of component generalized matrices, the assembly of system matrices, and the computation of normal modes; and
c. The retrieval of component response.

The type of component modes analysis presented uses constraint modes and normal modes exclusively. This method has the advantages of programing simplicity, generality of application, and provides good engineering accuracy. Computational efficiency is greater for structures having a large proportion of interior degrees of freedom relative to boundary freedoms.

NASTRAN/DMAP

This program was written by Robert J. Guyan of Rockwell International Corp. for **Johnson Space Center.** *For further information, Circle C on the COSMIC Request Card.*
MSC-19632

NASA

MINIVER

Miniature version of Real/Ideal Gas Aero-Heating & Ablation Computer Program

The determination of heat-transfer multiplication factors, special flow-field simulation techniques, different heat-transfer methods, different transition criteria, crossflow simulation, and a more efficient thin-skin thickness optimization procedure require a special analytical computer program.

The MINIVER computer program, is an automated method of using the simplistic approach to aerodynamic heating. The solutions are for a single location in contrast to many integral heat-transfer methods which treat the boundary-layer development over a particular geometry. One of the prime benefits in the use of the MINIVER computer code is the flexibility and economy which result from the use of a point solution technique.

The calculation procedures followed in MINIVER are as follows:

1. The definition of free-stream flow properties,
2. The determination of local boundary-layer edge static and total flow properties,
3. The determination of flow properties required by desired heat-transfer method,
4. The calculation of laminar and turbulent heat-transfer coefficients and recovery enthalpy,
5. The calculation of convective heat transfer based on transition criteria,
6. The calculation of radiation equilibrium temperature,
7. The calculation of thin-skin temperature response, and
8. The determination of the next time-step interval.

FORTRAN
CDC 6500/UNIVAC 1108/IBM 7094

This program was written by Douglas R. Hendler of McDonnell Douglas Corp. for **Marshall Space Flight Center.** *For further information, Circle D on the COSMIC Request Card.*
MFS-21951

NASA

ESOP Version IV

Energy Systems Optimization Program

The Energy Systems Optimization Program (ESOP) calculates energy requirements and evaluates yearly operational characteristics to satisfy these requirements. ESOP, Version IV, provides for improved analysis of low-grade heat utilization, waste-water treatment systems, and engine optimization to select the engine which will use the least energy.

There are six general analytical components of the program:

1. Waste Disposal — The Waste Disposal Calculation Section predicts the daily total energy required to operate a specific waste disposal system and the daily quantity of usable waste heat energy that is recovered from the specific disposal process.
2. Heating/Cooling Loads — The Loads Calculation Section predicts the heating or cooling loads on a building as a function of outside environment, desired inside conditions, building construction and geometry, domestic power usage, occupancy rate, and occupant metabolic rate for each hour of a 24-hour day.
3. Energy Requirements — The Energy Requirements Section calculates, on an hourly basis, the hourly, daily, seasonal, and yearly energy requirements.
4. Power Generation — The Power Generation Section calculates the required energy inputs to specific prime movers to deliver energy outputs, as defined by the Energy Requirements Section, and the amount of usable waste heat recovered from prime mover operation.
5. Waste-Water Treatment — The Waste-Water Treatment Section backs the changes in water quality that occur as the waste water passes through treatment proccesses.

(continued next page)

6. Conventional Utility System — The Conventional Utility System Section calculates the energy requirements of a commercial utility system that meets specific heating/cooling, hot-water, and domestic and auxiliary power demands.

The program operates in interactive or batch mode and uses the UNIVAC MATH-PACK routines, ORTHLS and FITY.

FORTRAN
UNIVAC 1108, EXEC VIII

This program was written by Lockheed Electronics Co. for **Johnson Space Center.** *For further information, Circle E on the COSMIC Request Card.*
MSC-14854

NASA

Tangent-Ogive Nose Cones

Heating and shear stresses are calculated for tangent-ogive nose cones.

The slenderness of the tangent-ogive shape for sounding-rocket nose cones results in an attached nose shock wave during periods of supersonic and hypersonic flight in which significant aerodynamic heating is experienced. This computer program calculates the aerodynamic heating and shear stresses at the wall for tangent-ogive noses that are slender enough to maintain an attached nose shock during that portion of flight when heat transfer from the boundary layer to the wall is significant.

The solution method is derived from a combination of known analytical methods with a few new approximations and assumptions. The tangent-ogive and flow geometries are completely specified to the program by three input values. The effects of moderate angles of attack are accounted for by assuming the local flow to be similar to that on a cone of half angle equal to the ogive local surface angle plus the angle of attack. The applicable free-stream conditions can be derived by electing to define the prenose shock air properties by specifying two thermodynamic variables (temperature and pressure) and then obtaining all the other properties from the real-gas (equilibrium) Mollier approximations of Hansen.

The program always solves for the heating and shear data at 15 stations, of which 10 are equally spaced along the ogive and the last 5 are on a downstream cylinder. The user may elect to input the local-to-stagnation-point pressure ratio at each of the 15 points, and the program will get the entropy on the nose at the first station and expand isentropically to the input pressures at the local points. This solution assumes a constant entropy over the entire body.

In the alternate solution the program calculates the downstream-of-conical-nose shock properties including pressure and entropy at the first point and then, using these data as initial values, passes through a real-gas Prandtl-Meyer expansion to get the pressure at a second point. This pressure and the point 1 entropy are then used with air properties to define all external-to-boundary-layer properties at point 2. Next the program considers the local surface angle at point 2 to be a cone half angle and calculates a new cone(external-to-boundary-layer) entropy at point 2 which it uses, in the same manner as just described, to expand by the real-gas Prandtl-Meyer routine to obtain the point 3 pressure at the point 2 entropy. In this way the properties at each point on the ogive are derived at the approximate entropy of the immediate upstream point.

FORTRAN and Assembler
IBM 360

This program was written by Lawrence D. Wing of **Goddard Space Flight Center.** *For further information, Circle F on the COSMIC Request Card.*
GSC-11468

NASA

DYNGEN

Steady-state and transient performance of turbojet and turbofan engines

Digital, analog, and hybrid computer methods are available for use in generalized computer codes for transient engine analysis. A disadvantage which all methods have traditionally shared is the need to minimize the number of equations which require iterative solution. Therefore, transient engine simulations usually resort to assumptions and approximations in an effort to avoid iterative solution procedures. As a result, their steady-state solutions tend to disagree with the solutions produced by purely steady-state programs.

A computer program, DYNGEN, has been developed which analyzes both the steady-state and transient performance of turbojet and turbofan engines. DYNGEN solves the system of differential equations which model the dynamics of the engine by a method substantially different from the forward-difference integration techniques frequently used in digital engine simulations. The new method used by DYNGEN is similar to the well-known Euler method of solving differential equations. It gives the analyst freedom in selecting the equations needed to describe the system and eliminates the discrepancies which often occur between answers generated by transient and steady-state simulations.

The program does not require small time steps to obtain a stable solution. This ability to use large time steps (about 0.10 second) is an advantage in engine simulation since in the past it has often been necessary to select integration time steps small enough to guarantee stability for high-frequency dynamics typical of mass and energy storage in unsteady flow.

FORTRAN IV
IBM 7000 Series
UNIVAC 1106
IBM TSS 360/67

This program was written by James F. Sellers and Carl J. Daniele of **Lewis Research Center.** *For further information, Circle G [IBM 7094 Model 2], Circle H [UNIVAC1106], or Circle I [IBM TSS 360/67] on the COSMIC Request Card.*
LEW-12506

NASA

Venting for Condensation in Gas Lines

Analysis of venting to prevent improper flow

A new computer program considers transient condensation phenomena in a vented gas stream. It provides information on the quantity of condensate and the effect of line heat transfer and temperature on minimizing or eliminating condensate that might affect gas flow adversely.

The program provides a complete thermodynamic mapping of the vent system. Inert pressurized gases, such as oxygen and nitrogen, containing significant content of a condensable material, such as water vapor, are vented through an orifice and are discharged to the ambient through a line. Time transient flow rates, fluid pressure and temperature distribution down the line, line temperatures, and condensation are calculated.

Whether flow choking occurs at either the valve orifice or the line exit, or both, is determined. The line exit condition is determined by either choked flow or pressure level at the ambient. Flow rates are determined by either choked flow at the valve or by iteration to meet exit boundary conditions. If choking occurs at the orifice, flow pressure losses at the orifice are iterated to meet exit boundary conditions.

FORTRAN
IBM 360

This program was written by Rex A. Moses of Rockwell International Corp. for **Johnson Space Center.** *For further information, Circle J on the COSMIC Request Card.*
MSC-19621

NASA

REJECT

Flow field of supersonic ejector nozzles for turbine engines

A computer program, REJECT, has been developed for determining the performance and flow-field characteristics of supersonic ejector nozzles. The computer program provides an accurate and economical method of designing a wide variety of ejector nozzles over the range of flow conditions of interest. It includes real sonic "line" effects and an interaction analysis for the mixing process between the primary and secondary flows of the ejector nozzle.

The primary flow field is determined by the method of characteristics, starting from an initial datum line called the sonic line. The viscous interaction between the two streams occurs along the interface and results in a transfer of energy from the primary stream to the secondary stream. In the present analysis the two-stream mixing is computed on the basis of a quasi-constant-pressure mixing process. Two conditions are applied at each point along the jet boundary or interface: (1) the local static pressure must be equal for both streams at their boundary, and (2) continuity between the two streams must be preserved. The latter condition requires that the amount of secondary flow entrained by the mixing process plus the unmixed flow be equal to the secondary flow supplied to the ejector. These conditions are used to determine the jet boundary and consequently the local flow conditions in the neighborhood of the shroud wall. Thus, the mixing process is treated as an interaction analysis rather than simply superimposing the mixing region on the inviscid flow field at the minimum secondary flow area as had been done previously.

A large number of cases have been calculated with this analysis and compared with appropriate experimental data with high correlation.

FORTRAN IV
IBM 360, 7094
CDC 6600
UNIVAC 1108

This program was written by Bernhard H. Anderson of **Lewis Research Center.** *For further information, Circle K on the COSMIC Request Card.*
LEW-12375

NASA

BUCLAP2

Instability analysis of laminated curved plates subjected to combined in-plane loads

A method was needed to predict the buckling of rectangular flat and curved laminated plates subjected to in-plane normal and shearing loads, with each lamina composed of orthotropic material with arbitrary orientation of the orthotropic axes. To meet this need, a method of analysis has been presented, and a computer program, BUCLAP2, based on this method has been coded. The program is used to study the buckling behavior of selected laminated curved plates.

The method of analysis starts with nonlinear engineering strains to derive stability equations from the energy by variational methods. The applied loads are considered constant throughout the plate, and the analysis ignores prebuckling displacements. Periodic behavior is required along the length; then the equations are solved exactly, with provisions for arbitrary elastic constraints on the longitudinal edges. The solution is applicable to: (a) finite-length plates when the plate is specially orthotropic and the combined in-plane external loads do not include shear and (b) infinitely long plates for all other cases. The edges across the width of the finite plate must be simply supported.

A stiffness matrix is set up with elements that are transcendental functions of the external loading. After the boundary conditions are applied, the minimum load is extracted by setting the determinant of the stiffness matrix equal to zero for any chosen axial number of half-waves. This load is determined by an iteration procedure (based on the number of eigenvalues below the trial value), and the lowest of all such loads for various half-wave numbers is the critical load of the structure. Given the geometry, the material properties, and the selected boundary conditions, the program calculates the minimum buckling load for various wavelengths.

(continued next page)

SCOPE 3.1 or KRONOS 2.0
CDC FORTRAN IV,
COMPASS CDC 6000

This program was written by D. W. Halstead, L. L. Tripp, M. Tamekuni, L. L. Baker, and A. V. Viswanathan of The Boeing Co. for **Langley Research Center.** *For further information, Circle L on the COSMIC Request Card.*
LAR-11696

NASA

Swept-Tapered-Wing Aerodynamics

Effects of jet blowing at low subsonic speeds

A computer program has been developed to calculate the effects, on lift and drag, of blowing two jets over a swept tapered wing at low subsonic speeds. The algorithm used is based on a vortex lattice representation of the wing lifting surface and a line source-sink distribution to represent the effects of the exhaust jets. The method assumes that the flow external to the jet exhaust is steady, irrotational, inviscid, and incompressible. It is also assumed that: (a) the jet is not deflected by the free stream, (b) the jet exhausts do not intersect or wash the wing, and (c) the jet cross-sectional shape is not distorted by the wing flow field or by any cross-flow components of the free stream velocity.

Each wing half is subdivided along the span and chords into 50 or fewer elemental areas. In the present program version the number of spanwise and chordwise panels is arbitrary; however, all calculations are made with 5 equally-spaced chordwise and 10 equally-spaced spanwise panels on each wing half, unless otherwise specified. Each elemental area is represented by a horseshoe vortex with the bound portion lying along the local quarter-chord line of the element. The trailing vortices lie streamwise along the inboard and outboard edges of each panel on the wing chord plane.

The induced effects of the jet exhaust are simulated with a distribution of line sinks and sources located on the longitudinal axis of the jet. The axis of the jet is divided into a number of segments over which the sink or source strength is assumed to be linear. This continuous line sink-source distribution is equivalent to a series of triangular elemental distributions. The predictions of this relatively simple procedure are in good agreement with experimentally measured interference lift and interference-induced drag.

FORTRAN IV
CDC 6000

This program was written by Lawrence E. Putnam of **Langley Research Center.** *For further information, Circle M on the COSMIC Request Card.*
LAR-11701

NASA

SESOP

Program for solar-energy heating-systems analysis

The design of efficient solar-energy systems for heating, air-conditioning, and other utilities in homes and buildings requires a reliable analysis of the energy needs in operating the building under consideration.

A computer program has been developed for the analysis of heating, ventilation, and air-conditioning systems with the utilization of solar energy for space heating and domestic hot-water heating. Hot-water demand profiles are calculated by the use of empirical equations with the number of occupants per dwelling unit and the number of dwelling units as the independent variables. The space heating-and-cooling loads are calculated for each building based on: (a) outside environment, (b) desired inside conditions, (c) building construction and geometry, (d) domestic power usage, (e) occupancy rate, and (f) occupant metabolic rate. Upon the completion of calculation of the loads for each of the buildings, the loads are summed to determine the requirements of the central utility systems.

Based upon input descriptions of the environment and the solar collectors, an analysis is performed to determine a profile of the amount of useful energy which can be collected by the solar collectors. The program uses the load profiles and solar-energy profiles to determine the energy required by alternative systems to meet the utility demands.

FORTRAN
UNIVAC 1100, EXEC VIII

This program was written by Lockheed Electronics Co. for **Johnson Space Center.** *For further information, Circle N on the COSMIC Request Card.*
MSC-14853

NASA

Machinery

Hardware, Techniques, and Processes

Concentric-Tube Differential Drive

A remote manipulator with concentric gear shaft has seven degrees of freedom.

Marshall Space Flight Center, Alabama

This novel remote manipulator consists essentially of gear shafts that are placed concentrically, with bevel gears located at each joint. By locking of various sets of gears and rotating others one or several degrees of rotational freedom may be achieved. A special differential prevents cross-coupling between joints.

Up to seven degrees of freedom (see Figure 1) can be stacked in one composite differential and still allow independent, simultaneous operation.

Figure 2 shows how a seven-degree-of-freedom differential allows the power package to be completely remote from the arm. The system uses long tubes or ball cables to transmit power to the arm.

Among the advantages of this teleoperator are: light weight, accessibility of components, continuous rotation of joints, possibility of underwater use if arm is filled with incompressible fluid (light oil), and possibility of miniaturization.

This work was done by Ray E. Marlow of Sperry Rand Corp. for **Marshall Space Flight Center.** *For further information, Circle 72 on the TSP Request Card.*

This invention has been patented by NASA [U.S. Patent No. 3,922,950]. Inquiries concerning nonexclusive or exclusive license for its commercial development should be addressed to the Patent Counsel, Marshall Space Flight Center [see page 2]. Refer to MFS-22707.

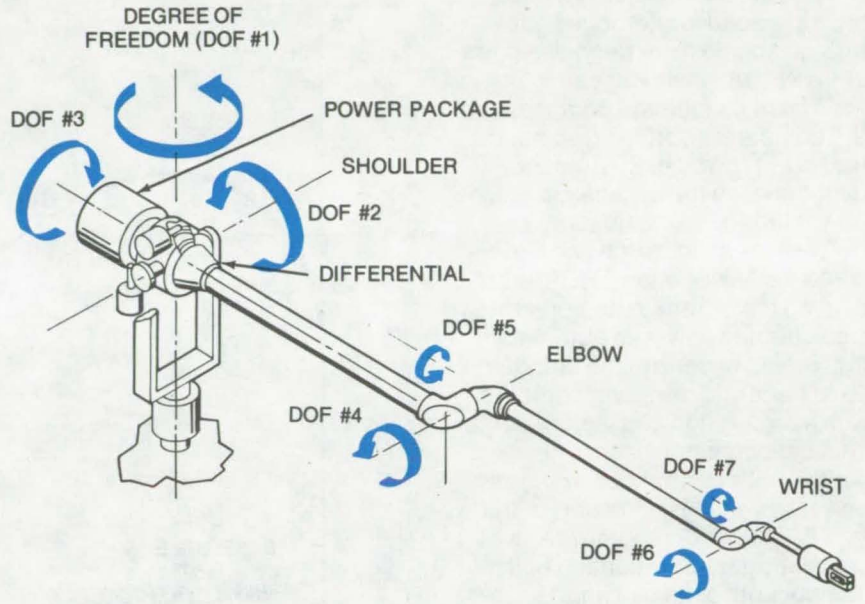

Figure 1. A conceptual model of the **Remote Manipulator** has three degrees of freedom (DOF's 1, 2, and 3) in the shoulder mount and four more on the arm. The weight of the power package helps balance the arm.

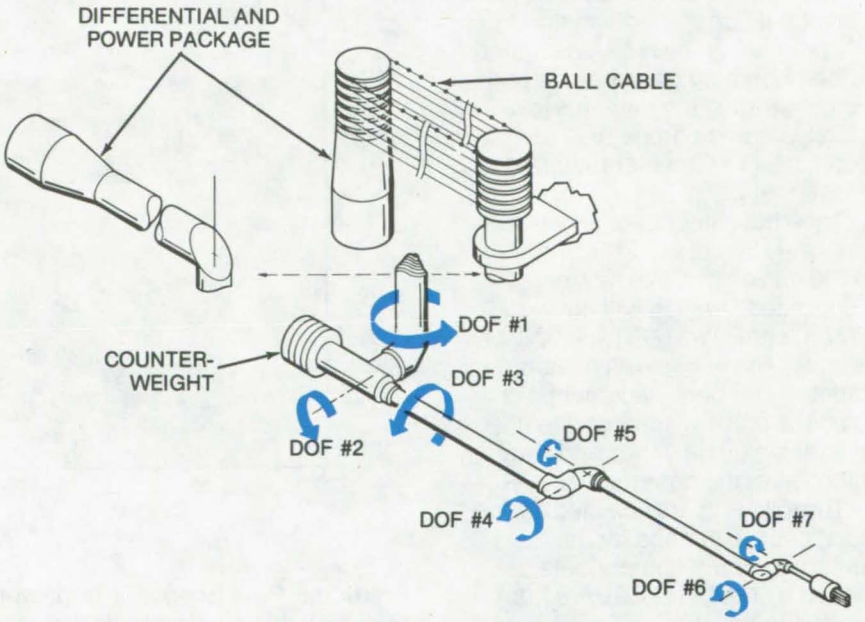

Figure 2. In another version, a **Separate Power Package** is made possible by using long tubes or ball cables to transmit power to the arm.

NASA

Improved Automobile Gas Turbine Engine

Design of turbomachinery components for an improved automotive gas turbine engine

Lewis Research Center, Cleveland, Ohio

Turbomachinery components for an "upgraded" automotive gas turbine engine have been designed at the NASA Lewis Research Center. These include the compressor, the compressor-driven turbine, the free power turbine, the transition duct between the turbines, and the power turbine exit diffuser.

The Energy Research and Development Administration (ERDA) is conducting a program to demonstrate a gas turbine powered automobile that meets or betters the stringent 1978 Federal Emissions Standards with acceleration characteristics and fuel economy that are competitive with current conventionally powered vehicles. One part of the joint ERDA/NASA program involves an experimental evaluation of the components of an existing "baseline" (sixth-generation, Chrysler Corporation) engine and a current (Chrysler Corporation) vehicle. The major part of the ERDA program consists of the design and fabrication of the "upgraded" engine by Chrysler using the NASA-designed turbomachinery components and demonstrating the engine's low emissions and competitive fuel economy in a Chrysler-modified passenger car.

The "baseline" engine delivers 112 kW (150 hp) in a 2000 Kg (4400 lb) vehicle. The new or "upgraded" engine will deliver 75 kW (100 hp) in a 1600 Kg (3500 lb) vehicle. The engine will have the capability for power augmentation to 90 kW (120 hp) through the use of variable guide vanes and water injection at the compressor inlet.

The following are selected design point characteristics for the turbomachinery components designed by NASA for ERDA's "upgraded" engine:

Compressor — Mass flow rate 0.59 kg/sec; rotating speed 58,500 rpm; total pressure ratio 4.08; and total efficiency 0.775. A backswept

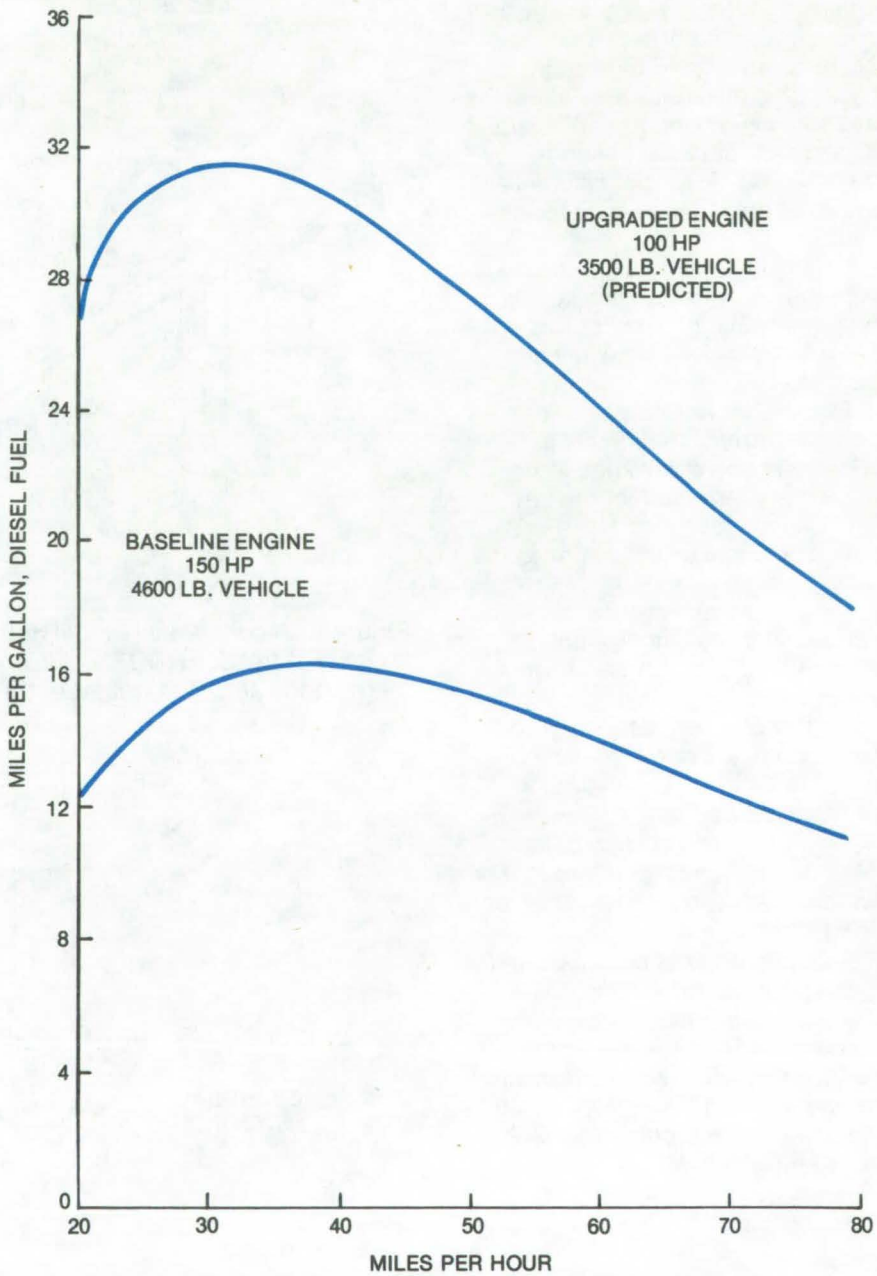

Predicted **Fuel Economy** improvement of the upgraded gas turbine engine/vehicle combination vs. the baseline engine/vehicle

impeller was designed for the compressor in order to attain the efficiency and operating range goals of this program. Design inlet Mach number for the diffuser is 0.85.

Compressor-drive turbine — Mass flow rate 0.598 kg/sec; turbine inlet temperature 1325 K (1925 °F); work factor 2.1; total efficiency 0.85; radius ratio 0.7973; tip diameter of 11.15 cm (4.39 in).

Free power turbine — Rotative speed 46,150 rpm; tip diameter 15.41 cm (6.07 in); hub-to-tip ratio 0.78; total efficiency 0.85; work factor 1.247.

The transition duct and the turbine exit diffuser were designed to each have an optimum area ratio based on empirical studies.

The figure shows predicted fuel economy improvement of the upgraded engine/vehicle combination as compared with road test data from the present ERDA baseline engine/vehicle combination. The improvements are a result of the combined effects of reduced weight, reduced power-to-weight ratio, increased turbine inlet temperature and improved component efficiencies at part power.

This work was done by Milton G. Kofskey, Theodore Katsanis, Richard J. Roelke, Kerry L. McLallin, and Robert Y. Wong of **Lewis Research Center** *and Lawrence F. Schumann and Michael R. Galvas of the U.S. Army Air Mobility R&D Laboratory. Further information may be found in:*

NASA TM-X-71714 [N75-24106] "Aerodynamic Design of a Free Power Turbine for a 75 kW Gas Turbine Automotive Engine,"
NASA TM-X-71717 [N75-21633] "The Aerodynamic Design of a Compressor-Drive Turbine for Use in a 75 kW Automotive Engine," and
NASA TM-X-71719 [N75-24116] "A Compressor Designed for the Energy Research and Development Agency Automotive Gas Turbine Program."

Copies of these reports may be obtained at cost from the Aerospace Research Applications Center, Indiana University [see inside back cover].

LEW-12521

NASA

Efficient Low Static-Volume Water Heater

A concept for an efficient fast-response form of demand heater with an easily temperature-controlled heating element

Marshall Space Flight Center, Alabama

At high temperatures, steam forms around heating elements which are in direct contact with water and drastically reduces their efficiency. Moreover, thermal gradient mixing is an inefficient form of heat transfer. The critical energy shortage requires a more efficient design.

A transfer of technology is suggested by a recent development in cooling techniques for high-power transmitter tubes. The cooling fluid is circulated through a matrix of fused metallic spheres which introduces turbulent flow and minimizes boundary-layer effects, yielding a heat transfer which is greater than that of the fluid without turbulent flow. Based on this, a proposed demand water heater could provide a compact heating source for industrial applications and homes. The proposed heater is readily attached to existing cold water lines, is electrically safe to operate, and provides a relatively unlimited supply of hot water. A Calrod heating element is surrounded by a matrix of fused sintered copper or brass balls, and the assembly is then installed in the piping of a water system. As water flows through the matrix, the sintered balls cause turbulent flow and heating.

Control of the water temperature is achieved using a temperature-sensing element attached to the outer jacket of the assembly. If necessary, a mixing faucet can be used to provide a mixture of hot and cold water. Possible applications include laundromats, where there is no way of knowing in advance what the actual hot water demand may be; and laboratories and photographic labs, where present immersion heaters are difficult to use and where hot water lines are not conveniently available.

This work was done by Robert L. Brown of **Marshall Space Flight Center.** *No further documentation is available.*

Inquiries concerning rights for the commercial use of this invention should be addressed to the Patent Counsel, Marshall Space Flight Center [see page 2]. Refer to MFS-22469

NASA

Cyclical Bidirectional Rotary Actuator

A thermally powered actuator has been developed to rotate a magnetometer during calibration.

Goddard Space Flight Center, Greenbelt, Maryland

A magnetometer can be used to measure the strength of the Earth's magnetic field. It also provides navigational guidance for unmanned spacecraft. When guiding these craft, the instrument requires precise calibration; if ambient magnetic field strength readings waver as the magnetometer is rotated, it needs to be calibrated. In one method of rotating the device, flipping the instrument end-over-end on axis via a thermally-powered rotary actuator, one or more bimetallic springs, wound much like clock springs, are used. The springs are attached to a shaft which turns the magnetometer.

Until now, this simple design lacked provisions for locking the shaft in position. Also the spring material lacked position memory.

A thermally-powered rotary actuator has been designed to flip a magnetometer between one of two positions located 180° apart and permits instrument calibration. A pair of heat-extensible springs, selectively rotate the shaft from one position to the other when electric

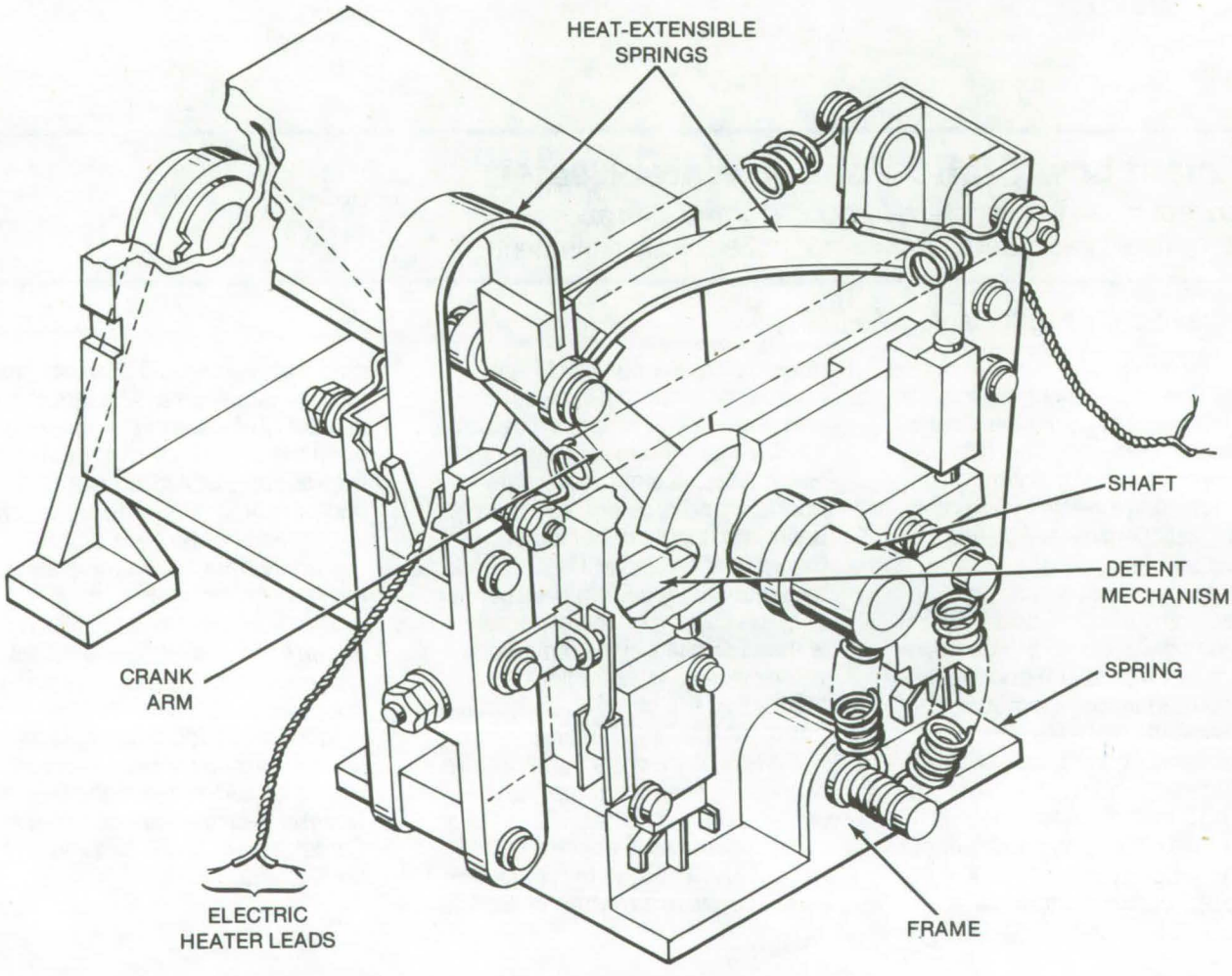

The **Cyclical Bidirectional Rotary Actuator** includes a rotatable frame that supports the shaft and a pair of heat-extensible springs. One end of the springs is coupled to the frame, and the other end is coupled to the shaft for respectively applying clockwise and counterclockwise torque to the shaft upon application of heat. This permits the shaft to be positioned in either of two positions 180° apart.

heaters bonded to them are energized. A detent mechanism locks the rotatable shaft in one of the two positions. The major elements include a frame which supports a shaft and the pair of heat-extensible springs. These have first and second ends (the first is coupled to the frame, and the second is coupled to the shaft) for applying clockwise and counterclockwise torque to the shaft when the springs are heated. A crank arm positions the shaft in the first and second positions via projections, stops, and springs. The detent mechanism locks the shaft in position.

With the crank arm starting in the position shown in the illustration, electric current is applied to the heater windings mounted integrally with the left-hand spring. Its temperature then rises above the transition temperature of the alloy. During the extension of the spring caused by heating, the H-shaped member connected to the spring pivots around its anchor pin, which disengages the tapered tip from the detent. After disengagement, the shaft rotates the crank-arm projection clockwise away from the mechanical stop on the right side of the actuator.

During the first 90° of shaft rotation, both flexible springs become fully compressed. The left-hand heat-extensible spring is partially entended and pushes the toggle spring crank closer to the right-hand H-shaped member. As soon as the shaft rotates more than 90°, the fully compressed flexible springs expand, pushing the shaft through its complete arc of rotation. As the shaft approaches 180°, the detent engages the notch to lock the shaft (a mechanical stop prevents the shaft from rotating more than 180°). The left-hand heat-extensible spring is extended more fully than the one on the right. When the right-hand spring is heated, the process is reversed.

This work was done by William C. Stange of **Goddard Space Flight Center.** *For further information, including a detailed description of the actuator, Circle 73 on the TSP Request Card.*

This invention is owned by NASA, and a patent application has been filed. Inquiries concerning nonexclusive or exclusive license for its commercial development should be addressed to the Patent Counsel, Goddard Space Flight Center [see page 2]. Refer to GSC-11883, GSC-11974, and GSC-11975.

NASA

Field Sampling Fine-Vacuum Systems

A portable pumping system can be used for onsite sampling of vacuum systems at 10^{-7} torr.

John F. Kennedy Space Center, Florida

Onsite sampling followed by quantitative laboratory analysis of residual gases is now possible with a small portable pumping station consisting of a roughing pump, an air-cooled diffusion pump, and a liquid nitrogen cold trap. Duplicate samples are collected into 40-liter stainless-steel flasks, which are then taken to the laboratory for analysis. The residual gas analyzer, a mass spectrometer, need not be moved to the sampling site.

Comparisons between laboratory results and onsite analytical results were made with two different gas mixtures: N_2, O_2, He, Ar, and CO_2; and He, Ar, O_2, and N_2. Good agreement was obtained except when high concentrations of helium (He) were present. Industries that deal with cryogenic fluids or low-pressure gas systems will save time and maintenance costs with this new technique.

This work was done by E. W. Fickey and D. M. Smoot of The Bendix Corp. for **Kennedy Space Center.** *For further information, Circle 74 on the TSP Request Card. KSC-10596*

NASA

Optical Bias Assembly

An optical bias assembly, consisting of a tungsten lamp source, optical filters, fiber optics bundle, aperture mask, relay lens, and folding mirror, is used to achieve linear response in an optical detection system. The tungsten lamp source provides sufficient background illumination to make an input optical flux small compared to the background, thus linearizing the input flux.
(See page 58.)

Tracking System for Moving Subjects

An electronic system automatically focuses a camera or a spotlight on a moving subject. The subject is equipped with a miniature ultrasonic or radio transmitter; its signal is picked up by two or more detectors, depending on the number of dimensions of the subject's motion. These signals are phase detected and fed to a computer which determines the position of the subject and sends command signals to a servo for the camera or the spotlight.
(See page 36.)

Integral Fan/Water Separator

Centrifugal force is used to remove moisture from a gas.

Lyndon B. Johnson Space Center, Houston, Texas

A new fan/water separator is a lightweight compact unit in which the centrifugal force created by a rotating fan wheel separates moisture from gas. The portable separator can be worn with a pressurized suit, where it will remove moisture that accumulates from breathing and perspiration. In conventional systems with heat-exchange condensers the water flow capacity may be restricted by clogging or by gas pockets trapped within the assembly pores.

Speed	15,000 rpm
Oxygen flow rate	3.6 kg/h (8 lb/h)
Pressure rise	1,493 N/m² (6 in. H_2O)
Inlet pressure	27.6×10^3 N/m² (4 psia)
Inlet temperature	10° C (50° F)
Power consumption	22 W
Design water removal rate	0.37 kg/h (0.808 lb/h)

Separator Specifications

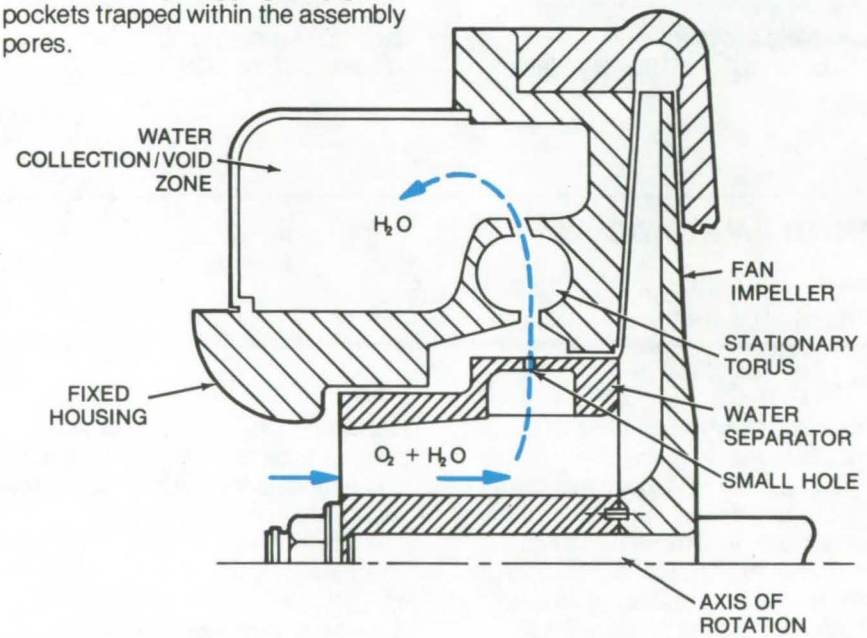

Fan/Water Separator

The basic design of the separator is shown in the cross-section drawing. A force field is created by the rotating fan impeller. The impeller is made up of two parts: a water separator and a radially bladed fan. As the oxygen/water mixture enters the system, it is subjected to rotation by the rotating water separator. The centrifugal action forces the moisture toward a small hole built into the separator wall.

Water droplets move through the hole and collect in the stationary torus section. Continuous pressure from the incoming droplets forces the water to move from the torus into the water collection/void zone.

The currently tested separator has the specifications shown in the table.

This work was done by Richard L. Johnson of The Garrett Corp. for **Johnson Space Center.** *For further information, Circle 75 on the TSP Request Card.*
MSC-14756

NASA

Crosswind Landing-Gear Position Indicator

A new position indicator for airplane landing-gear systems prevents wheel misalinements.

Langley Research Center, Hampton, Virginia

The aircraft position indicator shown was designed at Langley Research Center for use on airplanes equipped with an adjustable or automatic crosswind landing-gear system. The indicator display shows the wheel alinement relative to the runway and aircraft centerline in such a manner that the flight crew will not mistakenly adjust the wheels in the wrong direction.

When the wheel-alinement system is operated in an automatic mode, the indicating system is used to monitor and detect improper wheel alinement. The co-located (common-rotational-axis) needles of this instrument show "crab angle" and wheel alinement in a clear and accurate manner. The indicator system (see illustration) consists of the following:

- A compass card driven by a gyro slaved to the compass heading
- A fixed airplane symbol
- A double bar needle (runway symbol) which points to the landing-runway magnetic heading
- A single bar needle which indicates the preset (or automatic-setting) angle of the wheels relative to the aircraft axis
- A runway-heading selector knob which is used to select the desired runway
- Suitable electronic circuits to move the various needles and controls.

When the pilot selects the runway heading, the runway needle (double bar) alines with the proper compass heading as seen on the compass card. The pilot flies the aircraft to the extended-runway centerline and then "crabs" into the local wind for the approach. The "crab angle" is then the angular difference between the centerline of the fixed aircraft symbol and the double needle. The pilot then alines the landing gear of the aircraft with the runway centerline, and the landing-gear indicator shows when the two are alined as the single and double bar needles are superimposed and, thus, makes no mistake possible on wheel alinement. When the wheels are alined automatically (operated by the angle difference between runway heading and aircraft gyrocompass heading by electronic circuits), the system can be monitored by the pilot, and a malfunction of the automatic mode can be detected.

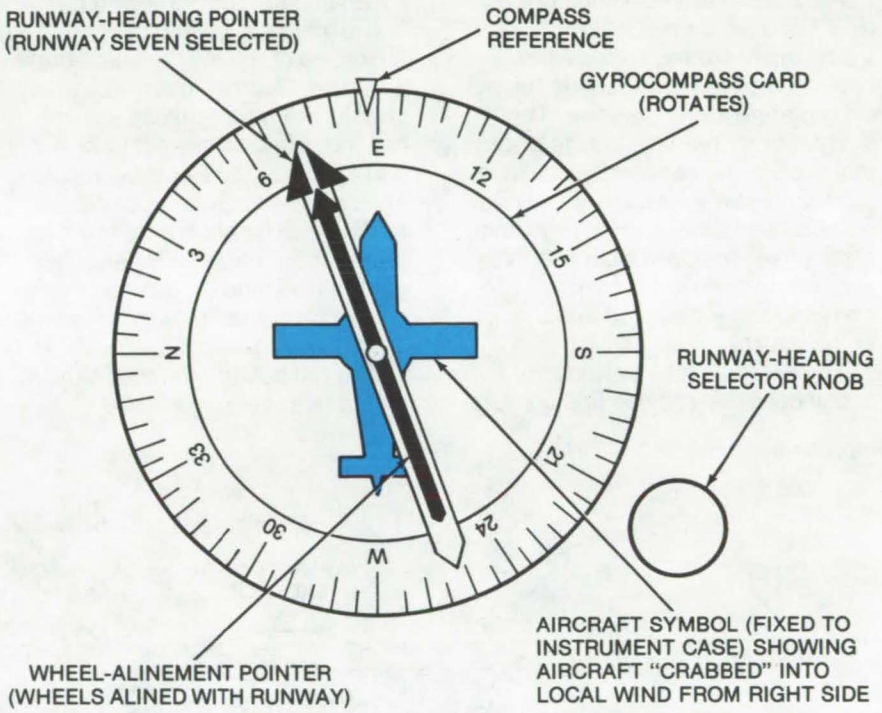

The co-located needles (pointers) of the **Aircraft Position Indicator** show "crab angle" and wheel alinement clearly and accurately. The system is designed for airplanes with adjustable/automatic crosswind landing-gear systems.

This work was done by Robert A. Champine of **Langley Research Center.** *No further documentation is available.*

Inquiries concerning rights for the commercial use of this invention should be addressed to the Patent Counsel, Langley Research Center [see page 2]. Refer to LAR-11941.

NASA

Pointing Control/Roll Positioning Mechanism

A telescope mount provides torquing for a fine-pointing servosystem, in both pitch and yaw.

Marshall Space Flight Center, Alabama

An experiment pointing control (EPC) and a roll positioning mechanism were developed to provide a pointing capability for an orbiting-telescope canister. The system comprises two large rings that support the canister and provide pitch-and-yaw torquing for the fine pointing servosystem. The system also senses rotation about two axes and has an open-loop roll drive. The combined mechanisms are shown in the figure.

The EPC has four actuator assemblies that provide fine pointing ($\pm 2^{\circ}$) in pitch and yaw, and the entire gimbal system can be rotated by means of the roll drive-and-brake actuator. Each actuator assembly consists of a frictionless flexure bearing, a brushless dc torque motor, and a multispeed electrical resolver. The resolver provides position feedback. The pitch actuator pair connect the canister to the inner gimbal ring, and the yaw actuators connect the inner gimbal ring to the outer roll ring.

The roll positioning mechanism includes a drive-and-brake assembly, a roll-position indicator assembly, a ring-and-gear assembly, and four roller cluster assemblies. It provides the drive capability in roll and a means of sensing the amount and speed of rotation.

During pointing tests, pitch and yaw are monitored automatically by a dual-axis laser autocollimator. The autocollimator system consists of a high-quality, optically-flat target mirror; a laser-powered, interferometric optical head; a laser power supply; and an electronic signal-processing assembly. Signals

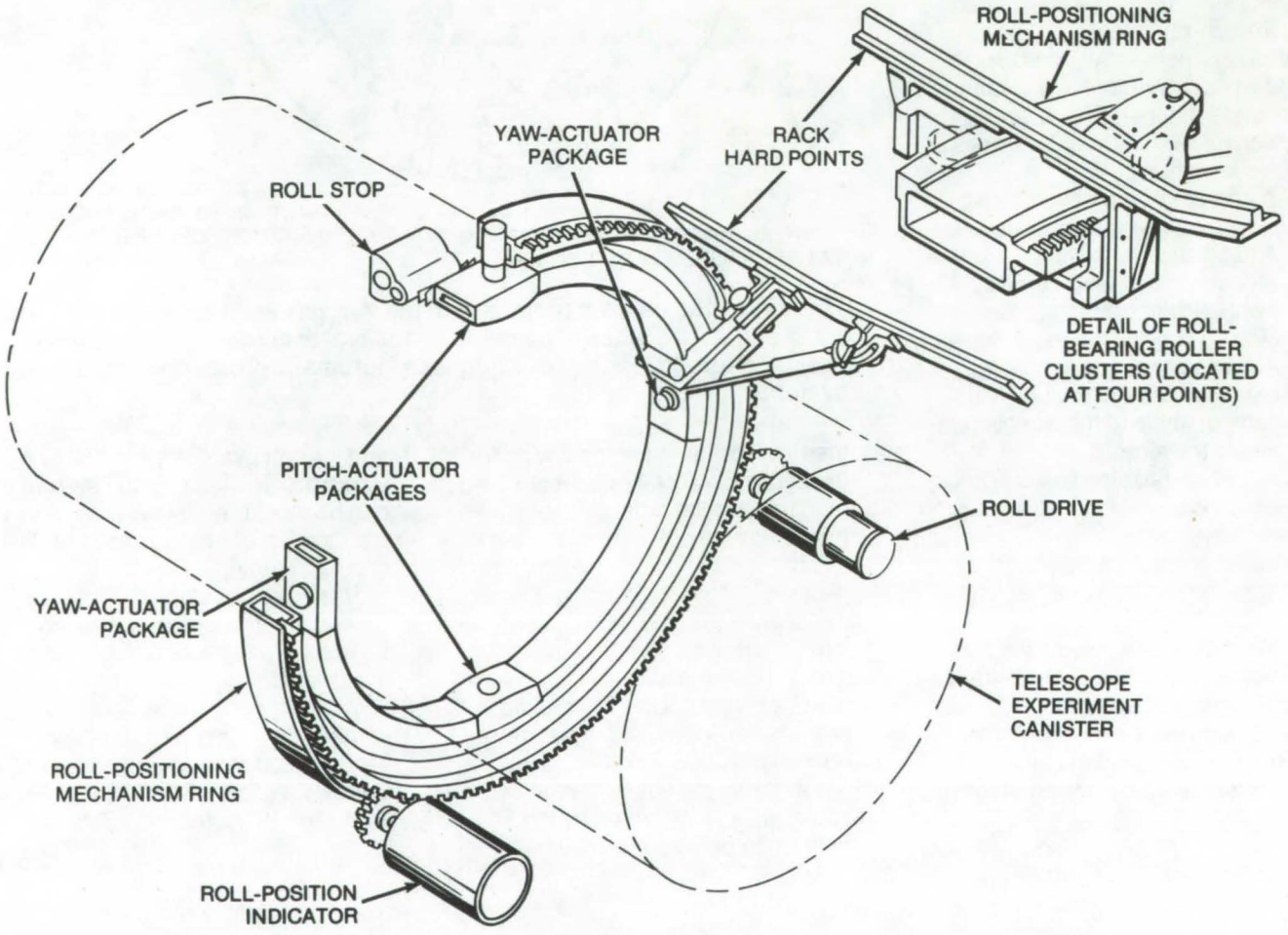

In the **Fine-Pointing Mechanism** the pointing control moves the canister in pitch and yaw and reads out the movement. The roll-positioning mechanism rotates the system and senses the amount of rotation.

from the optical head are electronically processed and are provided in two forms; digitally on a display and as analog voltages conducted to a control console. The output signals consist of rate and position information for pitch-and-yaw motion. Although commercial units are available that can perform some of these functions, no known available instrument can provide an equivalent combined performance, range, and accuracy in angular position and rate sensing.

Although the design of this system is based on well known concepts, the use of flexure bearings (EPC actuator packages) offers a combination of performance, simplicity, and reliability superior to most other bearing configurations. Because flexure bearings require no lubrication, are insensitive to extremes of temperature and pressure, and allow low torque, have little noise, friction, and hysteresis, they are ideally suited for use in precision pointing and tracking systems.

This work was done by W. E. Kohman of The Perkin-Elmer Corp. for **Marshall Space Flight Center.** *For further information, Circle 76 on the TSP Request Card.*
MFS-22809

NASA

Improved Data Display for Milling Machine

Digital display of coordinate-axis position to the nearest 0.0001 in. and a process sequence-number indicator

Lyndon B. Johnson Space Center, Houston, Texas

A problem occurs when operating a specific type of commercially-available, numerically-controlled milling machine in conjunction with its tape controller: There is no visual display or readout which allows the machine operator to verify the position of any machine axis. Furthermore, in the automatic mode, a program sequence number is used to identify each block of information on the tape program. As each program sequence number is read from the tape, it is displayed on the screen at the operator's console. The sequence number consists of a letter address, N, followed by two digits ranging from 00 to 99. However, because the majority of the items produced on this machine require many more steps in their manufacture, the present two-digit display is inadequate to allow the operator to check his program.

These problems have been solved by the adoption of an axis-position-and-sequence-number indicator system designed to work in conjunction with the numerical tape controller. There is a visual display of the exact positions of the X, Y, and Z axes of the machine, to the nearest 0.0001 in. (0.00025 cm), and the sequence-number display shows sequential blocks of input data up to a maximum of 999.

The unit consists of four identical printed-circuit cards (see Figure 1), a self-contained power supply, and all the necessary interface wiring to the tape controller. It is mounted above the right panel of the operator's control station (see Figure 2). Each axis, and the sequence number, requires one card, and each card consists of all the necessary logic elements to convert the binary-coded decimal information of the machine controller to the code required for the seven-segment display.

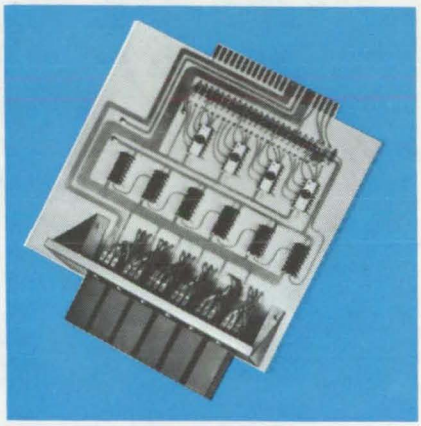

Figure 1. A **Code-Conversion** printed-circuit card for the data display.

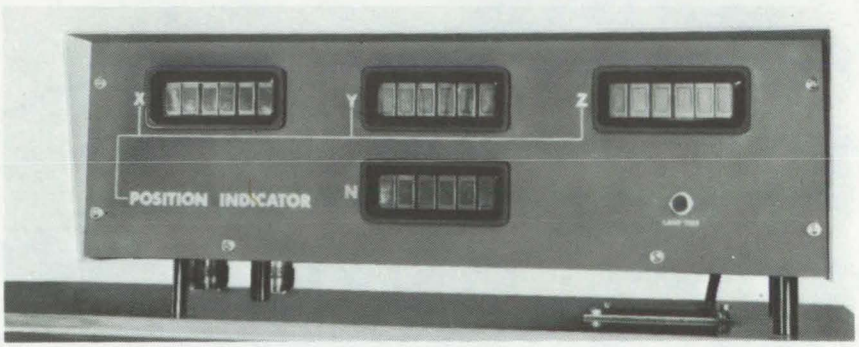

Figure 2. The **Display Console** shows the X, Y, and Z coordinates of the machine as well as the program sequence number.

This work was done by Walter M. Surrency and Paul S. Moravek of **Johnson Space Center.** *For further information, Circle 77 on the TSP Request Card.*
MSC-14742

NASA

Fabrication Technology

Hardware, Techniques, and Processes

Low-Cost Solar Reflectors

Foamed glass is an inexpensive lightweight substrate for reflective elements in solar energy converters.

NASA Pasadena Office, Pasadena, California

Reflective elements used in solar energy converters are made from a reflective surface supported by a substrate. The substrate is shaped for efficient collection of solar energy. However, the shaping process is costly when the substrates are made from quartz, plastics, honeycombs, metal weldments, fiber resins, or spun epoxies.

Recently, a less-expensive lightweight substrate has been made from foamed glass. The foamed glass is basically a cellular glass insulation which withstands temperatures from 5 to 700 K (-450° to 800° F). The material is not combustible and sustains pressures up to 0.7×10^6 N/m² (100 psi). It is a very good thermal insulator both because of the low heat transmissivity of the glass and because the foaming process produces sealed glass cells which are impermeable. Since water and vapor cannot enter the sealed cells, insulating efficiency, shape, and weight are stable during the lifetime of the material.

Normally the foamed glass is obtained in blocks. The block then is shaped by using an accurately-finished aluminum or steel master. The master is as an inverse of the desired shape (e.g., a convex master for a concave shape). Strips of fine sandpaper are attached to the master (see Figure 1), and the master is moved gently over the foamed glass to lap it to the desired shape.

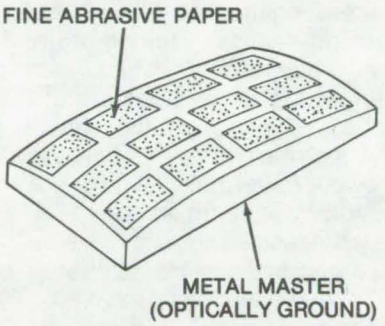

Figure 1. A **Metal Master** is used to shape the foamed-glass substrate. A block of foamed glass is moved over the abrasive to lap it to shape. Lapping is done with very little pressure and a rolling motion until the desired curvature is produced.

After the shaping is completed a sheet of back-silvered glass is applied to the finished surface. The sheet is bonded to the contoured block so that the glass surface is exposed to the outside, and the silvered surface is protected when cemented to the contoured substrate. The sheet is forced to the shape of the concavity by the differential pressure of vacuum and atmosphere across the sheet, and it is permanently held in that flexed state by the cured epoxy cement

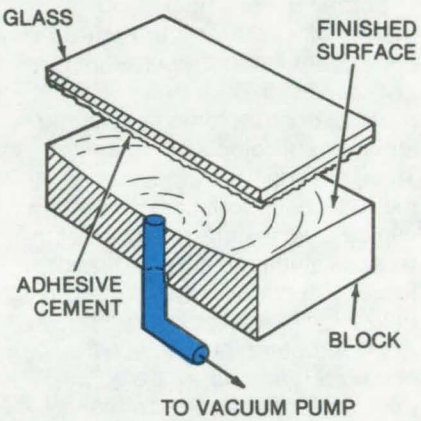

Figure 2. A **Cross Section of a Single Block** is shown during the bonding process. The reflective glass sheet is forced to the shape of the substrate via a vacuum.

(see Figure 2). Vacuum is applied beneath the sheet or to a bag around the composite.

This work was done by Maurice J. Argoud, Jack Jolley, and Walter L. Walker of Caltech/JPL for **NASA Pasadena Office.** *For further information, including design and production data, Circle 78 on the TSP Request Card.*

This invention is owned by NASA, and a patent application has been filed. Inquiries concerning nonexclusive or exclusive license for its commercial development should be addressed to the Patent Counsel, NASA Pasadena Office [see page 2]. *Refer to NPO-13707.*

NASA

Battery-Cell Thermal Test Facility

A vacuum-enclosed system is used to analyze battery thermal output and electrical performance, to help improve battery efficiencies.

Marshall Space Flight Center, Alabama

Since the electrical performance of a battery is temperature dependent, its thermal output is a critical design parameter. This is particularly true for systems with a limited heat-rejection capability. Thus, data on the instantaneous thermal characteristics of a battery can be used to determine its instantaneous electrical efficiency and thereby provide for more effective utilization of available power.

Prior testing methods do not consider the importance of temperature changes on the electrical characteristics of batteries. In the case of nickel cadmium cells, electrical efficiency decreases with increasing temperature, increasing the state of charge and decreasing the charge rate. As temperature increases, the cell becomes more inefficient, thus generating more heat which in turn increases cell temperature. Liquid calorimeters, which maintain a constant cell temperature, have been used to obtain data on cell thermal characteristics. However, thermal lag limits accuracy to approximately 17 percent, and equipment is expensive, requires considerable setup time, and cannot be used with large cells.

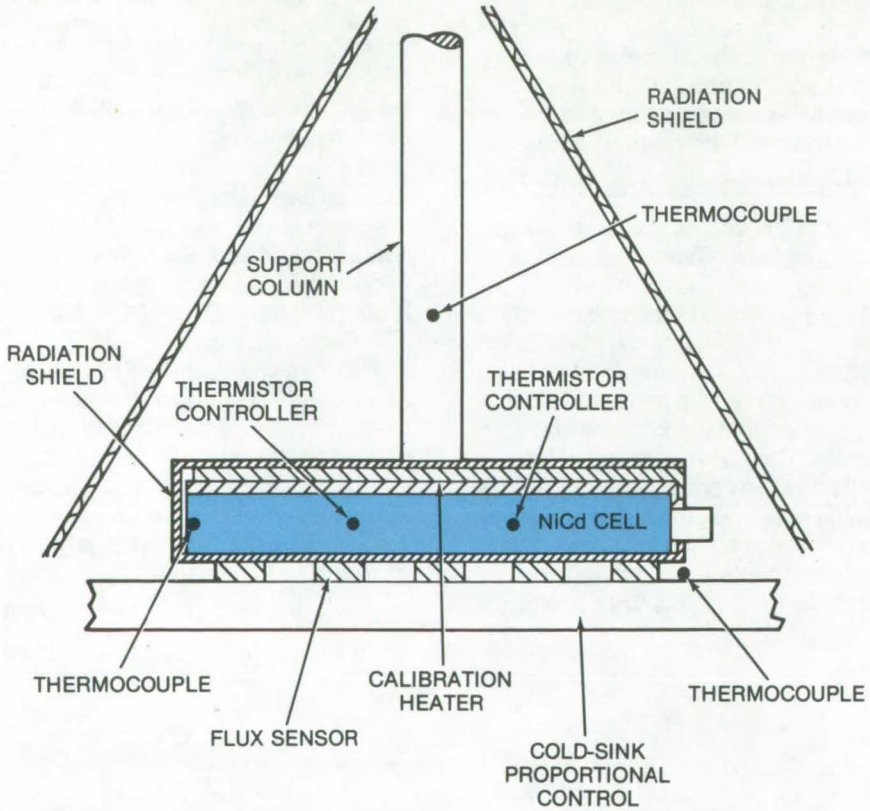

The Test Configuration, shown above with a NiCd cell, is placed inside a vacuum chamber at 10^{-7} torr.

A new test system makes it possible to obtain, simultaneously, the instantaneous thermal and electrical characteristics of batteries. The system consists of an instrumented thermal vacuum chamber, having a capacity of 0.4 m^3 (14 ft^3), an operating vacuum of 1.3×10^{-5} N/m^2 (10^{-7} torr), and a test temperature range of 239 to 344 K (-30° to 160°F). The details of the inner chamber are shown in the figure. The test cell with a calibration heater attached to its upper face is mounted on a series of heat flux sensors. The sensors measure the bidirectional heat flow between the cell and the cold sink and can be of thermopile or any other construction that can measure the heat flux.

Radiation and convection current losses are minimized by two radiation shields and by the operating vacuum. Losses through the support column maintaining the cell in position, and through the electrical cabling from the cell, are determined by establishing an energy balance when calibrating the test setup with the calibration heater. Typical measured losses are less than 2 percent.

The key to satisfactory performance lies in maintaining the cell temperature constant within 0.1°C of the test temperature. This control is achieved by a master-submaster controller that operates a heater in the cold-sink circulating unit. The controller responds to minute changes in the resistance of a thermistor attached to the cell. When the cell begins to generate heat, the controller reduces the temperature of the cold sink and extracts heat from the cell through the flux sensors, thereby maintaining the cell at a constant test temperature.

When heat flows in either direction through the flux sensors, a voltage is generated in proportion to the quantity of heat flowing. The flux sensor output is recorded on a voltage recording device. Simultaneously, the electrical performance characteristics of the cell are also recorded. The accuracy of the test program is established by a simple energy balance based on the integrated electrical power in and out through the cell and the integrated thermal energy measured through the flux sensors.

This work was done by John A. Sanders of Martin Marietta Corp. for **Marshall Space Flight Center.** *For further information, including schematics and test data, Circle 79 on the TSP Request Card.*
MFS-23040

NASA

Uniform Solar Cells

Trimming has been found more cost effective than individual selection in producing matched solar cells.

Goddard Space Flight Center, Greenbelt, Maryland

Solar cells with outputs matched to ±0.5 percent are required as radiation sensors on scanners which are used to calibrate solar-cell simulators for a uniform simulator output. Formerly the matched cells were obtained by testing thousands of cells manufactured to broader tolerances to select 150 cells with outputs matched within ±0.5 percent.

Because individual selection was time consuming and costly, a faster technique has been developed in which the cells are individually trimmed to meet specifications. Cells are selected at random from a lot with an output variation of ±5 percent. These are then attached to a scanner, which is mounted on a workbench. Each cell is indexed, using, as an illumination standard, a 1,000-watt quartz-iodine lamp operated at 8.3 amperes. Each cell is tested to determine which has the smallest output under an illumination of 1 solar constant.

All other cells are then matched to the lowest-output (reference) cell by covering a portion of the cell with a narrow strip of aluminized adhesive backed Mylar. The position of the strip is adjusted by trial and error to obtain cell output within ±0.5 percent of the reference-cell output. Because many fewer cells are handled, a matched set can be obtained more quickly (and at lower cost) than by selecting from among thousands of cells.

This work was done by Northrop Services, Inc. for **Goddard Space Flight Center.** *No further documentation is available.*
GSC-11941

NASA

Spotting Small Liquid Leaks

A simple technique helps locate minute liquid leaks.

John F. Kennedy Space Center, Florida

Minute leaks in fittings of petroleum-base fuels may occur in inaccessible places. To avoid the necessity of hand-cleaning the entire suspected area and then taking the time to observe it for leakage, a very efficient improvement has been made with the use of trichlorotrifluoroethane.

The solvent is liberally applied to the surface area being inspected. (It may be brushed on or squirted from a plastic squeeze bottle). The solvent will clean the surface well; and because it is highly volatile, it will leave a dry surface before any further leakage has had a chance to occur. At this point, any leaks will be readily visible on the clean dry surface.

This work was done by Charles R. Gilley and John R. Schanbacher of The Boeing Co. for **Kennedy Space Center.** *No further documentation is available.*
KSC-10667

NASA

Combined Joining Process for Dissimilar Metals: A Concept

Combined brazing and diffusion bonding of aluminum and stainless steel may save time and simplify processing.

Lyndon B. Johnson Space Center, Houston, Texas

NASA has investigated heat dissipators that consist of aluminum cold plates attached to stainless-steel connecting ports for corrosion resistance. Not only might the cold plates be useful with various electronic and mechanical products, but also the techniques investigated for bonding aluminum to stainless steel could have wide applications.

The conventional technique for joining the two metals consisted of an initial aluminum/aluminum silicon fluxless-brazing step. This was followed by diffusion bonding the stainless-steel part to the brazed aluminum. The separate diffusion-bonding step required a high platen pressure and 5 hours of processing time.

A combined joining process has been proposed in which the two metals are diffusion bonded in less time and with a much lower platen pressure. In the conventional technique, the aluminum cold plate is vacuum fluxless-brazed in a retort for 10 minutes at 1,055° to 1,095° F (570° to 590° C) and under a platen pressure of from 100 to 200 psi (0.69×10^6 to 1.38×10^6 N/m^2). The subsequent diffusion-bonding step is carried out at 850° F (455° C) for up to 5 hours at a platen pressure of 2,000 psi (13.8×10^6 N/m^2).

In the proposed combined process, the metals are brazed and diffusion bonded in the same retort assembly. The aluminum is brazed as in the conventional technique. For the diffusion bonding, the temperature is lowered to 950° F (510° C), and the platen pressure is increased to 500 psi (3.45×10^6 N/m^2). The process requires only from 1 to 4 hours, and tests have shown that the resulting bond can withstand internal pressures up to 1,000 psi (6.9×10^6 N/m^2).

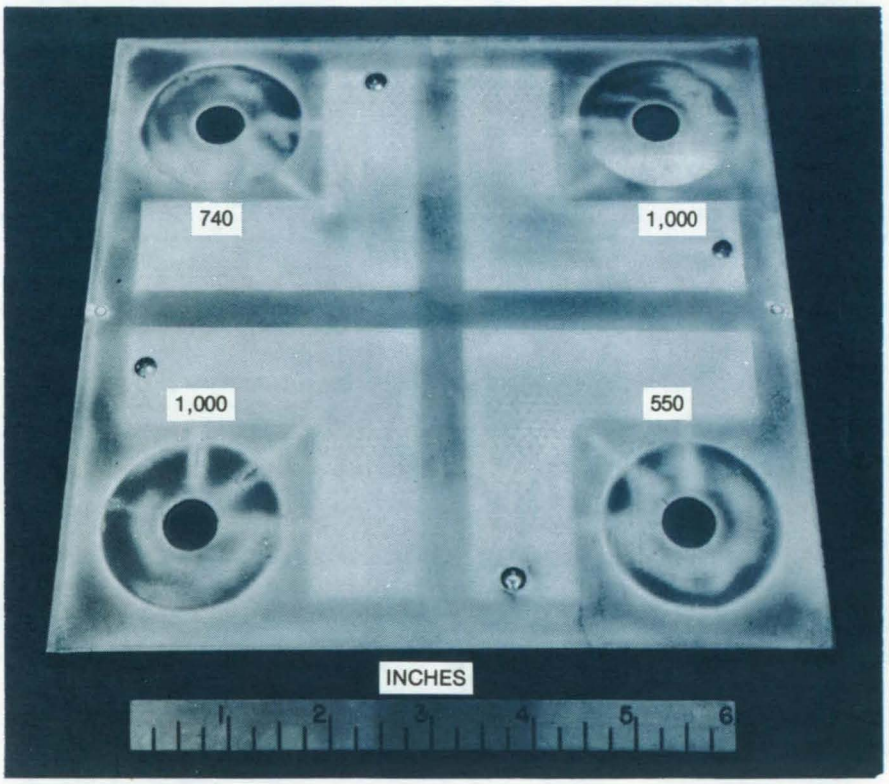

Figure 1. A **Standard Cold Plate Specimen** is shown, with the final pressure in psi shown for each section.

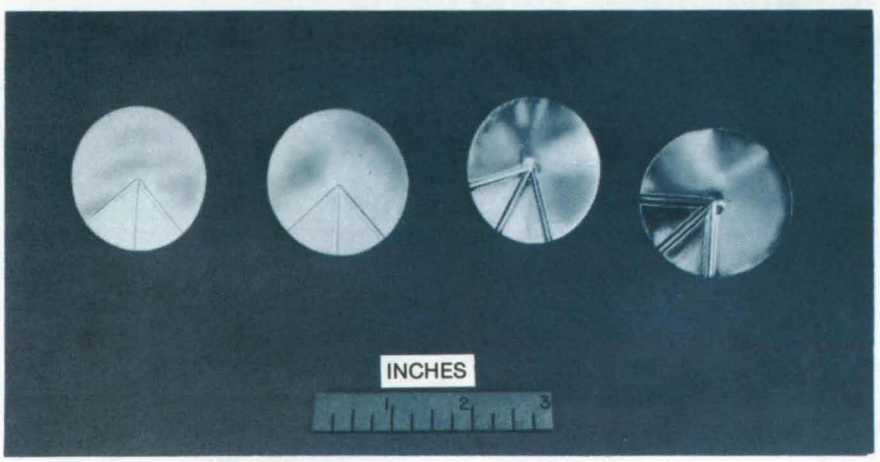

Figure 2. Four **Stainless-Steel Disks** used to simulate integral port fittings are shown.

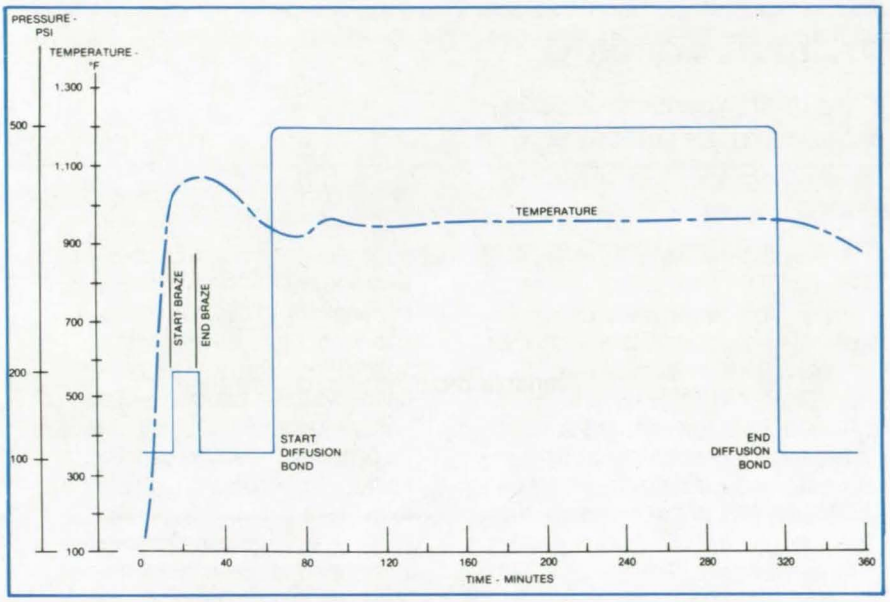

Figure 3. A **Process Chart** shows pressure and temperature as a function of time for the experimental two-stage braze diffusion bonding.

The photograph in Figure 1 shows the standard cold plate test specimen developed for this program. The numbers on the cold plate show the final pressures (psi) used in the four sections. Four stainless-steel disks (Figure 2) are used to simulate integral port fittings required for actual fittings. The process chart in Figure 3 gives pressure and temperature as a function of time for the experimental two-stage braze diffusion bonding of these test specimens.

This work was done by Charles S. Beuyukian and Mike J. Mitchell of Rockwell International Corp. for **Johnson Space Center.** *No further documentation is available.*
MSC-19323

NASA

Nondestructive Inspection of Multilayered Insulation

Radio-frequency techniques are used to measure layer density and metal loss.

Marshall Space Flight Center, Alabama

Nondestructive radio-frequency techniques can be used in the inspection and evaluation of multilayered cryogenic insulation materials. The use of nondestructive techniques in this connection is believed to be unique. Defects or damage in multilayered insulation (MLI) blankets could consist of: (a) metal loss due to corrosion or abrasion, (b) areas of increased layer density, or (c) areas where the insulation has been torn. The new process permits the inspection of MLI blankets without requiring any contact between the blankets and the inspection apparatus. The electromagnetic inspection approach allows the assessment of both thickness variations and loss of metallization from the reflector layers.

The technique involves probing the MLI blanket throughout its thickness with an electromagnetic field that intersects with the metal in the MLI. The field is generated by an induction coil. The coil impedance is a function of the interaction between the field and the MLI. Therefore, the condition of the MLI can be related to the measured coil impedance. A novel feature of this approach is that both the resistive and the reactive components of the probe coil impedance are measured directly. The values of these two components can be related independently to layer density and to metal loss, allowing the inspection process to distinguish between these types of defects.

This work was done by Joseph A. Zelik of McDonnell Douglas Corp. for **Marshall Space Flight Center.** *For further information, Circle 80 on the TSP Request Card.*
MFS-22191

NASA

Reliability of Hybrid Microcircuit Bonding

Microcircuit failure due to differential thermal expansion depends on the technique used to mount components to the substrate.

Marshall Space Flight Center, Alabama

One means of fabricating hybrid microcircuits is to bond the various circuit elements (transistors, integrated circuits, resistors, and the like) to the alumina substrate with an epoxy resin or solder. A problem with this fabrication method is that although the components operate as specified at normal laboratory ambient temperatures, they fail during elevated temperature cycling tests. The reason: present bonding materials are not sufficiently flexible and therefore subject the circuit elements to excess mechanical stress (due to differential thermal expansions). The result of the different rates of expansion is component rupture, termination debonding, solder joint failure, or substrate metalization lifting.

A report documents the effects of differential thermal expansion on ceramic chip capacitors, one of the types of components so adversely affected. It indicates that the mounting techniques used to bond the capacitors to the alumina substrate have a definite effect on the thermally induced stress, and thus the failure rate of the components. The report experimentally observes that the stresses in more compliant bonding systems, such as soft lead/tin and indium solders, are significantly lower than those in hard solder and epoxy systems. The report further states that the harder (or higher-melting-point) solders are less susceptible to thermal cycling effects but that they are more likely to fail during initial processing operations.

Strain-gage techniques are used to determine thermally-induced expansion stresses on the capacitors and the alumina substrates. Samples of the capacitors are bonded to the substrate samples, using standard 10 percent tin/90 percent lead solder, 60 percent tin/40 percent lead solder, an indium solder, a two-component epoxy adhesive, and a nonconductive epoxy adhesive. A strain gage is attached to each capacitor sample as shown. A matching strain gage is then bonded to a second capacitor at one end only. This capacitor is allowed to expand and contract freely through the temperature cycling and is the standard for the strain-gage measurements.

The capacitors with attached strain gages are placed in a temperature chamber and cycled. The value of strain recorded represents a difference in the dimensional changes of the two capacitors. With these values, strain in micrometers per meter (μm/m) is plotted against time for each sample, using the various bonding agents.

This work was done by S. V. Caruso, D. L. Kinser, S. M. Graff, and R. V. Allen of **Marshall Space Flight Center.** *For further information, Circle 81 on the TSP Request Card.*
MFS-23358

NASA

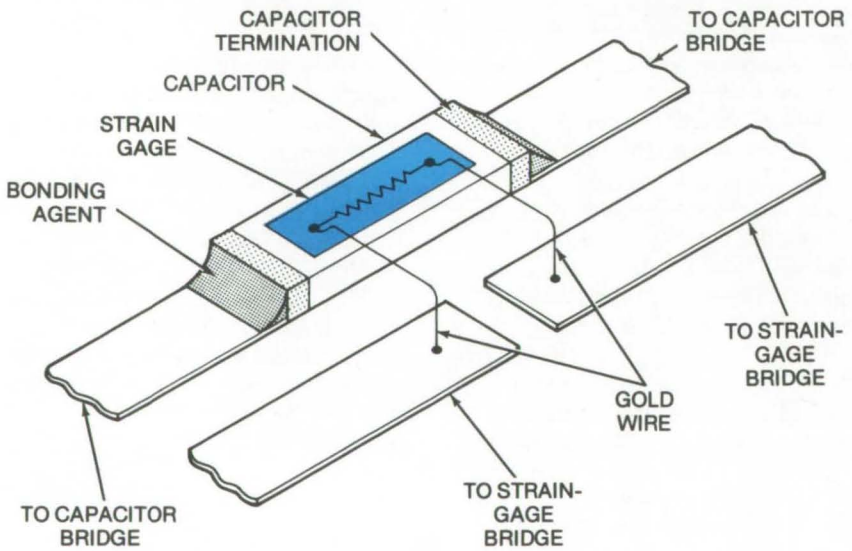

Capacitor Assembly for Strain Measurements as a function of time and temperature: A ceramic chip capacitor is bonded to an aluminia substrate.

Roll-Forming Tubes to Header Plates

A technique for attaching and sealing tubes to header plates

Lewis Research Center, Cleveland, Ohio

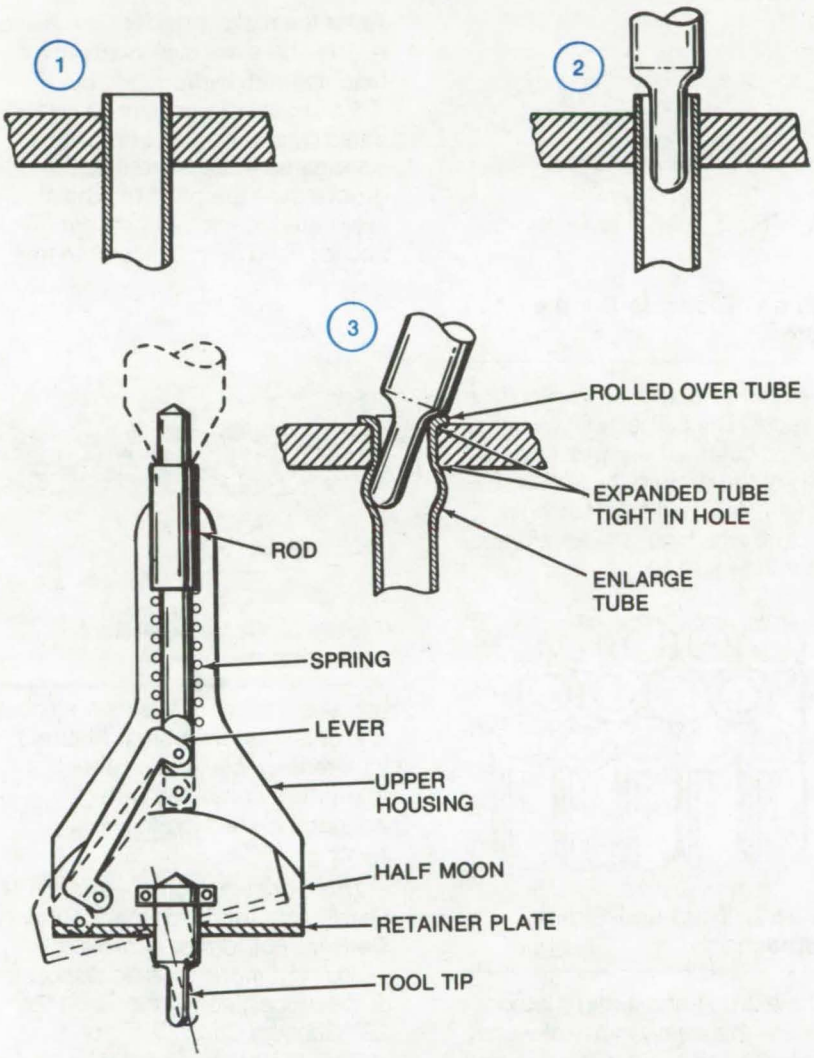

The **Roll-Forming Tool Assembly** can be used with interchangeable tool tips that may be made in various sizes for use with various sizes of tubes and thicknesses of header plates.

A technique has been developed for attaching and sealing tubes to header plates, as in a heat exchanger, by expanding the tubes above and below the header plates with a unique roll-forming tool. This technique is particularly useful for attaching small tubes which are difficult to roll into conventional grooves in header plate tube holes, and for attaching when welding, brazing or soldering is not desirable.

The technique consists of rotating a unique tool assembly by means of a drill press or hand drill to expand the tube above and below the header plate in a single operation.

As shown in the figure, the tool tip is mounted in a ball bearing and is free to rotate about its longitudinal axis. The tool tip and bearing are mounted in a hemispherical plate ("half moon"). The "half moon" is connected to the housing assembly by a lever. The rod through the housing transmits external pressure to the lever and controls the angular displacement of the tool tip. In operation, the entire tool assembly is mounted in a drill and the tool tip inserted into the end of the tube. With the drill rotating, pressure on the rod is transmitted through the level to tilt the "half moon" and the tool tip away from the longitudinal axis and cause the tool tip to circumscribe a conical revolution.

This work was done by Karl Kramer of **Lewis Research Center.** *For further information, Circle 82 on the TSP Request Card.*
LEW-10513

NASA

Metal Structures With Parallel Pores

Four methods of fabricating porous metal parts such as electrodes produce parallel pores, resulting in a more efficient structure.

Goddard Space Flight Center, Greenbelt, Maryland

The fabrication of porous metal parts by powder metallurgy procedures is a well-established technology. Plates for electrochemical cells and electrodes for certain types of fuel cells, for instance, are presently made by such procedures. One characteristic of the process, random pore structure, does not offer optimum pore geometry for these applications. Parallel pores of a uniform dimension would probably be more suitable.

Four methods of fabricating metal plates having uniformly-sized parallel pores have been studied: (1) the elongate-bundle method, (2) the wind-and-sinter method, (3) the extrude-and-sinter method, and (4) the corrugate-stack method.

The elongate-bundle method consists of enclosing a copper rod within a thick-walled nickel tube. The tube is machined to obtain a billet having a square cross section. The billet is elongated by a factor of 81 and then is cut into 81 sections. These sections are reassembled into a 9-by-9 array that is about the same size as the original billet but contains 81 copper rods, each one-ninth its starting diameter. This new billet can again be elongated, cut into 81 sections, and reassembled as before. The process may be repeated several times to yield copper rod filaments of the desired size. After reduction, the billet is sliced, and the copper is leached out, leaving a porous nickel plate as shown in Figure 1. Stainless steel structures with pores of approximately 4 μm in diameter and 100 μm in length can be made by this method.

The wind-and-sinter technique consists of winding fine nickel-coated copper wire onto a spool. The wound wire is sintered to form a coherent mass and is removed from the spool. The coil is cut perpendicular to the wires to yield slices of the desired thickness. The copper is leached out, leaving a structure which has the appearance shown in Figure 2.

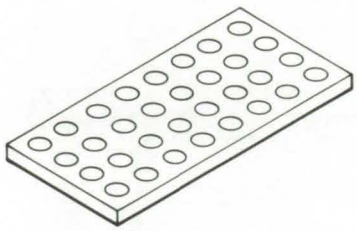

Figure 1. **Elongate-Bundle Approach**

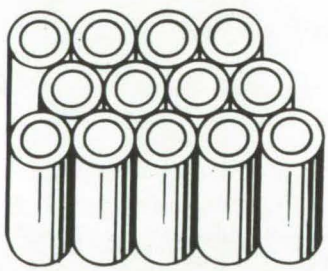

Figure 2. **Wind-and-Sinter Approach**

The extrude-and-sinter method begins with a heavy slurry of water, chopped fused-quartz fibers, nickel powder, a wetting agent, and a thickener. The mix is forced through a small orifice, alining the quartz fibers parallel to the extrusion axis. The extruded material is cut into convenient lengths, stacked, and compacted. The compact is fired at a low temperature to remove the water and organic matter and is fired again at a higher temperature to sinter the nickel powder. The fused-quartz fibers are dissolved out by leaching with hydrofluoric acid.

Corrugate-stack plates are fabricated by stacking electroformed, corrugated metal sheets so that groove axes are parallel. The stack is sintered to form a coherent mass and is sliced perpendicular to the grooves. Adjacent sheets may nest and obliterate the pores; Figure 3 illustrates uncorrugated sheets alternately combined with nonparallel stacking to avoid nesting.

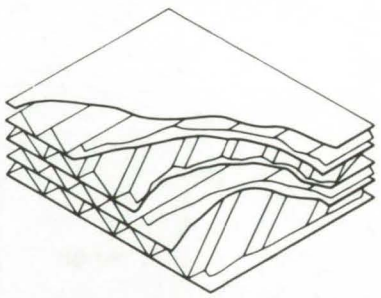

Figure 3. **Corrugate-Stack Approach**

This work was done by Joseph M. Sherfey of **Goddard Space Flight Center.** *For further information, including a more detailed discussion of the processes, Circle 83 on the TSP Request Card.*

This invention is owned by NASA, and a patent application has been filed. Inquiries concerning nonexclusive or exclusive license for its commercial development should be addressed to the Patent Counsel, Goddard Space Flight Center [see page 2]. Refer to GSC-10984.

NASA

Metalworking Method for Composites

Drawing and rolling can reduce fabrication costs of Al/C composites.

Marshall Space Flight Center, Alabama

A study was conducted to find effective fabrication methods for aluminum/boron (Al/B) and aluminum/graphite (Al/C) composites. Standard metalworking methods were examined, such as drawing (through conical converging), rolling, extrusion, and swaging. These processes are well established in the metal industry; and if any are found suitable for composites, inexpensive modifications can be made to existing equipment for economical composite fabrication.

The Al/B composite fabrication was investigated in three phases. In the first phase a limited number of Al/B flats were prepared by diffusion bonding. The purpose was to identify the composite matrix most suitable to such processing. The second phase, conducted concurrently with the first, was to design and construct experimental equipment for rolling and drawing the Al/B composites. The third phase involved experiments with existing metalworking equipment based on the results of the first and second phases.

The studies have shown that hot/cold drawing is a viable method for the production of 1/2-inch (12.7-mm) Al/B tubes. Heating the preforms uniformly, (acrylic) binder removal, and drawing speed are the most critical parameters and must be established for a particular tube size. However, upscaling to full-size tubes was exceedingly difficult, primarily because of the difficulty in procuring equipment necessary for such large sizes. Similarly, the rolling of small Al/B preforms was satisfactorily demonstrated, but could not be carried into the upscaling phase because of equipment cost limitations. Rolling was abandoned in favor of drawing because a fully equipped drawbench was readily available.

The properties of the small composite tubes and flats obtained were comparable to those prepared by other means. Metallographic analysis showed that the matrix-clad filament approach yielded excellent filament distribution. Of particular significance was the low cost potential offered by drawing (and to some extent rolling) as a means of tube fabrication, because every processing step can be automatic and continuous.

While developments in the Al/B program could be fairly well predicted, the very nature of the commercial graphite yarn imposed severe restrictions in following conventional metalworking procedures for Al/C. It was observed, for example, that even mild reductions on Al/C matrix-clad filament preforms could not be tolerated and that severe fiber fracture was encountered despite considerable care. Metalworking processes were, therefore, abandoned in favor of resistance heating and ion-beam (or electron-beam) heating to eliminate any applied pressure and to maintain a protective atmosphere. Composites prepared by these two methods were far superior in consolidation, filament distribution, and filament-matrix compatibility.

In summary, modern metalworking methods, particularly drawing and rolling, are adaptable to Al/B composite fabrication. The speed of Al/B composite fabrication, which is generally connected with low cost, is not as fast as the fabrication of homogeneous metals. However, it is sufficiently fast to reduce the fabrication costs.

Graphite composites, on the other hand, are not amenable to standard metal processing methods. If, however, electron-beam heating methodology is pursued, it may be possible to reduce fabrication costs of Al/C significantly even though capital expense for equipment would be high. However, it seems certain that graphite multiend yarns will always be more difficult to fabricate into metal-matrix composites in comparison to their boron counterparts.

This work was done by A. P. Divecha of Commonwealth Scientific Corp. for **Marshall Space Flight Center.** *For further information, including a description of procedures and apparatus, Circle 84 on the TSP Request Card.*

Inquiries concerning rights for the commercial use of this invention should be addressed to the Patent Counsel, Marshall Space Flight Center *[see page 2]*. *Refer to MFS-23354.*

NASA

Mathematics and Information Sciences

Estimation of Spares

A simplified manual technique to determine the number of spare parts required for a given risk level

Lyndon B. Johnson Space Center, Houston, Texas

Conventional methods for the probability basis of spares determination require the use of statistical tables or graphs (e.g., a cumulative Poisson distribution), the manual computation of complex equations, or the use of computer devices. A new approach employs short-cut approximations in lieu of computer-assisted or complex computational analyses to arrive at initial sparing estimates. The method involves an easily remembered procedure.

As an example, suppose a part has a unit reliability of 0.6. How many spares (N_S) are required to meet a sufficiency risk level of 99 percent (i.e., no more than a 1-percent risk that sufficient spares will not be available)? The unreliability of the part is

$$Q_u = 1 - 0.6 = 0.4$$

and the probability of not having adequate spare parts is

$$Q_S = 1 - 0.99 = 0.01$$

A worksheet is set up as shown in the figure.

N_t	$\frac{Q_u}{N_t}$	PRIOR RESULT	PRESENT RESULT
1	$\frac{0.4}{1} = 0.4$	1.0	0.4
2	$\frac{0.4}{2} = 0.2$	0.4	0.08
3	$\frac{0.4}{3} = 0.133$	0.08	0.011
4	$\frac{0.4}{4} = 0.1$	0.011	0.001

WORKSHEET FOR SPARES DETERMINATION

Column 1 contains, in increasing order, a sequence of trial numbers, 1, 2, 3, etc. In column 2 of row 1, $Q_u = 0.4$ is divided by $N_t = 1$. Column 3 of row 1 (a prior result) is initially unity. Column 4 is obtained by multiplying columns 2 and 3 ($0.4 \times 1.0 = 0.4$). Since column 4 is greater than $Q_S = 0.01$, the procedure is continued in row 2. As before, column 2 of row 2 is obtained by dividing Q_u by N_t ($0.4 \div 2 = 0.2$). The prior result 0.4 is repeated from column 4 of row 1. Column 4 of row 2 is obtained by multiplying columns 2 and 3 ($0.2 \times 0.4 = 0.08$).

This process is continued until column 4 is less than $Q_S = 0.01$. The number of spares required is then one less than the final value of N_t, or

$$N_S = N_t - 1 = 4 - 1 = 3$$

For a unit reliability of 0.9 or greater, the error in the above procedure can be shown to be less than 10 percent.

This work was done by Michael A. Mezzacappa of Rockwell International Corp. for **Johnson Space Center.** *For further information, Circle 85 on the TSP Request Card.*
MSC-19469

NASA

Computer Programs

These programs may be obtained at very reasonable cost from COSMIC, a facility sponsored by NASA to make new programs available to the public. For information on program price, size, and availability, circle the reference letter on the COSMIC Request Card in this issue.

Linear Stochastic Optimal Control and Estimation

A digital program for solving the LSOCE problem

A digital program has been written which solves the Linear Stochastic Control and Estimation (LSOCE) problem by using a time-domain formulation.

The LSOCE problem is defined as that of designing controls for a linear time-invariant system, which is disturbed by white noise, in such a way as to minimize a quadratic performance index. The major subroutine solves the algebraic matrix Riccati equation by using an eigenvector method. Other major subroutines provided are a Lyapunov equation subroutine, an eigenvalue subroutine, an eigenvector subroutine, and a subroutine for solving the matrix Riccati differential equation. Program LSOCE is designed so that the user has options to solve all or part of the LSOCE problem.

(continued next page)

The LSOCE was written so as to handle systems of any order and is restricted only by computer storage size and accuracy.

FORTRAN IV
IBM 7094

This program was written by Lucille C. Geyser and F. K. Bruce Lehtinen of **Lewis Research Center.** *For further information, Circle O on the COSMIC Request Card.*
LEW-12505

NASA

Guide for Testing Numerical-Integration Subroutines

A technique for testing algorithms used to solve differential equations

A numerical technique has been designed for testing algorithms that are used to find solutions to differential equations. When evaluating a method for the solution of differential equations, it is important to consider discretization (or truncation) error, stability characteristics (error propagation), and the effect of round-off error. Mathematical analysis usually can give separate indications of these. However, analytical results for different methods may be incomplete or difficult to compare, and a rigorous analysis requires simplifying assumptions for any nontrivial problem. Consequently, numerical results are frequently used to compare different methods.

As a rule, numerical tests show clearly the advantages of a method but give little information about its limitations. It is highly desirable that numerical tests give as complete a picture as possible, especially when used to assess the relative merits of different techniques. To simplify this task, a guide has been prepared which is easy to follow and which yields enough information to make a reasonable evaluation of a method. The guide consists of suggested procedures and a set of test problems.

The guide presents a reasonably complete evaluation of a subroutine for the integration of ordinary differential equations. Results for the variable-order Adams method are given to illustrate how the guide might be used and to document the capabilities of the method.

In connection with the problem of comparing solutions which have been obtained on machines with different word lengths, it should be noted that word length has no significant effect on results unless round-off error is a factor. If results are given for enough different error tolerances (or step sizes), it is possible to tell by inspection where round-off starts causing a deterioration in performance. The smallest error achieved with a method on a test problem gives an indication of its round-off characteristics.

A set of test problems is presented which can be used along with the guide to evaluate various methods of solving differential equations. These could serve as a tentative general standard for such evaluations. Since a standard should include the points where results are to be tabulated, a set of output points is suggested for each test problem.

This work was done by Fred T. Krogh of Caltech/JPL for **NASA Pasadena Office.** *To obtain a copy of the report, Circle P on the TSP Request Card.*
NPO-11644

NASA

Business Capabilities File

An automated search system to help find the right business for the right job

A computerized file-creation and update system identifies businesses by their functional capabilities and geographic location. The file is easy to maintain and update with new businesses and capabilities.

This management information system was originally designed to generate reports on minority-owned firms in one geographical area. It may be used as is; or by merely changing the column headings, it can be used with a data base on organizations of most any type or location. It will identify sources by specific requirements and by specific or general location.

Documents are keypunched and input to the program. Records are then sorted before creating or updating the master file. Reports are formatted and edited for the production of error messages, and edited data are sorted and passed to the report writer. Multiple copies of the following reports are output: (a) Company Register, (b) Capabilities Index, (c) Capabilities Index Headings and Particular Interests, (d) Item Description Cross-Reference by Keyword, and (e) Batch List and Error Report.

ANS COBOL V4
IBM OS 360/370

This program was written by Walter H. Anderson of Caltech/JPL and Dominic A. Costanza of Informatics Inc. for **NASA Pasadena Office.** *For further information, Circle Q on the COSMIC Request Card.*
NPO-13834

NASA

Subject Index

WHERE IS THE WORLD'S LARGEST BANK OF TECHNICAL DATA

?

It's in Bloomington and Pittsburgh, it's in Storrs, Connecticut and Research Triangle Park, North Carolina; and it's in Albuquerque and Los Angeles.

NASA IAC's — INDUSTRIA

You can get more information and more data on more technical subjects through NASA's network of IAC's than anywhere else in the world. About 8,000,000 documents and growing at the rate of 50,000 more each month!

Major sources include:

- 750,000 NASA Technical Reports
- Selected Water Resources Abstracts
- NASA Scientific and Technical Aerospace Reports
- Air Pollution Technical Information Center
- NASA International Aerospace Abstracts
- Chem Abstracts Condensates
- Engineering Index
- Nuclear Science Abstracts
- NASA Tech Briefs
- Government Reports Announcements

and many other specialized files on food technology, textile technology, metallurgy, medicine, business, economics, social sciences, and physical science.

☆U.S. GOVERNMENT PRINTING OFFICE: 1976 0—203-137

The IAC's are one of the most economical ways of staying competitive in today's world of exploding technology. The help available from the network ranges from literature searches through expert technical assistance.

Literature Searches

Help in designing your search, typically from 30 to 300 abstracts in as narrow or broad an area as you need, and complete reports when you need them. The most complete "search before research" available!

Current Awareness

Consult with our applications engineers to design your personal program — selected monthly or quarterly abstracts on new developments in your speciality. It's like having your own journal!

Technical Assistance

Our applications engineers will help you evaluate and apply your literature-search results. They can help find answers to your technical problems and put you in touch with scientists and engineers at NASA Field Centers.

To obtain more information about how NASA's IAC's can help you —
Check the IAC box on the TSP Request Card in this issue,
Or write or call the IAC nearest you.

APPLICATIONS CENTERS

How to get reports and other documents discussed in this issue of Tech Briefs

Many of the innovations in Tech Briefs are described in detail in reports available at a reasonable cost through one or more of the IAC's. To order a report, call or write the IAC referenced at the end of the Tech Brief article at the address below. Be sure to list the titles and accession numbers (N76-..., N75-..., etc.) of those you wish to purchase.

Aerospace Research Applications Center (ARAC)
Indiana University
400 E. 7th St.
Bloomington, Ind. 47401
Dr. Robert D. Shriner, Director
Phone: (812) 337-7833

Knowledge Availability Systems Center (KASC)
University of Pittsburgh
Pittsburgh, Pa. 15260
Edmond Howie, Director
Phone: (412) 624-5211

New England Research Application Center (NERAC)
Mansfield Professional Park
Storrs, Conn. 06268
Dr. Daniel U. Wilde, Director
Phone: (203) 486-4533

North Carolina Science & Technology
Research Center (NC/STRC)
P.O. Box 12235
Research Triangle Park, N.C. 27709
Peter J. Chenery, Director
Phone: (919) 549-8291, Ext. 210

Technology Application Center (TAC)
University of New Mexico
Albuquerque, N.M. 87131
Dr. Carey O'Bryan, Director
Phone: (505) 277-4000

Western Research Application Center (WESRAC)
University of Southern California
University Park
Los Angeles, Calif. 90007
Radford King, Director
Phone: (213) 746-6132

National Aeronautics and
Space Administration

Washington, D.C.
20546

Official Business
Penalty for Private Use, $300

SPECIAL FOURTH CLASS MAIL
BOOK

Postage and Fees Paid
National Aeronautics and
Space Administration
NASA-451

U.S.MAIL

NASA

An Energy Conservation House being built by NASA uses solar collectors, waste-water recycling, and other space spinoffs. It will be open to the public this year.

Instrumentation for monitoring spacecraft control gyros resulted in a method to detect faults in railroad roller bearings.